INTERNATIONAL DOCTORAL
SCHOOL OF THE USC

Carlos Alberto
Pena Puga

PhD Thesis

# Liquid systems for the valorisation of lignocellulosic biopolymers

Santiago de Compostela, 2022

**Doctoral Programme in Chemical and Environmental Engineering**

TESE DE DOUTORAMENTO

# LIQUID SYSTEMS FOR THE VALORISATION OF LIGNOCELLULOSIC BIOPOLYMERS

Carlos Alberto Pena Puga

**ESCOLA DE DOUTORAMENTO INTERNACIONAL DA UNIVERSIDADE DE SANTIAGO DE COMPOSTELA**
**PROGRAMA DE DOUTORAMENTO EN ENXEÑARÍA QUÍMICA E AMBIENTAL**

SANTIAGO DE COMPOSTELA

2022

# DECLARACIÓN DO AUTOR DA TESE

## (Statement by the author of the thesis, in Galician)

D. Carlos Alberto Pena Puga

Título da tese: Liquid systems for the valorisation of lignocellulosic biopolymers

Presento a miña tese, seguindo o procedemento axeitado ao Regulamento, e declaro que:

1) A tese abarca os resultados da elaboración do meu traballo.
2) No seu caso, na tese se fai referencia ás colaboracións que tivo este traballo.
3) Confirmo que a tese non incorre en ningún tipo de plaxio doutros autores nin de traballos presentados por min para a obtención doutros títulos.
4) A tese é a versión definitiva presentada para a súa defensa e coincide a versión impresa coa presentada en formato electrónico.

E comprométome a presentar o Compromiso Documental de Supervisión no caso de que o orixinal non estea na Escola.

En Santiago de Compostela, a 29 de xullo de 2022.

# AUTORIZACIÓN DOS DIRECTORES/TITOR DA TESE

## (Authorisation by the directors/tutor of the thesis, in Galician)

**Liquid systems for the valorisation of lignocellulosic biopolymers**

D. Héctor Rodríguez Martínez e Dna. Eva Rodil Rodríguez, Profesores Titulares de Universidade do Departamento de Enxeñaría Química da Universidade de Santiago de Compostela

INFORMAN:

Que a presente tese se corresponde co traballo realizado por D. Carlos Alberto Pena Puga, baixo a nosa dirección/titorización, e autorizamos a súa presentación, considerando que reúne os requisitos esixidos no Regulamento de Estudos de Doutoramento da USC, e que como directores desta non incorre nas causas de abstención establecidas na Lei 40/2015.

De acordo co indicado no Regulamento de Estudos de Doutoramento, declaramos tamén que a presente tese de doutoramento é idónea para ser defendida en base á modalidade de monográfica con reprodución de publicacións, onde a participación do doutorando foi decisiva para a súa elaboración e as publicacións se axustan ao Plan de Investigación.

En Santiago de Compostela, a 29 de xullo de 2022.

Héctor Rodríguez Martínez

Eva Rodil Rodríguez

# Acknowledgements

The present thesis is the compilation of the work that I have carried out over the last years. This period has been a tremendously enriching experience, which has given me the opportunity to meet and interact with great people. The collaboration with them has contributed to arrive, through a rewarding path, to a successful end of my predoctoral stage, crystallised in this thesis volume. I would like to start my list of acknowledgments with Dr. Héctor Rodríguez, the person who introduced me to the research world and the person who can help you with all kind of doubts, problems, and inexplicable things. He was accompanied in the direction of my PhD studies by Dr. Eva Rodil, who was always supportive and ready to help me with whatever I might need. Without their assistance, this goal (unthinkable for me only some years ago) would have been impossible to achieve. I am also grateful to Prof. Ana Soto, coordinator of the research group Sustainable Separation Processes of the University of Santiago de Compostela (USC), for her valuable advices and, of course, for accepting me in the research group during all these years. I feel indebted to all of them since, independently of the knowledge gained in the context of research or the field of chemical and environmental engineering, this period of my life has also had a fascinating impact at a personal level. It has been also a pleasure to count on the assistance of Prof. Alberto Arce, Dr. Alberto Arce Jr., and Dr. Óscar Rodríguez, always helpful and contributing to create a pleasant work environment.

Throughout all these years, I have received additional assistance from different people in the USC, helping me in one way or another to succeed in my research endeavours. In this regard, I would like to express my gratitude to Ms. Mar Orge and Ms. Mónica Dosil (research group GI-1613) for their assistance with some analytical determinations and in helping to fix the never-ending problems with the HPLC apparatus; to Dr. Álvaro Gil (Institute of Materials) for collaboration in the characterisation of cellulose samples; to Dr. José B. Quintana and Dr. Rosario Rodil (research group GI-1626) for solving doubts related to the analytical procedures for identification of phenolic compounds; and to Dr. Thelmo Lu-Chau (research group GI-

1613) for assisting me in the initial steps with enzymatic reactions. Moreover, the utilisation of the analytical facilities of the Network of Infrastructures to Support Research and Technological Development (RIAIDT) of the USC has been continuous (and essential!) during the development of my PhD research work. I am thankful to the personnel in charge of the different units, with a special mention to the endless patience that Dr. Bruno Dacuña (X-ray unit) and Dr. Manuel Martín (NMR unit) have had with me. The acknowledgement is extended to Eduardo Gómez (Technical Service), who has always made an effort to find fast and efficient solutions to the various breakdowns of the apparatus that I have had to face. Beyond the USC walls, I also want to acknowledge the fruitful discussions maintained with Dr. Alberto V. Puga (Rovira i Virgili University, Tarragona) on the reactivity of cellulose, and with Prof. Rafał M. Łukasik (National Laboratory of Energy and Geology, Lisbon) on biomass treatments and experimental design.

Part of this work was carried out during a research stay in the Centre of Biological Engineering (University of Minho, Braga) under the supervision of Dr. Michele Michelin. I must thank her for her closeness and predisposition to clarify the many doubts that were permanently arising in my mind. She and Dr. Lina F. Ballesteros taught me methods for characterisation of lignin that allowed me to progress in that research line. In this stay I was very lucky to meet people (Aloia, Claudia, Sara...) who made me feel comfortable from the beginning, with the city of Braga becoming a second home to me.

During these exciting years, I have shared the laboratory with people who have made the long working hours more enjoyable: Marlen, Iria, Raquel, Néstor, Iago, Mohammed, Fernanda... A long list of people that I will always remember with a pleasant memory. A special mention to colleagues with whom I have not only shared moments in the laboratory but also wonderful leisure times outside it: Alba, Cris, Leti, and Paula. Part of the work collected in this thesis took place in a pandemic time with severe mobility restrictions and, undoubtedly, they made this confusing period more bearable.

In this thanking list, my family and the friends from Carballo -and everywhere else- could not be missing. They have seen how I was not sharing as much time with them as they deserved, and how the plans were suddenly changing in a good number of occasions (here I also have to include my motorbike!). Nevertheless, I have

continuously felt their unconditional support, and I keep knowing that I can always count on them.

Finally, I would like to thank the financial support provided by Xunta de Galicia through projects ED431B 2017/023, ED431D 2017/06 (Galician Network of Ionic Liquids) and ED431B 2020/021, as well as by the "Galicia-Norte de Portugal" European Group of Territorial Cooperation through its mobility programme Iacobus.

Carlos Pena

Santiago de Compostela, July 2022

# Abstract

Lignocellulosic biomass is a key biorenewable source in the transition of the current industrial platform for the production of chemicals and materials to a more sustainable scheme. It is presently accepted that the viable exploitation of this type of biomass should include an integral valorisation of its major constituent biopolymers. The work of this thesis focuses on the two main ones: cellulose and lignin. In a first part, the pretreatment of cellulose with liquid formulations based on ionic liquids was studied, with the purpose of improving its reactivity. Better reaction rates were observed both in the enzyme hydrolysis and in the carboxymethylation of the pretreated samples. In a second part, the depolymerisation of lignin via aqueous solutions of an ionic liquid or alternative aqueous systems was explored. Although in limited yields, a number of value-added phenolic compounds were identified after the treatments.

# Contents

# 1. INTRODUCTION

# INTRODUCTION

## 1.1. Lignocellulosic biomass as a key feedstock for the sustainability of the chemical industry

Since the last years of the 20th century, the tendency of the industry to shift to more sustainable processes has been gradually consolidated. The establishment by the United Nations, in 2015, of its 2030 Agenda for Sustainable Development (https://sdgs.un.org/2030agenda) has stimulated an acceleration of this tendency in recent times. A key element for the movement of the current industrial platform of production of chemicals and materials towards more sustainable positions is the substitution of fossil and non-renewable resources by others with a more satisfying (bio)renewable character in the industry. The global volume of industrial production, however, is already large at present, and expected to keep increasing over at least the next decades due to a continuous improvement of the human development indices (https://hdr.undp.org/data-center/human-development-index#/indicies/HDI), as well as to the mere growth of the total world population (https://population.un.org/wpp/Graphs/DemographicProfiles/Line/900). Thus, this large and growing volume poses a critical challenge for the identification of raw materials with the capacity to feed the referred industrial platform in a sustained manner. An attractive candidate that seems to be called to play a significant role in this regard is lignocellulosic biomass (Bozell et al., 2007), a biorenewable source produced by Nature at a sufficiently fast rate as to cover the present and projected human demand of chemical industry production (Huber et al., 2006). Beyond its abundancy, additional appealing attributes of lignocellulosic biomass include a reasonably homogeneous geodistribution (much better than that of the current fossil resources of reference) and, in contrast to other biorenewable sources, the fact that it avoids competition or direct interaction with the human food market (FitzPatrick et al., 2010).

Lignocellulosic biomass has been used by humankind in a variety of forms since prehistoric times. However, it was not until the identification of cellulose by the French scientist Anselme Payen in the second half of the 19th century that its embedded chemical richness began to be unveiled. The major components of lignocelluloses are cellulose, hemicellulose and lignin – three biopolymers arranged in a complex non-

uniform 3D structure in the cell walls (Figure 1.1). Cellulose is a linear long-chain polysaccharide of repeating β-(1,4)-glycosidically bonded D-glucose units, which exist as pyranose rings in a thermodynamically preferred configuration, and with a strong network of intra- and intermolecular hydrogen bonds; hemicellulose is an amorphous and branched polysaccharide built of several C5 and C6 sugar moities (xylose, arabinose, glucose, mannose...), any of which can be potentially substituted by acetyl groups; and lignin is a highly branched polyphenol biosynthesised by the random recombination of phenoxy radicals of three different monolignols (coniferyl, sinapyl, and *p*-coumaryl alcohols), deriving in phenylpropane units linked together by ether linkages and different types of carbon-carbon bonds (Brandt et al., 2013; Huber et al., 2006; Schmidt et al., 2013; Usmani et al., 2020). The specific composition is a function

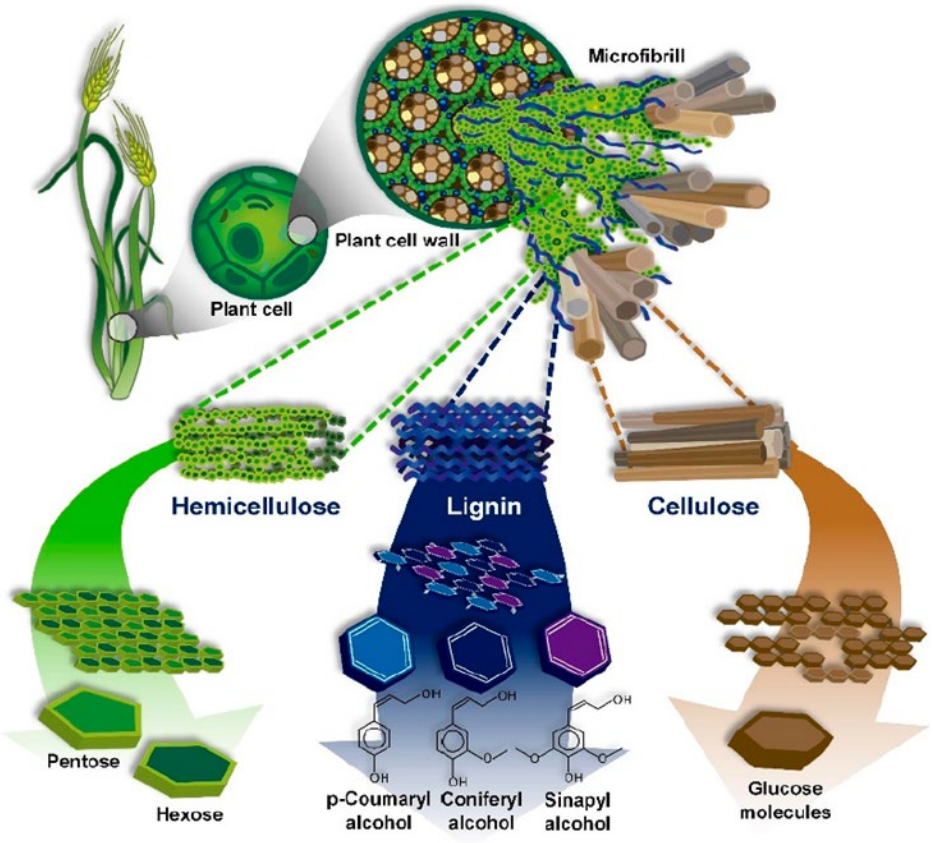


Figure 1.1. Structure of lignocellulosic biomass and its biopolymers: cellulose, hemicellulose, and lignin. Reproduced from Hernández-Beltrán et al. (2019) with permission by MDPI.

of the species, tissue, maturity etc., but in general it can be stated that lignocelluloses contain aproximately 25-50 % cellulose, 15-35 % hemicellulose, and 10-35 % lignin (Usmani et al., 2020). Despite some excepcions (e.g. the lower lignin content of straws of different substrates), this is generally illustrated in Table 1.1 for a variety of lignocelluloses. In woody biomass, these three biopolymers do typically represent more than 95 % in dry weight (Isikgor et al., 2015). The remaining non-polymeric fraction is constituted by proteins, oils, extractives, and ashes. In view of the diverse nature and inherent chemical richness of their components, it is evident that lignocelluloses have an undeniable potential to serve as biorenewable feedstock in the development of chemical processes for the production of a broad portfolio of chemicals and materials (see Figure 1.2); that is, the development of biorefineries (Cherubini et al., 2009).

**Table 1.1.** Approximate percent composition of cellulose, hemicellulose, and lignin (in a dry basis) for different lignocellulosic substrates. Adapted from Hernández-Beltrán et al. (2019).

| Lignocellulosic substrate | Composition (% dry basis) | | |
|---|---|---|---|
| | Cellulose | Hemicellulose | Lignin |
| Bamboo stem | 43.0 | 22.1 | 27.1 |
| Birch | 40.1 | 17.5 | 24.2 |
| Corn cob | 42.0 | 45.9 | 2.8 |
| Corn stalk | 36.4 | 30.3 | 6.9 |
| Corn stover | 42.2 | 22.3 | 19.5 |
| Corn straw | 49.3 | 28.8 | 7.5 |
| Cotton stalk | 41.6 | 23.6 | 23.3 |
| Eucalyptus | 52.1 | 24.5 | 25.2 |
| Giant reed | 41.5 | 20.5 | 18.4 |
| Maize straw | 38.3 | 29.8 | 3.8 |
| Meadow grass | 41.3 | 28.1 | 30.1 |
| Miscanthus | 36.3 | 22.1 | 22.6 |
| Oat straw | 35.0 | 28.2 | 4.1 |
| Pinewood | 38.2 | 24.1 | 34.4 |
| Poplar | 46.0 | 16.7 | 26.6 |
| Rice hulls | 36.0 | 12.0 | 26.0 |
| Rice straw | 37.8 | 29.6 | 14.8 |
| Sorghum straw | 26.9 | 32.6 | 10.2 |
| Spruce | 24.7 | 10.2 | 35.0 |
| Sugarcane bagasse | 46.1 | 20.1 | 20.3 |
| Sunflower stalk | 34.0 | 20.8 | 29.7 |
| Wheat straw | 43.4 | 26.9 | 22.2 |
| Willow sawdust | 35.6 | 21.5 | 28.7 |

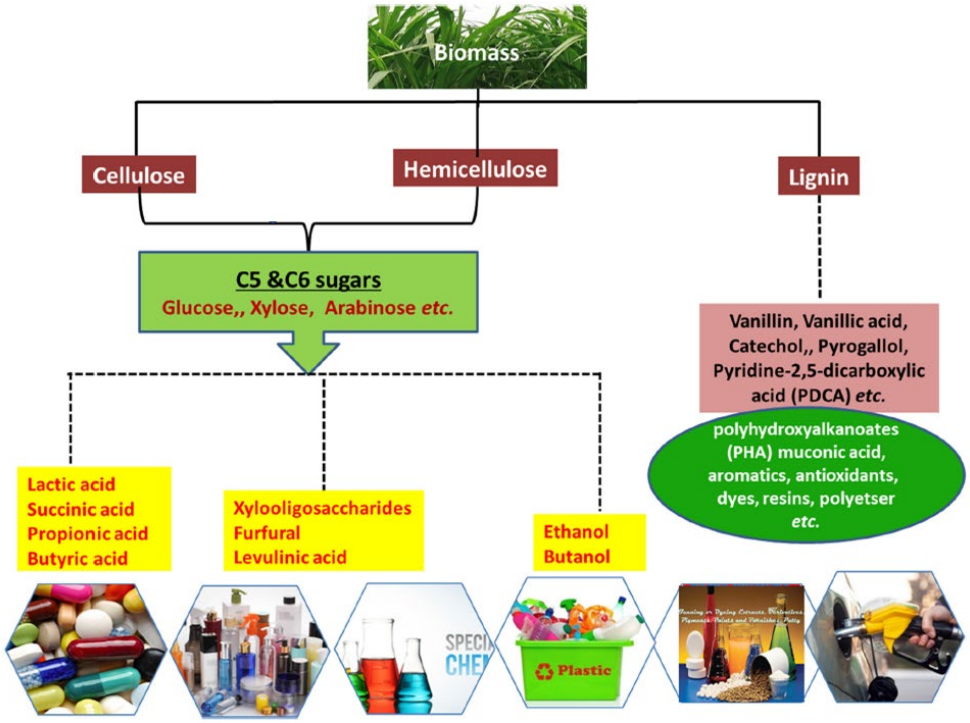


Figure 1.2. Illustrative example of a possible biorefinery scheme for the production of a broad portfolio of chemicals and materials. Reproduced from Singhvi and Gokhale (2019) by permission of Springer-Verlag.

# 1.2. Cellulose and lignin in the biorefinery

A biorefinery can be defined as an industrial plant where biomass is processed sustainably into a spectrum of marketable products and energy (Cherubini et al., 2009). Perhaps with a question mark on the "sustainably" aspect, the industrial exploitation of lignocellulosic biomass in the chemical sector has been traditionally focused on the valorisation of cellulose, for example in the pulp and paper sector or in the production of cellulosic fuels; thus neglecting the potential of hemicellulose and lignin to contribute to the biorefinery paradigm. However, at present there exists a generalised consensus that, for the viability of biorefinery schemes fed with lignocelluloses, an integral valorisation of the other major biopolymers is needed (FitzPatrick et al., 2010; Verma and Kuila, 2020; Yoo et al., 2020; Zakzeski et al., 2010). A first alternative towards this objective in the framework of sustainability may be the development of better approaches for the direct pretreatment of the lignocellulosic biomass, seeking an

improvement in the accessibility and/or fractionation of its constituent biopolymers. A second possibility may reside in alternative technologies for better processing of the different biopolymers once they have been isolated by classical or new methods, trying to provide the best value to the final products derived from them in the most efficient manner. This PhD Thesis will focus in the latter, and particularly in alternative approaches for improved processing of cellulose and of lignin.

***Cellulose***

Cellulose is the most abundant biopolymer in Nature. It is not toxic and is very well geodistributed (in line with what has been already said for lignocellulosic biomass in general), and estimations indicate that it is produced naturally at a rate higher than the capacity of the overall chemical industry worldwide (Klemm et al., 1998). Thus, it holds a strong potential to serve as alternative raw material of biorenewable character for the high-volume production of numerous chemical products and materials through cellulosic biorefinery schemes. However, this potential is, in part, limited by a significant recalcitrance, caused by a high degree of crystallinity, as noted below.

Cellulose chains in natural lignocellulosic matrices typically exhibit a combination of highly ordered crystalline regions and disordered amorphous regions (Sjöström, 1993). The crystalline structures in the ordered and rigid regions are constituted by intra- and intermolecular hydrogen bonds between the individual chains. Figure 1.3 illustrates these hydrogen bond networks for the two main allomorphs of cellulose:

- Cellulose I is the typical crystalline structure of native celluloses. It has two subtypes: cellulose $I_\alpha$ (produced by microbes, with a triclinic structure) and cellulose $I_\beta$ (present in higher plants, with a monoclinic structure) (Nagarajan et al., 2017). The compactness of this structure makes it recalcitrant to reactions (Ferro et al., 2020).
- Cellulose II is usually obtained from cellulose I by means of treatments in alkaline media (mercerisation processes), or via solubilisation and subsequent recrystallisation; although cases of native cellulose II have been sporadically identified (Kuga et al., 1993; O'Sullivan, 1997; Shibazaki et al, 1998). It is a more reactive and thermodynamically more stable structure than cellulose I (Ferro et al., 2020).

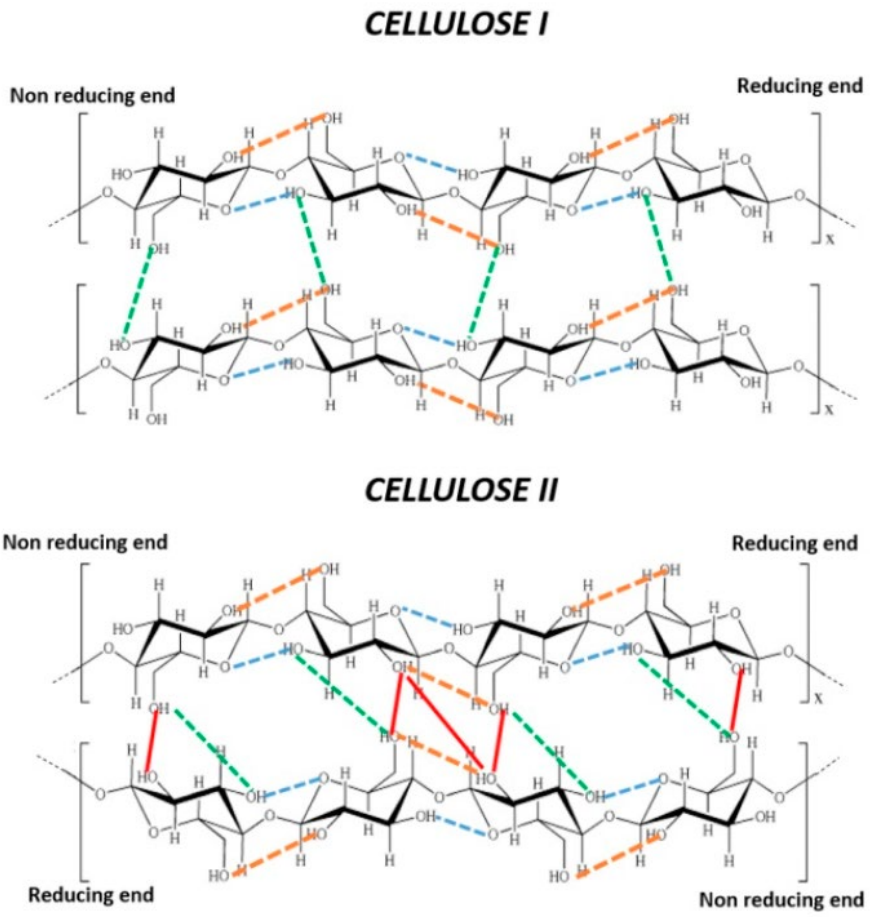


**Figure 1.3. Comparison of intramolecular and intermolecular hydrogen bonds in cellulose I and cellulose II: intramolecular 2(OH)···O-6 (orange lines), intramolecular O(3)H-O pyranosidic (blue lines), intermolecular O(6)H-O(3') (green lines), and intermolecular O(2)H-O(2) and O(6)H-O(2') (red lines). Reproduced from Ferro et al. (2020) by permission of MDPI.**

Other allomorphs of cellulose, denoted as cellulose III and cellulose IV, have been identified upon treatment of cellulose I or cellulose II with ammonia, optionally followed by a thermal treatment, but their stability is clearly lower, and for practical purposes they are of minor importance (O'Sullivan, 1997; Park et al., 2010).

Leaving aside the direct production of fibres from cotton plantations, cellulose is industrially obtained mostly from (woody) lignocellulosic feedstock via a pulping process (e.g. *kraft*, sulfite...) (Krässig et al., 2012). This pulping step barely affects the high degree of crystallinity and the type of crystalline structure of the cellulose

naturally present in the lignocellulosic source. Thus, a high proportion of cellulose I crystalline allomorph is preserved in the current methods of isolating cellulose from the native lignocellulosic matrices. While this rigid and highly ordered molecular structure provides desirable mechanical properties for a number of applications (e.g. paper, packaging...), it also imposes a substantial limitation to its chemical reactivity and subsequent transformation into a large variety of value-added products (including cellulose-derived polymeric materials and non-polymeric chemicals such as cellulosic bioethanol, 5-hydroxymethylfurfural, etc.) (Klemm et al., 2005; Nagarajan et al., 2017; Wyman et al., 2005). If the latter perspective is targeted, then cellulose is typically subjected to a pretreatment stage, where the native cellulose I form is transformed into the more thermodynamically stable and more accessible crystalline form cellulose II (Langan et al., 2001). A concomitant reduction in crystallinity may also occur during this pretreatment stage (Ferro et al., 2020), and in fact this is a desirable effect, since the barriers associated with the ordered arrangement of any of the cellulose crystalline structures (even cellulose II) in terms of reactivity are suppressed in the amorphous cellulose, boosting the corresponding reaction kinetics.

The current pretreatment methods can be based on two different approaches: dissolution followed by regeneration through a precipitation mechanism; or non-dissolving procedures that typically use volatile organic solvents or aqueous NaOH solutions (mercerisation) (Duchemin, 2015; Ferro et al., 2020; Park et al., 2010). In either case, these procedures typically involve the utilisation of harsh temperature and/or pressure conditions, along with the use of volatile organic solvents or strong acids or bases of poor green credentials (El Seoud et al., 2008; Klemm et al., 2005; Zhang et al., 2018). Thus, there is an interest in the development of new pretreatment methods with better performance in terms of sustainability.

***Lignin***

Lignin is Nature's dominant aromatic polymer (Ragauskas et al., 2014). It is a three-dimensional heteromorphic polymer, mainly built through the random interlinkage of three repetitive units: *p*-hydroxyphenyl (commonly known as H-unit), guaiacyl (or G-unit), and syringyl (or S-unit), generated from the primary monolignols *p*-coumaryl alcohol, coniferyl alcohol, and sinapyl alcohol, respectively (Ragauskas et al., 2014; Ralph et al., 2019). Figure 1.4 illustrates this aspect. This attractive chemical

composition has led to the suggestion of lignin as a resource of great potential in value-added applications, for example in the fields of bioplastics, resins, lubricants, and aerogels (Liu et al., 2019, Singhvi and Kim, 2021), and in general to a variety of fuels and chemicals from this biorenewable resource (Ragauskas et al., 2014). Nevertheless, with its commercial production mainly linked to the chemical pulping industry (Saake and Lehnen, 2012), lignin has been commonly regarded as a low-value byproduct, or even as a residue, due to the difficulty in transforming it into valuable substances in a sufficiently attractive manner for the chemical industry (Hu et al., 2018). In fact, the burning of lignin has been traditionally performed in most large-scale industrial processes handling polysaccharides from plants, with the simple aim of generation of power contributing to meet the energy needs of the corresponding process (Liu and Bao, 2019; Ragauskas et al., 2014; Saake and Lehnen, 2012). Even the option of its mere degradation to reduce the oxygen demand in wastewater effluents that contain it, without any kind of valorisation, has been considered (Fedyaeva et al., 2020; Makhotkina et al., 2008).

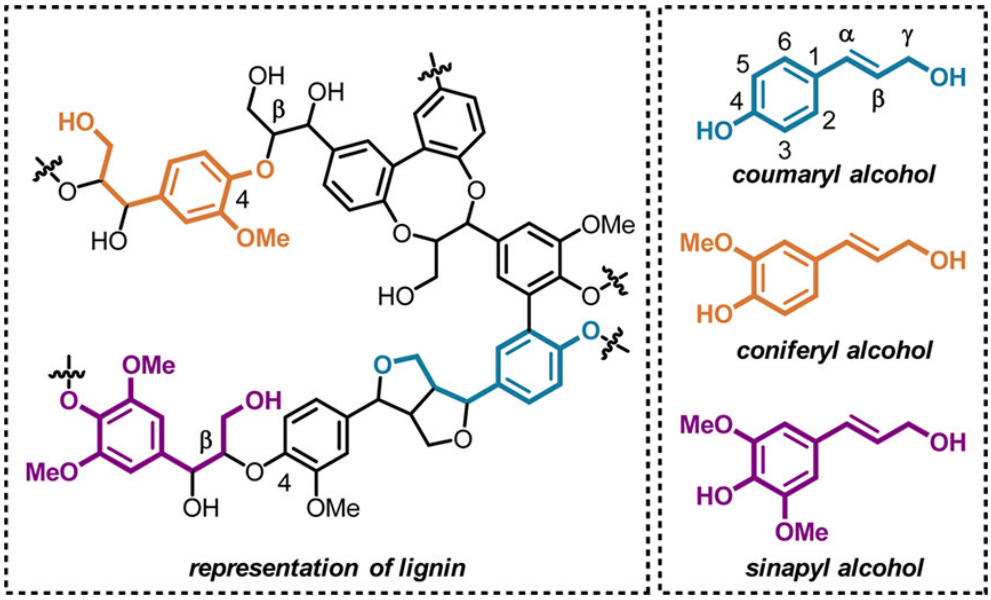


Figure 1.4. Representative depiction of the chemical structure of lignin, including identified elements of its main repetitive units (left), derived from their corresponding monolignols (right). Reproduced from Kärkäs et al. (2016) by permission of the American Chemical Society.

For the fraction of lignin that actually makes it to the market, applications (either as the crude lignin obtained as byproduct of the pulping process or after a sulfonation process rendering water-soluble lignosulfonates) are mostly based on its dispersing, binding, complexing, and emulsion-stabilising properties (Saake and Lehnen, 2012). Beyond these material applications, the most paradigmatic effort in valorisation of lignin through its conversion to value-added low-molecular chemicals is the production of vanillin, although its higher costs compared to the production of vanillin from petrochemical feedstocks has prevented its widespread consolidation (Saake and Lehnen, 2012). In general, lignin depolymerisation is challenging because of the broad distribution of bond strengths in the various C-O and C-C linkages and the tendency of the generated low-molar-mass species to undergo recondensation, often yielding more recalcitrant species (Ragauskas et al., 2014). In this complicated context, most of the efforts made to develop innovative processes to obtain value-added products from lignin through its depolymerisation do normally involve the use of solvents with poor green credentials and/or high temperatures and pressures (Casimiro et al., 2022; Dai et al., 2018; Ragauskas et al., 2014; Wang et al., 2018; Yamaguchi et al., 2020), thus hampering the environmental benefit of valorising a biorenewable resource.

## 1.3. Seeking a better strategy for improving the processability of cellulose

In the quest for broadening the portfolio of tailored and smart materials based on cellulose, the historical focus has been mostly put in the development of mercerisation processes with aqueous alkali solutions or of derivatising solvent for this unique biopolymer (Liebert, 2010). The discovery of novel fluid media capable of dissolving cellulose without derivatisation (e.g. ionic liquids, aqueous onium hydroxydes, concentrated acids...) has raised interest in the development of new dissolution-based processes in recent years (Abe et al., 2015; Nagarajan et al., 2017; Wang et al., 2012). However, with the exception of those cases in which a direct transformation of cellulose into the desired products in the same dissolving medium, the involvement of non-volatile or poorly volatile compounds in these fluid media makes it necessary to recover the dissolved cellulose via a non-vaporisation approach; for example by precipitation from the solution upon the addition of an antisolvent. Among the latter, water may

arguably be the most popular in the literature, and certainly its intrinsic properties are unbeatable from a sustainability perspective. Nevertheless, its high specific heat and heat of vaporisation, together with a relatively high boiling temperature, are likely to imply an excessive energy penalty in the necessary stage of recovery of the cellulose-dissolving fluid. In addition, the simple addition of water as antisolvent often results in gelation, which complicates the biomass recovery due to limited mass transfer. Although this can be alleviated using different antisolvent compositions (Dibble et al., 2011), it will inherently introduce undesirable further complications in the recycling process. Within that context, a mercerisation-type (i.e. non-dissolving) process would be more advantageous, as the cellulose could be mainly recovered by pressing and/or filtration.

Within the new non-derivatising solvents for cellulose that have started to be explored in the present century, ionic liquids have been found to dissolve cellulose in relevant amounts under relatively mild conditions (Swatloski et al., 2002; Zakrzewska et al., 2010). Together with other attractive characteristics of these low-melting organic salts (Freemantle, 2010), such as a negligible vapour pressure (thus not contributing to air pollution or to the generation of flammable atmospheres) and a reasonably good thermal stability, the above-mentioned cellulose dissolution capacity has opened the door to the consideration of ionic liquids as the basis of new cellulose processing technology with good performance from a sustainability perspective. An example of such a technology for a large market is the Ioncell-F process for the production of regenerated cellulose fibres, which avoids the use of the very toxic carbon disulfide necessary in the state-of-the-art Viscose process (Asaadi et al., 2018; Sixta et al., 2015).

In the evolution of the interest on ionic liquids as potential fluids in technologies for the pretreatment of cellulose, the focus has been limited to ionic liquids with the ability to dissolve cellulose (Wang et al., 2012), thus having to face the problem of cellulose regeneration and efficient ionic liquid recycling that has been commented above. These problems would considerably neutralise the advantage of using a non-volatile, non-flammable ionic liquid as a safer pretreatment fluid. However, the capacity of ionic liquids to interact with cellulose does not have to be restricted to those able to dissolve it in appreciable concentrations. This would be similar to a strategy already insinuated in research works for the pretreatment of lignocellulosic materials, where other ionic liquids were considered in addition to those able to disolve cellulose

in relevant amounts. Such is the case, for instance, of choline acetate and choline lysinate, with negligible capacity for cellulose dissolution (Liu et al., 2012; Zhang et al., 2012), but efficient in pretreating/delignifying switchgrass, and for which an effective interaction with the crystalline structure of cellulose in that context was evidenced through X-ray diffraction analyses (Sun et al., 2014). This capacity of establishing an effective interaction with the crystalline structure of cellulose of some ionic liquids with negligible cellulose dissolution capacity enables the possibility of combining the potentially favourable attributes of ionic liquids (e.g. negligible vapour pressure, non-flammability, and avoidance of extreme pH conditions) with a mercerisation-like approach in which the large energy penaly brought about by the vaporisation of the antisolvent (see above) would be avoided. In that regard, for the case of pretreatment of isolated cellulose in the context of the cellulose processing industry, some tetraalkylphosphonium acetates could be ionic liquid candidates of great potential, as they have been found not to dissolve cellulose when in neat, but to be capable of dissolving it when combined with specific co-solvents (Holding et al., 2014, 2017).

## 1.4. Approaches based on liquid systems for the valorisation of lignin at mild conditions

Processes such as pyrolysis, hydrogenolysis, hydrodeoxygenation... are among the strategies currently explored for the valorisation of lignin, either towards materials applications or through depolymerisation to yield chemicals of low molar mass, in spite of their significant energy requirements in the form of elevated temperatures and/or pressures (Ragauskas et al., 2014).

Trying to look for more sustainable alternatives at milder conditions, approaches based on liquid systems for the treatment of lignin seem more plausible. In this regard, enzyme-based methods do typically operate at atmospheric pressure and in the vicinity of ambient temperature. One type of enzyme with the potential for lignin depolymerisation is lacasse, which is commonly used to transform lignin via oxidation. The effect of laccase on a lignin substrate can be improved with the assistance of a redox mediator acting as an electron shuttle between the enzyme and the substrate, and thus configuring a system referred to as laccase-mediator system (Munk et al., 2018). In the scientific literature, these systems have been essentially applied under homogeneous

conditions, with the tested lignin fully solubilised in aqueous media, due to the use of highly sulfonated lignin or as a result of a sufficiently acid or alkaline pH (Liu et al., 2012). Investigation of laccase-mediator systems for processing lignins with a low (or negligible) sulfonation degree (and hence with limited water solubility) under mild pH conditions remains unexplored, despite their potential to lead to lignin valorisation processes with improved green credentials.

A further aspect to consider in seeking the improvement of the performance of a given laccase-based system is the utilisation of an additive. One interesting option may be an ionic liquid, especially one of those known to be suitable for the dissolution, fractionation or pretreatment in general of lignocellulosic biomass (Rodríguez, 2021); as long as it is reasonably compatible with the enzymes in the medium. Its action on the lignin may complement nicely the action of the laccase-mediator tandem, while presenting some good characteristics in terms of the sustainability coordinates (see section 1.3) and preserving the mild conditions of the process.

Since ionic liquids have been credited with the potential to act as both solvents and catalysts in the depolymerisation of lignin (Chatel and Rogers, 2014; Prado et al., 2016), the alternative of using them as the treatment liquid has been also explored in recent years. As compared to other solvents of organic nature, ionic liquids can certainly improve the sustainability credentials of the lignin depolymerisation processes thanks to the inherent characteristics already mentioned in section 1.3 (Freemantle, 2010). Nevertheless, to date the research works exploring ionic liquids for depolymerisation of lignin have involved relatively harsh conditions: temperatures higher than 100 °C, oxygen pressures, additional metal/acid catalysts, etc. (Geniselli da Silva, 2021). Moreover, the relatively high viscosity can be a relevant drawback in the utilisation of the pure ionic liquid as treatment fluid. So, one convenient possibility may be the dilution of the ionic liquid with water, thus using it in the form of aqueous solution with a much lower viscosity. As a consequence, the resistance to the necessary solid-liquid mass transfer in the treatment process will be largely diminished. Concomitantly, the combination of ionic liquid and water will enable the capacity to modulate the lignin dissolution capacity of the liquid system by adjusting its concentration.

The depolymerisation of lignin for the production of valuable chemicals via a photoreaction catalysed by nanoparticles is another approach reported in the literature

that works at very mild conditions (Colmenares et al., 2017; Li et al., 2015; Sun et al., 2018). The catalytic nanoparticles, together with a source of UV light, can be used along in aqueous media, or their combination with the processes described above can be also considered.

# 2. OBJECTIVES

# OBJECTIVES

The general objective of this doctoral thesis is to develop scientific knowledge on the potential use of liquid systems comprising ionic liquids and/or molecular solvents in new technologies with greener credentials for the more sustainable valorisation of cellulose and lignin, which are two of the main polymeric components of lignocellulosic biomass. This general objective will be reached through the development of specific objectives related to each of the mentioned biopolymers, as detailed below.

***Better cellulose pretreatment approaches***

An efficient non-dissolving pretreatment of cellulose will be sought using pretreatment liquids based on the ionic liquid tetrabutylphosphonium acetate ([$P_{4444}$][OAc]) and mild conditions (atmospheric pressure and low or moderate temperature). Preliminary attempts will be carried out with microcrystalline cellulose powder, and then more defined experiments will be performed with the popular commercial cellulose Avicel PH-101.

Besides the pure [$P_{4444}$][OAc], its combinations with conventional molecular solvents with acceptably good green credentials will be investigated. Representative polar protic and polar aprotic solvents will be selected in order to evaluate this effect on the pretreatment performance. The possibility of carrying out the pretreatments at lower temperatures than with the pure ionic liquid will be explored, through the development of appropriate solid-liquid equilibrium studies. In a similar vein, the potential eutectic behaviour of [$P_{4444}$][OAc] with its homologous halides will be ascertained to evaluate the possibility of using a lower temperature in the pretreatment while preserving an integrally ionic nature of the pretreatment fluid.

Analysis of the cellulose crystallinity reduction caused by the pretreatments, as well as of other properties such as degree of polymerisation or thermal stability, will be performed on the pretreated samples. The improvement in reactivity imparted by the pretreatments to the cellulose will be assessed by means of the investigation of its kinetics of enzymatic hydrolysis.

Finally, a selection of the pretreated samples will be explored in the context of a practical application: the production of carboxymethylcellulose (CMC) through the corresponding carboxymethylation reaction. Carboxymethylation levels of commercial

interest will be sought by carrying the reaction under milder conditions than the current benchmark process.

***Better lignin valorisation approaches***

A first strategy will pursue the direct use of aqueous solutions of the ionic liquid 1-ethyl-3-methylimidazolium acetate ([$C_2$mim][OAc]), at ambient temperature and pressure, for the depolymerisation of a technical lignin (Indulin AT) with generation of value-added phenolic compounds. Identification of these compounds will be attempted, and the structure of the recovered solids will be investigated and compared to the one of the raw lignin. The assistance of these treatments with UV irradiation in the presence of nanoparticles that might catalyse the depolymerisation of lignin by photoreaction will be explored.

In a second approach, the effect of [$C_2$mim][OAc] will be studied in the depolymerisation of lignin by the action of a recombinant laccase from the fungus *Myceliophthora thermophila*, or of a laccase-mediator system composed of this laccase and the popular mediator 2,2'-azino-bis(3-ethylbenzothiazoline-6-sulfonic acid) diammonium salt (commonly abbreviated and referred to as ABTS). An attempt will be carried out to identify the phenolic compounds produced in these biological treatments at different conditions, always operating at ambient temperature. The solids recovered will be investigated from the point of view of their structure in comparison to the raw Indulin AT, and their antimicrobial activity will be tested against representative pathogenic bacteria.

# 3. LIQUIDS BASED ON [$P_{4\,4\,4\,4}$][OAc] FOR THE NON-DISSOLVING PRETREATMENT OF CELLULOSE

The content of this chapter was published as:

- C. A. Pena[a], A. Soto[a], A. King[b], H. Rodríguez[a] (2019). [a]Department of Chemical Engineering, Universidade de Santiago de Compostela, E-15782 Santiago de Compostela, Spain. [b]Department of Chemistry, University of Helsinki, A. I. Virtasen Aukio 1, 00014 Helsinki, Finland.
"Improved Reactivity of Cellulose via its Crystallinity Reduction by Non-Dissolving Pretreatment with an Ionic Liquid", ACS Sustainable Chemistry and Engineering, 7, 9164-9171. https://doi.org/10.1021/acssuschemeng.8b06357

- C. A. Pena[a], A. Soto[a], H. Rodríguez[a] (2021). [a]CRETUS Institute, Department of Chemical Engineering, Universidade de Santiago de Compostela, E–15782 Santiago de Compostela, Spain.
"Tetrabutylphosphonium acetate and its eutectic mixtures with common-cation halides as solvents for carbon dioxide capture", Chemical Engineering Journal, 409, 128191. https://doi.org/10.1016/j.cej.2020.128191

- C. A. Pena[a], A. V. Puga[b], A. Metlen[c], A. Soto[a], Héctor Rodríguez[a] (2022). [a]CRETUS, Department of Chemical Engineering, Universidade de Santiago de Compostela, E15782 Santiago de Compostela, Spain. [b]Departament d'Enginyeria Química, Universitat Rovira i Virgili, 43007 Tarragona, Spain. [c]AMT1-Translations & Chemistry, 2910 Essen, Antwerp, Belgium.
"Liquid Systems Based on Tetra(*n*-butyl)phosphonium Acetate for the Non-dissolving Pretreatment of a Microcrystalline Cellulose (Avicel PH-101)", Biomacromolecules, 23, 1970-1980. https://doi.org/10.1021/acs.biomac.1c01683

# LIQUIDS BASED ON [P4444][OAc] FOR THE NON-DISSOLVING PRETREATMENT OF CELLULOSE

## 3.1. Motivation

The existence of ionic liquids capable of interacting effectively with the crystalline structure of cellulose, while exhibiting a negligible capacity to dissolve it, may enable the development of a pretreatment strategy combining the advantageous properties of ionic liquids as process auxiliary substances with the energy savings and process simplification associated to a mercerisation-like approach, as compared to a dissolution-regeneration approach with subsequent recovery of the pretreatment fluid (see section 1.3). Tetraalkylphosphonium acetates may be adequate ionic liquid candidates for this type of strategy. In their pure state, they have a negligible cellulose dissolution capacity; but, on the other hand, their combination with certain co-solvents leads to a relevant cellulose dissolution capacity (Holding et al., 2014, 2017). Thus, their ability to interact with the cellulose crystalline structure in a non-dissolving context seems plausible.

Within the family of tetraalkylphosphonium acetates, a promising candidate for the described purpose is the member with four butyl substituents in the cation: tetrabutylphosphonium acetate ([P4444][OAc]). This ionic liquid has the potential to be produced industrially at a competitive cost via an adequately integrated synthetic route (Bradaric et al., 2003; Ferguson et al., 2012) and, in contrast to some of its homologues incorporating longer alkyl substituents, it has been reported to exhibit low toxicity towards a number of microorganisms (Mikkola et al., 2015; Ruokonen et al., 2016). In addition, it may be expected to present good thermal stability, at least in relative terms with regard to other ionic liquids (Freemantle, 2010). All of these are relevant aspects for its utilisation in processes implemented at industrial level.

One of the possible disadvantages of [P4444][OAc] may be the relatively high temperatures needed if it is applied as a neat solvent (Rico del Cerro et al., 2020). One option for lowering the temperature at which the [P4444][OAc]-based non-dissolving pretreatment can be performed is by combining it with a second substance so that the

melting temperature of the resulting mixtures is lower. In that vein, the combination with a second ionic substance (ideally a homologous ionic liquid) would integrally preserve the advantageous non-volatile character of the pretreatment liquid. An alternative is the combination with a molecular solvent, which instead will help to reduce not only the melting temperature, but also, and considerably, the viscosity of the pretreatment liquid. Water and organic substances such as ethanol and dimethylsulfoxide (DMSO), which have reasonably good green credentials within their respective categories of polar protic solvents and polar aprotic solvents (Alder et al., 2016), are interesting candidates for combination with [$P_{4444}$][OAc].

The evaluation of the effectiveness of a pretreatment based on the simple contact of cellulose and [$P_{4444}$][OAc] or a [$P_{4444}$][OAc]-based mixture, with easy recovery of the pretreated cellulose by filtration, may be carried out in a practical way through the analysis of the kinetics of a simple reaction such as the enzymatic hydrolysis of the pretreated cellulose. The establishment of a connection between the observed improved reactivity and a structural element such as the cellulose crystallinity reduction caused by the pretreatment would be valuable. Other aspects, such as thermal stability and degree of polymerisation of the pretreated cellulose, and the actual preservation of the non-dissolving character, should also deserve attention.

In a first set of experiments, trends and influence of variables will be preliminary explored with the pretreatment of microcrystalline cellulose (MCC) powder. In a second set of advanced experiments, the widely used commercial microcrystalline cellulose type branded as Avicel PH-101 (Park et al., 2010), henceforth referred to as just “Avicel” for simplicity, will be pretreated, facilitating the more standardised interpretation of the results by those skilled in the art. For the latter, the pretreated Avicel will be finally evaluated with an application-oriented perspective in the reaction for the formation of a classical cellulose-modified product such as carboxymethylcellulose (CMC).

# 3.2. Experimental

## 3.2.1. Materials

Two microcrystalline celluloses were used: microcrystalline cellulose powder (MCC) and Avicel PH-101, both commercialised by Sigma-Aldrich (product references 435236 and 11365, respectively). Both were dried in an oven at 383 K for ca. 2 days, to adjust their water content to ca. 1.5 %, as determined from the weight loss of a thermogravimetric analysis consisting on a heating ramp at 20 K/min from room temperature to 383 K followed by a 15-min isotherm. This analysis was performed in a TA Instruments TGA Q500 thermogravimetric analyser (Figure 3.1) using $N_2$ flow rates of 40 mL/min and 60 mL/min as balance purge gas and sample purge gas respectively.

**Figure 3.1. TA Instruments DSC Q2000 differential scanning calorimeter (left) and TA Instruments TGA Q500 thermogravimetric analyser.**

Ethanol (Panreac, 99.8 %) and DMSO (Sigma-Aldrich, 99.99 %) were used as received. Their water content was measured by the Karl Fischer titration method in a Metrohm 899 coulometer (Figure 3.2), ensuring that it corresponded to mass fractions lower than 0.0002. Bidistilled water was obtained from a Bibby Aquatron A4000D system (Figure 3.3).

The ionic liquid [P4444]Cl was provided by Iolitec with nominal purity greater than 95 %, whereas [P4444]Br was supplied by Aldrich with a nominal purity of 98 %. The ionic liquid [P4444][OAc] was synthesised in-house by a metathesis reaction

between [$P_{4444}$]Cl and potassium acetate (K[OAc]), supplied by Sigma-Aldrich with purity 99 %, following a similar procedure to that described by Mikkola et al. (2015). In detail, [$P_{4444}$]Cl and K[OAc] (the latter in a 15 % excess with respect to the stoichiometric amount) were dissolved separately in ethanol, and then these solutions were mixed and stirred overnight in a beaker at room temperature. The generated precipitate (KCl) was removed by vacuum filtration through a sintered funnel, and the ethanol was eliminated from the filtrate by rotary evaporation. The residue (crude [$P_{4444}$][OAc]) was dissolved in acetone (Scharlau, ≥99.8 %) and placed in a freezer at

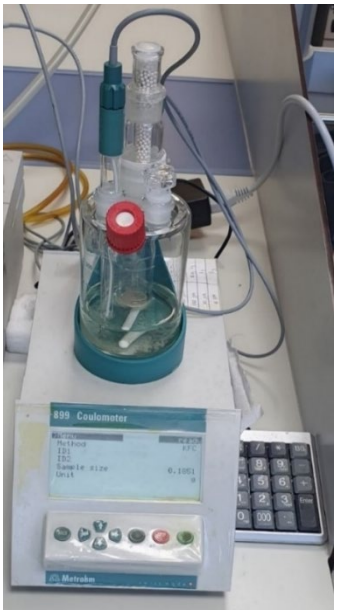


Figure 3.2. Metrohm 899 coulometer (Karl Fischer titrator).

Figure 3.3. Bibby Aquatron A4000D water still for the production of bidistilled water.

ca. 255 K for24 h, to promote the precipitation of the K[OAc] added in excess and of any remaining KCl. Filtration of precipitate, elimination of acetone by rotary evaporation, redissolution in fresh acetone, and placement in the freezer were repeated until no further precipitation was observed; and a final step of rotary evaporation was performed prior to the purification procedure described in the next paragraph.

All three phosphonium salts were subjected to purification under reduced pressure (absolute pressure lower than 1 Pa) while being magnetically stirred and heated at ca. 380 K (in the case of [P4444]Cl and [P4444]Br) or ca. 345 K (in the case of [P4444][OAc]). The preservation of the desired chemical identities and the absence of organic impurities at relevant levels after this purification step were confirmed by $^{1}H$ and $^{13}C$ NMR spectroscopy in a Varian Mercury 300 spectrometer (Figure 3.4), using DMSO-$d_6$ (Sigma-Aldrich, 99 %, atomic deuteration level of 99.5 D %) as deuterated solvent of the samples. The corresponding spectra are included in Figures A.1 to A.6 in Appendix A. For [P4444][OAc], the residual $K^+$ and $Cl^-$ concentrations were, respectively, <4 ppm (determined by ICP-OES using a PerkinElmer Optima 4300 DV spectrometer equipped with a 40-MHz RF plasma generator (Figure 3.5)) and 1000 ppm (determined by ion chromatography using a Metrohm 861 Advanced Compact IC chromatograph equipped with a Metrosep A Supp5 250/4.0-mm column, with an aqueous solution of 3.2 mM sodium carbonate and 1.0 mM sodium bicarbonate as the mobile phase (Figure 3.6)). The water content of the purified ionic liquids was determined by means of Karl Fischer titration (Figure 3.2), and water mass fractions lower than 300 ppm were found in all cases.

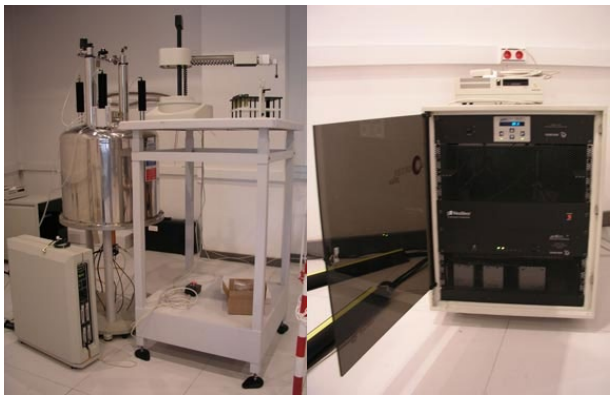

Figure 3.4. Varian Mercury 300 NMR spectrometer.

Figure 3.5. PerkinElmer Optima 4300 DV ICP-OES spectrometer.

Figure 3.6. Metrohm 861 Advanced Compact IC cromatograph.

### 3.2.2. Characterisation of the ionic liquids and pretreatment fluids

Thermal and physical properties were included in the characterisation of the ionic liquids and pretreatment fluids. In particular, their thermal stability and solid-liquid transitions were investigated, as well as their viscosity and density.

***Thermal stability***

Analysis of the thermal stability of the phosphonium salts was carried out by thermogravimetric analysis (TGA) in a dynamic mode and in an isothermal mode. A TA Instruments Q500 thermogravimetric analyser (Figure 3.1) was used, with a weight

precision of 0.01 %. For each run, ca. 5-20 mg of sample was placed in an open platinum pan, and loaded into the measuring chamber. Nitrogen (Nippon Gases, 99.999 %) was used as sample purge gas (flow rate of 60 mL/min) and as balance purge gas (flow rate of 40 mL/min). In the dynamic mode runs, the thermal programme consisted of a heating ramp at a rate of 5 K/min (for [P4444]Cl and [P4444]Br) or 10 K/min (for [P4444][OAc]) from room temperature until a final temperature of 773 K. Analysis of the TGA curves thus obtained was performed with the software Universal Analysis 2000, version 4.5.0.5, by TA Instruments; and an uncertainty of 1 K was estimated for the recorded decomposition temperatures. In the isothermal mode runs, the samples were held at a fixed temperature for 24 h. Due to the hygroscopicity of the ionic liquids, each of these isotherms was preceded by another 60-min isotherm at 383 K to eliminate the water that the samples could have picked up from the ambient while mounting them in the TGA apparatus.

***Melting temperatures and solid-liquid equilibria***

Melting temperatures of the phosphonium salts and solid-liquid equilibrium behaviours of binary systems comprising them were determined by differential scanning calorimetry (DSC), using a TA Instruments Q2000 differential scanning calorimeter with an RCS 90 refrigerated cooling system attached (Figure 3.1). For the binary systems, samples with a step composition of ca. 0.10 in mole fraction, and covering the entire composition range, were prepared in small glass vials (with the assistance of a Mettler-Toledo XPE 205 analytical balance (Figure 3.7) with an uncertainty of $10^{-4}$ g) and subsequently homogenised via magnetic stirring at ambient temperature or with mild to moderate heating. For the DSC runs, about 5-20 mg of each sample was transferred to a 40-mL DSC aluminium pan (manufactured by TA Instruments) and sealed hermetically with the corresponding aluminium lid (also manufactured by TA Instruments). The sealed capsule was loaded by means of an autosampler into the measuring chamber of the DSC apparatus, and an analogous capsule with no sample was used as the empty reference. A flow rate of 50 mL/min of nitrogen (Nippon Gases, 99.999 %) was applied as purge gas. The thermal programme consisted of an initial heating ramp at 5 K/min from ambient temperature to a certain "top temperature" (ranging from 343 K to 393 K, depending on the melting of the sample), followed by two cycles, each of them comprising a cooling ramp at −5 K/min

down to a "bottom temperature" (nominally 183 K, although, due to the loss of baseline stability at very low temperatures, the portion of thermograms below 200 K was systematically disregarded) and a heating ramp at 5 K/min back to the "top temperature", with intercalated 10-min isotherms in between ramps. It was verified that the signals of the two cycles were repetitive. The signal of the last heating ramp was used to evaluate the thermal events of the sample: glass transition temperatures (at the midpoint of the sigmoidal portion of the thermogram resulting from the variation in heat capacity) and/or melting temperatures (at the onset of the corresponding endothermic peak), with an estimated uncertainty of 1 K. Enthalpies of fusion were calculated by integrating the endothermic peaks associated with the melting, with an estimated uncertainty of 0.1 kJ/mol. All the analyses of the thermograms were performed with the software Universal Analysis 2000, version 4.5.0.5, by TA Instruments.

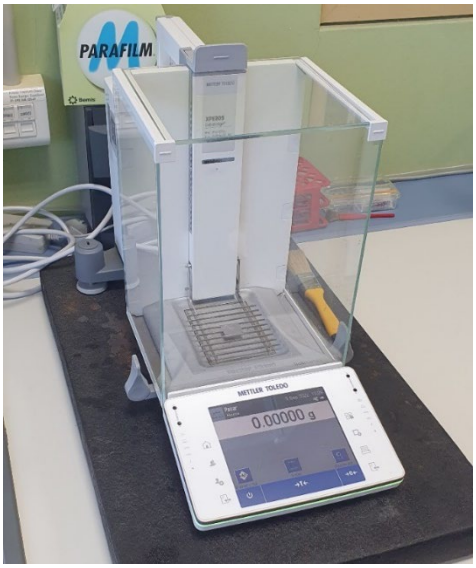


Figure 3.7. Mettler-Toledo XPE 205 analytical balance.

***Viscosity and density***

For the liquid systems used in the pretreatment of MCC, kinematic viscosities were determined at different temperatures with micro-Ubbelohde glass capillary viscometers manufactured, calibrated, and certified by Schott. An automatic Lauda

PVS1 Process Viscosity System was used, equipped with a photoelectric cell for the precise determination of the efflux time (resolution of 0.01 s) of the liquid samples through the viscometers. The temperature during the measurements was kept constant by means of a Lauda D20 KP clear-view thermostatic water bath with a Lauda DLK 10 through-flow cooler coupled (Figure 3.8). For each sample, a minimum of three consistent efflux time measurements were performed, and the average efflux time $t$ was used in the calculation of the kinematic viscosity ($\nu$):

$$\nu = K \times t \tag{3.1}$$

where $K$ is the certified capillary constant provided by the manufacturer. There was no need to use any kinetic energy correction factors for $t$, since all efflux times were sufficiently long, according to the correction tables of each viscometer, also supplied by the manufacturer. After checking that the obtained value of $\nu$ lay within the prescribed range for the capillary viscometer specifically used, the dynamic viscosity ($\eta$) was obtained, with an estimated uncertainty of 0.5 %, as follows:

$$\eta = \nu \times \rho \tag{3.2}$$

where $\rho$ stands for the density of the liquid sample. This density was measured, with an uncertainty of $3 \times 10^{-5}$ g/cm$^3$, in an Anton Paar vibrating U-tube DMA 5000 density meter (Figure 3.9) with automatic correction of the influence of the viscosity and a built-in system based on the Peltier effect to accurately control the temperature during the measurement.

Figure 3.8. Example of micro-Ubbelohde capillary viscometer (left), and PVS1 systems installed in a Lauda D20 KP thermostat with a Lauda DLK 10 cooler attached (right).


Figure 3.9. Anton Paar DMA 5000 oscillating U-tube density meter.

For the liquid systems used in the pretreatment of Avicel, density and viscosity at different temperatures were simultaneously determined in an Anton Paar DMA 5000 M oscillating U-tube density meter with an attached Anton Paar LOVIS 2000 ME microviscometer module based on the rolling ball principle (Figure 3.10). The density meter chamber has two integrated Pt100 platinum thermometers together with Peltier elements for the precise thermostating of the sample (temperature accuracy: 0.01 K) and performs an automatic correction of viscosity-related errors over the full viscosity range. Uncertainty of the density values obtained

Figure 3.10. Anton Paar DMA 5000 M oscillating U-tube density meter with an attached Anton Paar LOVIS 2000 ME microviscometer module.

was estimated to be $1 \times 10^{-5}$ g/cm$^3$. The capillary of the microviscometer module, located in a temperature-controlled block (temperature accuracy: 0.02 K), was adjusted with a certified viscosity standard fluid by Anton Paar. The dynamic viscosity values thus obtained are accurate to within 0.5 %.

### 3.2.3. Pretreatment of cellulose

In each pretreatment experiment, 10.0 g of the selected pretreatment fluid was placed in a jacketed glass cell, and 1.00 g of cellulose was added (thus making a solid-to-liquid ratio of 10 g of solid per 100 g of liquid). The glass cell was stoppered, and water from a Selecta Ultraterm 200 thermostatic bath was circulated through the jacket to keep the mixture at the desired temperature (with an uncertainty of 0.1 K). The solid–liquid contact was promoted via mechanical stirring using an IKA RW 16 Basic overhead stirrer (Figure 3.11). After the desired pretreatment time, the stirring was ceased and

Figure 3.11. IKA RW 16 Basic overhead stirrer installed on a jacketed glass cell used for cellulose pretreatments.

the content of the cell was filtered under soft vacuum using a fritted glass Allihn filter tube coupled with a Buchner flask. The recovered solid was washed with portions of 50 mL of bidistilled water until a residual concentration of ionic liquid lower than 50 ppm in the washing waters was obtained. This residual concentration was ascertained by UV absorbance at a wavelength of $\lambda$ = 195 nm (except in the case of pretreatments with the mixture of $[P_{4444}][OAc]$ + $[P_{4444}]Br$, for which $\lambda$ = 210 nm provided better resolution), measured with an Agilent 8453 UV–vis spectrophotometer equipped with a deuterium plasma discharge lamp (Figure 3.12), and with the assistance of the corresponding calibration curves. In the particular cases of utilisation of a pretreatment fluid involving DMSO, the residual concentration of this compound was verified to be below the detection threshold by one of the following methods: determination of the sulfur content of the washed solid with a Thermo Finnigan Flash 1112 elemental analyser (detection threshold: 100 ppm) (Figure 3.13), when pretreating MCC; or measurement of the total sulfur content in the washing water with an Oxford Instruments Lab-X3500S spectrometer (detection threshold: 2.5 ppm) (Figure 3.14), when pretreating Avicel. Once sufficiently washed, the pretreated cellulose sample was placed in a mortar and dried in an oven at 383 K, with periodical soft grinding with the help of a pestle to avoid agglomeration of particles, until obtaining a water content similar to that of the non-pretreated cellulose (as determined by TGA – see section 3.2.2.).

Figure 3.12. Agilent 8453 UV-visible spectrophotometer.

Figure 3.13. Thermo Finnigan Flash 1112 elemental analyser.

Figure 3.14. Oxford Instruments Lab-X3500S spectrometer.

For verification of the non-dissolving character of the studied pretreatments, 2.00 g of the pretreatment fluid was placed into the jacketed glass cells and thermostated at the specific pretreatment temperatures, and ca. 0.01 g of cellulose was added, thus yielding a ratio of 0.5 g of cellulose per 100 g of liquid. After stirring the heterogeneous mixture magnetically for 24 h, a sample was taken for analysis by confocal microscopy in a Leica TCS SP5 X microscope using a UV 405 nm diode and a Scan-DIC-Pol filter (Figure 3.15).

All weighing related to the cellulose pretreatment experiments was carried out with a Mettler-Toledo XPE 205 analytical balance precise to within $10^{-4}$ g (Figure 3.7).

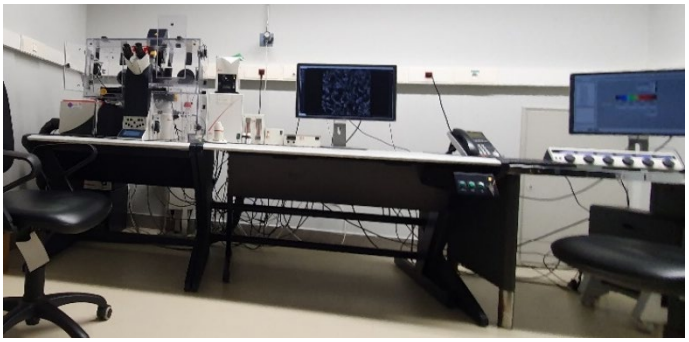

Figure 3.15. Leica TCS SP5 X microscope.

## 3.2.4. Characterisation of the cellulose samples

The characterisation of the cellulose samples comprised an analysis of their thermal stability and the determination of their crystallinity index and degree of polymerisation.

***Thermal stability***

The thermal stability of the raw and pretreated cellulose samples was analysed by TGA in dynamic mode, using the TA Instruments Q500 thermogravimetric analyser shown in Figure 3.1, following the procedure described in section 3.2.2.

***Crystallinity index (CI)***

The *CI* of cellulose samples was determined by powder X-ray diffraction (PXRD). In the experiments with MCC, a Philips diffractometer operated by a PW1710 control unit was used, with a PW1820/00 vertical goniometer, an Enraf Nonius FR590 generator working at 40 kV and 30 mA, and a PW1711/10 proportional detector (Figure 3.16). In the experiments with Avicel, a Bruker D8-Advance diffractometer was used, equipped with a LYNXEYE-2 detector (Figure 3.17). Both apparatus included a rotary sample holder for Bragg–Brentano geometry, and in both cases the X-rays were produced in a Cu-sealed tube and the radiation was monochromatised with a graphite monochromator ($\lambda$(K$\alpha$1) = 1.5406 Å). The diffractograms were recorded in an angular range 13–30°, with a step of 0.02° and an accumulation time of 6 s. The samples were rotated during the analysis in order to get the optimal peak profiles as well as to minimise the effect of preferential orientation. Subtraction of the amorphous content,

Figure 3.16. Philips X-ray diffractometer.


Figure 3.17. Bruker D8-Advance X-ray diffractometer.

currently considered as the strategy to lead to numerically most reliable results (Ahvenianen et al., 2016; Park et al., 2010), was carried out thanks to the parallel analysis of a cellulose sample totally amorphised. To obtain the latter, a sample of raw cellulose was introduced together with a zirconia ball of 2 cm of diameter in the 20 $cm^3$ zirconia chamber of a Retsch MM-2 vibration mill (Figure 3.18), leaving more than 50 % of free space in the chamber for the milling to be performed correctly (according to the specifications by the manufacturer). This ball-milling was carried out for 30 min with

a vibration frequency of 900 cycles/min. The *CI* was calculated as the difference of the areas under the curves of the specific cellulose sample and the one totally amorphised, after a process of normalisation of the curves. Each reported diffractogram is the average of two independent replicates.

Figure 3.18. Retsch MM-2 vibration mill.

***Degree of polymerisation (DP)***

The *DP* was determined via a procedure based on the measurement of the intrinsic viscosity (The United States Pharmacopeia, 2017). Initially, 0.130 g of cellulose sample was dissolved in 5.0 mL of a 0.5 M solution of bis(ethylenediamine)copper(II) hydroxide (supplied by Sigma-Aldrich as an aqueous solution of concentration 1.0 M) under an inert atmosphere of argon (Praxair, ≥99.9 %). The kinematic viscosity of this solution was measured with micro-Ubbelohde glass capillary viscometers (Figure 3.8), following the procedure described for this type of viscometers in section 3.2.2. The quotient of this kinematic viscosity over the one of the 0.5 M aqueous solution of bis(ethylenediamine)copper(II) hydroxide (without any cellulose dissolved) is the dynamic relative viscosity, which can be related through literature tables with the product of the intrinsic viscosity, $[\eta]_c$ (The United States Pharmacopeia, 2017). Then, the *DP* can be obtained by means of the following expression:

$$DP = \frac{95 \times [\eta]_c}{w \times \left(\frac{100 - \%\, LOD}{100}\right)} \quad (3.3)$$

where $w$ is the mass (in grams) of the cellulose dissolved in the 0.5 M aqueous solution of bis(ethylenediamine)copper(II) hydroxide and $\%LOD$ is the percentage of weight loss observed by TGA of the cellulose sample after having been subjected to the drying process in the oven, as described in section 3.2.1.

### 3.2.5. Kinetics of the enzymatic hydrolysis of cellulose samples

Citric acid (Sigma-Aldrich, 99.5 %) and sodium citrate (Sigma-Aldrich, 99 %) were used to prepare an aqueous 0.01 M citrate buffer (pH = 5). For the hydrolysis of MCC samples, 0.20 g of cellulose was added to 6.67 g of the aqueous buffer in a jacketed glass cell thermostated at 323.2 K. With magnetic stirring of the content of the cell, 0.1071 mL of cellulase solution (Celluclast 1.5L, by Novozymes), with an activity of 70 FPU/mL, and 0.0586 mL of β-glucosidase solution (NS50010, by Novozymes), with an activity of 640 UI/mL, were added to the medium, thus yielding a cellulase activity of 37.5 FPU/g of cellulose, and a β-glucosidase activity of 5 UI per each FPU. In the case of hydrolyses of Avicel samples, 0.10 g of solid was placed in the jacketed glass cell along with 10 mL of the aqueous buffer. The content was also magnetically stirred and thermostated at 323.2 K, and a volume of 30 µL of a 1:3 dilution of the commercial enzyme blend Cellitec CTec2 by Novozymes, containing cellulases, *β*-glucosidases, and hemicellulase, was added to initiate the hydrolysis.

In the course of each experiment, aliquots of the liquid were taken at different times as the hydrolysis progressed, and their glucose concentration was analysed with a commercial enzymatic kit by Spinreact. The method of the enzymatic kit for monitoring glucose is based on the oxidation of glucose to gluconic acid by glucose oxidase, producing an equimolar amount of hydrogen peroxide. The latter is then detected by a chromogenic oxygen acceptor (phenol + 4-aminophenazone) in the presence of peroxidase, yielding an intense colour that can be quantified by the measurement of the absorbance at 505 nm. Within the adequate range, this absorbance is proportional to the glucose concentration in the sample (Spinreact, 2016; Trinder, 1969). Samples were filtered through 0.45-µm pore size disposable filters and diluted with a 9 g/L solution of sodium chloride (Sigma-Aldrich, 99.5 %), following the

instructions by the manufacturer. Subsequently, they were incubated for 30 min in a thermostated Selecta Boxcult orbital shaker (Figure 3.19) at 298 K, with a stirring angular velocity of 150 rpm.

The absorbance was measured in an Agilent 8453 UV–vis spectrophotometer (Figure 3.12) using a deuterium plasma discharge lamp and a quartz cuvette with a 10 mm light path. A standard glucose solution of 1 g/L was used to determine the absorbance correction factor. The accuracy of the enzymatic kit method was verified by testing it with aqueous solutions of known concentration of glucose (Sigma-Aldrich, 99.5 %). All determinations of glucose concentration were carried out in triplicate, typically with a repeatability of 3-4 %, and the average values were reported.

Figure 3.19. Selecta Boxcult thermostated orbital shaker.

## 3.2.6. Carboxymethylation of cellulose samples

In a typical carboxymethylation experiment, 0.100 g of cellulose sample and 0.120 g of sodium chloroacetate (Sigma-Aldrich, for synthesis) were weighed in a 10 mL glass tube and suspended in 2.0 mL of 2-propanol (Scharlau, ≥99.5 %). The tube was then immersed in an oil bath preheated at 313 K, and the suspension was magnetically stirred at 1000 rpm for 2 min. Then, 0.1 mL of a ca. 20 % w/v aqueous solution of

sodium hydroxide (Sigma-Aldrich, ≥98 %), corresponding to an equimolar $[OH]^-$/anhydroglucose unit ratio, was added. The suspension was further stirred for the desired time (1 h or 3 h) and, after this reaction period, the tube was taken out of the bath and allowed to settle and cool down to room temperature, followed by centrifugation of its content at 2000 rpm for 3 min. The supernatant was carefully decanted using a pipette, and the sedimented solid was washed with 2-propanol (3 × 1 mL) by stirring at room temperature for 2 min and then centrifuging-decanting as described above. The resulting solid was suspended in 6 mL of methanol (Merck, ≥99.9 %), and the stirred mixture was neutralised until pH ≈ 6 (as measured using pH indicator paper) by adding a few drops of glacial acetic acid (Scharlau, extrapure). The solid was separated by filtration on a sintered glass funnel (pore size: 3), washed with methanol (5 × 2 mL), and dried under an air stream by suction. The final carboxymethylcellulose (CMC) samples had a white color, and their texture ranged from powdery solids to slightly sticky flakes depending on their degrees of substitution.

The degree of substitution (*DS*) of the CMCs was determined by attenuated total reflectance Fourier-transform infrared (ATR-FTIR) spectroscopy, suitable for *DS* determination with a small amount of cellulose sample (<10 mg). After recording the spectra on a Jasco FT/IR-6700 instrument (Figure 3.20), *DS* values were estimated from the absorbance ratio ($R_{CM}$) between the signals for the asymmetric carboxylic stretching and the methylenic/methinic stretching, designated as $\nu_{as}(COO^-)$ and $\nu(CH)$ respectively. This ratio was calculated as $R_{CM} = I_{COO}/I_{CH}$, where $I_{COO}$ and $I_{CH}$ are the peak heights, after baseline correction, of the $\nu_{as}(COO^-)$ and $\nu(CH)$ signals found at ca. 1590 and 2900 $cm^{-1}$, respectively. Calibration of this ATR-FTIR method was done by correlating $R_{CM}$ to actual *DS* figures, determined by acid-base back-titration for a series of CMC samples, as described in the rest of this section.

***Calibration of the ATR-FTIR method***

For calibration of the ATR-FTIR method for determination of *DS* of CMC with low amount of sample, the *DS* for a series of CMC samples in sufficiently large amounts were


**Figure 3.20. Jasco FT/IR spectrophotometer.**

determined by acid-base back-titration, and then correlated to the $R_{CM}$ values obtained by ATR-FTIR. In order to cover a wide *DS* range, such CMCs comprised a commercial one (sodium carboxymethylcellulose, MW ~ 250,000, degree of substitution 1.2, Sigma-Aldrich) and a range of samples prepared by standard procedures varying solvent composition (2-propanol/water ratios) and/or reaction time – see Table 3.1 and the next paragraph.

**Table 3.1.** Carboxymethylcellulose samples used for the calibration of the ATR-FTIR method for the determination of *DS* via the conventional titration method.

| Entry | 2-Propanol/$H_2O$ ratio (v/v) | Time (h) | $R_{CM}$ [ATR-FTIR] | *DS* [titration] |
|---|---|---|---|---|
| 1[a] | - | - | 5.14 | 1.18 |
| 2[b] | 10.8 | 3 | 3.76 | 0.76 |
| 3[b] | 10.8 | 3 | 3.91 | 0.81 |
| 4[b] | 2 | 3 | 1.59 | 0.18 |
| 5[b] | 2 | 1 | 0.93 | 0.16 |
| 6[b] | 2 | 0.5 | 0.93 | 0.14 |
| 7[b] | 1 | 3 | 0.54 | 0.09 |
| 8[c] | 2 | 3 | 1.45 | 0.23 |
| 9[c] | 2 | 0.5 | 1.11 | 0.18 |
| 10[b] | 0 | 3 | 0 | 0 |

[a] *From commercial sodium carboxymethylcellulose (MW ~ 250,000, degree of substitution 1.2, Sigma-Aldrich) after acidification.*

[b] *From Avicel after carboxymethylation and subsequent acidification.*

[c] *From Avicel after pretreatment with $[P_{4\,4\,4\,4}][OAc]$ + DMSO ($x_{DMSO}$ = 0.20), carboxymethylation and subsequent acidification.*

Initially a series of cellulose samples in sufficiently large amount were carboxylated under a variety of conditions to obtain CMC samples covering a range of *DS* values. This carboxymethylation was performed by a procedure adapted from Pushpamalar et al. (2006). Typically, a cellulose sample (0.500 g) was weighted in a 25 mL round-bottomed flask, and it was suspended in 10 mL of a mixture of 2-propanol and water (see Table 3.1 for the different 2-propanol/water volumetric ratios used). A volume of 1.0 mL of a 20 % w/v aqueous solution of sodium hydroxyde was then added dropwise under magnetic stirring, and the resulting suspension further stirred at 500 rpm for 1 h at room temperature. The flask was then immersed in an oil bath preheated at 313 K and the suspension stirred at 700 rpm for 2 min. Sodium chloroacetate (Sigma-Aldrich, for synthesis) was added in an amount of 0.600 g, and the suspension was stirred at 700 rpm for the desired time (see Table 3.1). After reaction, the flask was taken out of the bath, allowed to cool down to room temperature and the solid separated by filtration through a sintered glass funnel (pore size: 3), washed with 2-propanol (3 × 3 mL) and air-dried by suction. The collected solid was suspended in methanol and the stirred mixture neutralised until pH ≈ 6 by adding the required amount of glacial acetic acid. The solid was separated by filtration on a sintered glass funnel (pore size: 3), washed with methanol (5 × 3 mL) and dried under an air stream by suction. The final sodium carboxymethylcellulose (Na-CMC) samples had a white colour and their texture ranged from powdery solids to slightly sticky flakes depending on their *DS*.

The next step consisted in the acidification of the Na-CMC samples obtained. Their conversion into the acid form was carried out by adapting procedures described in the literature (Eyler et al., 1947; Pushpamalar et al., 2006). The procedure varied slightly depending on whether the CMC was commercial or had been synthesised from cellulose in our laboratories:

a) For samples prepared in-house from cellulose, in a typical acidification procedure Na-CMC (0.500 g) was dispersed in 10 mL of ethanol (Scharlau Pharmpur®, 96 % v/v) in a 25 mL round-bottomed flask connected to a condenser. The suspension was heated in an oil bath at 363 K and stirred at 1000 rpm until boiling. Then, 1.7 mL of aqueous solution of nitric acid 2.0 M (Baker, 65 %) was added dropwise and the boiling mixture stirred for 5 min at 1000 rpm, and then for further 15 min outside the oil bath while

cooling down to room temperature. The solid was separated by filtration through a sintered glass funnel (pore size: 3), washed with ethanol (5 × 4 mL), further washed with an ethanol/water mixture (80:20 v/v, ca. 50 mL) until the pH of the liquor was higher than 6 as detected by using pH indicator paper, and air-dried by suction.

b) Acidification of commercial Na-CMC was performed under a more diluted and less aqueous regime to avoid gel formation, a phenomenon which seriously hinders solid recovery. Thus, 1.00 g of Na-CMC was dispersed in 200 mL of methanol in a 500 mL round-bottomed flask connected to a condenser, and 2.0 mL of nitric acid was added dropwise. The resulting suspension was heated in an oil bath at 353 K and stirred at 1000 rpm until boiling, then stirred for 5 min at 1000 rpm while boiling, and taken out of the oil bath while cooling down to room temperature under stirring. The solid was separated by filtration through a sintered glass funnel, washed with methanol (5 × 10 mL), further washed with a methanol/water mixture (80:20 v/v, ca. 200 mL) until the pH of the liquor was higher than 6 as detected by using pH indicator paper, and air-dried by suction.

In both cases, the resulting solid was identified as the acid form of carboxymethylcellulose (H-CMC) based on ATR-FTIR spectroscopy (see an illustrative example in Figure 3.21). Before titration, the H-CMC was placed in a Petri dish and dried in an oven at 378 K until constant weight. The resulting weight was taken as its dry weight for *DS* quantification.

Finally, the *DS* of CMC samples was accurately determined by an acid-base back-titration method in aqueous solution consisting of a prior basification of H-CMC samples using a sodium hydroxide solution, and the titration of the remaining free $[OH]^-$ by a hydrochloric acid solution. The difference between such remaining $[OH]^-$ and that of a blank titration of an equal amount of sodium hydroxide (without H-CMC) is used to determine the amount of moles of acid in the CMC sample. In a typical back-titration procedure, an accurately weighted sample of one of the prepared H-CMC materials (ca. 0.30 g, corrected to only account for its dry weight, as described above) was dispersed in deionised water (60 mL) in an Erlenmeyer flask and heated to boiling on a hot plate. At this stage, an aqueous sodium hydroxide solution (0.2 M, 20.00 mL) was added, and the mixture shaken. Samples of high *DS* (greater than 0.6) readily dissolved

after a few seconds, whereas the solid remained suspended for samples of lower *DS*. In either case, the aqueous mixtures were titrated with an aqueous solution of hydrochloric acid (Panreac, for analysis, 37 %), standardised by conventional methods (0.0997 M) using phenolphthalein as an indicator. The blank titrations were performed by a similar procedure, yet in the absence of H-CMC.

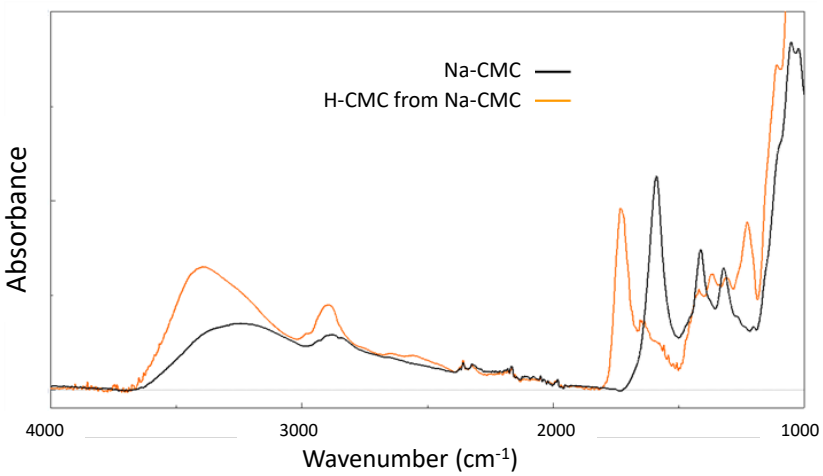


**Figure 3.21. ATR-FTIR spectra of sodium carboxymethylcellulose (Na-CMC) prepared from Avicel after 3 h reaction time, as for Entry 3 in Table 3.1, as compared to its acid form (H-CMC) prepared for determination of *DS* by titration. The effective conversion from sodium to protonic form is confirmed by the disappearance of the asymmetric carboxylate stretching band (*ca.* 1590 cm$^{-1}$) and the appearance of the carboxylic (C=O) stretching signal (*ca.* 1730 cm$^{-1}$).**

The molar concentration of carboxymethyl groups of the H-CMC ($C_{CM}$, expressed in mol$_{acid}$/g$_{H\text{-}CMC}$) was calculated according to the following equation:

$$C_{CM} = \frac{(V_{HCl,blank} - V_{HCl,sample}) \times C_{HCl}}{m_{sample}} \qquad (3.4)$$

where $V_{HCl,blank}$ and $V_{HCl,sample}$ are the volumes (in litres) of the HCl solution employed for the blank and sample titrations, $C_{HCl}$ is the concentration of the standardised HCl solution (0.0997 M), and $m_{sample}$ is the mass of dry H-CMC. The determination of *DS* was then done by considering that:

$$DS = \frac{n_{CM}}{n_{AG}} \qquad (3.5)$$

where $n_{CM}$ and $n_{AG}$ are the moles of carboxymethyl groups and anhydroglucose units, respectively, in an H-CMC sample (assumed to be equal to those of the parent Na-CMC sample). Operating with the above equations, we can get:

$$DS = \frac{MW_{AG} \times C_{CM}}{1 - MW_{CM} \times C_{CM}} \quad (3.6)$$

where $MW_{AG}$ and $MW_{CM}$ are the molar weights of anhydroglucose ($C_6H_{10}O_5$) and carboxymethyl ($CH_2COO$) units, respectively (Eyler et al., 1947). The *DS* values thereby obtained are listed in Table 3.1. The linear regression correlating these *DS* values with the $R_{CM}$ values obtained by the ATR-FTIR method for the same samples (see numerical values also in Table 3.1) is shown in Figure 3.22, where a satisfactory correlation ($R^2 = 0.981$) can be observed.

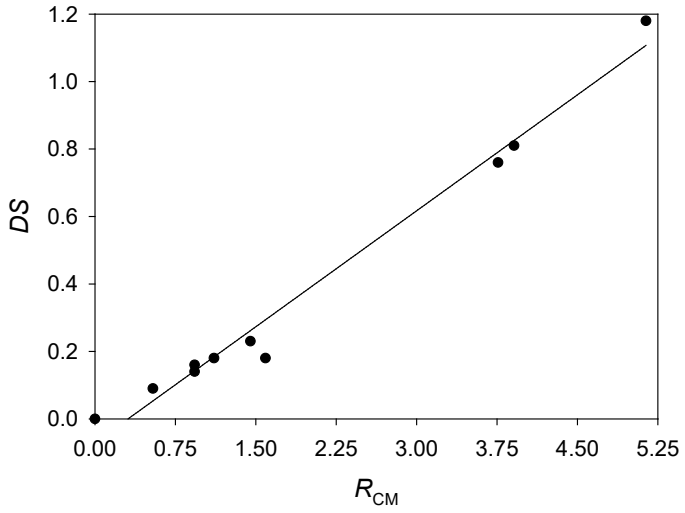


**Figure 3.22. Correlation between *DS* determined by acid-base back-titration and the carboxylate *vs.* methylenic/methinic absorbance ratio measured by ATR-FTIR ($R_{CM}$) for the samples listed in Table 3.1. Parameters of the linear fit: slope = 0.229; intercept = -0.072.**

# 3.3. Results and discussion

## 3.3.1. Preliminary pretreatment studies with MCC

### 3.3.1.1. Thermal characterisation of the ionic liquid [P4444][OAc]

The purified [P4444][OAc] is solid at room temperature. To determine the temperature range in which it can be utilised as a stable liquid, its solid/liquid transition and its thermal stability were analysed by DSC and TGA, respectively. From the DSC analysis, an onset melting temperature of 331 K was found. Regarding the thermal stability, an

onset decomposition temperature of 590 K was found by dynamic TGA (Figure 3.23). If an onset with the tangent to the TGA curve at the point of 5 % decomposition is used instead of the regular onset with the tangent at the inflection point, the so-called 5 % onset decomposition temperature ($T_{d,5\%onset}$) can be obtained, which is a more conservative and realistic value of the maximum temperature at which the ionic liquid can be actually considered as thermally stable (Clough et al., 2013; Smiglak et al., 2008). In this case, the obtained value of $T_{d,5\%onset}$ was 527 K, substantially lower than the regular onset decomposition temperature. However, even the $T_{d,5\%onset}$ value corresponds to a dynamic TGA experiment and overestimates the maximum temperature at which the ionic liquid can be actually used in mid- and long-term processes. To guarantee more scrupulously the thermal stability of the ionic liquid in cellulose pretreatments with a possible duration of several hours, isothermal TGA runs with a duration of 24 h were performed at various temperatures lower than the $T_{d,5\%onset}$ value previously found. The signals corresponding to these isothermal TGA experiments are shown in Figure 3.24, where it can be observed that the ionic liquid

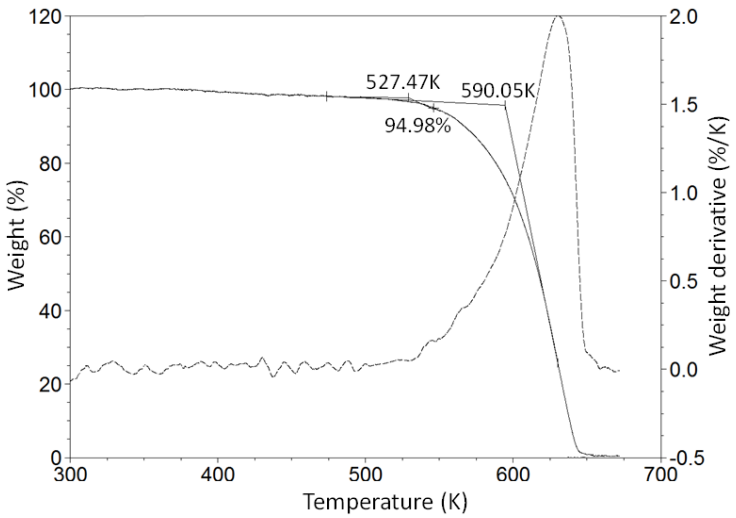


**Figure 3.23. Dynamic TGA thermogram of [P4444][OAc], showing the determination of the regular onset decomposition temperature and of the 5 % onset decomposition temperature. The solid line represents the weight percentage as a function of temperature, whereas the dashed line represents its first derivative.**

undergoes substantial decomposition at temperatures notably lower than $T_{d,5\%onset}$. For example, decomposition of a large percent of the initial sample is observed at 463.2 or 483.2 K after the first hours. A negligible decomposition rate was observed at 403.2 K, interestingly higher than the temperature of 383.2 K found under an analogous analysis for 1-ethyl-3-methylimidazolium acetate, an archetypal ionic liquid in the processing of (ligno)cellulosic materials (Clough et al., 2013). Therefore, this value can be taken as a better estimation of the maximum temperature at which a process involving [$P_{4\,4\,4\,4}$][OAc] should operate.

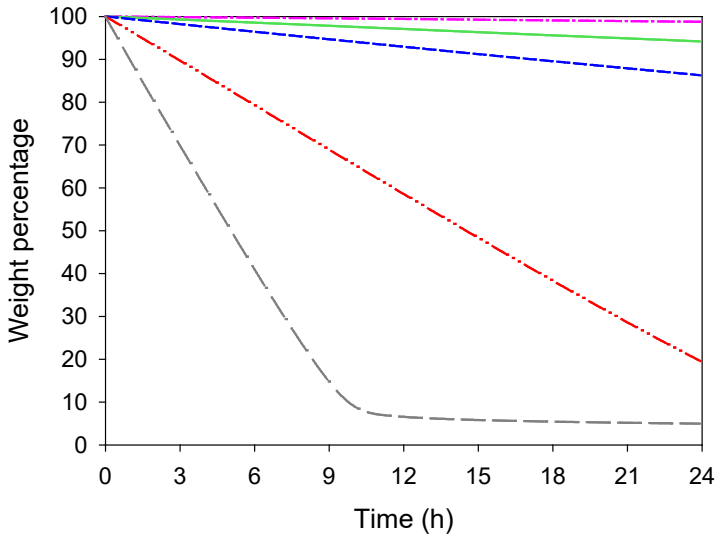


**Figure 3.24. Isothermal TGA curves for [$P_{4\,4\,4\,4}$][OAc], at different temperatures (from top to bottom): 403.2 K (magenta, dot-dash line), 423.2 K (green, solid line), 443.2 K (blue, short-dashed line), 463.2 K (red, dot-dot-dash line), and 483.2 K (grey, long-dashed line).**

Interestingly, the isothermal TGA data in Figure 3.24 allow the modelling of the kinetics of thermal decomposition of [$P_{4\,4\,4\,4}$][OAc], for example following the procedure described by Clough et al. (2013), who assumed that this thermal decomposition was a pseudo-zeroth order reaction. According to this procedure, the time necessary to reach a 1 % decomposition in isothermal TGA experiments ($t_{0.99}$) was computed for different absolute temperatures ($T$), and a clear exponential decay was observed when plotting one magnitude against the other (Figure 3.25A; numerical values listed in Table 3.2). Denoting the molar proportion of ionic liquid that decomposes as a function of time as

$d\alpha/dt$, the linearised form of the Arrhenius-type equation for the thermal decomposition of [P4444][OAc] would be:

$$\ln\left(\frac{d\alpha}{dt}\right) = \ln A - \frac{E_a}{R} \times \frac{1}{T} \qquad (3.7)$$

with $A$ and $E_a$ being respectively the pre-exponential factor and the activation energy parameter to be fit, and $R$ the universal gas constant. The representation of the natural logarithm against the inverse of the absolute temperature (Figure 3.25B) yielded a good linear fit ($R^2$ = 0.990), from which values of $A$ = 6.60 × $10^8$ $min^{-1}$ and $E_a$ = 107 kJ/mol could be obtained. Thus, the following Arrhenius-type equation for the description of the thermal decomposition of [P4444][OAc] was concluded:

$$\ln\left(\frac{d\alpha}{dt}\right) = 6.60 \times 10^8 \times \exp\left(-\frac{107}{R \times T}\right) \qquad (3.8)$$

where $R$ is expressed in $kJ \cdot mol^{-1} \cdot K^{-1}$, $T$ in K, and $t$ in minutes. The plot of this equation in Figure 3.25A corroborates the acceptably good fit that it provides of the experimental data.

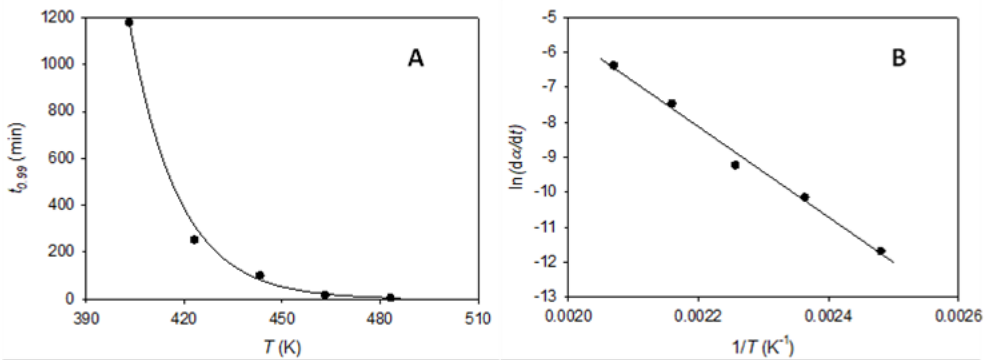


**Figure 3.25.** A) Time necessary to achieve a 1 % decomposition ($t_{0.99}$) of [P4444][OAc] in isothermal TGA experiments, as a function of temperature ($T$); with the solid line corresponding to the exponential fit provided by the Arrhenius equation. B) Linear fit of the plot of ln(d$\alpha$/d$t$) against 1/$T$.

**Table 3.2.** Time $t_{0.99}$ at which a 1 % decomposition of a [P4444][OAc] sample is achieved in an isothermal TGA run at temperature $T$.

| $T$ (K) | $t_{0.99}$ (min) |
|---|---|
| 403.2 | 1174 |
| 423.2 | 235.4 |
| 443.2 | 101.1 |
| 463.2 | 17.42 |
| 483.2 | 5.85 |

In view of all this thermal analysis, a compromise temperature of 343.2 K (70.0 °C) was selected to carry out the MCC pretreatment experiments. This was a temperature intended to keep to a minimum the cost of heating of the system, while being sufficiently above the reported melting temperature and safely below the temperatures at which noticeable thermal decomposition was observed in the isothermal TGA analysis. In fact, by applying equation 3.8 to this temperature, an extrapolated time of 5000 h (more than 200 days) would be necessary for the ionic liquid to undergo a 1 % decomposition. Moreover, it is worth noting that this is a temperature lower than the ones typically used in pretreatment of cellulose with ionic liquids (Zhang et al., 2012).

### 3.3.1.2. Pretreatment with pure [$P_{4444}$][OAc]: effect of time

In a first instance, and besides evidence from direct visual observation, a verification of the lack of capacity of [$P_{4444}$][OAc] to dissolve MCC at the selected temperature of 343.2 K (hence corroborating the non-dissolving nature of the pretreatment method proposed) was performed. In a glass cell thermostated at that temperature, MCC and [$P_{4444}$][OAc] were placed in a ratio of 0.5 g of MCC per 100 g of [$P_{4444}$][OAc]. After vigorous stirring for 24 h at 343.2 K, a sample was taken, and its microscopic photograph (by confocal microscopy) is shown in Figure 3.26. The clear observance of undissolved microcrystalline solids constitutes an evidence of the negligible cellulose dissolution capacity of [$P_{4444}$][OAc] (at least, lower than 0.5 g of cellulose per 100 g of ionic liquid), and thus the non-dissolving character of the pretreatments can be assumed.

Different pretreatment times (2 h, 4 h, and 8 h) were investigated in the pretreatment of MCC with pure [$P_{4444}$][OAc] at 343.2 K. The PXRD diffractograms obtained for the pretreated samples are shown in Figure 3.27, along with the diffractogram corresponding to the untreated cellulose. A gradual decrease in the intensity of the crystalline peaks with an increase in the pretreatment time is clearly observed. The associated *CI* values were calculated: 48 % for the untreated sample; 38 % for the 2-hour pretreatment, 30 % for 4 h, and 24 % for 8 h. Thus, the simple, non-dissolving pretreatment with pure [$P_{4444}$][OAc] leads to a significant decrease in the degree of crystallinity of MCC upon pretreatment, at any of the tested pretreatment times.

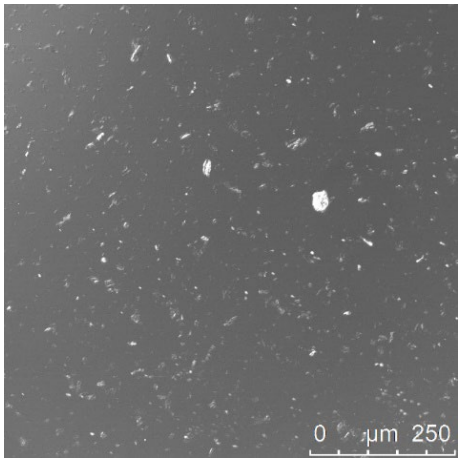


Figure 3.26. Microscope image, at a magnification of 20×, of a mixture of MCC and [P4444][OAc] in a ratio of 0.5 g of cellulose per 100 g of ionic liquid, after vigorous stirring for 24 h at 343.2 K.

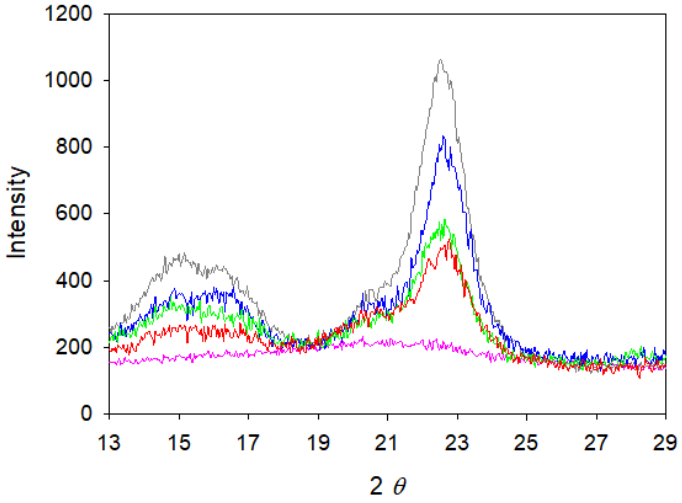


Figure 3.27. PXRD diffractograms of MCC pretreated with pure [P4444][OAc] at 343.2 K, with a load of 10 g of cellulose per 100 g of ionic liquid, during different times. From top to bottom at a 2$\theta$ value of 23°: without pretreatment (grey), 2 h (blue), 4 h (green), 8 h (red). The diffractogram of totally amorphised MCC is also shown (magenta).

To find out if the observed reduction in the degree of crystallinity resulted in an improved reactivity of the cellulose, its enzymatic hydrolysis by the action of cellulases

and $\beta$-glucosidases was selected as a model reaction.* Thus, a study of the kinetics of enzymatic hydrolysis of the pretreated MCC samples was carried out. The corresponding time courses are shown in Figure 3.28, together with the base case of hydrolysis of untreated MCC. As observed, all pretreated MCC samples hydrolysed at a faster rate than the untreated sample. For a given hydrolysis reaction time, the longer the pretreatment time, the higher the conversion achieved. This evolution of hydrolysis kinetics is in line with the degrees of decrystallisation presented in the paragraph above.

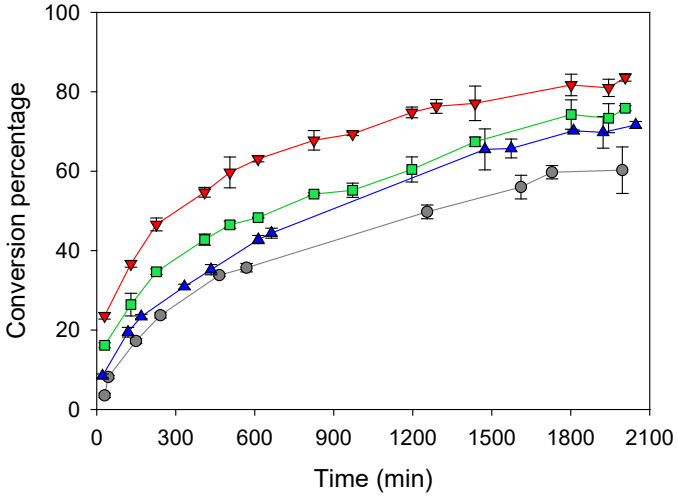


**Figure 3.28. Evolution, as a function of time, of the percentage of conversion of cellulose into glucose in the reaction of enzymatic hydrolysis of the MCC pretreated with pure [$P_{4\,4\,4\,4}$][OAc] at 343.2 K during different pretreatment times: 2 h (blue, triangles), 4 h (green, squares), and 8 h (red, inverted triangles). The kinetics of hydrolysis of untreated MCC are also shown (grey, circles).**

Given the interest, for many applications, of pretreatment procedures that do not affect negatively the length of the cellulose chains, an investigation of the *DP* was also carried out. Values of 224, 228, and 224 were respectively found for the MCC samples pretreated during 2, 4, and 8 h. If the uncertainty of the method for the experimental determination of *DP* is taken into account, all these values can be considered as equivalent, and not significantly different of the value of 228 found for the untreated

* Please note that this enzymatic hydrolysis was chosen only for the sake of evidencing an improved reactivity; not as a process target itself, as it is normally the case in works involving the pretreatment and subsequent saccharification of lignocellulosic biomass.

MCC. Therefore, it can be assumed that the cellulose chains were not degraded during the pretreatments.

Similarly, the preservation of the thermal stability of cellulose upon its pretreatment may be another aspect of interest. The determination of the $T_{d,5\%onset}$ for the MCC samples pretreated during different times was carried out, and the following values were obtained: 562 K for the MCC samples pretreated during 2 h and during 4 h, and 559 K for the sample corresponding to the pretreatment during 8 h. This means just a very small decrease (essentially negligible for practical purposes) in thermal stability with regard to the $T_{d,5\%onset}$ of 569 K obtained for the untreated MCC. This preservation of thermal stability constitutes and advantage of the method presented herein with respect to other strategies previously reported for cellulose decrystallisation with ionic liquids (Zhang et al., 2012).

### 3.3.1.3. Effect of water or DMSO as co-solvents of [P4 4 4 4][OAc] in the pretreatment fluid

Besides the use of neat [P4 4 4 4][OAc] as fluid for the non-dissolving pretreatment of MCC, some mixtures of this ionic liquid with water or DMSO were also tested for such purpose. The use of these molecular co-solvents would lead to a series of beneficial aspects: lowering the cost per unit mass, lowering the melting temperature of the fluid (as dictated by the colligative properties), and lowering the viscosity. The latter was experimentally quantified for mixtures with mole fractions of co-solvent of 0.20 and 0.40, with Table 3.3 providing a comparison of the dynamic viscosities of the pure ionic liquid and of the selected mixtures at the common temperature of 343.15 K (a temperature at which all systems are totally fluid). A remarkable decrease in viscosity is observed when any of the molecular co-solvents is used, even for the lowest co-solvent mole fraction tested. The density of the studied mixtures, also experimentally determined since it was necessary for the calculation of the dynamic viscosity from the kinematic viscosity, is also included in Table 3.3; although in the case of this property the influence of the co-solvents is more limited.

**Table 3.3.** Density ($\rho$) and dynamic viscosity ($\eta$) at 343.15 K for pure [$P_{4\,4\,4\,4}$][OAc] and for its mixtures with water or DMSO at selected mole fractions ($x_2$) of the molecular co-solvent; and crystallinity index (*CI*) and degree of polymerisation (*DP*) of the MCC pretreated with those fluids at 343.2 K for 2 h with a load of 10 g of cellulose per 100 g of solvent.

| Co-solvent | $x_2$ | $\rho$ (g/cm$^3$) | $\eta$ (mPa·s) | *CI* (%) | *DP* |
|---|---|---|---|---|---|
| None | --- | 0.90886 | 43.90 | 38 | 224 |
| Water | 0.20 | 0.91084 | 31.12 | 31 | 228 |
| Water | 0.40 | 0.91316 | 22.78 | 34 | 226 |
| DMSO | 0.20 | 0.91603 | 28.85 | 12 | 219 |
| DMSO | 0.40 | 0.92530 | 18.81 | --- | --- |

For evaluation of the effect of the molecular co-solvents in the pretreatment of MCC, the temperature of 343.2 K was chosen to allow direct comparison with the pretreatment carried out with the neat ionic liquid (despite the fact that lower temperatures could be an option if using the mixtures of ionic liquid and molecular co-solvent). Although the pretreatment efficiency (crystallinity reduction) with neat [$P_{4\,4\,4\,4}$][OAc] was more effective at longer times, for this new set of pretreatments a duration of 2 h was preferred considering the overall energy demands and productivity in an industrial context.

Figure 3.29 shows the PXRD diffractograms of the MCC samples pretreated with the mixtures of [$P_{4\,4\,4\,4}$][OAc] + $H_2O$. Compared to the MCC pretreated with pure ionic liquid, a lower degree of crystallinity is observed. However, the difference between the diffractograms for the two investigated concentrations of water in the mixture is rather small. This has its reflection in the *CI* values that were calculated, which are numerically displayed in Table 3.3. As observed, the *CI* obtained for MCC pretreated with the mixtures of ionic liquid and water is clearly lower than that for MCC pretreated with the neat ionic liquid, but the variation of the concentration of the mixture from a water mole fraction ($x_{water}$) of 0.20 to 0.40 has little influence in the crystallinity reduction achieved. Interestingly, the *CI* for the pretreatment with the mixture of composition $x_{water}$ = 0.20 is slightly lower than that corresponding to the pretreatment with the mixture of composition $x_{water}$ = 0.40; a fact that invites to think of the existence of an optimum composition in the pretreatment system [$P_{4\,4\,4\,4}$][OAc] + $H_2O$ for which the reduction in crystallinity is maximised. Such an optimum might be the result of the best balance between the favourable viscosity reduction induced by the presence of water (which improves the contact of the cellulose with the pretreatment fluid) and the detrimental effect that it would have on the capacity of the pretreatment fluid to interact with the

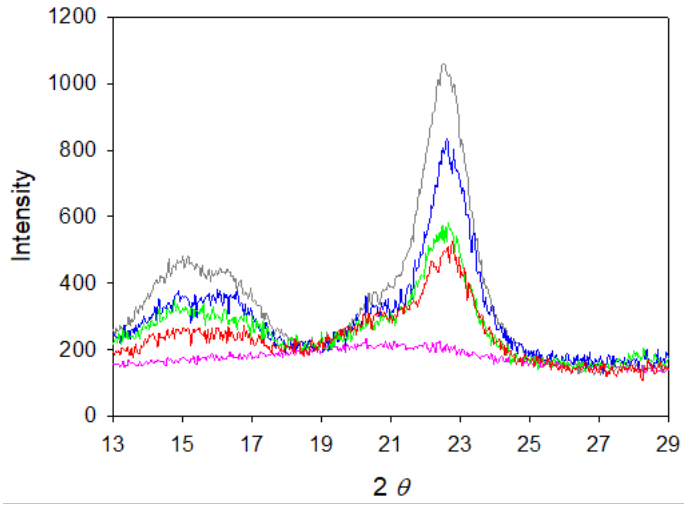


**Figure 3.29. PXRD diffractograms of MCC pretreated with pure [P4 4 4 4][OAc] and with mixtures of [P4 4 4 4][OAc] + H2O at different water mole fractions ($x_{water}$), at a temperature 343.2 K, with a load of 10 g of cellulose per 100 g of solvent, during 2 h. Pretreatment fluid (from top to bottom at a 2$\theta$ value of 23°: pure [P4 4 4 4][OAc] (blue); [P4 4 4 4][OAc] + H2O, $x_{water}$ = 0.40 (red); and [P4 4 4 4][OAc] + H2O, $x_{water}$ = 0.20 (green). The diffractogram of totally amorphised MCC is also shown (magenta).**

cellulose chains (pure water is totally ineffective as pretreatment fluid). The latter would be due to the very high hydrogen bond donor ability of water, which would counteract the anion basicity that is necessary to interact with the cellulose substrate for disruption of its hydrogen-bonding network (Wang et al., 2012).

Regarding the system [P4 4 4 4][OAc] + DMSO as pretreatment fluid, an important effect of gelation of cellulose was observed during the washing step when the concentration of 0.40 in mole fraction of DMSO ($x_{DMSO}$) was used, thus generating agglomerates that would need copious amounts of water to effectively wash away the retained ionic liquid. This is an indication of partial dissolution and is consistent with results previously reported in the literature that demonstrate the requirement for a significant proportion of dipolar aprotic co-solvent, such as DMSO, to maximise cellulose dissolution in tetraalkylphosphonium acetate homologues (Holding et al., 2014, 2017). Therefore, further characterisation associated with the pretreatment with such DMSO concentration was disregarded. With $x_{DMSO}$ = 0.20 in the pretreatment fluid, an incipient manifestation of gelation could be also observed, but this did not pose a problem in performing effectively the washing step. The PXRD diffractogram of the MCC pretreated with this mixture is shown in Figure 3.30, where a strong reduction of the

area under the curve (directly related to the degree of crystallinity) is observed in comparison to the diffractogram of the MCC pretreated with pure [$P_{4444}$][OAc] at equivalent conditions. Moreover, a transition from the crystalline structure Cellulose I to the more thermodinamically stable Cellulose II is manifested by the shift of the main peak from 22.5° (characteristic of Cellulose I) to the region 20-21.5° (characteristic of Cellulose II) (Wu et al., 2018). Compared to the *CI* of 38 % obtained when using the neat ionic liquid for the pretreatment, the *CI* found for the MCC pretreated with the [$P_{4444}$][OAc] + DMSO system was very much lower: 12 %. Despite this stark crystallinity reduction and the allomorphic transformation from Cellulose I to Cellulose II, the pretreatment with the explored mixture of [$P_{4444}$][OAc] and DMSO is still of a non-dissolving nature, based on the avoidance of significant gelation upon regeneration. This aspect was further evidenced through the development of dissolution tests and subsequent analysis by confocal microscopy (Figure 3.31), where the solubility of MCC in the [$P_{4444}$][OAc] + DMSO mixture ($x_{DMSO}$ = 0.20) at 343.2 K was proven to be lower than 0.5 g of cellulose per 100 g of solvent. However, it should be taken into account that this might be highly temperature-dependent.

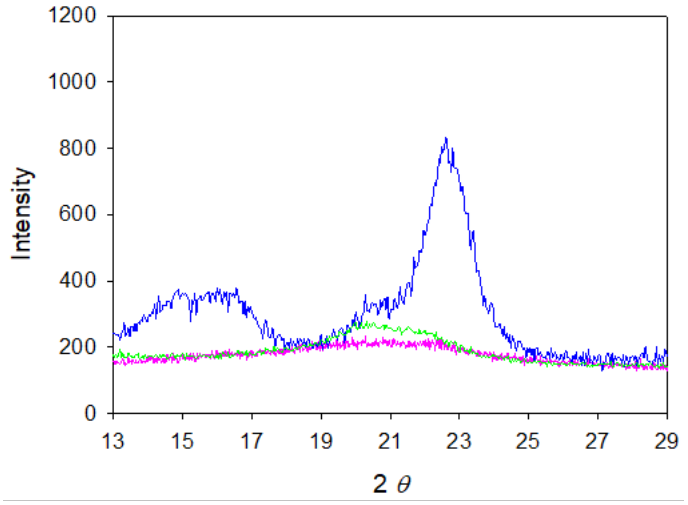


**Figure 3.30. PXRD diffractograms of cellulose pretreated with pure [$P_{4444}$][OAc] (blue, top signal) and with a mixture of [$P_{4444}$][OAc] + DMSO at a 0.20 mole fraction of DMSO (green, intermediate signal), at a temperature 343.2 K, with a load of 10 g of cellulose per 100 g of solvent, during 2 h. The diffractogram of totally amorphised MCC is also shown (magenta, bottom signal).**

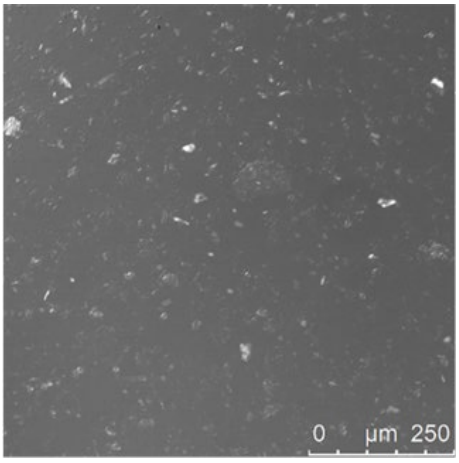


**Figure 3.31. Microscope image, at a magnification of 20×, of a mixture of MCC and [P4444][OAc] + DMSO with a mole fraction $x_{DMSO}$ = 0.20, in a ratio of 0.5 g of cellulose per 100 g of pretreatment fluid, after vigorous stirring for 24 h at 343.2 K.**

Figure 3.32 shows the kinetics of the enzymatic hydrolysis of the MCC samples pretreated with mixtures of [P4444][OAc] + (water or DMSO), as well as a comparison with the kinetics corresponding to the MCC pretreated under analogous conditions with pure [P4444][OAc]. For both co-solvents, a good correspondence is observed between the level of crystallinity reduction caused by the pretreatment and the improvement in the hydrolysis kinetics. Thus, in the case of water as co-solvent (Figure 3.32A), the fastest kinetics are found for the cellulose pretreated with the [P4444][OAc] + $H_2O$ mixture with $x_{water}$ = 0.20 (the one for which a lower *CI* was achieved). The cellulose pretreated with the [P4444][OAc] + $H_2O$ mixture with $x_{water}$ = 0.40 leads to somewhat slower kinetics, but still faster than the case of the cellulose pretreated with ionic liquid in the absence of water. Equivalently, in Figure 3.32B it can be seen how the kinetics of hydrolysis of the cellulose pretreated with the [P4444][OAc] + DMSO mixture with $x_{DMSO}$ = 0.20 (which underwent a very strong reduction in its crystallinity) is much faster than that of the cellulose pretreated with the pure ionic liquid. The strong improvement in the kinetics in this case is likely related not just to the reduction in crystallinity caused by the pretreatment, but perhaps also to the transformation of the crystalline fraction from Cellulose I to Cellulose II (see Figure 3.30) that concomitantly occurred (Nagarajan et al., 2017). Nevertheless, this statement may be somewhat controversial, due to the

difficulty in separating the effect of the presence of different phases of unambiguously defined crystallinity versus accessibility to enzymes or other reagents.

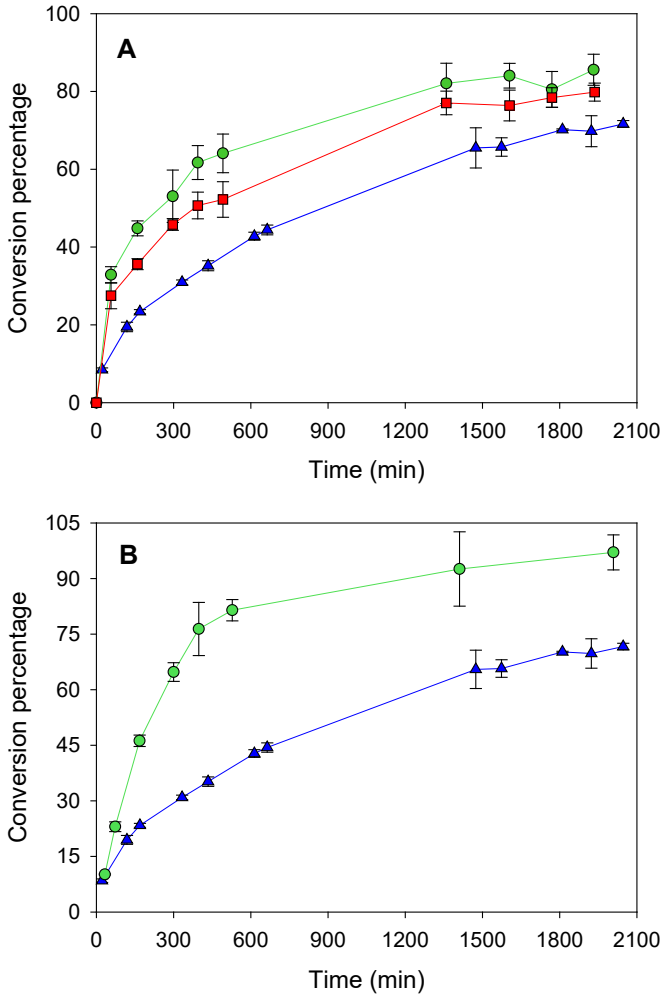


**Figure 3.32. Evolution, as a function of time, of the percentage of conversion of cellulose into glucose in the reaction of enzymatic hydrolysis of the MCC pretreated, at 343.2 K during 2 h, with pure [P4444][OAc] (blue, triangles) and with [P4444][OAc] + $H_2O$ (plot A) or [P4444][OAc] + DMSO (plot B) mixtures of different composition: $x_{co\text{-}solvent}$ = 0.20 (green, circles) or $x_{co\text{-}solvent}$ = 0.40 (red, squares).**

As in the case of pretreatment with pure [P4444][OAc], the *DP* of the MCC pretreated with the mixtures of this ionic liquid with water or DMSO was also analysed. Values of 228 and 226 were obtained in the case of pretreatment with the mixtures with water at $x_{water}$ = 0.20 and $x_{water}$ = 0.40, respectively; and 219 in the case of pretreatment

with the mixture with DMSO at $x_{DMSO}$ = 0.20 (Table 3.3). By comparison of these values with *DP* = 228 for the untreated MCC, it can be stated that the use of the [P4444][OAc] + $H_2O$ mixtures as pretreatment fluids, as in the case of pure [P4444][OAc], does not cause any significant reduction of the length of the cellulose chains. Regarding the use of the [P4444][OAc] + DMSO mixture, a little reduction in such length is observed, although the potential for utilisation of the thus pretreated cellulose in applications requiring the retention of fibrous properties is essentially preserved.

### 3.3.1.4. Relationship between crystallinity index and rate of hydrolysis

A relationship of the reactivity of cellulose with its crystallinity index has been established by different authors in the literature (Hall et al., 2010; Li et al., 2014). The results of diffractometry and hydrolysis kinetics presented herein, for the raw MCC and for all six MCC samples pretreated at different conditions (namely: pretreatment with pure [P4444][OAc] during 2 h, 4 h, or 8 h; pretreatment with [P4444][OAc] + $H_2O$ during 2 h with water molar fraction of 0.20 or 0.40; and pretreatment with [P4444][OAc] + DMSO during 2 h with DMSO molar fraction of 0.20), also suggest the existence of such a relationship. In Figure 3.33, the percentage of conversion of cellulose samples in the

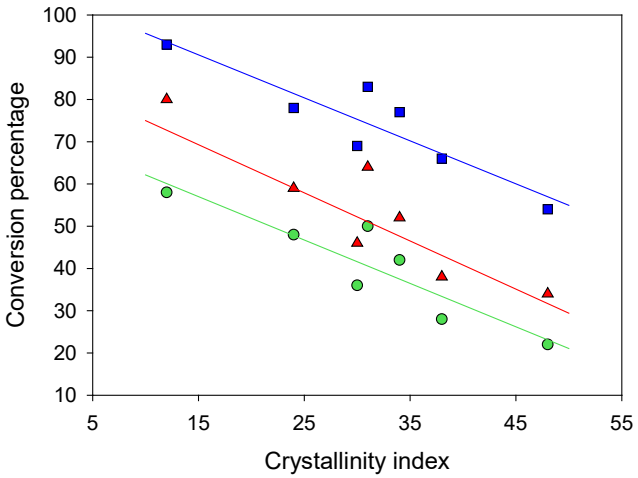


**Figure 3.33. Conversion of the enzymatic hydrolysis of MCC, as a function of the crystallinity index of the MCC sample, for selected reaction times (from bottom to top): 250 min (green, circles), 500 min (red, triangles), and 1500 min (blue, squares). The conversion values at the specified times were approximated as linear interpolations in the respective hydrolysis time courses. Lines correspond to the best linear fit for each series, and are provided as guide to the eye.**

enzymatic hydrolysis reaction is plotted against the crystallinity index of those cellulose samples, for different fixed hydrolysis times. For the different reaction times analysed (250, 500, and 1500 min), a rough trend can be observed, with the degree of conversion being higher as the crystallinity of the sample is lower. Thus, from this point of view, and among all the variations investigated in the present section 3.3.1, the pretreatment of MCC with the mixture of [$P_{4444}$][OAc] + DMSO ($x_{DMSO}$ = 0.20) would be preferred to improve its reactivity.

## 3.3.2. Advanced pretreatment studies with Avicel PH-101

### 3.3.2.1. Liquid systems and temperatures for pretreatment

As already reported in section 3.3.1.1, pure [$P_{4444}$][OAc] has a melting temperature of 331 K at atmospheric pressure, and thus a temperature of 343.2 K (70.0 °C) can be appropriate for its utilisation in the liquid state. In that context, such temperature was selected for the use of [$P_{4444}$][OAc] for the non-dissolving pretreatment of Avicel.

One possibility to carry out the pretreatment with a similar effect, but at a lower temperature (with the associated savings in energy demand), and while fully keeping the intrinsic advantages of ionic liquids, is the combination of [$P_{4444}$][OAc] with a second ionic liquid with which it would display a eutectic behaviour. Since one of the routes of synthesis of [$P_{4444}$][OAc] (particularly the one used herein) consists of a metathesis reaction of a halide of the cation with potassium acetate, it could make sense to select either [$P_{4444}$]Cl or [$P_{4444}$]Br as second ionic liquid candidates. The utilisation of a combination of [$P_{4444}$][OAc] and the analogous halide would avoid the most costly part of the process of preparation of [$P_{4444}$][OAc] by the aforementioned metathetic route, namely the complete exchange of anions in the desired product. With respect to pure [$P_{4444}$][OAc], the combinations [$P_{4444}$][OAc] + [$P_{4444}$]Cl or [$P_{4444}$][OAc] + [$P_{4444}$]Br imply only a partial replacement of the acetate anions (key in the interaction of the ionic liquid with cellulose due to their basicity) with halides that also exhibit some basicity – they are Lewis bases. Thus, the potential of these mixtures to perform an effective pretreatment of cellulose (already knowing that [$P_{4444}$][OAc] is capable of doing so) would be high. Therefore, the solid-liquid equilibria of the systems [$P_{4444}$][OAc] + [$P_{4444}$]Cl and [$P_{4444}$][OAc] + [$P_{4444}$]Br were investigated to ascertain

whether or not they displayed a eutectic behaviour. The corresponding phase diagrams, constructed from DSC thermograms of samples covering the entire composition range of each system, are shown as temperature-composition plots in Figure 3.34 (and the numerical values used to build such plots can be consulted in Tables B.1 and B.2 in Appendix B). As observed, both systems exhibit a eutectic

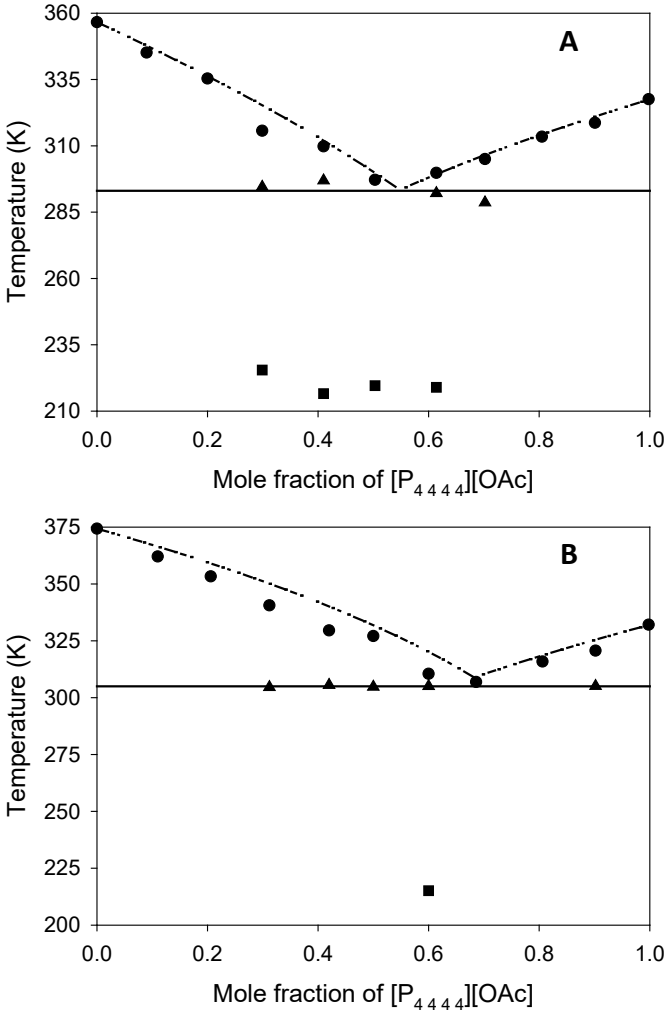


**Figure 3.34. Temperature-composition diagrams for the solid-liquid equilibrium of the systems [P4444][OAc] + [P4444]Cl (A) and [P4444][OAc] + [P4444]Br (B). Legend: ▲, melting of the eutectic composition; ●, melting of the excess compound; ■, glass transition. The horizontal solid lines represent the eutectic lines (calculated as the average of the eutectic melting temperatures observed). The dashed lines correspond to the Schröder-van Laar model (eq. 3.9).**

behaviour with miscibility of the compounds in the liquid phase and immiscibility in the solid phase (no solid solution). The eutectic temperatures obtained were 297 K for [$P_{4444}$][OAc] + [$P_{4444}$]Cl at a nearly equimolar composition, and 305 K for [$P_{4444}$][OAc] + [$P_{4444}$]Br, with a [$P_{4444}$][OAc] mole fraction of ca. 0.70. These represent a substantial depression of the melting temperature from the parent compounds – not just from [$P_{4444}$][OAc], but also from the halides, as melting temperatures of 361 K for [$P_{4444}$]Cl and of 374 K for [$P_{4444}$]Br were found by DSC.* Therefore, it was decided to use these eutectic compositions as pretreatment fluids for Avicel at a temperature of 313.2 K (40.0 °C). For direct comparison with the performance of pure [$P_{4444}$][OAc], equivalent pretreatments at 343.2 K were also included in the study.

As an additional note, complementing the information on the solid-liquid equilibria developed, Figures 3.34 also shows that the melting curves of the two systems (especially in the case of the [$P_{4444}$][OAc] + [$P_{4444}$]Cl mixture) are very well described by the simplified version of the Schröder-van Laar model:

$$T_m = \left( \frac{1}{T_{m,i}} - \frac{\ln x_i}{\Delta H_{m,i}/R} \right)^{-1} \tag{3.9}$$

where $T_m$ is the observed melting temperature; $x_i$, $\Delta H_{m,i}$, and $T_{m,i}$ are respectively the mole fraction, molar enthalpy of fusion,† and melting temperature of the excess component in the evaluated melting curve; and $R$ is the universal gas constant (Cortesão et al., 2017). Besides other simplifications (see, for instance, the analysis by Martins et al. (2019)), this equation assumes that an ideal liquid solution (activity coefficient equal to the unity) is in equilibrium with pure solid (Cortesão et al., 2017). The good description that it provides of the solid-liquid equilibria of the eutectic systems investigated, as assessed in Figure 3.34, can be taken as an indicator of the quite ideal mixing of [$P_{4444}$][OAc] and [$P_{4444}$]Cl, and of [$P_{4444}$][OAc] and [$P_{4444}$]Br, with values of the activity coefficients close to the unity. This should not be unexpected, since each pair of ionic liquids has the same bulky cation in common, and the two anions involved

* In the literature, Adamová et al. (2012) have reported a melting temperature of 70.6 °C (344 K) for [$P_{4444}$]Cl, significantly lower than the value reported herein. This difference may be due, at least in part, to the higher water content of their sample: 0.0006 in mass fraction, which is double than ours, rendering it difficult to establish a fair comparison with our value.

† The numerical values for $\Delta H_{m,i}$, obtained from integration of the endothermic melting peaks in the corresponding DSC thermograms, were: 14.1 kJ/mol for [$P_{4444}$][OAc], 10.9 kJ/mol for [$P_{4444}$]Cl, and 16.8 kJ/mol for [$P_{4444}$]Br.

are notably smaller, thus accommodating well and without much difference in the void spaces left by the network of the bulky cations in its three-dimensional arrangement. It can be added that the participation of [P4444]Cl or [P4444]Br in lowering the melting temperature of [P4444][OAc] does not compromise the thermal stability of the resulting liquid. A dynamic TGA analysis yielded 5 % onset decomposition temperatures ($T_{d,5\%onset}$) of 590 K for [P4444]Cl and 609 K for [P4444]Br (Figure 3.35), higher than the $T_{d,5\%onset}$ = 527 K found for [P4444][OAc] (see section 3.3.1.1). Following a similar

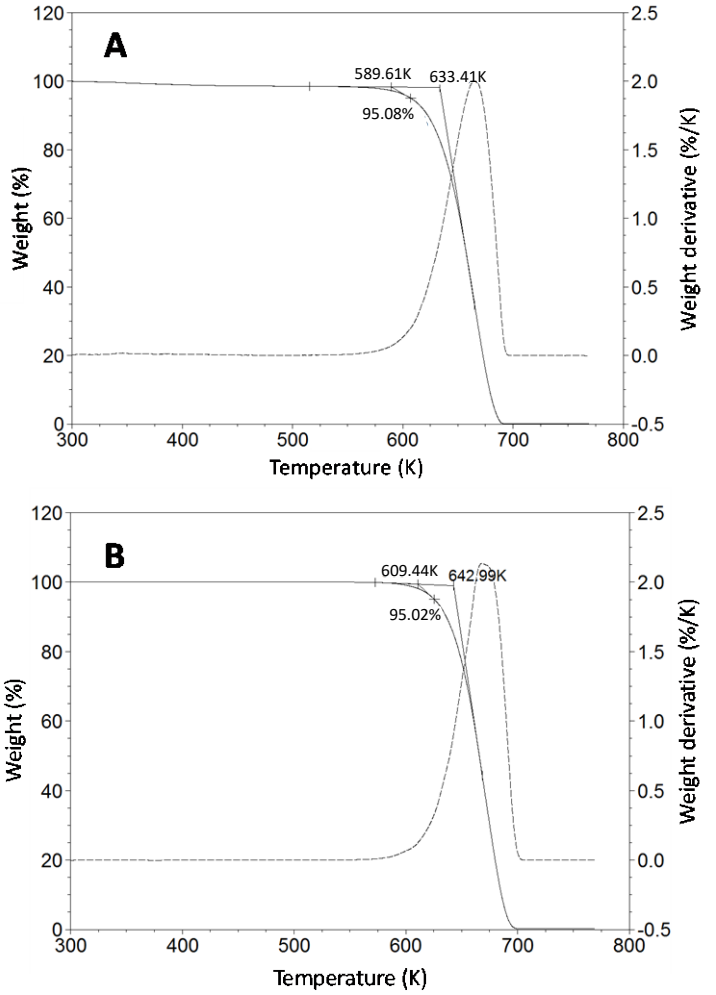


Figure 3.35. Dynamic TGA thermograms of [P4444]Cl (plot A) and [P4444]Br (plot B), showing the determination of the regular onset decomposition temperature and of the 5 % onset decomposition temperature. The solid line represents the weight percentage as a function of temperature, whereas the dashed line represents its first derivative.

procedure to what was done in section 3.3.1.1 to analyse the termal stability of [$P_{4444}$][OAc] in the mid-long term, and taking as reference the values of $T_{d,5\%onset}$ mentioned, 24-hour isothermal TGA runs were performed for [$P_{4444}$]Cl and for [$P_{4444}$]Br at different temperatures (below their respective $T_{d,5\%onset}$ values). The corresponding isothermal thermograms are shown in Figure 3.36, revealing for

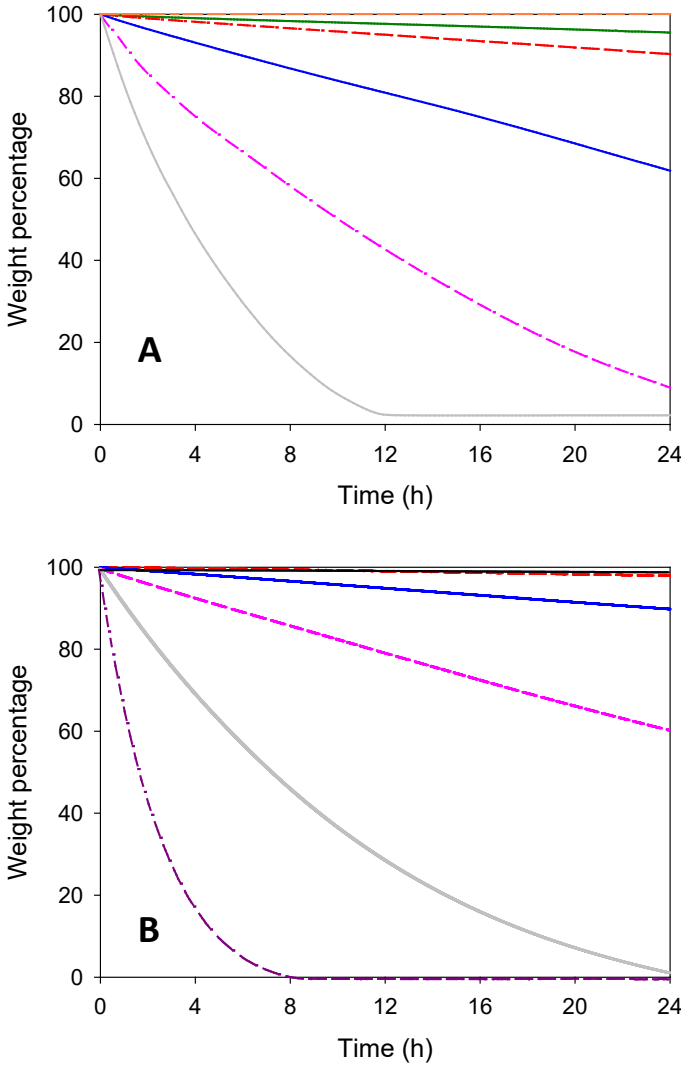


**Figure 3.36. Isothermal TGA curves for [$P_{4444}$]Cl (plot A) and [$P_{4444}$]Br (plot B) at different temperatures. From top to bottom: 473.2 K (orange dashed line, only in the plot for [$P_{4444}$]Cl), 493.2 K (green solid line), 513.2 K (red dashed line), 533.2 K (blue solid line), 553.2 K (pink dashed line), 573.2 K (grey solid line), and 593.2 K (purple dashed line, only in the plot for [$P_{4444}$]Br).**

example a decomposition lower than 1 % after 24 h at temperatures as high as 473.2 K for [P4444]Cl or 493.2 K for [P4444]Br. The sets of isothermal TGA thermograms were used to model the kinetics of thermal decomposition of [P4444]Cl and [P4444]Br with the Arrhenius equation, analogously to how it was done for [P4444][OAc] in section 3.3.1.1. The $t_{0.99}$ values for the different temperatures are listed in Table 3.4, and the plot of $t_{0.99}$ as a function of temperature is shown in Figure 3.37A. From the plot in Figure 3.37B, corresponding to the linearised version of the Arrhenius-type equation (equation 3.7), the following expressions could be obtained, respectively, for the thermal decomposition of [P4444]Cl and of [P4444]Br:

$$\ln\left(\frac{d\alpha}{dt}\right) = 4.05 \times 10^{9} \times \exp\left(-\frac{133}{R \times T}\right) \quad (3.10)$$

$$\ln\left(\frac{d\alpha}{dt}\right) = 5.06 \times 10^{14} \times \exp\left(-\frac{193}{R \times T}\right) \quad (3.11)$$

where all symbols have the same meaning as in equation 3.7, and where $R$ is expressed

**Table 3.4.** Time $t_{0.99}$ at which a 1 % decomposition of a sample of [P4444]Cl or [P4444]Br is achieved in an isothermal TGA run at temperature $T$.

| $T$ (K) | $t_{0.99}$ (min) | |
|---|---|---|
| | [P4444]Cl | [P4444]Br |
| 493.2 | 257 | - |
| 513.2 | 112 | 770 |
| 533.2 | 29.6 | 154 |
| 553.2 | 6.60 | 31.5 |
| 573.2 | 3.68 | 7.11 |
| 593.2 | - | 1.78 |

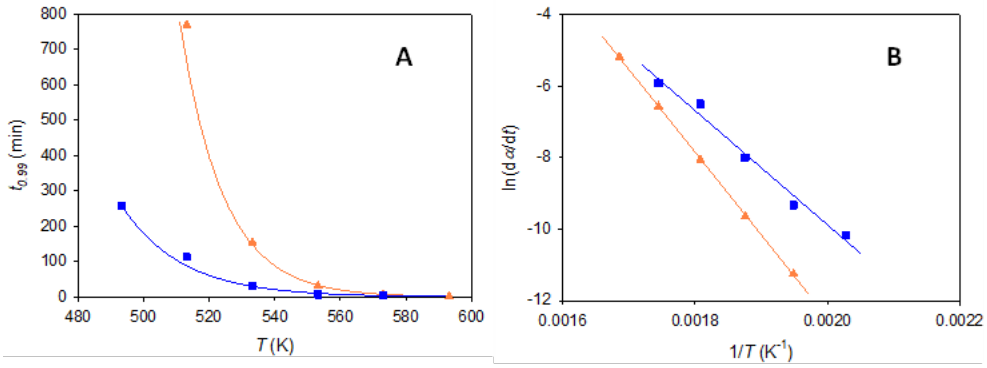


Figure 3.37. A) Time necessary to achieve a 1 % decomposition ($t_{0.99}$) of [P4444]Cl (blue squares) or of [P4444]Br (orange triangles) in isothermal TGA experiments, as a function of temperature ($T$); with the solid lines corresponding to the exponential fit provided by the Arrhenius-type equations. B) Linear fit of the plot of ln($d\alpha/dt$) against 1/$T$, with the same colour code.

in $kJ \cdot mol^{-1} \cdot K^{-1}$, $T$ in K, and $t$ in minutes. From Figure 3.37A it is clear that equations 3.10 and 3.11 constitute a good model for the thermal decomposition of these ionic liquids. By extrapolation of these equations, it could be estimated that, at a temperature of 343.2 K, even after one year the fraction thermally decomposed would be negligible (lower than 0.01 %) in any of these compounds.

An alternative for the pretreatment at lower temperatures is the use of mixtures of $[P_{4444}][OAc]$ with molecular solvents. As already pointed out in section 3.3.1.3, these molecular solvents will bring along the inconveniences of their volatility and the risks associated with it (flammability, atmospheric pollution, loss of solvent by evaporation, etc.), in particular if they are organic. However, they will also lead to a number of process advantages: lowering the viscosity of the pretreatment fluid, decreasing its cost per unit mass, and also the possibility of potentially reducing the melting temperature in a significant manner with respect to pure $[P_{4444}][OAc]$. In view of the good results achieved by the mixture of $[P_{4444}][OAc]$ and DMSO in the pretreatment of MCC (see section 3.3.1), this combination was attempted again herein, for the pretreatment of the Avicel cellulose standard. On the contrary, due to the modest results obtained with the mixture $[P_{4444}][OAc] + H_2O$ in the pretreatment of MCC (see also section 3.3.1), water was discarded as a co-solvent of $[P_{4444}][OAc]$ in the pretreatment studies of Avicel. Instead, another polar protic solvent was selected, namely ethanol; thus still providing a contrast point with the polar aprotic nature of DMSO. As in section 3.3.1, two different concentrations of molecular co-solvent, namely 0.20 and 0.40 in mole fraction, were selected in each case. For the rigorous choice of an appropriate pretreatment temperature, the solid–liquid equilibria of the binary systems $[P_{4444}][OAc]$ + ethanol and $[P_{4444}][OAc]$ + DMSO were experimentally investigated at atmospheric pressure. The temperature-composition diagrams built from DSC analyses of the corresponding mixtures covering the entire compositional ranges are shown in Figure 3.38 (and the numerical values of the corresponding solid-liquid equilibrium data are presented in Tables B.3 and B.4 in Appendix B). A sustained decrease in the melting temperature was observed in the system $[P_{4444}][OAc]$ + ethanol with an increase in the concentration of ethanol, at least up to an ethanol mole fraction of 0.70. In the ethanol mole fraction range 0.70–1.00, no solid–liquid transition could be detected within the reliable experimental temperature range of the DSC instrument used. Regarding the system $[P_{4444}][OAc]$ + DMSO, a clear eutectic behaviour was identified, with the eutectic

point corresponding to a composition of ca. 0.70 in mole fraction of DMSO and a temperature of 261 K. By inspection of these diagrams, a temperature of 313.2 K (40.0 °C) was initially selected for the low-temperature pretreatments since all mixtures [P4444][OAc] + (ethanol or DMSO) with a co-solvent mole fraction of 0.20 and 0.40 are liquid at this temperature. However, preliminary tests for the pretreatment of

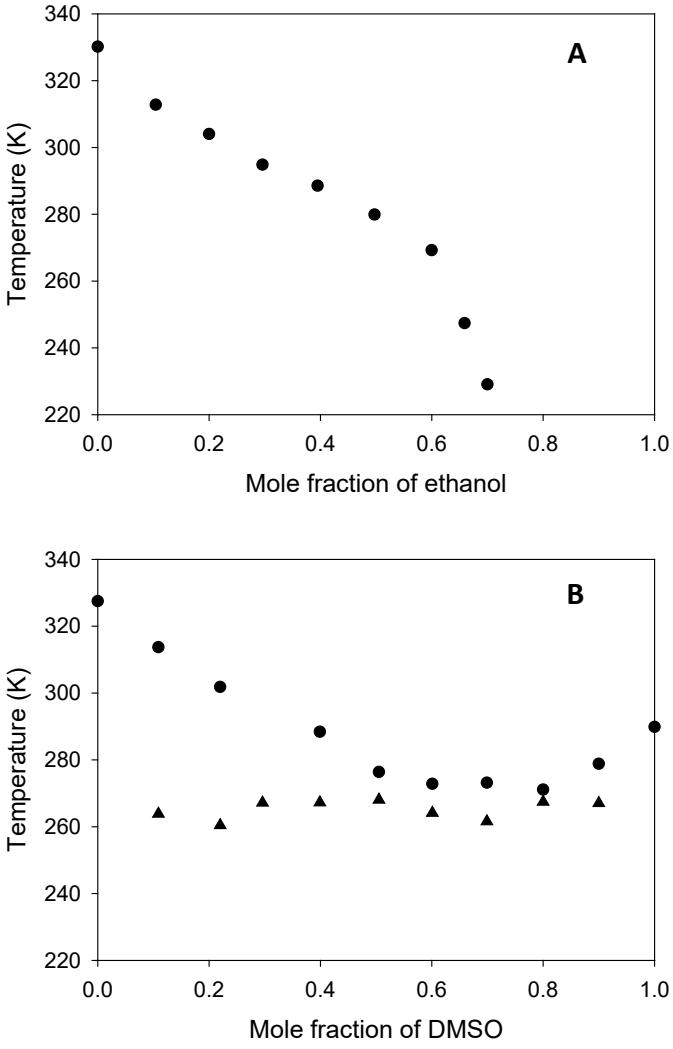


**Figure 3.38. Temperature-composition diagrams for the solid-liquid phase equilibria of the binary systems [P4444][OAc] + ethanol (plot A) and [P4444][OAc] + DMSO (plot B – Legend: ●, excess component melting; ▲, eutectic melting). For samples with an ethanol mole fraction higher than 0.70, no thermal events were detected above ca. 200 K (the lower limit of the reliable temperature range of the DSC instrument used).**

Avicel showed an impracticably high viscosity at this low temperature, which could be notably mitigated if operating at 323.2 K (50.0 °C). Therefore, this temperature of 323.2 K was the final choice to uniformly perform the low-temperature pretreatments with the combinations of ionic liquid and molecular solvent. For direct comparison with pure [$P_{4444}$][OAc], analogous pretreatments at 343.2 K were also performed.

It can be noted additionally that, contrary to the solid-liquid equilibria presented in Figure 3.34 for the mixtures of pairs of phosphonium ionic liquids, in the case of the solid-liquid equilibrium exhibited by [$P_{4444}$][OAc] + DMSO the Schröder-van Laar equation did not provide an acceptable description. This has to be due to not complying with some of the assumptions of the model, such as ideal liquid solution in equilibrium with pure solid (vide supra).

As a complementary characterisation of all these liquid systems intended for the pretreatment of Avicel cellulose at more than one temperature, two of their key properties from an industrial process design perspective, namely density ($\rho$) and viscosity ($\eta$), were measured as a function of temperature. The detailed numerical values of the measurements and their graphical evolution with absolute temperature ($T$) are presented in Table 3.5 and Figures 3.39 to 3.41. The density data sets were correlated by means of a polynomial equation:

$$\rho = a + b \times T + c \times T^2 \qquad (3.12)$$

where $a$, $b$, and $c$ are the fit parameters. The statistical Fisher's $F$-test (Devore, 2004) was used to evaluate the statistical significance of the quadratic term; with the

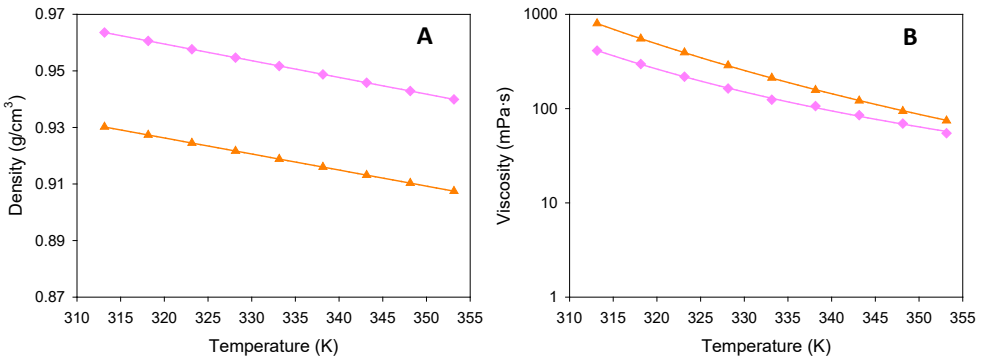


**Figure 3.39. Density (A) and viscosity (B) for the eutectic compositions of the mixtures [$P_{4444}$][OAc] + [$P_{4444}$]Cl ($x_{[P4444][OAc]}$ = 0.50) (orange) and [$P_{4444}$][OAc] + [$P_{4444}$]Br ($x_{[P4444][OAc]}$ = 0.70) (pink). Solid lines correspond to the fits provided by equations 3.12 and 3.13 (see fit parameters in Table 3.6).**

corresponding transformation into a linear fit in those cases in which such term was found to be non-significant. The viscosity data sets were correlated with the Vogel-Fulcher-Tammann equation in its modified version by Cohen and Turnbull (1959):

$$\eta = A \times T^2 \times exp\left(\frac{k}{T-T_0}\right) \qquad (3.13)$$

where $A$, $k$, and $T_0$ are the fit parameters. Their numerical values are collected in Table 3.6, and the quality of the correlation can be visualised in Figures 3.39 to 3.41.

**Table 3.5.** Experimentally measured density ($\rho$) and viscosity ($\eta$) of the pretreatments fluids based on the combination of [P4 4 4 4][OAc] with [P4 4 4 4]Cl, [P4 4 4 4]Br, ethanol, or DMSO, at different temperatures $T$.

| $T$ (K) | $\rho$ (g/cm$^3$) | $\eta$ (mPa·s) | $T$ (K) | $\rho$ (g/cm$^3$) | $\eta$ (mPa·s) |
|---|---|---|---|---|---|
| [P4 4 4 4][OAc] + [P4 4 4 4]Cl, $x_{[P4444][OAc]}$ = 0.50 | | | [P4 4 4 4][OAc] + [P4 4 4 4]Br, $x_{[P4444][OAc]}$ = 0.70 | | |
| 313.15 | 0.93018 | 799.4 | 313.15 | 0.96358 | 412.5 |
| 318.15 | 0.92734 | 550.8 | 318.15 | 0.96062 | 297.0 |
| 323.15 | 0.92449 | 393.7 | 323.15 | 0.95766 | 217.8 |
| 328.15 | 0.92166 | 286.9 | 328.15 | 0.95470 | 163.3 |
| 333.15 | 0.91882 | 211.6 | 333.15 | 0.95174 | 124.3 |
| 338.15 | 0.91599 | 157.0 | 338.15 | 0.94877 | 106.3 |
| 343.15 | 0.91315 | 121.1 | 343.15 | 0.94583 | 85.20 |
| 348.15 | 0.91031 | 93.92 | 348.15 | 0.94289 | 69.35 |
| 353.15 | 0.90748 | 74.37 | 353.15 | 0.93994 | 54.82 |
| [P4 4 4 4][OAc] + etanol, $x_{ethanol}$ = 0.20 | | | [P4 4 4 4][OAc] + etanol, $x_{ethanol}$ = 0.40 | | |
| 313.15 | 0.92125 | 133.2 | 313.15 | 0.91316 | 71.05 |
| 318.15 | 0.91826 | 100.9 | 318.15 | 0.91011 | 55.75 |
| 323.15 | 0.91527 | 77.94 | 323.15 | 0.90707 | 44.57 |
| 328.15 | 0.91229 | 61.19 | 328.15 | 0.90404 | 35.97 |
| 333.15 | 0.90932 | 48.77 | 333.15 | 0.90100 | 29.50 |
| 338.15 | 0.90635 | 39.57 | 338.15 | 0.89797 | 24.56 |
| 343.15 | 0.90338 | 32.38 | 343.15 | 0.89494 | 20.63 |
| 348.15 | 0.90042 | 31.52 | 348.15 | 0.89192 | 17.58 |
| 353.15 | 0.89747 | 27.29 | 353.15 | 0.88890 | 14.91 |
| [P4 4 4 4][OAc] + DMSO, $x_{DMSO}$ = 0.20 | | | [P4 4 4 4][OAc] + DMSO, $x_{DMSO}$ = 0.40 | | |
| 313.15 | 0.93356 | 115.2 | 313.15 | 0.94390 | 68.53 |
| 318.15 | 0.93055 | 91.01 | 318.15 | 0.94078 | 53.42 |
| 323.15 | 0.92755 | 71.24 | 323.15 | 0.93768 | 42.35 |
| 328.15 | 0.92455 | 55.97 | 328.15 | 0.93458 | 34.06 |
| 333.15 | 0.92156 | 45.03 | 333.15 | 0.93148 | 27.76 |
| 338.15 | 0.91857 | 36.52 | 338.15 | 0.92840 | 22.91 |
| 343.15 | 0.91559 | 29.87 | 343.15 | 0.92531 | 19.49 |
| 348.15 | 0.91261 | 25.00 | 348.15 | 0.92223 | 16.70 |
| 353.15 | 0.90962 | 21.10 | 353.15 | 0.91914 | 14.20 |

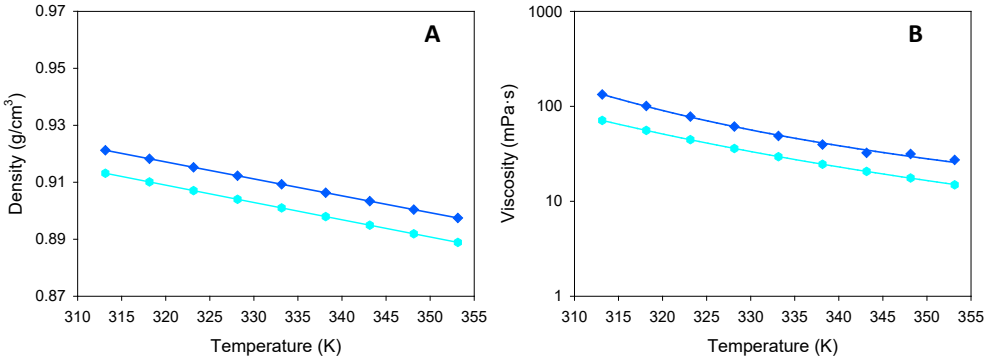


**Figure 3.40. Density (A) and viscosity (B) for mixtures [P4 4 4 4][OAc] + ethanol, with $x_{ethanol}$ = 0.20 (dark blue) and $x_{ethanol}$ = 0.40 (light blue). Solid lines correspond to the fits provided by equations 3.12 and 3.13 (see fit parameters in Table 3.6).**

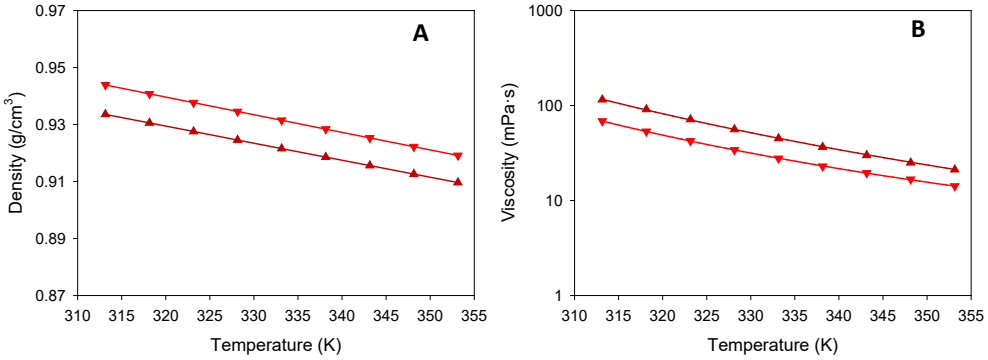


**Figure 3.41. Density (A) and viscosity (B) for mixtures [P4 4 4 4][OAc] + DMSO, with $x_{DMSO}$ = 0.20 (dark red) and $x_{DMSO}$ = 0.40 (light red). Solid lines correspond to the fits provided by equations 3.12 and 3.13 (see fit parameters in Table 3.6).**

**Table 3.6.** Parameters for the correlation of density (with equation 3.12) and viscosity (with equation 3.13), as a function of absolute temperature $T$ (in K), in the temperature range from 313.15 K to 353.15 K, for the pretreatment liquids based on the combination of [P4 4 4 4][OAc] with [P4 4 4 4]Cl, [P4 4 4 4]Br, ethanol, or DMSO.[a,b]

| Pretreatment liquid | $a$ | $b \times 10^4$ | $c \times 10^8$ | $A \times 10^4$ | $k$ | $T_0$ |
|---|---|---|---|---|---|---|
| [P4 4 4 4][OAc] + [P4 4 4 4]Cl, $x_{[P4444][OAc]}$ = 0.50 | 0.95287 | -5.6751 | - | 8.325 | 1524 | 173.3 |
| [P4 4 4 4][OAc] + [P4 4 4 4]Br, $x_{[P4444][OAc]}$ = 0.70 | 0.98721 | -5.9114 | - | 266.1 | 631.3 | 220.0 |
| [P4 4 4 4][OAc] + ethanol, $x_{ethanol}$ = 0.20 | 0.94535 | -6.0659 | 10.099 | 411.4 | 427.1 | 231.2 |
| [P4 4 4 4][OAc] + ethanol, $x_{ethanol}$ = 0.40 | 0.93765 | -6.1516 | 7.1645 | 28.76 | 1009 | 173.8 |
| [P4 4 4 4][OAc] + DMSO, $x_{DMSO}$ = 0.20 | 0.95747 | -5.9827 | - | 8.352 | 1471 | 149.2 |
| [P4 4 4 4][OAc] + DMSO, $x_{DMSO}$ = 0.40 | 0.96862 | -6.1860 | - | 45.52 | 842.8 | 188.2 |

[a] *Units of the parameters: a, g·cm$^{-3}$; b, g·cm$^{-3}$·K$^{-1}$; c, g·cm$^{-3}$·K$^{-2}$; A, mPa·s·K$^{-0.5}$; k, K; $T_0$, K.*

[b] *Parameter c is only displayed in those cases in which the quadratic term of the fit equation was found statistically significant by means of the F test.*

### 3.3.2.2. Pretreatment experiments: crystallinity reduction

Besides the evidence from direct visual observation, the non-dissolving character of the pretreatments to be investigated was confirmed by optical microscopy. Figure 3.42 shows microscope photographs of mixtures where Avicel and the pretreatment liquid were combined in a ratio of 0.5:100 (w/w) and stirred vigorously for 24 h at the corresponding pretreatment temperature. The presence of undissolved material in all cases (although with evident reduction of the size of the observable particles in some cases) indicates that the solubility of Avicel in the tested pretreatment fluids is lower than 0.5 g of cellulose per 100 g of fluid. Thus, the assumption of non-dissolving pretreatment was validated.

The PXRD diffractograms of the Avicel samples pretreated with the different liquid systems at the selected temperatures are shown in Figure 3.43, where the diffractogram of untreated Avicel is also shown for comparison. For the Avicel sample pretreated with pure [P4444][OAc] (at 343.2 K), a decrease in the intensity of the crystalline peaks is observed with respect to the Avicel sample with no pretreatment. The associated *CI* values are listed in Table 3.7, indicating a decrease from 51 % for the untreated sample to 46 % for the pretreated Avicel.

**Table 3.7.** Crystallinity index (*CI*), degree of polymerisation (*DP*), and 5 % onset decomposition temperature ($T_{d,5\%onset}$) for the samples of Avicel pretreated with the indicated liquids at the corresponding temperatures *T*.

| Pretreatment fluid | *T* (K) | *CI* (%) | *DP* | $T_{d,5\%onset}$ (K) |
|---|---|---|---|---|
| No pretreatment | — | 51 | 221 | 564 |
| [P4444][OAc] | 343.2 | 46 | 204 | 566 |
| [P4444][OAc] + [P4444]Cl, 50:50 mol/mol | 313.2 | 52 | 210 | 567 |
| | 343.2 | 50 | 212 | 560 |
| [P4444][OAc] + [P4444]Br, 70:30 mol/mol | 313.2 | 51 | 210 | 568 |
| | 343.2 | 51 | 211 | 570 |
| [P4444][OAc] + ethanol, $x_{ethanol}$ = 0.20 | 323.2 | 44 | 210 | 540 |
| | 343.2 | 46 | 209 | 543 |
| [P4444][OAc] + ethanol, $x_{ethanol}$ = 0.40 | 323.2 | 45 | 213 | 547 |
| | 343.2 | 48 | 212 | 562 |
| [P4444][OAc] + DMSO, $x_{DMSO}$ = 0.20 | 323.2 | 29 | 207 | 541 |
| | 343.2 | 20 | 202 | 544 |
| [P4444][OAc] + DMSO, $x_{DMSO}$ = 0.40 | 323.2 | 23 | 210 | 540 |
| | 343.2 | 28 | 211 | 548 |

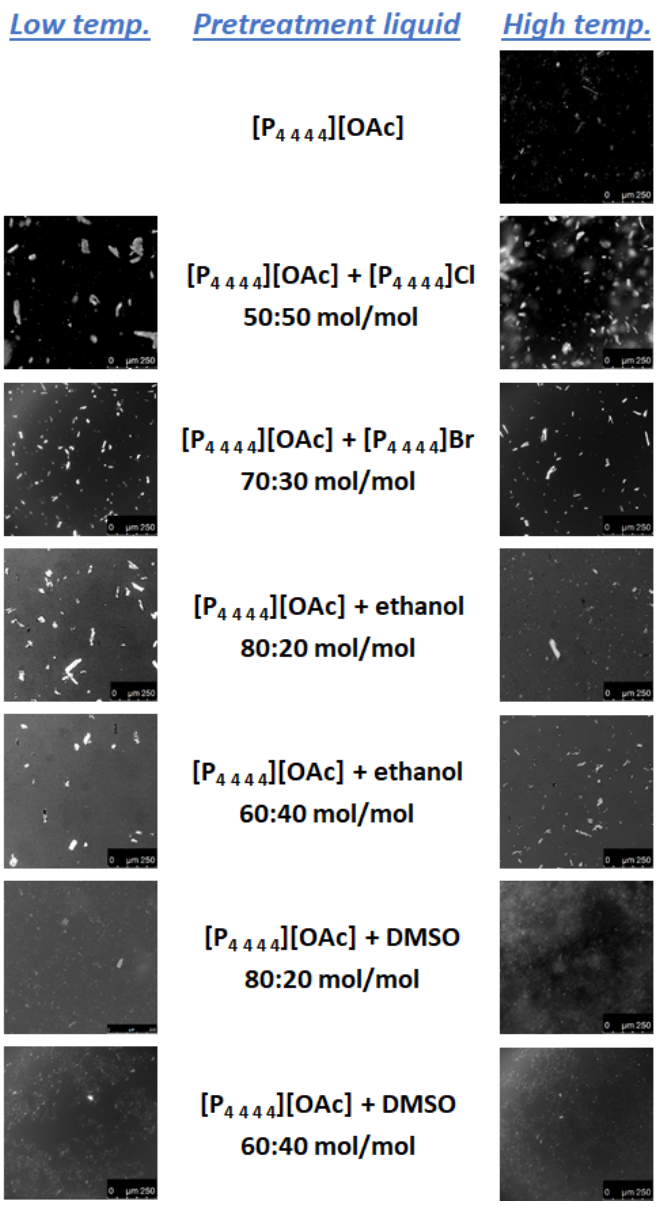


Figure 3.42. Microscope images, at a magnification of 20×, of mixtures of Avicel and pretreatment liquid in the ratio 0.5:100 (w/w), after vigorous stirring for 24 h at constant temperature. Photographs in column "*High temp.*" correspond to pretreatment temperature of 343.2 K; whereas photographs in column "*Low temp.*" correspond to pretreatment temperature of 313.2 K for the eutectics of [P4 4 4 4][OAc] + [P4 4 4 4]Cl and [P4 4 4 4][OAc] + [P4 4 4 4]Br, or 323.2 K for the mixtures of [P4 4 4 4][OAc] + (ethanol or DMSO).

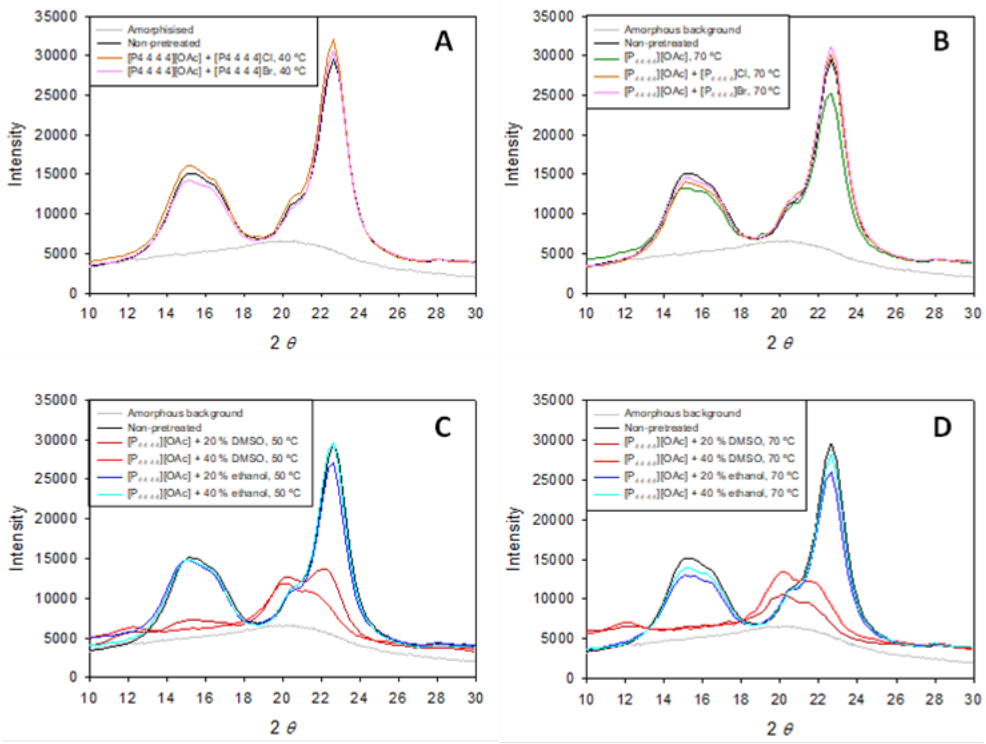


**Figure 3.43. PXRD diffractograms of samples pretreated at 313.2 K (plot A) or 343.2 K (plot B) with pure [P4444][OAc] (green line) or its eutectic mixtures with [P4444]Cl (orange line) and [P4444]Br (pink line); and at 323.2 K (plot C) or 343.2 K (plot D) with mixtures of [P4444][OAc] + ethanol with $x_{ethanol}$ = 0.20 (dark blue line) or $x_{ethanol}$ = 0.40 (light blue line), or with mixtures of [P4444][OAc] + DMSO with $x_{DMSO}$ = 0.20 (dark red line) or $x_{DMSO}$ = 0.40 (light red line). The diffractogram of non-pretreated Avicel cellulose (black line) is also shown in all plots as reference, as well as the diffractogram of the totally amorphised Avicel (grey line).**

Regarding the eutectic mixtures of phosphonium ionic liquids, none of their pretreatments (either at 313.2 K or at 343.2 K) caused a significant variation of the crystallinity with respect to the untreated Avicel, as evidenced in Figure 3.43AB, and also numerically by the corresponding *CI* values in Table 3.7. Besides the reduction in the intensity of the basicity caused by the partial replacement of acetate anions with halide anions (and therefore the reduction in the ability to interact with the hydroxyl groups of cellulose), another possible contributing factor to this lack of crystallinity reduction in the pretreatment could be the much higher viscosity of the eutectic mixtures at the investigated temperatures, as compared to the viscosity of pure [P4444][OAc] (see Tables 3.3 and 3.5). Such viscosity might hamper the necessary

mobility for interaction between the ions of the pretreatment liquid and the cellulose structures.

The PXRD diffractograms of the Avicel samples pretreated with the mixtures [$P_{4444}$][OAc] + (ethanol or DMSO) can be seen in Figure 3.43CD. The diffractograms of the pretreatments with [$P_{4444}$][OAc] + ethanol exhibit the same pattern of those pretreatments with integrally ionic fluids. The degree of crystallinity reduction achieved in these cases is similar to that obtained in the pretreatment with pure [$P_{4444}$][OAc], with the corresponding *CI* values listed in Table 3.7 showing a slightly larger decrystallisation effect in the pretreatments at 323.2 K. Regarding the [$P_{4444}$][OAc] + DMSO mixtures, a strong reduction of the areas under the signals can be observed, evidencing a remarkable decrease in the cellulose crystallinity. Moreover, a shift in the peaks is produced, from signals characteristic of the native Cellulose I crystalline structure (e.g. at 22.5°) to signals corresponding to the more thermodynamically stable Cellulose II crystalline structure (e.g. the region 20-21.5°) (Wu et al., 2018), similarly to what was described in section 3.3.1.3 for pretreated MCC samples with these pretreatment liquids. Despite the evidence of this allomorphic transformation, solubility tests revealed a solubility lower than 0.5 g per 100 g of pretreatment fluid for either of the investigated mixtures of [$P_{4444}$][OAc] and DMSO. The optical microscope photographs for such solubility tests in Figure 3.42 show undissolved particles after 24 h at the pretreatment temperature; however, it is clear that these particles are less and smaller in the mixtures with DMSO than in the other liquid systems tested. Therefore, it may be possible that the transformation of Cellulose I to Cellulose II exists as the result of a dynamic equilibrium of solubilisation of cellulose in the [$P_{4444}$][OAc] + DMSO pretreatment fluids, although keeping the overall solubility at levels that preserve the general non-dissolving character of the pretreatment at macroscopic scale.

The special performance of [$P_{4444}$][OAc] + DMSO in reducing the crystallinity of the Avicel sample should be attributed to the capacity of the polar aprotic solvent to disrupt the ionic association of [$P_{4444}$][OAc], thereby releasing more free ions through the solvation of cations and anions, without penalising the ability of these solvated ions to interact with cellulose, mainly by hydrogen bonding (Zhang et al., 2021). The known cellulose swelling ability of DMSO may enable an initial cellulose swelling step, enhancing the accessibility of [$P_{4444}$][OAc] to cellulose and therefore facilitating the

subsequent decrystallisation and allomorphic transformation (Zhang et al., 2021), in a similar fashion to what has been reported for the dissolution of cellulose in mixtures of tetrabutylammonium acetate and DMSO (Huang et al., 2016; Song et al., 2018).

The strong reduction of the crystallinity of Avicel in the pretreatment with the [P4444][OAc] + DMSO mixtures is obviously reflected in the remarkably lower *CI* values displayed in Table 3.7 for these cases. Interestingly, a different trend of *CI* with the pretreatment temperature is observed for the mixture with $x_{DMSO}$ = 0.20 (*CI* decreases from 29 % for the pretreatment at 323.2 K to 20 % for the pretreatment at 343.2 K) and the mixture with $x_{DMSO}$ = 0.40 (*CI* increases from 23 % for the pretreatment at 323.2 K to 28 % for the pretreatment at 343.2 K). These opposed trends are likely the result of a balance between two factors: the interaction forces (mainly hydrogen bonding) of the pretreatment liquid with the cellulose chains to modify their three-dimensional structure, which weaken with an increase in temperature; and the fluidicity (i.e., the inverse of the viscosity) of the pretreatment fluid, which facilitates the mass transfer stages in the mechanism of decrystallisation, and increases with increasing temperature. As observed in Table 3.5, the viscosities of the [P4444][OAc] + DMSO mixtures at 323.2 K are practically double than their values at 343.2 K. In the case of the mixture with a composition $x_{DMSO}$ = 0.20, the increased transport barrier is likely having a stronger overall effect in the pretreatment process than the enhancement of the hydrogen bonding interaction as a result of the lower temperature; with the contrary applying to the mixture with composition $x_{DMSO}$ = 0.40.

The preservation of the length of the polymeric chains and of the thermal stability are aspects of interest for a number of cellulose applications. The corresponding values of *DP* and $T_{d,5\%onset}$ (used herein as a numerical indicator of the thermal stability) for the Avicel samples resulting from the different pretreatments are listed in Table 3.7 (and the TGA thermograms from which the $T_{d,5\%onset}$ values were obtained are included in Figures C.1 to C.8 in Appendix C). Despite the important *CI* variations commented throughout this section, the described pretreatments led to only a small *DP* reduction of ca. 5-10 % with respect to the raw Avicel. Regarding the thermal stability, all the $T_{d,5\%onset}$ values of the pretreatments with integrally ionic fluids lie within ±2 % of the value of the untreated Avicel, thus implying a negligible effect in the thermal stability of the cellulosic material. For the pretreatments with mixtures of [P4444][OAc] and a molecular solvent, a small decrease in $T_{d,5\%onset}$ is systematically

observed, never larger than ca. 8 % (the lowest $T_{d,5\%onset}$ value being 540 K), and therefore it can still be considered that, for most practical purposes, the thermal stability of the pretreated Avicel is well preserved.

### 3.3.2.3. Proof of improved reactivity: kinetics of enzymatic hydrolysis

The kinetic curves of the enzymatic hydrolysis of the pretreated Avicel samples, as well as of untreated Avicel, are shown in Figure 3.44. All hydrolyses of the pretreated samples occurred faster than that of untreated Avicel, thus indicating an improvement in the reactivity conferred by the pretreatment stage. The fastest hydrolyses corresponded to the Avicel samples pretreated with [$P_{4444}$][OAc] + DMSO mixtures, for which the largest reduction in crystallinity was observed (see section 3.3.2.2). Interestingly, there is a good correspondence of the *CI* values obtained for the Avicel samples pretreated with these [$P_{4444}$][OAc] + DMSO mixtures (see Table 3.7) and their rate of enzymatic hydrolysis: the fastest hydrolysis of the samples pretreated at 323.2 K corresponds to pretreatment with the mixture with $x_{DMSO}$ = 0.40, whereas for the samples pretreated at 343.2 K, it corresponds to pretreatment with the mixture with $x_{DMSO}$ = 0.20 (Figure 3.44CD).

Expanding the exploration of a relation between the *CI* of Avicel samples and their enzymatic hydrolysis kinetics to the entire set of samples investigated herein, and in analogy to what was done in section 3.3.1.4, the plot in Figure 3.45 was built. In it, a reasonably linear trend can be observed (albeit with substantial scattering in the region of high crystallinity – see comments below) for different fixed hydrolysis times. This is in line with previous reports in the literature that relate cellulose crystallinity with its proneness to react (Hall et al., 2010; Li et al., 2014). Nevertheless, the correlation shown in Figure 3.45 does not intend to neglect the relevance of other factors that have to necessarily have an influence on the reactivity of the pretreated samples, particularly in the high crystallinity domain. For example, for the Avicel samples pretreated with the eutectics of [$P_{4444}$][OAc] + [$P_{4444}$]Cl and [$P_{4444}$][OAc] + [$P_{4444}$]Br, a certain improvement of the rate of enzymatic hydrolysis can be observed with respect to untreated Avicel (Figure 3.44AB), despite the inability of the corresponding pretreatments to induce any crystallinity reduction (Table 3.7). In a similar vein, the

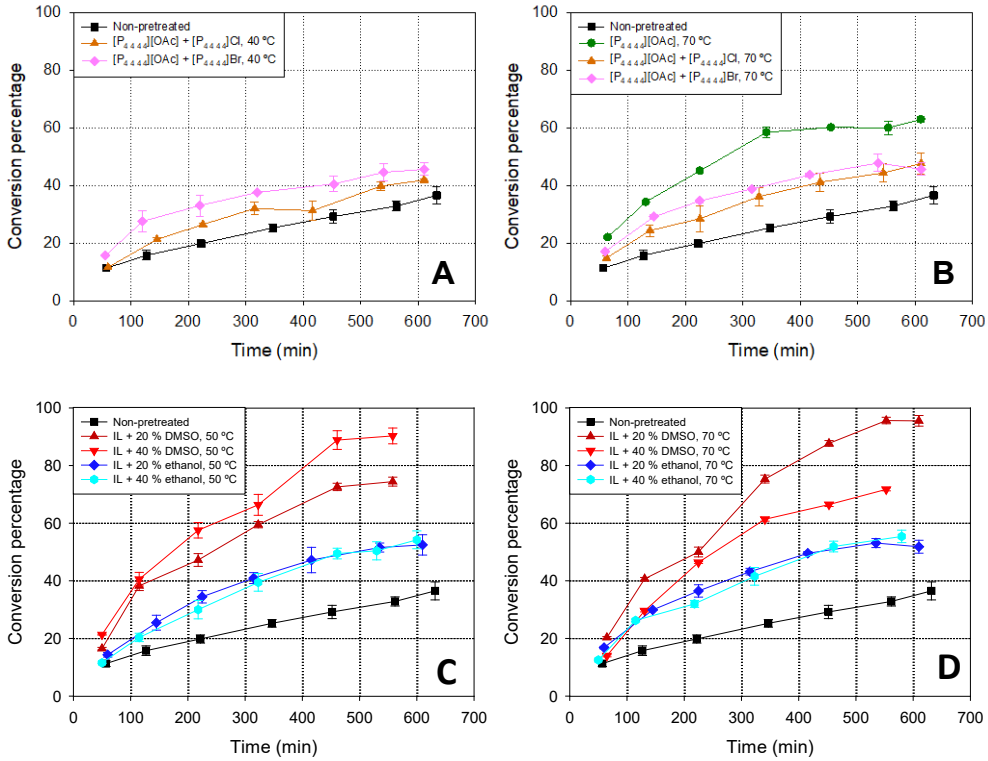


**Figure 3.44. Evolution with time of the percentage of conversion of cellulose into glucose in the reaction of enzymatic hydrolysis of the Avicel samples pretreated at 313.2 K (plot A) or 343.2 K (plot B) with pure [P4444][OAc] (green circles) or its eutectic mixtures with [P4444]Cl (orange triangles) and [P4444]Br (pink diamonds); and at 323.2 K (plot C) or 343.2 K (plot D) with mixtures of [P4444][OAc] (IL) + ethanol with $x_{ethanol}$ = 0.20 (dark blue diamonds) or $x_{ethanol}$ = 0.40 (light blue hexagons), or with mixtures of [P4444][OAc] (IL) + DMSO with $x_{DMSO}$ = 0.20 (dark red triangles) or $x_{DMSO}$ = 0.40 (light red inverted triangles). The corresponding curve for the hydrolysis of untreated Avicel (black squares) is also shown in all plots as a reference. Lines are a guide to the eye.**

hydrolyses of the samples pretreated with the [P4444][OAc] + ethanol mixtures proceeded somewhat slower than that of the sample pretreated with pure [P4444][OAc], in spite of a practically equivalent *CI* value. For this sample preteated with pure [P4444][OAc] it can be finally noted that, although the reduction in *CI* was rather moderate (from 51 % down to 46 %), the conversion percentage in its hydrolysis roughly duplicated that of untreated Avicel for any given time in the range tested.

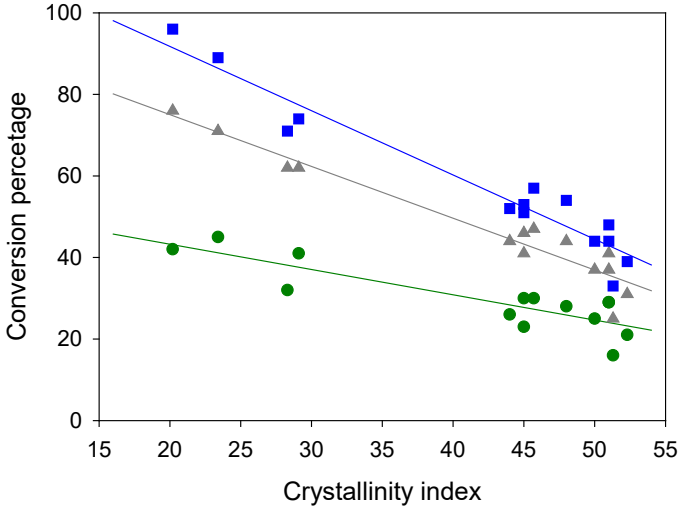


**Figure 3.45. Extension of the enzymatic hydrolysis of Avicel cellulose samples as a function of their crystallinity index, for selected reaction times: 150 min (green, circles), 350 min (grey, triangles), and 550 min (blue, squares). Conversion values at the specified times were obtained as linear interpolations in the respective hydrolysis time courses. Lines correspond to the best linear fit for each series.**

### 3.3.2.4. Application to cellulose carboxymethylation

Carboxymethylcellulose (CMC) is one of the most attractive cellulose-derived products due to its numerous fields of application: oil recovery drilling fluids, adhesives, coatings, detergents, and importantly the food, cosmetics, and pharma sectors (Majewicz and Podlas, 2000; Thielking and Schmidt, 2006). Such versatility is due to the thickening and gelling properties imparted by CMC salts to aqueous media, allowing rheology control at low cost and with little toxicity and remarkable biodegradability. The process of production of Na-CMC involves a first activation treatment of cellulose under strongly alkaline conditions with an excess of base (generally NaOH), followed by alkylation with chloroacetate at temperatures typically above 318-323 K (45-50 °C) in a heterogeneous regime with the cellulose suspended in a fibrous state in an intermediate-polarity alcohol (most commonly, 2-propanol) (Kono et al., 2016). Moreover, excess of base above 0.8 equivalents with respect to anhydroglucose units is typical, and hence, post-synthesis neutralisation of significant residual $[OH]^-$ is required (Klug and Tinsley, 1950; Thielking and Schmidt, 2006).

In view of the improved reactivity imparted by the pretreatments investigated (see section 3.3.2.3), a simplified and milder process for the preparation of Na-CMC from Avicel cellulose was investigated, avoiding the alkaline activation stage as well as the excess of base, and using a low reaction temperature – namely 313.2 K (40 °C). The samples pretreated at 343.2 K with [P4444][OAc] (*CI* = 46 %) and with the mixture of [P4444][OAc] + DMSO with $x_{DMSO}$ = 0.20 (*CI* = 20 %) were specifically selected for this study, together with untreated Avicel (*CI* = 51 %) for comparison. After a typical reaction time of 3 h, *DS* correlated inversely with *CI* of the feedstock, as it could be expected. The results are shown in Figure 3.46, whereas the ATR-FTIR spectra used for the calculation of the numerical *DS* values are displayed in Figure 3.47. Although even for the untreated Avicel its *DS* = 0.76 falls in the range of 0.7-1.22 which is industrially accepted for the use of CMC as thickening or gelling agent, it is worth noting that only 12 % of the initial $[OH]^-$ did not result in carboxymethylation for the sample pretreated with [P4444][OAc] + DMSO (*DS* = 0.88). This is an important fact since free $[OH]^-$ is known to promote the unproductive side reaction involving chloroacetate conversion into glycolate, and if unreacted, hydroxide must be neutralised prior to isolation of CMC (Klug and Tinsley, 1950; Thielking and Schmidt, 2006). This *DS* value of 0.88 obtained

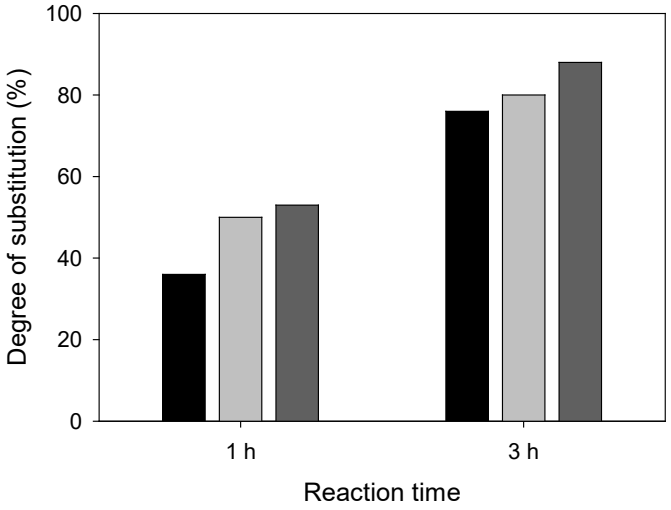


**Figure 3.46. Degree of substitution (*DS*) in the carboxymethylation of untreated Avicel (black columns) and of Avicel samples pretreated with pure [P4444][OAc] (light grey columns) or with a mixture of [P4444][OAc] + DMSO with $x_{DMSO}$ = 0.20 (dark grey columns), after reaction times of 1 h and of 3 h.**

for Avicel in just 3 h at 313.2 K without excess of NaOH is comparable, for example, to that of 0.89 reported by Klug and Tinsley (1950) for the preparation of CMC from chemically purified cotton linters under clearly harsher conditions (representative of the industrial state-of-the-art): pre-activation with NaOH in a 4-hour reaction at 328.2 K with NaOH excess of 103 mol% with respect to the anhydroglucose units.

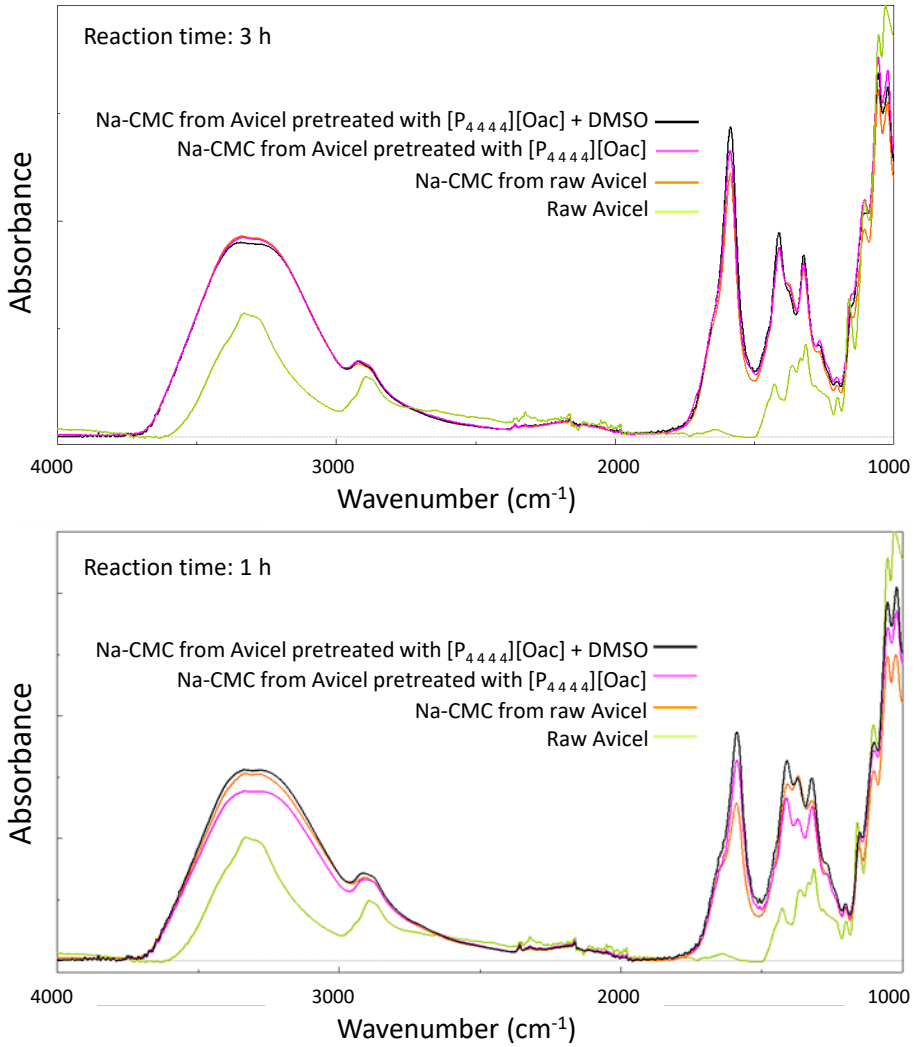


**Figure 3.47. ATR-FTIR spectra of sodium carboxymethylcellulose (Na-CMC) samples prepared after a reaction time of 3 h (top plot) or 1 h (bottom plot), from untreated Avicel or from Avicel pretreated with pure [P4444][OAc] or with a mixture of [P4444][OAc] + DMSO ($x_{DMSO}$ = 0.20). The spectrum of raw Avicel is also included for comparison. The extent of carboxymethylation can be observed by the increasing signal at ca. 1590 cm$^{-1}$. Normalisation of absorbance was performed at the area of ATR artifacts (ca. 2150 cm$^{-1}$) for a more realistic comparison.**

Shortening the reaction time to 1 h, the results (see also Figure 3.46 and, complementarily, Figure 3.47) show a more marked difference between the *DS* achieved with the untreated Avicel (0.36) and those of the pretreated samples (≥0.50). A *DS* = 0.53 for the sample pretreated with [$P_{4444}$][OAc] + DMSO represents, in fact, an improvement of 47 % in the substitution efficiency with respect to the untreated Avicel. Interestingly, the *DS* values achieved in this short 1-hour reaction time for the pretreated Avicel samples, and especially for that of lower crystallinity pretreated with the mixture of [$P_{4444}$][OAc] + DMSO, lie in the range of 0.5-0.6 at which Na-CMC becomes water-soluble, depending on substitution distribution (Kono et al., 2016; Thielking and Schmidt, 2006); and therefore they might already exhibit favourable gelling properties.

# 4. VALORISATION OF TECHNICAL LIGNIN WITH AQUEOUS MEDIA INVOLVING [$C_2$mim][OAc]

The content of this chapter has been submitted for publication as:

- C. A. Pena[a,b], L. F. Ballesteros[a], H. Rodríguez[b], E. Rodil[b], J. A. Teixeira[a], M. Michelin[a].
[a]Centre of Biological Engineering, University of Minho, Campus de Gualtar, 4710-057 Braga, Portugal. [b]CRETUS, Department of Chemical Engineering, Universidade de Santiago de Compostela, E–15782 Santiago de Compostela, Spain.
"Laccase-mediator system for the ionic liquid-assisted treatment of a technical lignin with partial dissolution". Submitted.

- C. A. Pena[a], E. Rodil[a], H. Rodríguez[a].
[a]CRETUS, Department of Chemical Engineering, Universidade de Santiago de Compostela, E–15782 Santiago de Compostela, Spain.
"Lignin depolymerisation with aqueous solutions of the ionic liquid 1-ethyl-3-methylimidazolium acetate". Submitted.

# VALORISATION OF TECHNICAL LIGNIN WITH AQUEOUS MEDIA INVOLVING [$C_2$mim][OAc]

## 4.1. Motivation

Processes for the efficient valorisation of lignin under mild conditions have enormous potential in the configuration of new transformative schemes of this aromatic biopolymer within the context of integral and truly sustainable biorefineries. The degree of success of these processes, however, is still rather limited at present, and a clear need for their improved development exists. Moreover, many of the investigations related to processes of this kind, such as enzymatic depolymerisation, have been performed using lignin samples with a high degree of sulfonation, which show good solubility in water over the entire pH range (Saake and Lehnen, 2012). Although this solubility imparted by the sulfonate substituents is interesting for some direct applications of these highly sulfonated lignins (or lignosulfonates), it must be taken into account that it does not reflect the behaviour of native lignin. Lignosulfonates are obtained from sulfite pulping, or by means of a sulfonation stage of lignins produced by other pulping processes. The reduced share of the sulfite process in the pulping market and the negative contribution of the sulfonation stage from a sustainability perspective invite to prefer the utilisation of non- or poorly-sulfonated lignins (hence with limited solubility in water at common pH values) in the development of lignin valorisation processes aimed to hold a relevant position in the market of lignin-derived products. In this regard, Indulin AT is the trade name of a technical lignin originally marketed by the company MeadWestvaco Specialty Chemicals, which derives from *kraft* pulping and presents a low degree of sulfonation (Saake and Lehnen, 2012). Thus, it may represent a better lignin model, from the point of view of future practical application at large scale, to be used in research for the development of lignin valorisation processes.

Given the appealing set of characteristics of ionic liquids for their use as auxiliary liquids in potentially greener processes (Freemantle, 2010), and the identification of their potential to act as both solvents and catalysts in the depolymerisation of lignin (Chatel and Rogers, 2014; Prado et al., 2016), one first possibility to explore for the depolymerisation of lignin using very mild conditions is the treatment of lignin directly

at ambient temperature and pressure with a liquid system based on an ionic liquid. The selection of 1-ethyl-3-methylimidazolium acetate ([$C_2$mim][OAc]) may be appropriate, as this is an archetypal ionic liquid in the pretreatment and dissolution/fractionation of lignocellulosic biomass, exhibiting also a remarkably high lignin dissolution capacity (Castro et al., 2014; Geniselli da Silva, 2021; Li et al., 2021; Radhakrishnan et al., 2021). Moreover, it presents other appealing attributes, such as reasonably good thermal stability, liquid character down to far below room temperature, good biocompatibility, and low toxicity (Freire et al., 2011; Geniselli da Silva, 2021; Leitch et al., 2020; Singer et al., 2011). There are some works in the literature exploring the use of this ionic liquid for the depolymerisation of lignin (Dutta et al., 2017; Li et al., 2021; Ninomiya et al., 2018; Singh et al., 2019), but the conditions applied were quite harsh. In applying ambient temperature and pressure, the problem may be the viscosity if using [$C_2$mim][OAc] pure. To avoid this issue, the mixing of the ionic liquid with water may be an option (Queirós et al., 2020). Besides a reduction in the viscosity of the liquid system, thus palliating potential problems in pumping and mass transfer, the combination of [$C_2$mim][OAc] with water will enable the modulation of the lignin solubility capacity of the resulting solution (Manna et al., 2021). In assisting the performance of the aqueous [$C_2$mim][OAc], UV irradiation in combination with nanoparticles, and optionally in the presence of a well known oxidant agent such as $H_2O_2$ (Chang et al., 2018), can be also explored fo the depolymerisation of lignin via nanoparticle-catalysed photoreaction (Colmenares et al., 2017; Li et al., 2015; Sun et al., 2018).

An alternative method, also involving mild conditions in aqueous media, consists of the utilisation of a biocatalyst, for example laccase, a popular enzyme for the transformation of lignin. A recombinant laccase may help to improve the performance of the enzyme on the lignin substrate. Besides genetic engineering tools, the participation of a mediator may also facilitate the action of the enzyme on the substrate. A popular choice as mediator in laccase-mediator systems is 2,2'-azino-bis(3-ethylbenzothiazoline-6-sulfonic acid), commonly abbreviated as ABTS (Feng et al., 2019; Shin et al., 2019). In general, the investigation of laccase-mediator systems of this kind for processing lignins with a low sulfonation degree (and hence with limited solubility in the aqueous medium) remains unexplored, despite their potential to lead to lignin valorisation processes with improved green credentials. One last agent to be

investigated towards a reinforcement of the treatment action of the liquid system on lignin is the participation of an ionic liquid as additive, for example the above-mentioned [C2mim][OAc]. This water-miscible ionic liquid is reasonably compatible with enzymes and, although it is known to induce a reduction in laccase activity (Harwardt et al., 2014; Stevens et al., 2019), this reduction can be compensated by its action as an adjuvant in the improvement of lignin treatment with a laccase-mediator system (Geniselli da Silva, 2021; Itoh and Takagi, 2021). It is worth to remind, at this point, that [C2mim][OAc] has an outstanding lignin dissolution capacity (Castro et al., 2014).

In the dissolution and fractionation of lignocellulosic materials with an adequate ionic liquid (e.g. [C2mim][OAc]), the potential build-up of lignin in the ionic liquid due to incomplete precipitation upon addition of an antisolvent (typically water or an aqueous mixture of solvents) represents a significant problem in the scalability and continuous operation of such fractionation strategies in a context of the real application (Rodríguez, 2021). With this in mind, the [C2mim][OAc]-containing liquid systems proposed herein (see the paragraphs above) for the treatment of lignin can be also understood as an approach to overcome the build-up issue by direct modification of lignin in the aqueous medium, subsequently followed by facilitated removal of the corresponding products from the ionic liquid medium (Castro et al., 2014; Rodríguez, 2021).

# 4.2. Experimental

## 4.2.1. Materials

Indulin AT, a technical pine *kraft* lignin commercialised by MeadWestvaco, was used as received. Its degree of sulfonation was measured by X-ray spectrometry in an Oxford Instruments Lab-X3500S spectrometer (Figure 3.14), resulting in a sulfur content of 2.1 %, lower than for other popular technical lignins.

The ionic liquid [C2mim][OAc] was purchased from Iolitec with a nominal purity >95 %. Prior to use, it was subjected to high vacuum (an absolute pressure of ca. 1 Pa) while magnetically stirred at ca. 343 K for a minimum of 48 h, for elimination of potential volatile impurities. After this purification step, the preservation of the

chemical identity of the ionic liquid, as well as the absence of organic impurities at relevant levels, was verified by $^{1}H$ and $^{13}C$ NMR spectroscopy (spectra available as Figures A.7 and A.8 in Appendix A). Its water content was lower than 0.05 wt%, as measured by Karl Fischer titration in a Metrohm 899 coulometer (Figure 3.2). Due to this low water content, it was neglected in the calculation for the preparation of aqueous solutions of this ionic liquid.

Titanium oxide ($TiO_2$) nanoparticles were supplied by Aldrich with a nominal purity >99.5 %. A particle size range of 20-50 nm was ascertained by transmission electron microscopy (TEM) analysis. Their crystalline structure was identified as anatase by means of X-ray diffraction (XRD). Silver chloride (AgCl) nanoparticles were synthesised from the bulk solid (Sigma-Aldrich, 99 %) following the procedure described by Rodríguez-Cabo et al. (2015). The range of their particle size, measured by TEM, was 5-20 nm, and the crystalline structure obtained by XRD was chlorargyrite. TEM photographies and XRD patterns for these nanoparticles are presented in Figure 4.1. TEM images were performed using a Philips CM-12 microscope with a Mega View Docu-II camera and an IMAX image analysis software SIS NT, whereas XRD patterns were acquired in an X-ray Philips powder diffractometer (Figure 3.14) operated by a PW 1710 control unit, with a Cu-Kα X-ray source (λ = 1.54 Å).

Hydrogen peroxide (Sigma-Aldrich, 30 % w/w) was diluted to the desired concentration by addition of water.

Acetic acid, sodium acetate, and 2,2′-azino-bis(3-ethylbenzothiazoline-6-sulfonic acid) diammonium salt (ABTS) were supplied by Sigma-Aldrich with nominal purities >99.5 %, >99 %, and >98 %, respectively. Molecular oxygen was supplied as compressed gas by Praxair with a purity of 99.5 %.

A commercial (recombinant) fungal laccase from the ascomycete *Myceliophthora thermophila* was supplied by Novozymes (code NS51003). The laccase activity of the enzyme extract was determined according to a slightly modified version of the procedure reported by Buswell et al. (1995), based on the monitoring of the oxidation reaction of the ABTS at 420 nm. First, the enzyme extract was diluted in 50 mM acetate buffer, pH 5.0 (made with acetic acid and sodium acetate), and then the reaction was

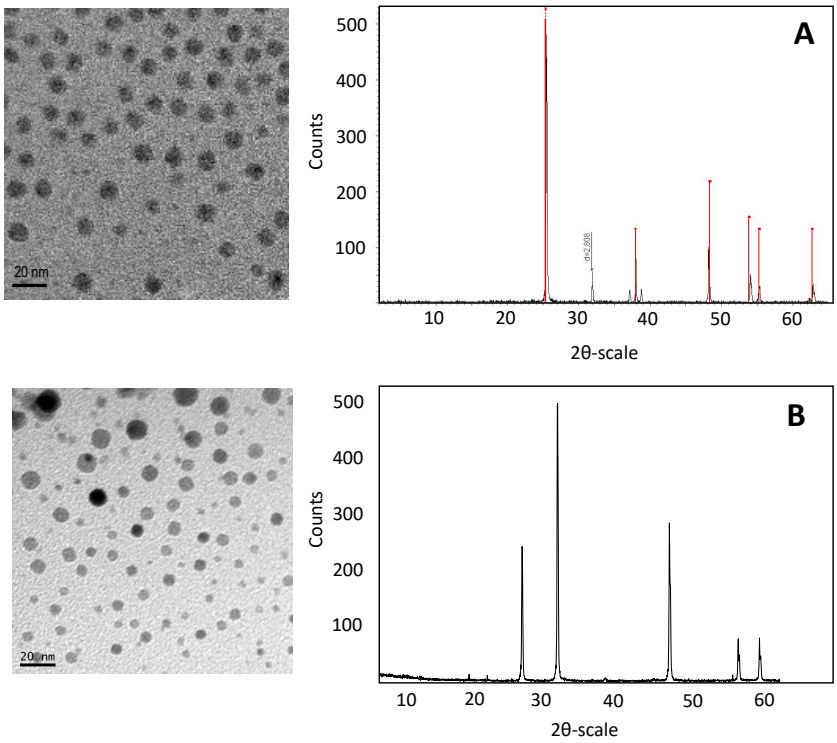


**Figure 4.1. TEM photographies (left column) and XRD patterns (right column) for $TiO_2$ nanoparticles (A) and AgCl nanoparticles (B).**

carried out at room temperature by adding 200 µL of the diluted enzyme to 2.0 mL of a a buffered ABTS solution (same buffer) to a final concentration of 1 mM in the assay. Mixing was done directly in a quartz cell placed in the measuring chamber of a Jasco V-560 UV-vis spectrophotometer (Figure 4.2), and absorbance measurements were recorded every 10 s during 1.5 min. The enzyme activity was found to be 945 U/mL, as calculated by the following expression:

$$Activity\ (\mathrm{U/L}) = \frac{\Delta E \times V_t}{\varepsilon \times l \times V_s} \times 10^6 \qquad (4.1)$$

where $\Delta E$ is the change in the extinction of light at 420 nm (in $min^{-1}$), $\varepsilon$ is the molar absorption coefficient of ABTS (in $M^{-1}{\cdot}cm^{-1}$), $l$ is the layer thickness that the light must pass in the cell (in cm), and $V_t$ and $V_s$ refer to the total volume of the assay and the volume of the enzyme, respectively. One enzymatic activity unit (U) was defined as the amount of enzyme required to oxidise 1 µmol of the substrate (ABTS) per minute at the assay reaction conditions.


Figure 4.2. Jasco V-560 spectrophotometer.

Gram-positive bacterium *Staphylococcus aureus* EG17 and Gram-negative bacterium *Escherichia coli* CECT 736 were obtained from the Centre of Biological Engineering collection of the University of Minho (Braga, Portugal).

Either bidistilled water or distilled + deionised water were used in all the experiments.

### 4.2.2. Treatment of lignin with aqueous solutions of [$C_2$mim][OAc]

Treatments of lignin in aqueous solutions of the ionic liquid [$C_2$mim][OAc] were carry out, at room temperature and atmospheric pressure, in Pyrex® tubes with an outside diameter of 16 mm and wall thickness of 1.8 mm. A solid load of 5 g of Indulin AT per 100 g of treatment fluid was systematically used, as well as magnetic stirring to facilitate an intimate contact between the lignin and the formulation. Two different concentrations of [$C_2$mim][OAc] were used in the treatments: either 10 % (w/w) or 70 % (w/w). Pure water (0 % of ionic liquid) was also used to establish a convenient reference case. Treatments with ionic liquid concentrations of 0 % and 10 % were executed with partial solubilisation, while the concentration of 70 % of [$C_2$mim][OAc] enabled a complete dissolution of the lignin load and required the addition of water as antisolvent (twice the volume of the treatment medium) to induce precipitation of the non-depolymerised fractions after the corresponding treatment time. In either case, the remaining solid materials were separated from the liquid phase by filtration, using

nylon filters with a pore diameter of 0.22 μm. Finally, the recovered solids were washed twice with water (10 mL each time).

For investigation of assistance of UV irradiation and/or nanoparticles in the treatments, a low-pressure mercury vapour lamp manufactured by UVP, model Pen-Ray 3SC-9 (Figure 4.3), was used as UV light source, with a maximum emission wavelength of 254 nm; and the $TiO_2$ and AgCl nanoparticles described in section 4.2.1 were used. Supplementation with hydrogen peroxide was also explored, adding in such cases $H_2O_2$ to the media about one minute before addition of the lignin for initiation of the treatments.

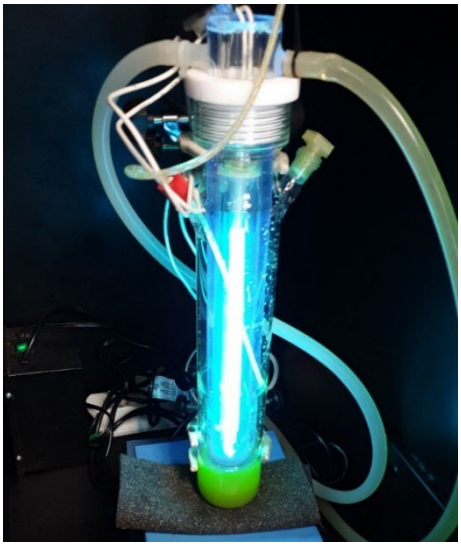

Figure 4.3. UVP Pen-Ray 3SC-9 low-pressure mercury vapour lamp, used as UV light source and shown here inside a cylinder-shaped Pyrex reactor.

In all experiments, the post-treatment aqueous phases obtained as filtrates and the washed solids recovered were analysed according to the descriptions provided in sections 4.2.4 and 4.2.5.

## 4.2.3. Treatment of lignin with laccase-based systems

For the treatment of lignin with the laccase-based systems, a solid load of 5 g of Indulin AT per 100 g of buffered aqueous medium was systematically used. Different buffered aqueous media were tested: a 0.1 M acetate buffer, pH 5.0 (treatment code 1), the same

buffer with a concentration of 25 mM ABTS mediator (treatment code 2), these two aforementioned treatments with oxygen pre-saturation (treatment codes 1O and 2O), and each of these media mixed in a 90:10 (w/w) ratio with the ionic liquid [$C_2$mim][OAc] (treatment codes 1-IL, 2-IL, 1O-IL, and 2O-IL). Both the lignin and the aqueous medium were placed in a glass Erlenmeyer flask and, in those cases including pre-saturation with oxygen, a stream of oxygen gas was bubbled for 30 min before the addition of the enzyme. An enzyme load of 25 U/$g_{lignin}$ was then added. Incubation was carried out at 298 K in a thermostated orbital shaker at ca. 150 rpm for 12 h, with monitoring of pH to ensure a maximum variation of ±0.1 units. After this time, the treatment was terminated by immersing the Erlenmeyer flask in boiling water for 20 min to denaturalise the enzyme. This time was precisely controlled to prevent different solubilisations or degradations of lignin induced by the high temperature at this stage. Control runs were performed in the absence of laccase, ABTS and oxygen pre-saturation, by subjecting the combination of lignin and acetate buffer (code Ctrl), or lignin and the mixture of buffer and [$C_2$mim][OAc] (code Ctrl-IL), to the same conditions described above, including the final step by immersion in boiling water. All treatments were carried out in triplicate.

In those experiments without ionic liquid, the separation of non-solubilised lignin from the reaction medium after treatment was carried out by simple centrifugation at 9000 rpm for 20 min in a Centurion Pro-Xtra3r refrigerated centrifuge (Figure 4.4). In treatments involving ionic liquid, filtration through an S3 sintered funnel in a Buchner flask under soft vacuum was performed. In either case, the aqueous phase (filtrate) was kept for subsequent analyses (see section 4.2.4), and the solids were washed with water twice, using 15 mL each time, to guarantee full removal of residual laccase and ionic liquid (if potentially present). Finally, the washed solids were dried by lyophilisation in a LaboGene CoolSafe 100-9 lyophiliser (Figure 4.5), and also subjected to subsequent characterisation, as described later in section 4.2.5.

***Enzyme stability***

The stability of the laccase over time was analysed under the treatment conditions indicated in this section. Briefly, the properly diluted enzyme extract was pre-incubated, at room temperature, with 0.1 M acetate buffer (pH 5.0) or a 90:10 (w/w)

Figure 4.4. Centurion Pro-Xtra3r refrigerated centrifuge.


Figure 4.5. LaboGene CoolSafe 100-9 lyophiliser.

mixture of 0.1 M acetate buffer and the ionic liquid [$C_2$mim][OAc]. Then, volumes of this mixture were taken at predetermined times during approximately 10 h, and the residual laccase activity was measured as already described in section 4.2.1.

## 4.2.4. Characterisation of the post-treatment aqueous phases

The characterisation of the aqueous phases obtained in the different treatments was focused on the identification and quantification of the phenolic compounds derived from the depolymerisation of lignin.

***Total phenolic content***

The concentration of total phenolic compounds in the aqueous phases was determined by means of a procedure adapted from that described by Makkar et al. (1993). According to this procedure, 0.5 mL of the conveniently diluted sample was mixed in test tubes with 0.25 mL of a 1 N aqueous solution of the Folin Ciocâlteu reagent, supplied by Sigma (Quality Level 100) with an original concentration of 2 N, and then 1.25 mL of a 20 % (w/w) solution of $Na_2CO_3 \cdot 10H_2O$ (Sigma-Aldrich, 99 %) was added. After 40 min of incubation at room temperature, the absorbance was recorded at 725 nm in a Biotek Cytation3 UV-visible spectrophotometer (Figure 4.6). The total


Figure 4.6. Biotek Cytation3 UV-visible spectrophotometer.

content of phenolic compounds was then obtained as equivalents of gallic acid, by means of the appropriate calibration curve (using anhydrous gallic acid purchased from Sigma with nominal purity >98 %).

***HPLC and UHPLC chromatography***

The aqueous samples obtained after the treatments of lignin with aqueous solutions of [C2mim][OAc] were analysed by high-performance liquid chromatography (HPLC) in an HP Series 1100 HPLC chromatograph equipped with an HP G1315A diode array detector (Figure 4.7). A Zorbax SB-C18 reversed-phase column (4.6 mm × 150 mm, 5 µm particle size) was used, together with a pre-column of the same kind, at 313 K. The injection volume was 4 µL, and the flow rate of the mobile phase was 1 mL/min. The HPLC-grade solvents used were aqueous 0.1 % formic acid (prepared from formic acid commercialised by Scharlau with nominal purity >98 %) as solvent A and acetonitrile (Supelco, >99.9 %) as solvent B. The elution gradient for solvent B was as follows: from minute 0 to 15, eluent B at 5 %; from minute 15 to 50, a linear increase to 60 %; from minute 50 to 55, a linear increase to 100 %; and concluding with a column recondition step consisting in a linear decrease to 5 % from minute 55 to 60, and remaining constant until minute 70. Phenolic compounds were identified by comparing their retention times and wavelengths of maximum absorbance peaks with several

Figure 4.7. HP Series 1100 HPLC chromatograph.

standards: benzyl phenyl ether (Aldrich, 98 %), catechin hydrate (Sigma-Aldrich, 98 %), chlorogenic acid (Sigma-Aldrich, >95 %), *trans*-cinnamic acid (Sigma-Aldrich, 99 %), *p*-coumaric acid (Sigma, ≥98 %), epicatechin (Sigma-Aldrich, 97 %), guaiacol (Sigma-Aldrich, 99 %), 4-hydroxybenzoic acid (Sigma-Aldrich, 99 %), isoeugenol (Aldrich, 98 %), (±)-naringenin (Aldrich, ≥95 %), quercetin dehydrate (Sigma-Aldrich, 98 %), syringaldehyde (Aldrich, 98 %), and vanillin (Sigma-Aldrich, 99 %).

The aqueous phases obtained after the treatments of lignin with laccase-based media were analysed by ultra-high-pressure liquid chromatography (UHPLC) in a Shimadzu Nexpera X2 UHPLC chromatograph equipped with a Shimadzu SPD-M20 A diode array detector (Figure 4.8). An Aquity UPLC BEH C18 reversed-phase column by Waters (2.1 mm × 100 mm, 1.7 μm particle size) was used, together with a pre-column of the same material, at 313 K. The injection volume was 1 μL, and the flow rate of the mobile phase was 0.4 mL/min. The HPLC-grade solvents used were aqueous 0.1 % formic acid (purchased from Fisher Chemical as an aqueous solution with a nominal purity of 98-100 %) as solvent A and acetonitrile (Fisher Scientific, ≥99.9 %) as solvent B. The elution gradient for solvent B was as follows: from minute 0.0 to 5.5, eluent B at 5 %; from minute 5.5 to 17.0, a linear increase to 60 %; from minute 17.0 to 18.5, a linear increase to 100 %; and column equilibration from minute 18.5 to 30.0 getting back through a linear decrease to 5 %. Phenolic compounds were identified by comparing their retention times with those of different standards, namely: caffeic acid (Sigma, >98 %), carvacrol (Sigma, 98 %), chlorogenic acid (Aldrich, 95 %), ellagic acid (Alfa Aesar, 97 %); *p*-coumaric acid (Sigma, >98 %), *p*-cymene (Sigma-Aldrich, 99 %), eugenol (Sigma, 99 %), ferulic acid (Sigma, ≥99 %), guaiacol (Sigma-Aldrich, 99 %), homovanillic acid (Sigma-Aldrich, >97 %), 3-hydroxytyrosol (Sigma-Aldrich, 98 %), methyl syringate (Sigma-Aldrich, product code S409448), naringenin (Sigma, >90 %); oleuropein (Sigma-Aldrich, >98 %), rosmarinic acid (Sigma, 96 %), syringaldehyde (Aldrich, 98 %), syringic acid (Sigma-Aldrich, ≥95 %), taxifolin (Sigma, >85 %), thymol (Sigma-Aldrich, ≥99 % ), tyrosol (Sigma-Aldrich, 98 % ), and vanillin (Sigma-Aldrich, 99 %).

Several wavelengths were evaluated, selecting for each compound the wavelength that offered the best resolution of its peak. Samples were run in triplicate, and the concentration results were expressed as average values after discarding possible outliers based on a statistical treatment at a 95 % confidence level.

Figure 4.8. Shimadzu Nexpera X2 UHPLC chromatograph.

### 4.2.5. Characterisation of the post-treatment recovered solids

In the characterisation of the solid samples recovered by filtration in the treatments, as well as of raw Indulin AT as a reference, different techniques were involved, as described below.

***NMR spectroscopy***

For analysis by two-dimensional $^{1}H$-$^{13}C$ heteronuclear single quantum coherence nuclear magnetic resonance (2D $^{1}H$-$^{13}C$ HSQC NMR) spectroscopy, aliquots of the solid samples were placed in 5-mm-diameter NMR tubes and dissolved with deuterated dimethyl sulfoxide (DMSO-$d_6$, provided by Sigma-Aldrich with a purity of 99 % and an atomic deuteration level of 99.5 D %). These tubes were charged in the spectrometer, where the procedure followed was similar to those previously reported in the literature by a number of authors (del Río et al., 2012; Feng et al., 2019; Kim and Ralph, 2010). An 11.7 T Bruker DRX-500 NMR spectrometer (Figure 4.9) operating at a frequency of

500 MHz for $^{1}H$, and equipped with a BBI probe with PFG gradient on the z-axis, was used to record the spectra at 300 K. The 2D $^{1}H$-$^{13}C$ HSQC NMR spectra were measured for each sample with the centre at 4.7 ppm and 100 ppm, and spectral widths of 11 ppm and 240 ppm, for the $^{1}H$ and $^{13}C$ dimensions respectively. The number of collected complex points was 2048 for the $^{1}H$ dimension, and 256 for the $^{13}C$ dimension. The spectra were acquired with a recycle delay ($d_1$) of 5 s and 64 scans per $t_1$ increment. The nominal value of $^{1}J_{CH}$ used for the INEPT periods was 140 Hz. The processing of the spectra was carried out with the software Mestrenova v.14.0, by Mestrelab Research Inc. Prior to application of the 2D Fourier transform, the FID files were apodised with a 90°-shifted sine-bell function in both dimensions and with line broadening of 8 Hz and 14 Hz for the $^{1}H$ and $^{13}C$ dimensions respectively. Then, they were zero-filled to 2048 and 512 points in the $^{1}H$ and $^{13}C$ dimensions, and subsequently the Fourier transformation was applied in both dimensions. Next, the spectra were phase-corrected and baseline-corrected in both dimensions, and finally subjected to a processing operation of $T_1$ noise reduction.

Figure 4.9. Bruker DRX-500 NMR spectrometer.

***Thermogravimetric analysis (TGA)***

The TGA analyses were carried out in a TA Instruments TGA Q500 thermogravimetric analyser (Figure 3.1), using flow rates of 40 mL/min and 60 mL/min of nitrogen gas (Nippon Gases, 99.999 %) as balance purge gas and sample purge gas, respectively. An amount of ca. 2-15 mg of each sample was placed in an open platinum pan, automatically introduced by the apparatus into the furnace chamber. The thermal programme consisted of a fast heating from room temperature to 378 K, followed by a 15-min isotherm at this temperature to eliminate traces of humidity, and continuing with a heating ramp at a rate of 10 K/min up to 1073 K. The software Universal Analysis 2000 by TA Instruments was used to process the thermograms.

***Differential scanning calorimetry (DSC)***

The DSC analyses were performed in a TA Instruments DSC Q2000 differential scanning calorimeter equipped with an RCS 90 refrigerated cooling system (Figure 3.1), and using a flow rate of 50 mL/min of nitrogen gas as purge gas in the measurement chamber. For each run, ca. 5-15 mg of sample was placed in a 40-μL aluminium pan hermetically closed with a lid of the same material. An analogous empty pan with lid was used as a reference. The thermal programme comprised three cycles, each of them consisting of a heating ramp at a rate of 10 K/min up to 473 K, a 5-min isotherm, a cooling ramp at a rate of -10 K/min down to 273 K, and another 5-min isotherm. Essential overlapping of the thermograms for the second and the third cycles was verified prior to validating the analyses. Glass transition temperatures (evaluated at the midpoint) were determined from the signal of the heating ramp of the third cycle with the corresponding function of the software Universal Analysis 2000 by TA Instruments.

***Attenuated total reflectance Fourier-transform infrared (ATR-FTIR) spectroscopy***

ATR-FTIR spectra were collected in a Bruker Alpha II spectrometer with a diamond crystal attenuated total internal reflectance accessory (Figure 4.10), from 4000 to 400 $cm^{-1}$, at a resolution of 2 $cm^{-1}$ and 4 scans per sample, using the software Opus.

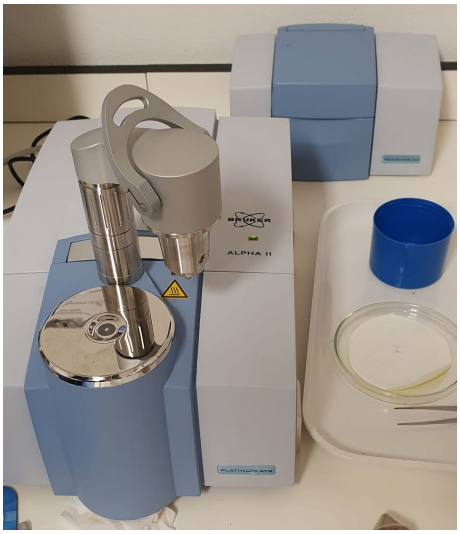


Figure 4.10. Bruker Alpha II ATR-FTIR spectrometer.

***Antioxidant activity***

The radical scavenging activity (RSA) of the lignin samples was determined by adapting a previously reported method (Michelin et al., 2018), with a 50 % (v/v) mixture of water and acetone (Fisher Scientific, ≥99.8 %) as the solvent instead of 80 % (v/v) aqueous ethanol. The method is based on the reduction of the stable free radical 2,2-diphenyl-1-picrylhydrazyl (DPPH, provided by Sigma-Aldrich with Quality Level 100) by an antioxidant, decreasing its absorbance at a wavelength of 515 nm. A commercial standard antioxidant, namely 2,6-di-*tert*-butyl-4-methylphenol, commonly referred to as butylated hydroxytoluene (BHT, supplied by Sigma-Aldrich with a nominal purity of 99 %), was used as a reference. The absorbances were measured in a Biotek Cytation3 UV vis spectrophotometer (Figure 4.6) after incubation of the samples in microplates for 30 min at room temperature in a light-protected environment.

***Minimal inhibitory concentration (MIC)***

The evaluation of MICs was carried out through a slightly modified version of the micro-dilution methodology described by the Clinical and Laboratory Standards Institute (CLSI, 2009). Initially, *S. aureus* and *E. coli* strains were grown into nutrient agar (NA, supplied by Oxoid) at 310 ± 2 K for 24 h. Subsequently, a single colony of each strain

was placed into 20 mL of Nutrient Broth (NB, supplied by Oxoid) and incubated at 310 ± 2 K and 150 rpm, for 18 h. Afterwards, both bacterial cell suspensions were adjusted to an optical density (80–82 % in the McFarland standards) between 0.09 and 0.11, measured at 620 nm, indicating a concentration of $1 \times 10^8$ CFU/mL. After that, the inocula were properly diluted in NB to $1 \times 10^6$ CFU/mL. On the other hand, solutions of the lignin samples diluted in DMSO (anhydrous, Invitrogen, >99.5 %) were prepared from concentrations of 300 mg/mL and serially diluted to obtain the following concentrations: 234.50, 117.25, 58.63, and 29.50 μg/mL. Concentrations above 234.50 μg/mL were not considered due to their too high absorbance.

Experiments were carried out in a sterile 96-well microplate, in which 100 μL of inoculum suspension was added to 100 μL sample. The microplate was incubated at 310 ± 2 K for 24 h and the absorbance was measured at 620 nm using a Tecan Sunrise spectrophotometric microplate reader. The behaviour of the samples was evaluated against growth and sterility controls, which consisted of 100 μL of NB plus 100 μL of inoculum suspension as a microbial growth control (negative control) and 200 μL of NB as a sterility control (positive control). Finally, the concentrations of each treatment capable of inhibiting growth when compared with the negative control were determined.

# 4.3. Results and discussion

## 4.3.1. Aqueous solutions of [$C_2$mim][OAc] as treatment media

### 4.3.1.1. Ionic liquid concentration and treatment time

Initial treatments of Indulin AT were performed with aqueous solutions of [$C_2$mim][OAc] for two different ionic liquid concentrations (10 % and 70 %) and for different treatment times (up to 6 h). A number of lignin-derived compounds were identified in the post-treatment aqueous phases, with the full list and corresponding yields (interpreted as mass of a compound per unit mass of the original Indulin AT) being listed in Table 4.1. It can be observed that, in line with what is typically reported

**Table 4.1**. Yield of compounds (expressed in g of compound per kg of lignin) identified in the post-treatment aqueous phases, with different concentrations of the ionic liquid in the treatment fluid and different treatment times. The letter (H, G, or S) in parenthesis next to the name of each compound indicates the type of lignin unit (*p*-hydroxyphenyl, guaiacyl, or syringyl, respectively) from which it originates.

| Compound* | Percentage of [$C_2$mim][OAc] | Treatment time (min) | | | | | | |
|---|---|---|---|---|---|---|---|---|
| | | 15 | 45 | 120 | 180 | 240 | 300 | 360 |
| *trans*-Cinnamic acid (H) | 0 | 0.00 | 0.00 | 0.04 | 0.06 | 0.06 | 0.02 | 0.00 |
| | 10 | 0.00 | 0.02 | 0.04 | 0.02 | 0.02 | 0.02 | 0.02 |
| | 70 | 0.02 | 0.00 | 0.00 | 0.00 | 0.00 | 0.00 | 0.00 |
| *p*-Coumaric acid (H) | 0 | 0.00 | 0.00 | 0.18 | 0.24 | 0.24 | 0.18 | 0.18 |
| | 10 | 0.00 | 0.00 | 0.18 | 0.28 | 0.28 | 0.18 | 0.18 |
| | 70 | 0.54 | 0.54 | 0.54 | 0.54 | 0.54 | 0.54 | 0.54 |
| Epicatechin (G) | 0 | 0.00 | 0.00 | 0.00 | 0.00 | 0.00 | 0.46 | 0.42 |
| | 10 | 0.00 | 0.00 | 0.56 | 0.46 | 0.46 | 0.56 | 0.46 |
| | 70 | 1.24 | 1.26 | 1.36 | 1.36 | 1.36 | 1.34 | 1.36 |
| Guaiacol (G) | 0 | 0.26 | 0.38 | 0.76 | 0.66 | 0.66 | 0.58 | 0.56 |
| | 10 | 0.26 | 0.50 | 1.06 | 0.96 | 0.96 | 0.90 | 0.92 |
| | 70 | 1.06 | 1.06 | 1.04 | 1.02 | 1.02 | 1.08 | 1.12 |
| Isoeugenol (G) | 0 | 0.00 | 0.00 | 0.06 | 0.06 | 0.06 | 0.06 | 0.08 |
| | 10 | 0.06 | 0.06 | 0.06 | 0.06 | 0.06 | 0.06 | 0.06 |
| | 70 | 0.18 | 0.16 | 0.16 | 0.14 | 0.14 | 0.16 | 0.16 |
| Naringenin (H) | 0 | 0.00 | 0.00 | 0.00 | 0.00 | 0.00 | 0.00 | 0.00 |
| | 10 | 0.00 | 0.06 | 0.00 | 0.00 | 0.00 | 0.00 | 0.06 |
| | 70 | 0.36 | 0.38 | 0.38 | 0.40 | 0.40 | 0.42 | 0.42 |
| Quercetin dehydrate (S) | 0 | 0.04 | 0.02 | 0.08 | 0.10 | 0.10 | 0.12 | 0.12 |
| | 10 | 0.04 | 0.02 | 0.08 | 0.08 | 0.08 | 0.10 | 0.10 |
| | 70 | 0.22 | 0.20 | 0.22 | 0.24 | 0.24 | 0.26 | 0.26 |
| Syringaldehyde (S) | 0 | 0.00 | 0.00 | 0.00 | 0.00 | 0.00 | 0.00 | 0.00 |
| | 10 | 0.00 | 0.00 | 0.00 | 0.04 | 0.04 | 0.04 | 0.04 |
| | 70 | 0.00 | 0.00 | 0.00 | 0.00 | 0.00 | 0.00 | 0.00 |
| Vanillin (G) | 0 | 0.34 | 0.52 | 1.36 | 1.38 | 1.38 | 1.42 | 1.30 |
| | 10 | 0.74 | 1.26 | 2.24 | 2.26 | 2.26 | 2.30 | 2.21 |
| | 70 | 2.94 | 2.96 | 3.02 | 3.40 | 3.40 | 3.38 | 3.28 |

** Benzyl phenyl ether, catechin hydrate, chlorogenic acid, and 4-hydroxybenzoic acid were also included in the list of standards scrutinised, but no significant concentration greater than 0.01 g/kg could be detected for them in any of the treatments.*

in the depolymerisation of *kraft* lignins (Casimiro et al., 2022; Wang et al., 2018), the phenolic compounds obtained in a higher yield are vanillin and guaiacol. These substances are likely produced by the cleavage of β-O-4 bonds in the lignin polymeric structure by the action of the ionic liquid (Cheng et al., 2012; George et al., 2011).

Figure 4.11 shows the evolution of vanillin and guaiacol yields with the treatment time, not only for the treatments with the aqueous solutions of [$C_2$mim][OAc] but also for analogous ones with plain water, for comparison purposes. Even in the case

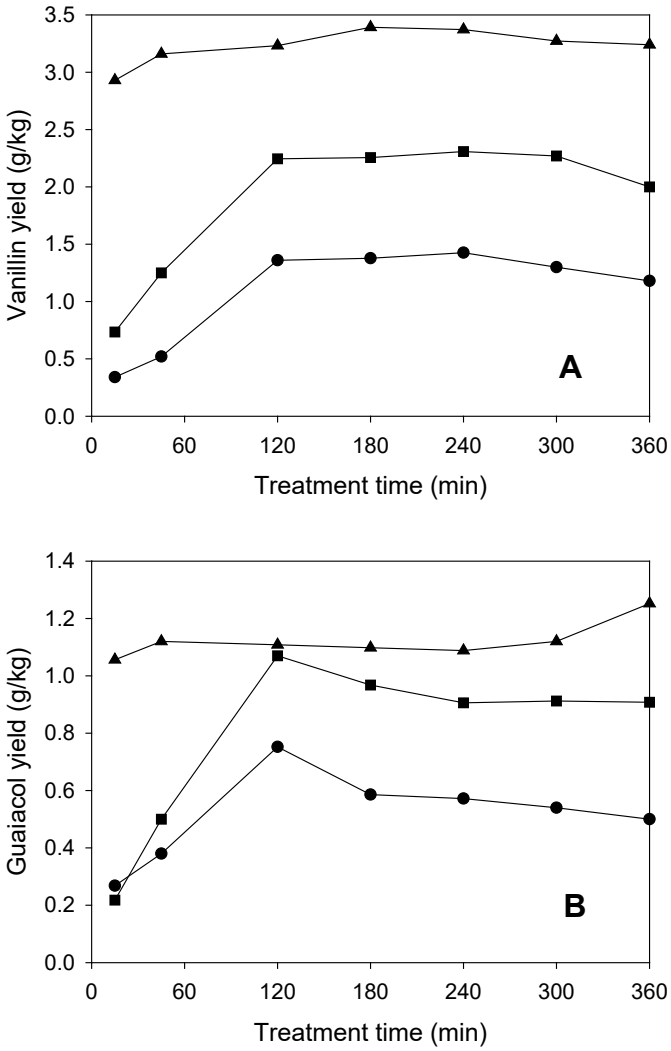


**Figure 4.11. Vanillin (A) and guaiacol (B) yields, represented as g of phenol per kg of original Indulin AT, for treatments with pure water (circles) and aqueous solutions with [C2mim][OAc] concentrations of 10 % (squares) and 70 % (triangles).**

of using just water, non-negligible yields of vanillin and guaiacol were obtained,probably due to the presence of these compounds or of easily hydrolysable fractions of low molecular weight in the raw Indulin AT. A significant increase of these yields, however, was found with increasing the presence of the ionic liquid in the treatment fluid, for any given treatment time. For the treatments with water and with 10 % [C2mim][OAc], the evolution with the treatment time is similar: an initial increase up to 2 h of treatment, followed by a stabilisation and small decrease at higher

treatment times in the case of vanillin, or followed directly by an appreciable decrease for treatment times of 3 h or longer in the case of guaiacol. This decrease observed for the longer treatment times may be a result of the degradation/oxidation that phenols are known to undergo in non-optimal contexts (Fache et al., 2016). Such decrease is not observed for the treatments with 70 % [$C_2$mim][OAc], for which both the vanillin and guaiacol yields remain reasonably stable, and even with a slight increase at higher times in the case of guaiacol, suggesting the preference for a 6-hour treatment in these conditions. The high concentration of ionic liquid may be providing, in this case, a protective environment against the mentioned degradation/oxidation phenomena.

Regarding the solid phases recovered after treatment (typically representing 80-90 % of the initial lignin before treatment), the HSQC NMR spectra for those samples obtained in the treatment with pure water and in that with the 70 % ionic liquid solution (treatment time: 6 h) are shown, as illustrative examples, in Figure 4.12, which also includes the equivalent spectrum for raw Indulin AT. In these spectra, the signal regions associated with the chemical structures shown in Figure 4.13 were identified and quantified. Structures *A*, *B*, *C*, and *J* correspond to lignin S-units, structures *FA* and *G* to lignin G-units, and structure *H* to lignin H-units (Casas et al., 2012; del Río et al., 2012; He et al., 2022; Strassberger et al., 2015). Since the absolute values of the integration of the signals are sensitive to the actual concentration of the solute in the preparation of the sample for NMR analysis and to subsequent processing (e.g. phase correction of the Fourier-transformed signal), area ratios have been used in order to establish valid comparisons (Ralph et al., 2019; Strassberger et al., 2015; Wang et al., 2018; Yang et al., 2022). In particular, area ratios related to the biggest area (the one corresponding to the $C_\beta$ region – see Figure 4.12) were calculated. Table 4.2 lists the numerical values of the so calculated ratios for raw Indulin AT and the two selected recovered solids. All ratios were found to be very small in comparison to the $G/C_\beta$ ratio (i.e., the ratio between the areas of the *G* region and the $C_\beta$ region). Therefore, this $G/C_\beta$ ratio was taken as a good indicator of the relative abundance of G-units versus S-units in the recovered lignin samples after the investigated treatments. In Figure 4.14, it can be seen how the $G/C_\beta$ ratio is considerably lower for the solid sample recovered after the treatment with the 70 % [$C_2$mim][OAc] solution than in the case of the solid sample recovered after the treatment with plain water. The latter, at the same time, is slightly

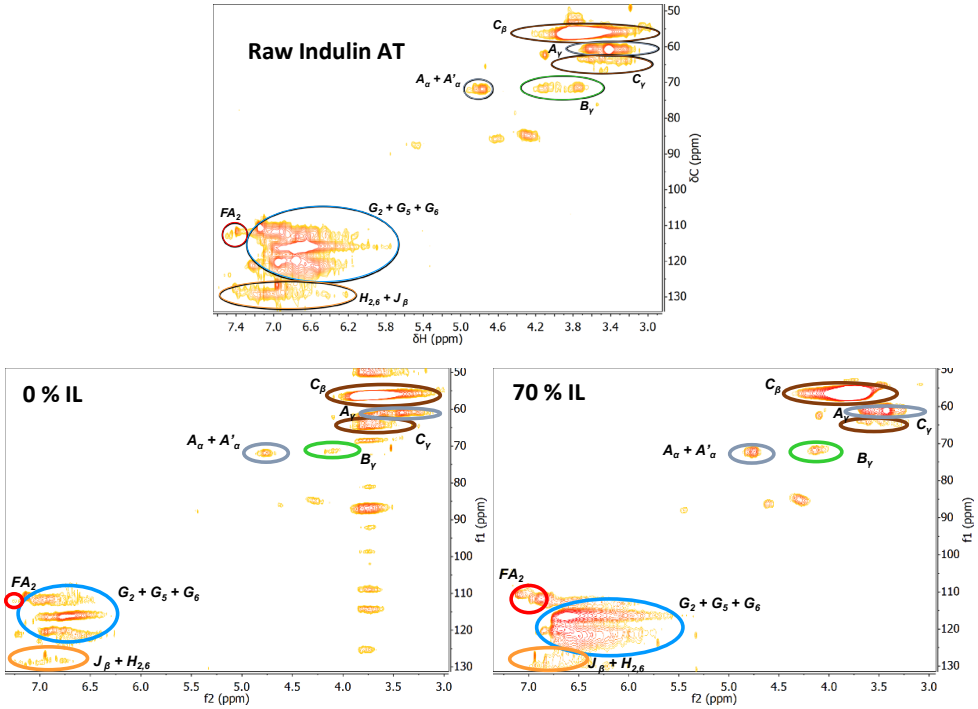


Figure 4.12. 2D $^{1}H$-$^{13}C$ HSQC NMR spectra of raw Indulin AT and of solid samples recovered after 6-hour treatments with water ("0 % IL") or with a 70 % solution of [$C_2$mim][OAc] ("70 % IL"), as noted in the labels in the upper left corner of each plot. The coloured ellipses in the spectra indicate signals associated with the different generic structures shown in Figure 4.13 with frames of the same colour.

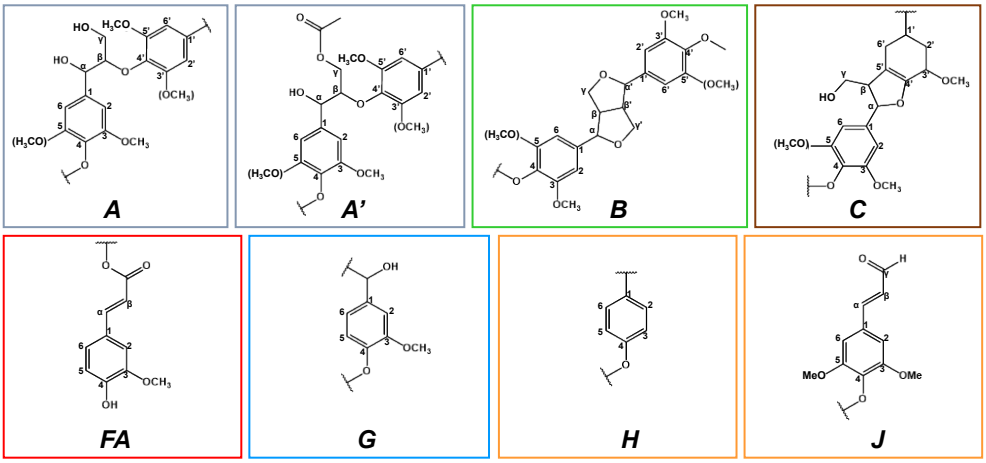


Figure 4.13. Structures associated with different signal regions identified in the 2D $^{1}H$-$^{13}C$ HSCQ NMR spectra of raw Indulin AT and solid samples recovered after the treatments.

**Table 4.2.** Area ratios of integrated regions in the $^{1}H$-$^{13}C$ HSQC NMR spectra of Figure 4.12.

| Ratio* | Raw Indulin AT | Treatment | |
|---|---|---|---|
| | | 0 % IL | 70 % IL |
| $A_\gamma / C_\beta$ | 0.11 | 0.10 | 0.10 |
| $C_\gamma / C_\beta$ | 0.04 | 0.03 | 0.03 |
| $B_\gamma / C_\beta$ | 0.04 | 0.02 | 0.02 |
| $(A_\alpha + A'_\alpha) / C_\beta$ | 0.02 | 0.03 | 0.02 |
| $(G_2 + G_5 + G_6) / C_\beta$ | 0.78 | 0.77 | 0.58 |
| $FA_2 / C_\beta$ | 0.01 | 0.01 | 0.01 |

** The notation used for the different areas of interest can be consulted in Figure 4.13.*

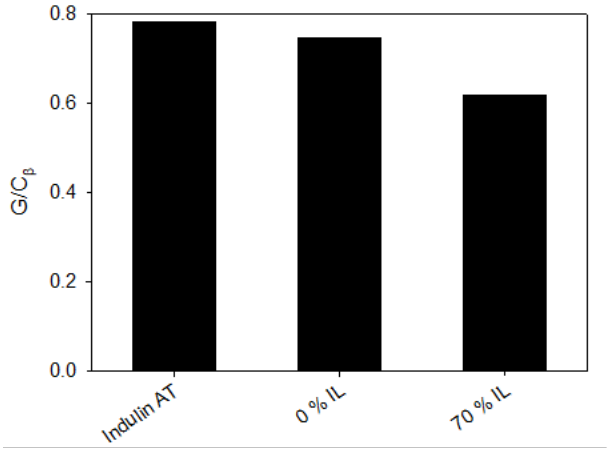


**Figure 4.14.** *G/ $C_\beta$* **ratio for raw Indulin AT and for the solid recovered after the 6-hour treatment with water ("0 % IL") or with a 70 % solution of [C2mim][OAc] ("70 % IL").**

lower than for untreated Indulin AT. This evolution is in good agreement with the trend followed by the yields of vanillin and guaiacol calculated from their concentrations in the post-treatment aqueous phases (see Figure 4.11): the higher yields of these phenolic compounds (derived from lignin G-units) in the aqueous phase correspond with the stronger relative diminution of G-units with respect to S-units (i.e. lower $G/C_\beta$ ratio) in the solid phase. Since this has not been accompanied by an increase in the signals associated to other lignin structures (condensation products proposed by Yang et al. (2022)), it can be guessed that the relative diminution of G-units should be connected with the depolymerisation of lignin for subsequent transformation into small phenolic compounds.

Since the thermal behaviour of lignin is highly influenced by its internal structure (Huang et al., 2018), a thermal analysis of the treated lignin samples was carried out to

seek complementary information on the mode of action of the treatment fluids investigated. In Figure 4.15, the TGA thermograms of raw Indulin AT and of the recovered solids from the treatments with plain water and with the 70 % solution of [$C_2$mim][OAc] are shown. In the three examples, after an initial weight loss in the temperature range up to ca. 473 K due to dehydration and vaporisation of low molar mass volatiles, the crucial decomposition step occurs in the range 473-773 K. In this stage, two maxima were identified in the derivative curve of the TGA thermogram for raw Indulin AT, with the second one corresponding to a smaller peak. These two peaks are associated to the decomposition of side chains and of C-C bonds, respectively (Huang et al., 2018). In the case of the solid recovered after treatment with the 70 % ionic liquid solution, those two peaks are also observed in the derivative curve; however, they are shifted to lower temperatures and are of an approximately equivalent size. This may indicate that a larger loss of side chains, relative to the breakage of C-C bonds, occurs during the treatment. Interestingly, in the treatment with just water (0 % of ionic liquid), only one peak was observed in the derivative curve of the TGA thermogram, although it might be the composed peak of the two aforementioned peaks overlapping largely, for example due to a more prolonged decomposition of the lignin side chains during the course of the dynamic TGA experiment. Finally, for the region above 773 K, which is associated with the decomposition of aromatic rings (Huang et al., 2018), no significant differences are observed among thermograms, thus indicating that the thermal destruction of such rings occurs in a similar fashion for the three samples. At the same time, the large residue observed at 1073 K (i.e. 800 °C, the temperature at which the TGA runs were stopped) invites to think that this thermal decomposition of the aromatic rings occurs to a limited extent. The numerical values of such solid residues at 1073 K, together with those of the temperatures of all the maxima of rate of decomposition ($T_{max}$) for the thermograms in Figures 4.15 are summarised in Table 4.3. A small reduction in the $T_{max}$ values can be observed in the solid recovered in the treatment with the 70 % [$C_2$mim][OAc] solution with respect to raw Indulin AT, and a slight increase in the residue at 1073 K is observed for the solid recovered in the treatment with just water; but in general it can be said that the thermal behaviour of the solids recovered is quite similar to that of the raw lignin.

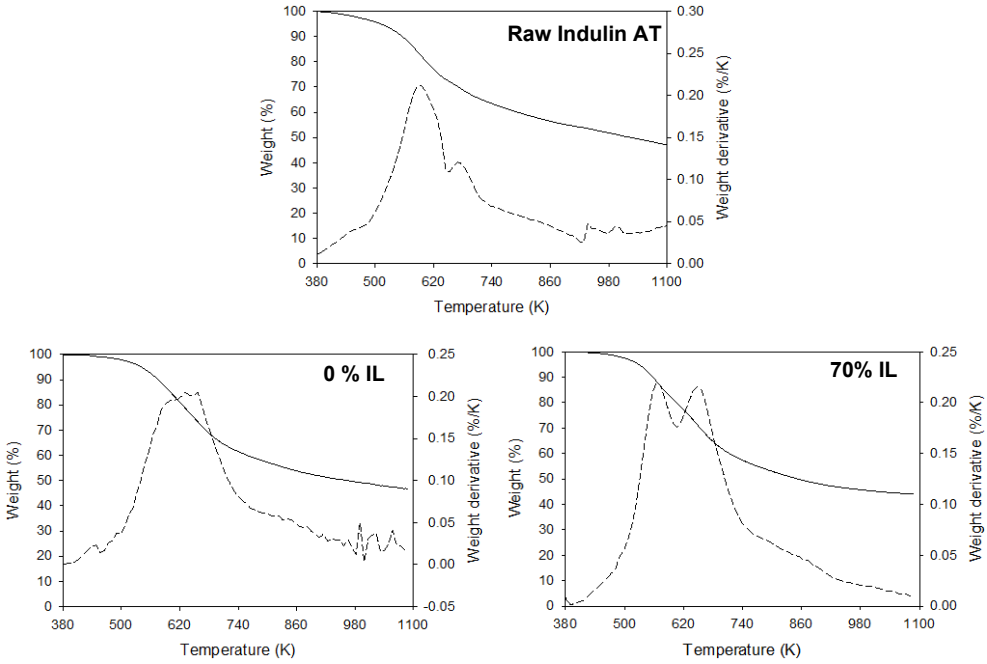


**Figure 4.15. TGA thermograms (solid lines), and the corresponding derivative curves (dashed lines) for raw Indulin AT and for the solids recovered after the 6-hour treatments with water ("0% IL") or with a 70 % [$C_2$mim][OAc] solution ("70 % IL").**

**Table 4.3.** Numerical values of temperature(s) of maxima of decomposition rate ($T_{max}$), residue at 1073 K, and glass transition temperature ($T_g$) for raw Indulin AT and for the solids recovered after the 6-hour treatments with water or with a 70 % [$C_2$mim][OAc] solution.

| Treatment | $T_{max}$ (K) | Residue at 1073 K (%) | $T_g$ (K) |
|---|---|---|---|
| None (raw Indulin AT) | 593, 678 | 45 | 427 |
| Water | 630 | 48 | 436 |
| 70 % [$C_2$mim][OAc] solution | 567, 650 | 44 | 425 |

By DSC analysis, the glass transition temperature ($T_g$) of the recovered solid samples in the selected treatments was found to be in the range 425-436 K, around that of the original Indulin AT (427 K). The numerical $T_g$ values are detailed in Table 4.3, whereas the processed DSC thermograms from which they were obtained are shown in Figure 4.16. The $T_g$ for raw Indulin AT is very close to that of 430 K reported by Li and McDonald (2014), especially if taking into account that the glass transition of lignin is highly influence by factors such as the water content of the sample (Glasser and Jain, 1993; Tejado et al., 2007). Even though efforts were made to maintain a very low and approximately constant water content for all the samples, part of the variation observed

in Table 4.3 for $T_g$ may be due to this factor. In any case, it is clear that the treatments with water or with the aqueous solution of [C2mim][OAc] do not imply a relevant modification of the glass transition behaviour of the lignin material.

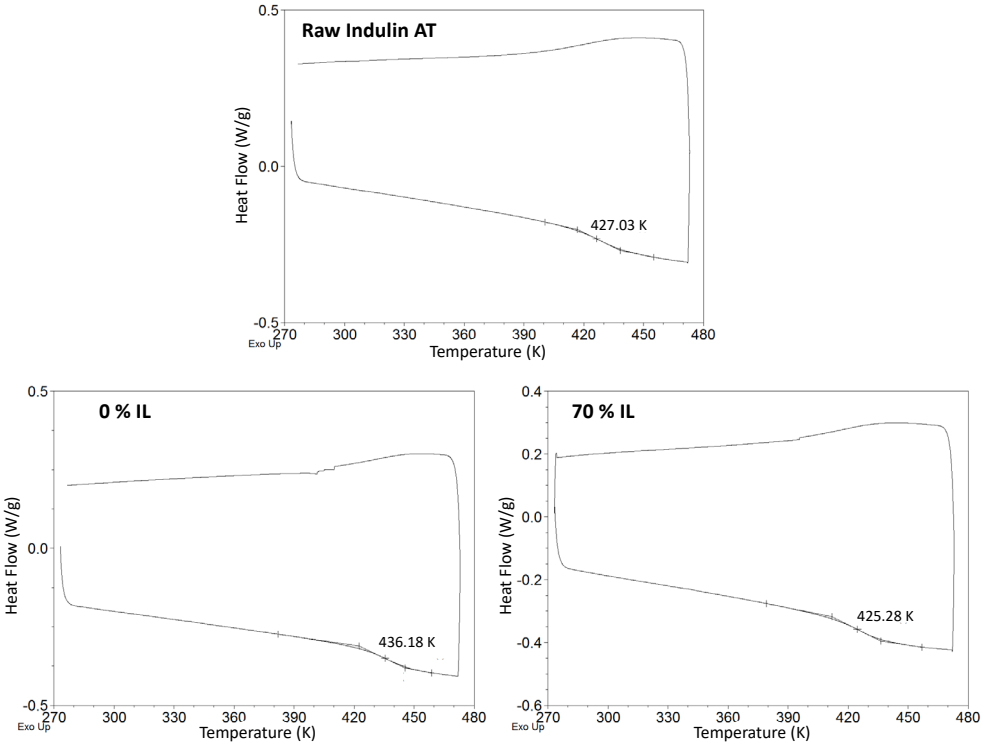


Figure 4.16. DSC thermograms (exo up) of raw Indulin AT and of the solid samples recovered after 6-hour treatments with water ("0 % IL") or a 70 % solution of [C2mim][OAc] ("70 % IL").

### 4.3.1.2. Treatments assisted by UV-irradiation photoreaction catalysed by nanoparticles

With the purpose of enhancing the performance of the treatment with aqueous solution of [C2mim][OAc], investigated in section 4.3.1.1, the deconstruction of lignin through photoreaction induced by UV light irradiation with $TiO_2$ or AgCl nanoparticles as catalysts was investigated. Since an excessively high concentration of nanoparticles can cause a shielding effect on the UV irradiation (El-Hosainy el al., 2022), a first variable to explore was the concentration of nanoparticles. Using the 70 % solution of [C2mim][OAc] as treatment fluid of reference, four concentrations of nanoparticles

were tested in quick 45-min treatments under UV irradiation, namely: 0.05 %, 0.10 %, 0.25 %, and 0.50 % (w/w). Focusing in the yield of the two major phenolic compounds identified in the post-treatment aqueous phases (vanillin and guaiacol), Figure 4.17 shows that the concentration of 0.05 % of $TiO_2$ nanoparticles leads to a simultaneous

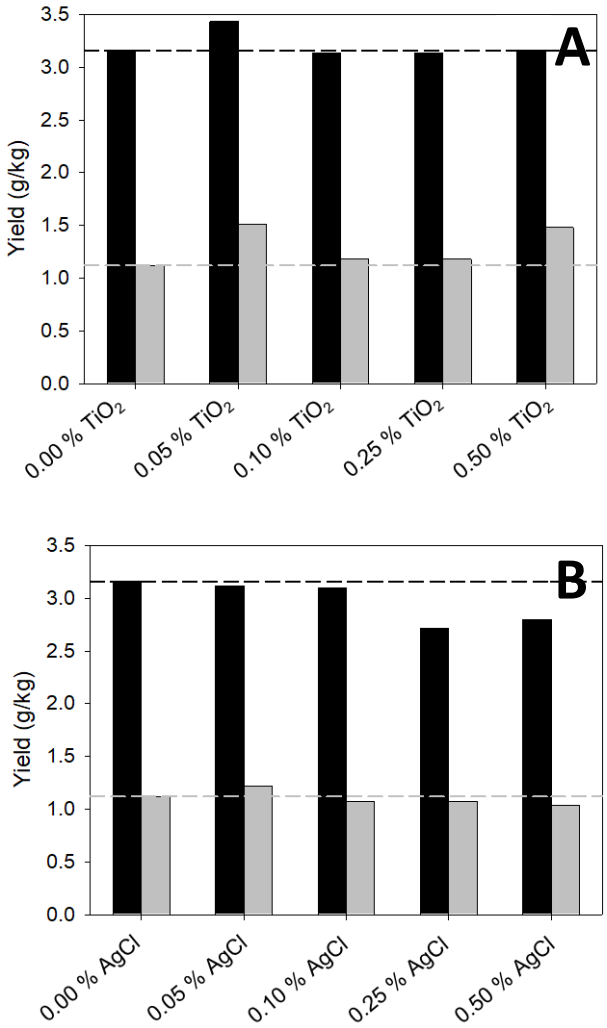


**Figure 4.17. Yields of vanillin (black bars) and guaiacol (grey bars) as a function of the concentration of $TiO_2$ nanoparticles (plot A) or AgCl nanoparticles (plot B) in 45-min treatments of Indulin AT with a 70 % solution of [$C_2$mim][OAc] assisted by UV irradiation. The horizontal lines (black for vanillin and grey for guaiacol) indicate the yields obtained in equivalent treatments with neither UV irradiation nor nanoparticles.**

improvement of the yields of both phenols with respect to the case of using UV irradiation without nanoparticles (which, in turn, provides results equivalent to the analogous treatment without irradiation). Treatments with the other concentrations of $TiO_2$ nanoparticles tested do not lead to such simultaneous improvement of both yields. Regarding the AgCl nanoparticles, no significant improvement of the phenols yields was detected at any concentration; and even a clear decrease in the yield of vanillin was observed for the highest concentrations (≥0.25 %). Therefore, the AgCl nanoparticles were discarded and a concentration of 0.05 % of $TiO_2$ nanoparticles was selected for further experiments.

Figure 4.18A shows the effect of applying UV irradiation and a 0.05 % concentration of $TiO_2$ nanoparticles in the 6-hour treatment of Indulin AT with either water ("0 % IL") or a 70 % solution of [C2mim][OAc]. Disappointingly, no significant variation was observed in the yields of vanillin or guaiacol. Trying to enhance the catalytic activity of the $TiO_2$ nanoparticles, hydrogen peroxide (at a concentration of 5 mM) was investigated as additive. However, these experiments involving $H_2O_2$ actually led to lower yields of the phenolic compounds, especially in the case of vanillin. Figure 4.18B presents the corresponding $G/C_\beta$ ratios of the post-treatment recovered solids (values calculated from the NMR spectra of Figure 4.19, and numerically listed in Table 4.4 together with the much lower ratios of the other identifiable regions with respect to region $C_\beta$), which can be analysed together with the yields in Figure 4.18A. It is observed that, for most of the UV-assisted experiments (the exception being the treatment with water in absence of $H_2O_2$), a decrease in the $G/C_\beta$ ratio value occurs without leading to a higher yield of vanillin and guaiacol, which are phenolic compounds derived from the lignin G-units. A plausible explanation may be that part of the G-units that leave the solid substrate do not end up transformed into the phenolic compounds of interest, as a result of a certain oxidising character of the $TiO_2$ nanoparticles (Kamwilaisak and Wright, 2012) and/or, even more notoriously, of the strong oxidising character of $H_2O_2$ (masking its potential effect to boost nanoparticles catalytic activity). Instead, fully oxidised compounds of low molecular weight might have been produced, such as $CO_2$ (Kamwilaisak and Wright, 2012), leaving the system, since neither an increase of other identified compounds nor new compounds were detected by HPLC in the analysis of the post-treatment aqueous phase of those experiments.

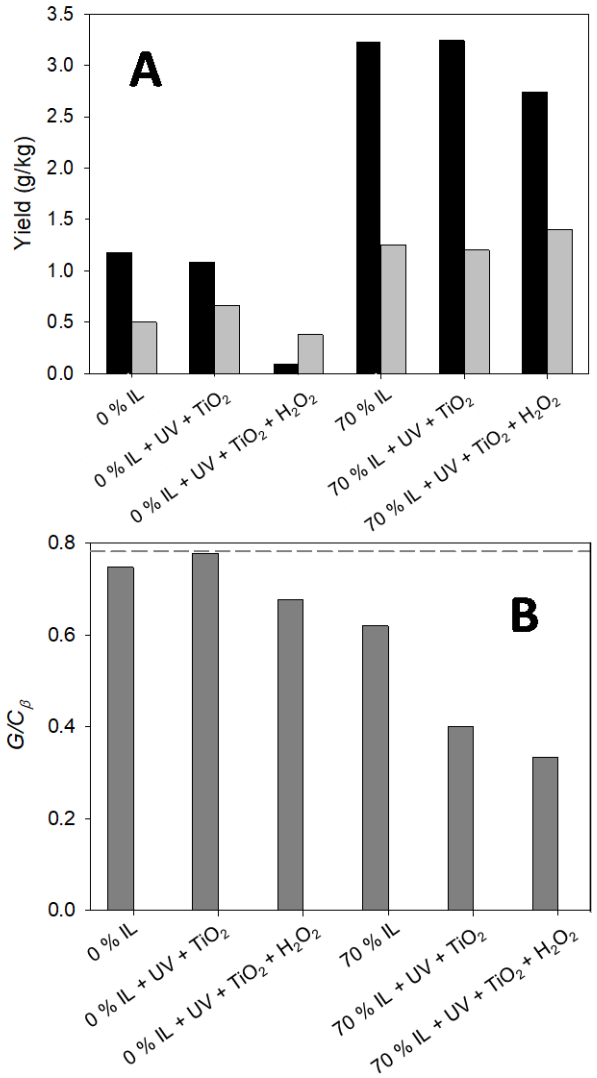


**Figure 4.18. A) Yields of vanillin (black bars) and guaiacol (light grey bars) for 6-hour treatments of Indulin AT with water ("0 % IL") or a 70 % solution of [$C_2$mim][OAc] ("70 % IL") assisted by UV irradiation, with 0.05 % $TiO_2$ nanoparticles and, optionally, a 5 mM concentration of $H_2O_2$. B) The corresponding *G/ C*$_\beta$ ratios (dark grey bars) of the recovered solids, with the *G/ C*$_\beta$ ratio for raw Indulin AT represented by the horizontal dashed line.**

Regarding the thermal analysis of the solids recovered after these treatments with irradiation (which consistently lied within the range 80-90 % with respect to the mass of the original lignin before treatment, as in the case of the treatments presented in section 4.3.1.1), their TGA thermograms are shown in Figure 4.20. Equivalent

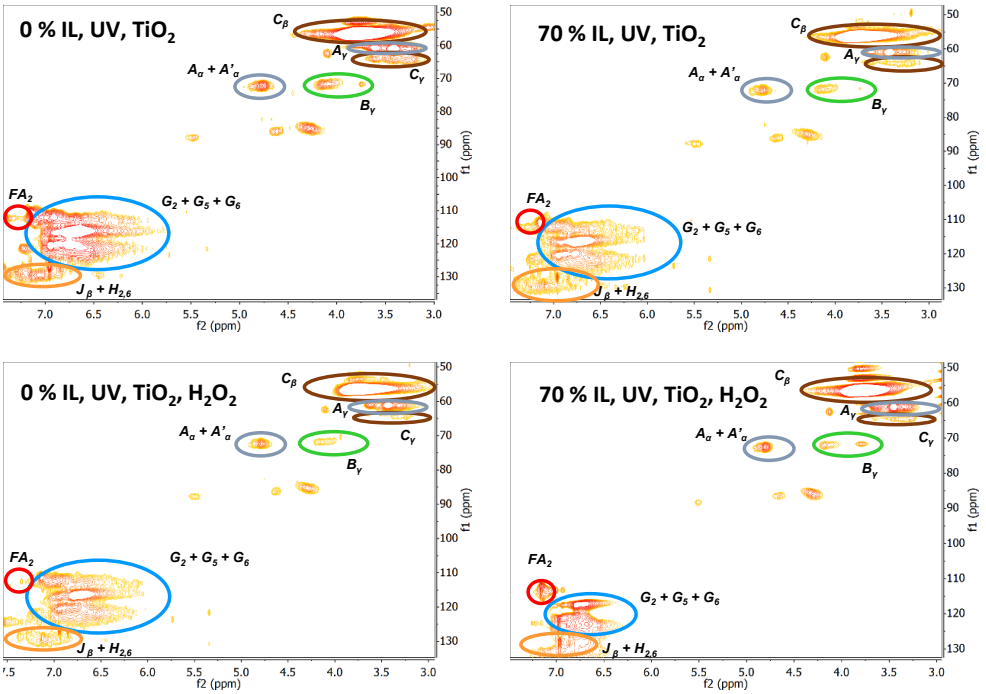


Figure 4.19. 2D $^{1}H$-$^{13}C$ HSQC NMR spectra of solid samples recovered after 6-hour treatments with water ("0 % IL") or with a 70 % solution of [C2mim][OAc] ("70 % IL") involving the assistance by UV irradiation with $TiO_2$ nanoparticles, optionally assisted with $H_2O_2$, as noted in the labels in the upper left corner of each plot. The coloured ellipses in the spectra indicate signals associated with the different generic structures shown in Figure 4.13 (see section 4.3.1.1), with frames of the same colour.

**Table 4.4.** Area ratios of integrated regions in the $^{1}H$-$^{13}C$ HSQC NMR spectra of Figure 4.19. The values for raw Indulin AT (from Table 4.2, section 4.3.1.1) are also included for comparison purposes.

| Ratio* | Raw Indulin AT | Treatment | | | |
|---|---|---|---|---|---|
| | | 0 % IL, UV, $TiO_2$ | 0 % IL, UV, $TiO_2$, $H_2O_2$ | 70 % IL, UV, $TiO_2$ | 70 % IL, UV, $TiO_2$, $H_2O_2$ |
| $A_\gamma / C_\beta$ | 0.11 | 0.10 | 0.09 | 0.10 | 0.10 |
| $C_\gamma / C_\beta$ | 0.04 | 0.03 | 0.03 | 0.03 | 0.02 |
| $B_\gamma / C_\beta$ | 0.04 | 0.02 | 0.03 | 0.02 | 0.02 |
| $(A_\alpha + A'_\alpha) / C_\beta$ | 0.02 | 0.02 | 0.03 | 0.02 | 0.02 |
| $(G_2 + G_5 + G_6) / C_\beta$ | 0.78 | 0.71 | 0.68 | 0.55 | 0.33 |
| $FA_2 / C_\beta$ | 0.01 | 0.01 | 0.01 | 0.02 | 0.04 |

** The notation used for the different areas of interest can be consulted in Figure 4.13.*

patterns to those identified in Figure 4.15 can be observed in this case, with only one peak in the derivative curve in the region of large decomposition for the treatments in

the absence of ionic liquid, and two peaks for those treatments involving the ionic liquid. An analogous trend to that already described in section 4.3.1.1 when commenting Figure 4.15 is observed, with a small shift, towards lower temperatures, of the maxima of rate of decomposition of the treatments comprising [$C_2$mim][OAc], in relation to raw Indulin AT. The numerical values are displayed in Table 4.5. This table also includes the percent residue obtained at 1073 K (final temperature of the TGA ramps) for the recovered solids in the treatments presented in this section, which, as in section 4.3.1.1, are reasonably similar to that of untreated Indulin AT. Thus, the most determining factor in the thermal decomposition mode of the recovered samples is the presence or not of the ionic liquid in the treatment fluid, whereas the irradiation with UV light and the presence of nanoparticles or $H_2O_2$ do not seem to have a relevant influence in this aspect.

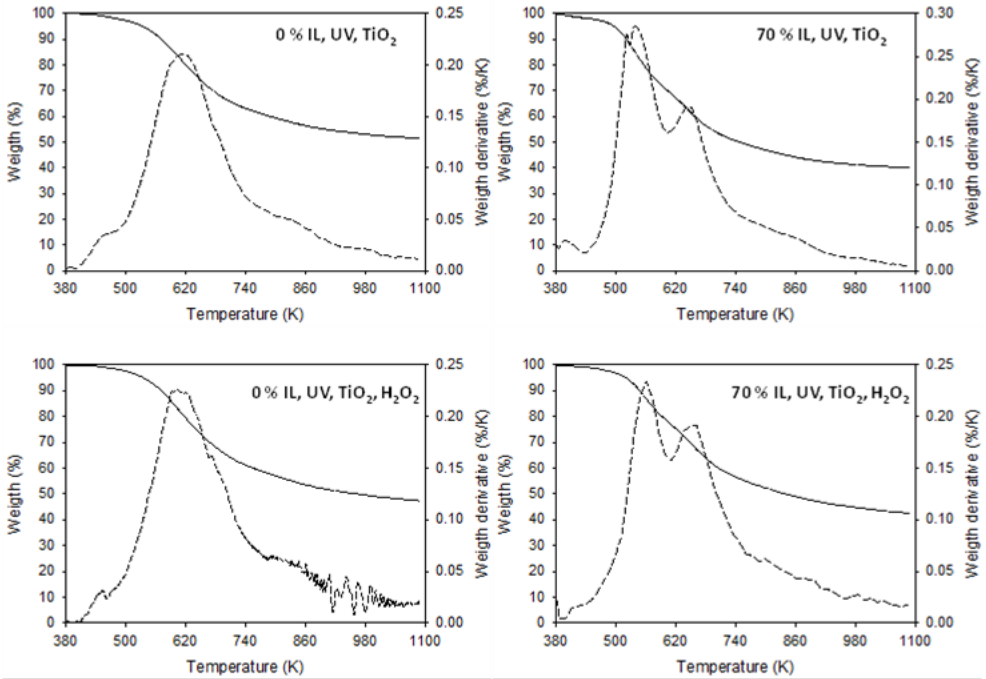


Figure 4.20. TGA thermograms (solid lines) and the corresponding derivative curves (dashed lines) for the solid samples recovered after 6-hour treatments using water ("0 % IL") or a 70 % [$C_2$mim][OAc] solution ("70 % IL") as treatment fluids, with the assistance of UV irradiation with $TiO_2$ nanoparticles, and optionally with $H_2O_2$, as noted in the labels in the upper right corner of each plot.

**Table 4.5.** Numerical values of temperature(s) of maxima of decomposition rate ($T_{max}$), residue at 1073 K, and glass transition temperature ($T_g$) for raw Indulin AT and for the solid samples recovered after 6-hour treatments using water or a 70 % [C2mim][OAc] solution ("70 % IL solution") as treatment fluids, with the assistance of UV irradiation with $TiO_2$ nanoparticles, and optionally with $H_2O_2$.

| Treatment | $T_{max}$ (K) | Residue at 1073 K (%) | $T_g$ (K) |
|---|---|---|---|
| None (raw Indulin AT) | 593, 678 | 45 | 427 |
| Water + UV + $TiO_2$ | 611 | 52 | 436 |
| Water + UV + $TiO_2$ + $H_2O_2$ | 608 | 48 | 436 |
| 70 % IL solution + UV + $TiO_2$ | 541, 645 | 41 | 435 |
| 70 % IL solution + UV + $TiO_2$ + $H_2O_2$ | 561, 652 | 43 | 434 |

The glass transition temperatures ($T_g$) of these solid samples, as determined by DSC (see spectra in Figure 4.21), are also included in Table 4.5. Once again, as in the case of the treatments discussed in section 4.3.1.1, these $T_g$ values are quite similar (only slightly higher) to that of raw Indulin AT; and the influence in this regard of the treatments discussed in the present section can be considered as rather small.

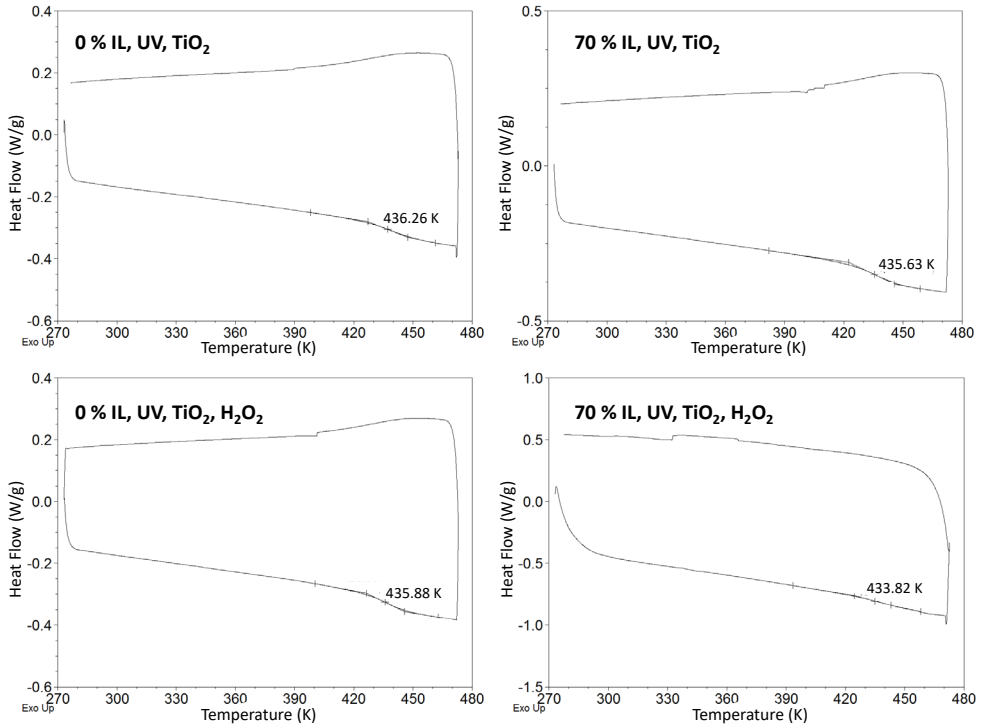


Figure 4.21. DSC thermograms (exo up) of the solid samples recovered after 6-hour treatments with water ("0 % IL", plots on the left hand side) or a 70 % solution of the ionic liquid ("70 % IL", plots on the right hand side) with the assistance of UV irradiation plus $TiO_2$ nanoparticles (plots in the top row), and optionally with $H_2O_2$ as well (plots in the bottom row).

## 4.3.2. Treatments with laccase-based systems

For facilitation of the understanding of the set of treatments carried out in this section and the codification used to refer to them, Table 4.6 presents all these codes, including both control experiences, with the different elements specifically involved in each treatment tested.

**Table 4.6.** Codes and elements involved in each of the lignin treatments studied in this section (including the two control experiences).

| Treatment code | Laccase | Mediator | Pre-saturation with $O_2$ | Ionic liquid |
|---|---|---|---|---|
| 1 | X | | | |
| 1-IL | X | | | X |
| 1O | X | | X | |
| 1O-IL | X | | X | X |
| 2 | X | X | | |
| 2-IL | X | X | | X |
| 2O | X | X | X | |
| 2O-IL | X | X | X | X |
| Ctrl | | | | |
| Ctrl-IL | | | | X |

Since a good number of the intended experiments imply the utilisation of the Novozymes NS51003 laccase in the presence of the ionic liquid [$C_2$mim][OAc] in the aqueous medium (see section 4.2.1 for further detail), first a test of stability of this enzyme in that environment was performed (see next section), prior to the proper experiments with subsequent characterisations of the post-treatment modified lignin (solid recovered) and the post-treatment aqueous phase obtained in each case.

### 4.3.2.1. Laccase stability

The commercial laccase from *M. thermophila* used in this work has a slightly acidic optimum pH. Maximal laccase activity was found in 0.1 M sodium acetate buffer (pH of 5.0). Upon addition of a 10 % (w/w) of the ionic liquid [$C_2$mim][OAc], the pH was found to rise to 6.1 (the ionic liquid is contributing acetate anions to the medium), and the residual activity of the enzyme in the presence of the ionic liquid corresponded to 52 % of the initial activity in the buffered medium with no ionic liquid, after 12 h of incubation. At higher ionic liquid concentrations the enzyme was not stable.

Domínguez et al. (2011) reported that the stability of laccase from *Trametes versicolor* decreases at high concentrations of imidazolium-based ionic liquids, and Stevens et al. (2020) reported that a laccase from the hyperthermophilic bacterium *Thermus thermophilus* lost more than 50 % activity in only 2 % (w/v) [$C_2$mim][OAc], despite its thermophilicity, with the cation favouring the binding of the ionic liquid to a region close to the active site. On the other hand, Harwardt et al. (2014) reported that the stability of laccase from *T. versicolor* at 15 % (v/v) [$C_2$mim][OAc] or [$C_2$mim][ethylsulfate] in buffer solution was higher compared to that of the same laccase in the plain buffer, and was also highly influenced by the anionic part of the ionic liquids. Thus, in addition to the ionic liquid, the source of laccase (microorganism) is an important point to be considered. In this case, in spite of the loss of activity of the selected enzyme in the presence of the 10 % of [$C_2$mim][OAc], it was speculated that the favourable action of [$C_2$mim][OAc] in the treatment could potentially lead to a globally better performance of the lignin treatments.

### 4.3.2.2. Modification of lignin with the laccase-based systems

Together with the yield of recovered solids, these post-treatment lignin samples have been subjeted to a structural and thermal analysis, and their antioxidant and antimicrobial activity has been explored.

***Solid recovery yield***

The percentages of lignin recovered after the different treatments of Indulin AT are shown in Figure 4.22. In general, all percentages are quite high, roughly lying in the range of 80–90 %. The fraction of sample lost is a result of the inherent solubility of part of Indulin AT in the tested media (ca. 8–9 %) and the action of laccase in generating additional soluble materials. No strong differences are observed among treatments, although a slightly higher solid recovery percentage can be noticed for the treatments with ionic liquid compared to their corresponding pairs. This may be due in part to the increase in pH caused by the presence of [$C_2$mim][OAc] in the treatment medium, which results in lower enzyme activity.

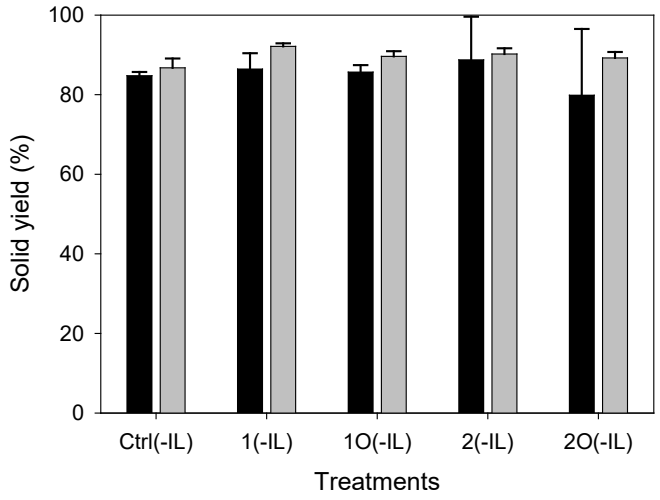


**Figure 4.22. Percentage of lignin sample recovered after the treatments. Black and grey bars correspond to the treatments without and with ionic liquid, respectively.**

### *Structural and thermal characterisation of the post-treatment solids*

Two-dimensional $^{1}H$-$^{13}C$ HSQC NMR spectroscopy is one of the most commonly used methods to determine molecular structures in lignin. In section 4.3.1.1, the spectrum of raw Indulin AT was already shown in Figure 4.12, indicating different regions of signals in the spectrum that could be associated with the chemical structures shown in Figure 4.13. Proceeding analogously with the 2D NMR spectra obtained for the lignin-modified samples obtained with the laccase-based treatments (including the control experiments) investigated in the present section (Figures 4.23-4.25), the areas under the peaks in the labelled regions were integrated. Due to the reasons already pointed out in section 4.3.1.1, the area ratios referred to the largest area (systematically the $C_\beta$ region) were preferred instead of the absolute area values. As observed in Table 4.7, most ratios are relatively small (lower than 0.15), and no significant variation or trend can be observed among treatments. The exception is the ratio between the $G_2$+$G_5$+$G_6$ region (or simply the $G$ region) and the $C_\beta$ region. Such ratio, denoted as the $G/C_\beta$ ratio, is shown in a graphical mode in Figure 4.26 for all treatments carried out. The $G$ region is constituted by signals from the atoms in the aromatic ring of guaiacyl units (G-units). Thus, the lower values of the $G/C_\beta$ ratios of the treated lignin, compared to the raw

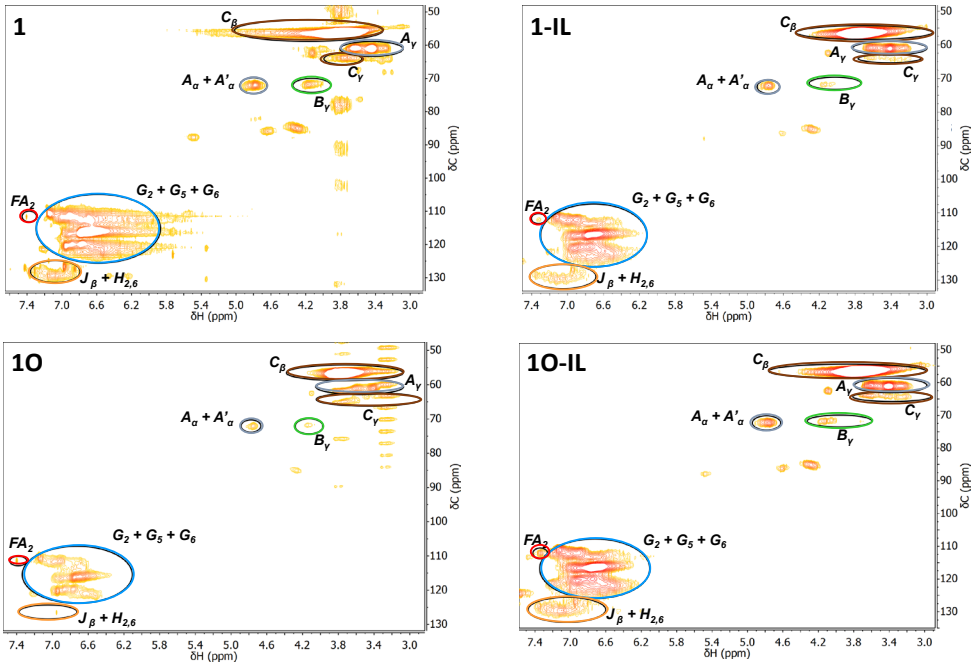


Figure 4.23. Two-dimensional $^{1}H$-$^{13}C$ HSQC NMR spectra of recovered solid samples in treatments with no ABTS. Treatment codes are displayed in the left top corner of each plot. Coloured ovals indicate regions integrated for quantification of different structures – See Figure 4.13.

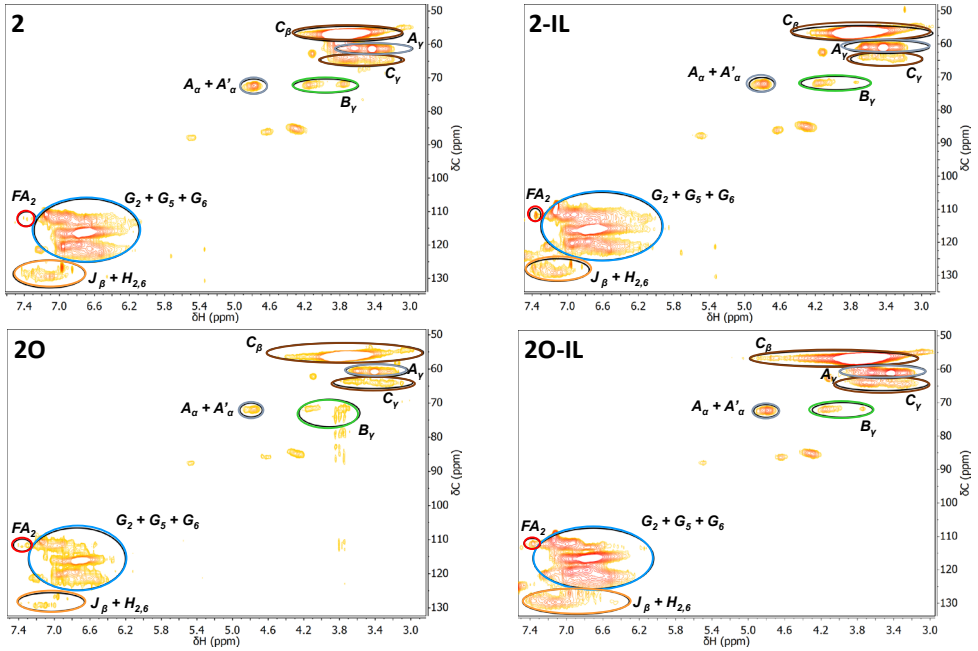


Figure 4.24. Two-dimensional $^{1}H$-$^{13}C$ HSQC NMR spectra of recovered solid samples in treatments involving ABTS as mediator. Treatment codes are displayed in the left top corner of each plot. Coloured ovals indicate regions integrated for quantification of different structures – See Figure 4.13.

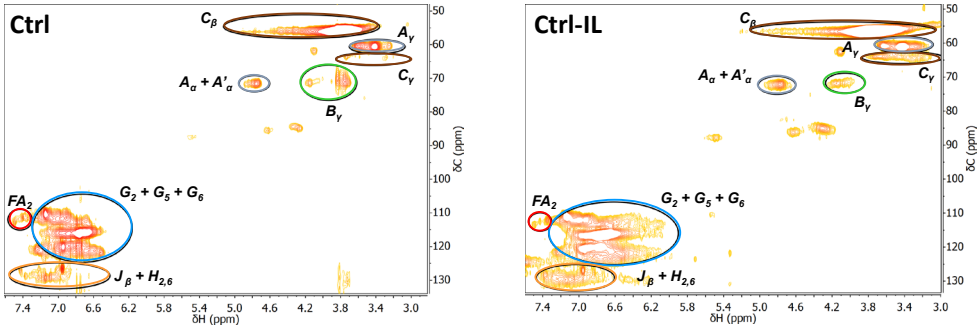


Figure 4.25. Two-dimensional $^{1}H$-$^{13}C$ HSQC NMR spectra of the control samples. Treatment codes are displayed in the left top corner of each plot. Coloured ovals indicate regions integrated for quantification of different structures – See Figure 4.13.

**Table 4.7.** Area ratios of integrated regions in the $^{1}H$-$^{13}C$ HSQC NMR spectra in Figures 4.23-4.25, associated with specific structures in accordance with the coding in Figure 4.13.

| Ratio | Raw Indulin AT | Treatment | | | | | | | | | |
|---|---|---|---|---|---|---|---|---|---|---|---|
| | | Ctrl | 1 | 1O | 2 | 2O | Ctrl-IL | 1-IL | 1O-IL | 2-IL | 2O-IL |
| $A_\gamma / C_\beta$ | 0.11 | 0.11 | 0.10 | 0.14 | 0.14 | 0.09 | 0.09 | 0.10 | 0.10 | 0.10 | 0.13 |
| $C_\gamma / C_\beta$ | 0.04 | 0.02 | 0.02 | 0.07 | 0.01 | 0.03 | 0.03 | 0.02 | 0.03 | 0.03 | 0.06 |
| $B_\gamma / C_\beta$ | 0.04 | 0.08 | 0.14 | 0.02 | 0.03 | 0.04 | 0.01 | 0.01 | 0.01 | 0.01 | 0.02 |
| $(A_\alpha + A'_\alpha) / C_\beta$ | 0.02 | 0.03 | 0.02 | 0.02 | 0.02 | 0.02 | 0.02 | 0.02 | 0.02 | 0.02 | 0.02 |
| $(G_2 + G_5 + G_6) / C_\beta$ | 0.78 | 0.79 | 0.68 | 0.49 | 0.65 | 0.40 | 0.57 | 0.58 | 0.57 | 0.62 | 0.53 |
| $FA_2 / C_\beta$ | 0.01 | 0.02 | 0.00 | 0.01 | 0.00 | 0.01 | 0.01 | 0.00 | 0.01 | 0.00 | 0.01 |
| *Expanded ratio* * | 0.76 | 0.76 | 0.58 | 0.41 | 0.59 | 0.36 | 0.56 | 0.57 | 0.57 | 0.58 | 0.52 |

** The expanded ratio refers to the ratio of the sum of areas of the aromatic/unsaturated regions ($G_2$+$G_5$+$G_6$ plus $FA_2$ plus $H_{2,6}$+$J_\beta$) and the sum of areas of the aliphatic oxygenated side chain regions ($A_\alpha$+$A'_\alpha$ plus $A_\gamma$ plus $B_\gamma$ plus $C_\beta$ plus $C_\gamma$).*

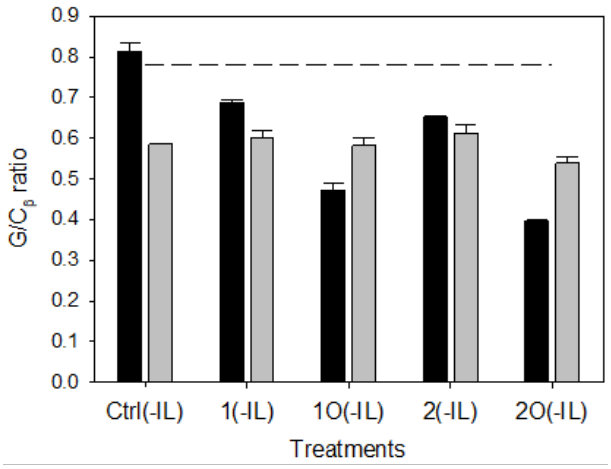


Figure 4.26. *G/ $C_\beta$* ratio calculated from the integration of selected areas in the HSCQ NMR spectra. The horizontal dashed line represents the value for raw Indulin AT, the black columns represent the lignin samples recovered from the treatments without ionic liquid, and the grey columns are those lignin samples recovered from the treatments with ionic liquid.

Indulin AT, indicate that the treatments tested cause a proportionally greater disappearance, in the lignin, of these G-units with regard to the non-aromatically bonded $C_\beta$ atoms. This is consistent with the reported consideration of the β-O-4 bond as being the most easily cleavable bond into lignins through oxidation, which in turn may facilitate the release of guaiacyl units from the solid phase (Dai et al, 2016). Similar conclusions to those from the $G/C_\beta$ ratios in Figure 4.26 would be achieved if calculating an "expanded ratio" using all identified aromatic/unsaturated regions ($G_2$+$G_5$+$G_6$ plus $FA_2$ plus $H_{2,6}$+$J_\beta$) in the numerator and all the identified aliphatic oxygenated side-chain regions ($A_\alpha$+$A'_\alpha$ plus $A_\gamma$ plus $B_\gamma$ plus $C_\beta$ plus $C_\gamma$) in the denominator (Longe et al., 2018) – see numerical values in the bottom row of Table 4.7. Longe et al. (2018) reported some changes in lignin structure after treatment with laccase and ABTS or violuric acid as mediators, for example a general decrease in the relative amount of *G*-units; and these changes appeared to be mediator-dependent. Rico et al. (2014) also reported a decrease in *G*-units after treatment of lignin with *M. thermophila* laccase and methyl syringate mediator.

If comparing the set of treatments without ionic liquid and the set of treatments with ionic liquid, clearly different trends can be observed in Figure 4.26. In the treatments carried out in absence of [$C_2$mim][OAc], an evident decreasing trend of the $G/C_\beta$ ratio occurs in the order: Ctrl > 1 > 2 > 1O > 2O; which corresponds in general with the intensity of the treatment: laccases only (1), laccases with ABTS (2), laccases with an $O_2$ pre-saturation of the medium (1O), and laccases with ABTS and the $O_2$ pre-saturation (2O). A specific comparison of the $G/C_\beta$ ratio for treatments 1 and 2 reveals that the redox potential of the ABTS mediator is more suitable than that of the laccases to react on the guaiacyl units. It is important to note that the laccase from *M. thermophila* used herein is a low redox potential laccase, specifically 465 mV (Munk et al., 2015); hence the importance of the ABTS to increase the oxidative capacity of the enzyme. In a similar manner, direct comparisons of treatments 1 and 1O and treatments 2 and 2O manifest the relevance of supplementation with $O_2$ over naturally dissolved $O_2$ in the transformation of these aromatic units with the investigated laccase(–mediator) system. Regarding the set of treatments involving [$C_2$mim][OAc], a similar value of $G/C_\beta$ ratio was obtained, independently of the treatment conditions, even for the control run (in absence of enzyme). This points to the presence of [$C_2$mim][OAc] as the main responsible actor for the elimination of the guaiacyl units

from the treated lignin, with the potential action of the enzyme being masked by such ionic liquid effect (for example, via the reduction of the laccase activity as a result of increased pH or ionic strength due to the [$C_2$mim][OAc] in the medium, among other possible effects). Evidence of this capacity of action of [$C_2$mim][OAc] on the lignin substrate was already presented in section 4.3.1.

Thermal stability and decomposition rate are greatly influenced by the internal structure of the lignin (Huang et al., 2018), as already mentioned in section 4.3.1.1. Figure 4.27 shows the TGA curves and the corresponding derivative curves for raw Indulin AT (it was already shown in Figure 4.15, but it is included again in this figure for direct visual comparative purposes) and the lignin samples recovered from treatments 2 and 2-IL, as representatives of treatments without and with ionic liquid, respectively. The behaviour observed is completely analogous to that described in section 4.3.1.1: an inital mass loss due to dehydration and removal of low molar mass volatiles (up to ca. 473 K); the main decomposition stage in the approximate range 473-773 K, with only one peak in the derivative curve (maximum of decomposition rate) in the case of the treatment without ionic liquid, and with two peaks in the case of the treatment in the presence of ionic liquid (and also for raw Indulin AT); and a final stage above 773 K, where the decomposition of the aromatic rings occurs following the same pattern in all cases. In the main decomposition step, for treatment 2 the only observed peak can be interpreted as a shift of the first peak of raw Indulin AT towards higher temperatures together with an overlapping with the second peak. In any case, the same TGA behaviours are reproduced for all the treatments with and without ionic liquid – see the corresponding thermograms in Figures D.1-D.4 in Appendix D. All numerical values of temperatures of the maxima of rate of decomposition ($T_{max}$) associated to the peaks in the main decomposition stage of the derivative curves are listed in Table 4.8. This table also includes the residue (char) observed at the end of the TGA thermograms, at 1073 K. The relatively large percentages are likely a result of the high percentage of guaiacyl units in Indulin AT (as compared to other lignins), since these units can easily undergo ionic condensation and radical coupling reactions at the *ortho* and *meta* positions for phenolic OH groups in aromatic ring (Casas et al., 2012; Faix et al., 1988). At a 95 % confidence level, there is no statistical difference among the residues at 1073 K for the samples from the treatments without the IL (1, 2, 1O, and 2O), nor among those for the samples from the treatments with the IL (1-IL, 2-IL, 1O-IL,

and 2O-IL). The mean residuals for these two sets were 43 % and 45 %, respectively; being essentially coincident with the value obtained for raw Indulin AT.

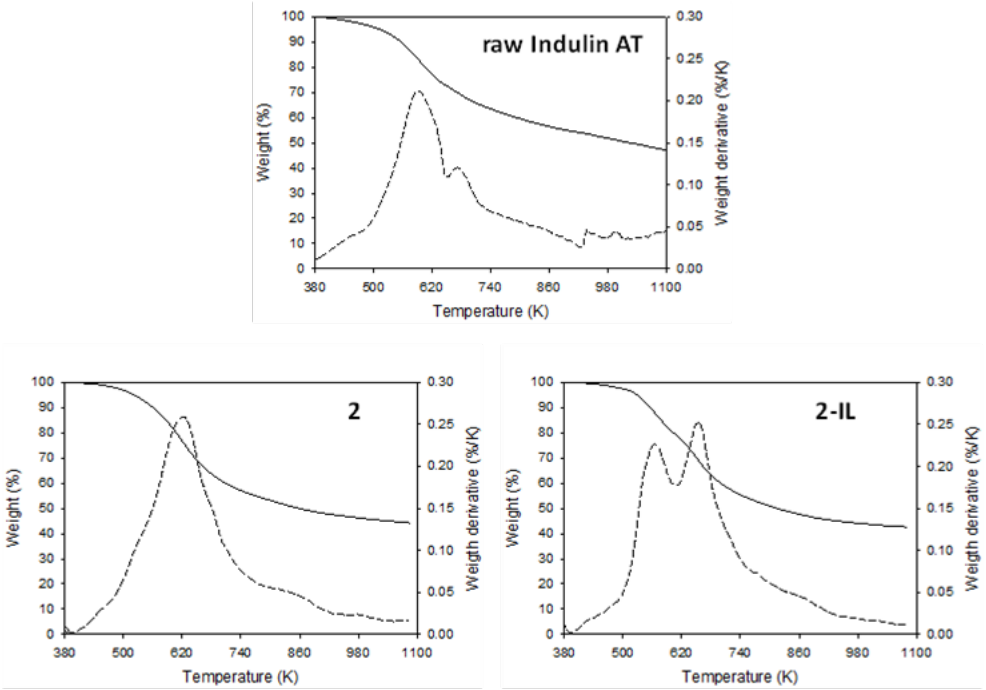


Figure 4.27. TGA thermograms (solid lines), and the corresponding derivative curves (dashed lines) for raw Indulin AT and for the solids recovered after the treatments 2 and 2-IL.

**Table 4.8.** Numerical values of temperature(s) of maxima of decomposition rate ($T_{max}$), residue at 1073 K, and glass transition temperature ($T_g$) for raw Indulin AT and for the solid samples recovered after the different laccase-based treatments.

| Treatment | $T_{max}$ (K) | Residue at 1073 K (%) | $T_g$ (K) |
|---|---|---|---|
| None (raw Indulin AT) | 593, 678 | 45 | 427 |
| Ctrl | 604, 692 | 45 | 433 |
| 1 | 606, 692 | 45 | 437 |
| 1O | 615 | 45 | 438 |
| 2 | 619 | 45 | 439 |
| 2O | 621 | 44 | 439 |
| Ctrl-IL | 563, 653 | 43 | 418 |
| 1-IL | 559, 651 | 43 | 400 |
| 1O-IL | 561, 653 | 43 | 409 |
| 2-IL | 562, 654 | 43 | 400 |
| 2O-IL | 562, 653 | 42 | 412 |

Glass transition ($T_g$) values obtained for the lignin samples recovered from the corresponding DSC thermograms for the treatment involving no ionic liquid are somewhat higher than the $T_g$ value of raw Indulin AT (427 K), lying in the narrow range 433-439 K, including the control sample. This slight increase in $T_g$ may be due to the dissolution of low molecular weight moieties in the aqueous phase (Ramezani and Sain, 2018), while the presence of enzyme and mediator in the treatments would have little influence on this regard. However, for the lignin samples recovered from treatments involving the ionic liquid, the $T_g$ obtained was somewhat lower than that of raw Indulin AT: in the range 400–418 K, also including the corresponding control sample (Ctrl-IL). This might be a result of a greater degree of deconstruction of the original lignin structure due to the applied treatment, compensating for the loss of those low molecular weight moieties getting into the aqueous phase. All individualised numerical values of $T_g$ are listed in Table 4.8, and a couple of illustrative DSC thermograms from which they were obtained are included in Figure 4.28. The rest of DSC thermograms of the solids recovered from the treatments discussed in this section can be consulted in Appendix D (Figures D.5-D.8).

In addition to the effect on $T_g$ discussed above, it is worth noting that in the DSC thermograms of IL treatments (including the Ctrl-IL run) a sharp peak representing an exothermic event was systematically observed at 329 K under heating; with the corresponding endothermic signal also appearing in the cooling ramp at 316 K – see Figure 4.28 and Appendix D (Figures D.5-D.8). The reason for this thermal transition could not be clearly identified, although it might be connected with a somewhat higher pH or a higher ionic strength induced by the presence of the ionic liquid in the treatment medium. The possibility of a potential reaction of [$C_2$mim][OAc] with lignin as responsible for the unexpected signal was ruled out, given the essentially identical FT-IR spectra of raw Indulin AT and the recovered samples, shown in Figure 4.29. The lack of relevant differences in the direct comparison and detailed analysis of the spectra of the Ctrl and Ctrl-IL samples (no enzyme or mediator involved, and the presence of ionic liquid being the only difference), in plots C and D of Figure 4.29, is particularly illustrative in this regard. Interestingly, several characteristic signals associated with different structural features of lignin can be observed in either of these two spectra (see vertical lines in plots C and D of Figure 4.29): quinonoid structures at 1645 $cm^{-1}$, aromatic skeletal vibrations and C=O stretch at 1595 $cm^{-1}$, aromatic skeletal vibration

at 1509 $cm^{-1}$, phenolic hydroxyl at 1384 $cm^{-1}$, syringyl ring vibration at 1333 $cm^{-1}$, guaiacyl ring breathing at 1265 $cm^{-1}$, and C-H out of plane vibrations of carbons 2, 5 and 6 of the guaiacyl ring at 857 $cm^{-1}$ and 813 $cm^{-1}$ (Feng et al., 2019). Stevens et al. (2019) also reported that alkaline lignin treated with laccases, ABTS, and aqueous ionic liquids ([$C_2$mim][OAc] among them) showed few structural changes, although the lignin was partially solubilised and converted to degradation products.

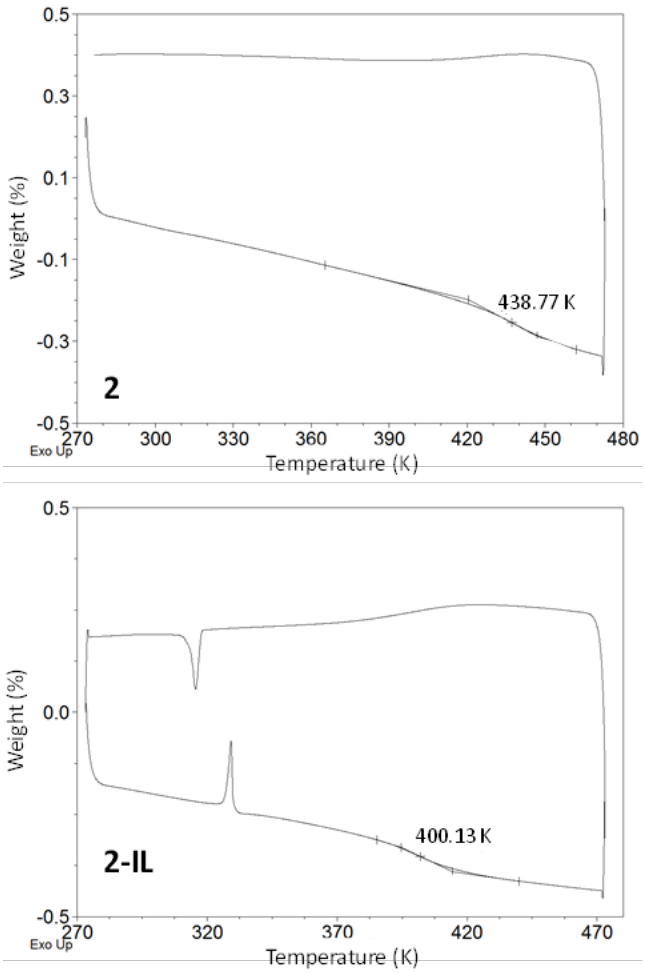


Figure 4.28. DSC thermograms (exo up) of the solid samples recovered after treatments 2 (top plot) and 2-IL (bottom plot).

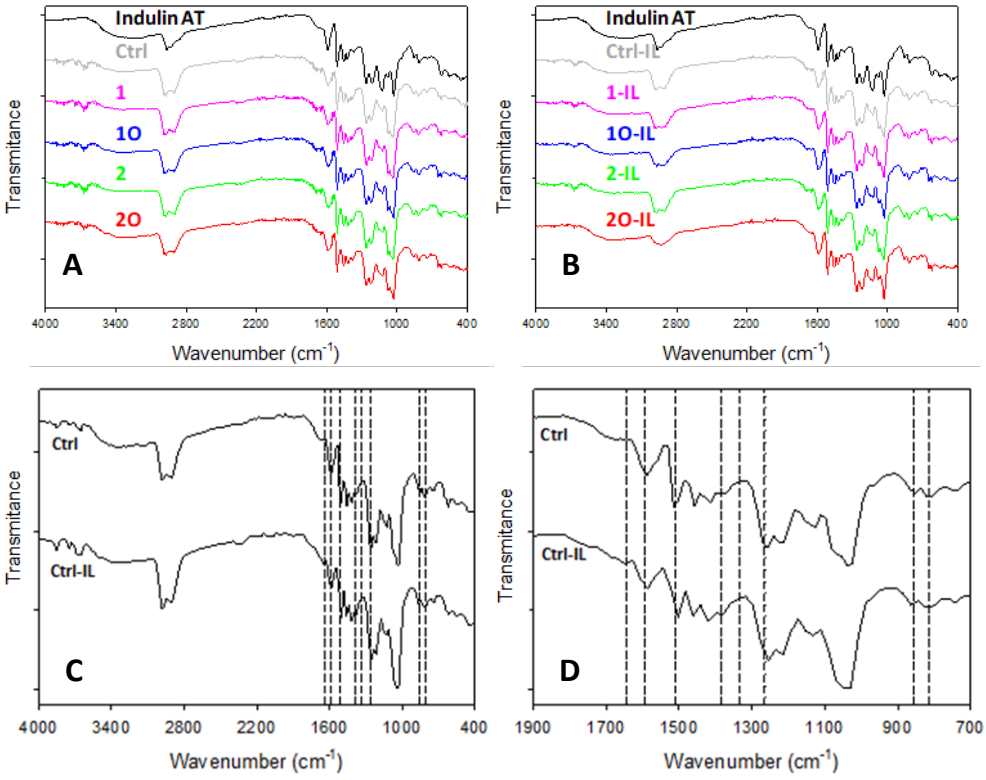


Figure 4.29. FTIR spectra of raw Indulin AT and of the solid samples recovered after each treatment: A) treatments in absence of ionic liquid; B) treatments involving [$C_2$mim][OAc]; C) detailed comparison of the spectra for the samples Ctrl and Ctrl-IL; D) Close-up of plot C in the wavelength range 700-1900 $cm^{-1}$. In plots A and B, treatment codes are displayed on the corresponding spectral lines in the same colour. In plots C and D the vertical dashed lines identify wavelengths corresponding to different structural features characteristic of lignin (see the text for further detail).

### *Antioxidant and antimicrobial capacities*

To evaluate the antioxidant capacity, the radical scavenging activity (RSA) was measured for all lignin samples recovered after the different treatments. The corresponding values, expressed as the percentage of total inhibition of DPPH oxidation, are listed in Table 4.9. For control runs, a small decrease in the RSA percentage with respect to raw Indulin AT (about 2–3 %) is already observed. For the sets of treatments with laccases, a smaller reduction than for the corresponding control run, or even an increase in the RSA percentage, are observed. Nevertheless, all values lie in the range 73–79 %, thus representing small variations, even statistically non-significant for several entries, with respect to the intrinsic antioxidant activity of the

lignin model tested (RSA of 76.5 %). Although somewhat lower, the RSA percentages of all lignin samples are still reasonably comparable to the value of 87.1 % obtained for a widely recognised antioxidant such as BHT. Thus, it can be stated that the quite good antioxidant activity exhibited by Indulin AT is barely affected by the treatments proposed in the present section. In parallel, the concentrations of the raw or treated lignin to achieve a 50 % inhibition of radical species ($IC_{50}$) were approximately double than those required in the case of BHT: 0.188–0.213 mg/mL versus 0.093 mg/mL. For this $IC_{50}$ parameter, again, the conditions of the different lignin treatments have little effect with respect to raw Indulin AT – see Table 4.9.

**Table 4.9**. RSA and $IC_{50}$ of raw Indulin AT and lignin samples recovered after the corresponding treatments. Values for the standard antioxidant BHT are added for comparison purposes. Values in parenthesis represent the radius of the confidence interval at a 95 % confidence level.

| Sample | RSA (%) | $IC_{50}$ (mg/mL) |
|---|---|---|
| Raw Indulin AT | 76.5 (1.6) | 0.188 (0.001) |
| Ctrl | 74.1 (0.2) | 0.211 (0.001) |
| 1 | 75.0 (0.4) | 0.202 (0.012) |
| 1O | 76.2 (0.7) | 0.209 (0.008) |
| 2 | 76.2 (0.2) | 0.200 (0.009) |
| 2O | 79.0 (1.7) | 0.191 (0.008) |
| Ctrl-IL | 73.2 (0.3) | 0.198 (0.001) |
| 1-IL | 74.2 (0.1) | 0.213 (0.014) |
| 1O-IL | 75.9 (0.3) | 0.191 (0.008) |
| 2-IL | 74.8 (0.2) | 0.191 (0.006) |
| 2O-IL | 76.3 (0.4) | 0.194 (0.000) |
| BHT | 87.1 (4.1) | 0.093 (0.004) |

The evaluation of the antimicrobial capacity was carried out for the lignin sample recovered from treatment 2O-IL, which exhibited the largest modification of its structure according to the NMR results in terms of $G/C_\beta$ ratio (see Figure 4.26). For comparison purposes, the lignin sample recovered from the equivalent treatment with no ionic liquid involved (treatment 2O) and raw Indulin AT were also tested. The obtained results are shown in Figure 4.30. As can be seen, a decrease ($p < 0.05$) in the *E. coli* and *S. aureus* growth (~30 % and ~10 %, respectively) was observed when raw Indulin AT was used, independently of the concentration tested. The lignin sample recovered from treatment 2O caused a significant inhibition ($p < 0.05$) against *S. aureus* growth from the concentration of 117.25 µg/mL onwards, achieving ~80 % inhibition

at 234.5 µg/mL. This lignin also led to a reduction ($p < 0.05$) of *E. coli* growth at a concentration of 234.5 µg/mL (24 % inhibition) when compared with the growth control. For other concentrations studied, the inhibition detected was lower (~13 %). The lignin sample recovered after treatment 2O-IL showed an inhibition over the Gram-positive strain (*S. aureus*) of 78 % at the concentration of 117.25 µg/mL ($p < 0.05$), while with the Gram-negative strain (*E. coli*) a 24 % inhibition was found at 234.5 µg/mL ($p < 0.05$). It is remarkable that the laccase-mediator system treatments, with or without ionic liquid, improved the antimicrobial capacity of lignin for the Gram-positive bacterium *S. aureus*. This can be related to the number of functional groups and the molecular weight of the treated lignin, as reported by Yun et al. (2021), who found that the studied original lignin and fractionated lignins can inhibit the growth of Gram-negative bacteria (*E. coli* and *Salmonella*) and Gram-positive bacteria (*Streptococcus* and *S. aureus*), in which the lignin fraction with the lowest molecular weight and highest phenolic hydroxyl content showed the best antimicrobial capacity.

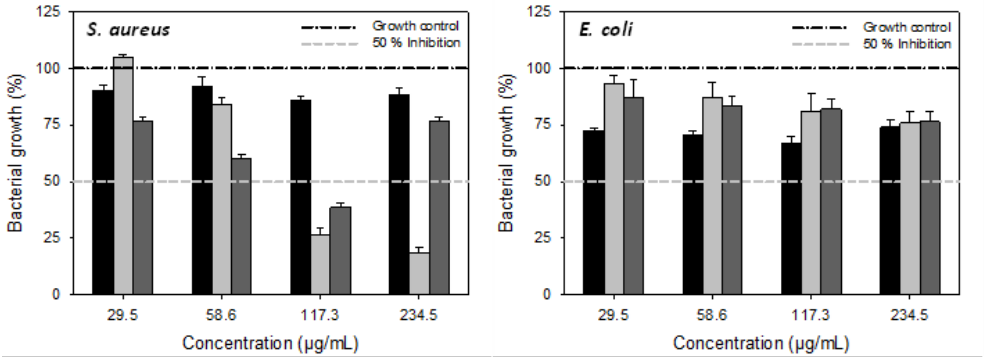


Figure 4.30. Bacterial growth as a result of the effect of different concentrations of raw Indulin AT (black bars) and lignin samples from treatment 2O (light grey bars) and treatment 2O-IL (dark grey bars) on *Staphylococcus aureus* (plot on the left) and *Escherichia coli* (plot on the right).

### 4.3.2.3. Lignin-derived compounds in the post-treatment liquid phases

The total concentration of phenolic compounds in the aqueous phase after each treatment, as determined by the method of Folin-Ciocâlteu, is shown in Figure 4.31. For all treatments involving the ionic liquid, these concentrations are notably higher than

for any of the treatments without it. As noted in section 4.3.2.1, the presence of [$C_2$mim][OAc] in the treatment fluid leads to a moderate increase in pH, which can facilitate the transfer of lignin material from the solid to the liquid phase in the form of phenolic compounds. Interestingly, among treatments with the participation of the ionic liquid, samples from treatments without a mediator (1-IL and 1O-IL) led to a phenolic concentration similar to that of the control run (Ctrl-IL), whereas those treatments with the combination enzyme + mediator resulted in a higher concentration of phenolic compounds in the aqueous phase, highlighting the contributing role of ABTS in the generation of water-soluble phenolic compounds during the lignin treatment. On the other hand, pre-saturation with oxygen did not cause any relevant effect on this total concentration of phenolic compounds in the aqueous phase, as is evident by comparing the bars of 1-IL and 1O-IL treatments, and 2-IL and 2O-IL treatments. One further aspect to be mentioned is that, for treatments in the absence of ionic liquid, the control run (Ctrl) provides a slightly higher concentration of phenolic compounds in the aqueous phase than all enzymatic treatments. This may be a result of the recondensation action of laccases on the lignin substrate, since the depolymerisation process is an equilibrium reaction that also involves the repolymerisation of low molecular weight oligomers. (Nanayakkara et al., 2014).

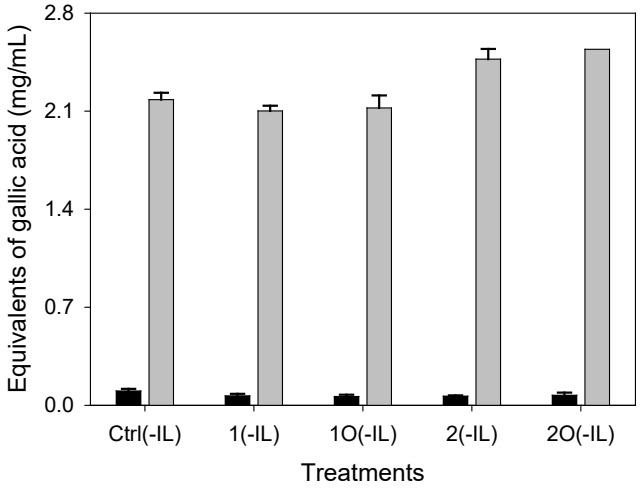


**Figure 4.31. Total concentration of phenolic compounds, expressed as equivalents of gallic acid, in the aqueous phase after each lignin treatment. Black and grey columns correspond to treatments without and with ionic liquid, respectively.**

A considerable number of compounds contributing to the total phenolic concentration were identified by UHPLC and individually quantified. Table 4.10 explicitly lists those for which concentrations higher than 100 mg/L were obtained in at least one of the treatments (other compounds that could be identified in at least one of the treatments, but never at a concentration higher than 100 mg/L, were: caffeic acid, chlorogenic acid, *p*-cymene, 3-hydroxytyrosol, methyl syringate, syringic acid, and tyrosol). While these phenolic compounds are barely present or cannot even be detected in the aqueous filtrate after simple washing of raw Indulin AT with plain water at room temperature, their presence in control samples becomes somewhat more relevant (especially in the case of Ctrl-IL), likely due to the boiling stage included in the experimental procedure. In treatments without ionic liquid, a clear boost in the concentrations of oleuropein (>6000 mg/L) and rosmarinic acid (>4000 mg/L) was identified in treatments involving the combination of enzyme and ABTS (treatments 2 and 2O) with respect to treatments without ABTS (treatments 1 and 1O). Curiously, for these two phenolic compounds, the use of only the enzyme without ABTS led to a decrease in their concentration, from the levels observed in the Ctrl sample to undetectable levels. Regarding treatments involving the ionic liquid, a similar boosting effect of treatments applying the combination of enzyme and ABTS (treatments 2-IL and 2O-IL) with respect to treatments without ABTS (treatments 1-IL and 1O-IL) was observed for the concentrations of guaiacol (>5000 mg/L) and syringaldehyde (>3500 mg/L). To a lesser extent, this effect was also observed in other phenolic compounds with appreciable concentrations, such as ellagic acid, ferulic acid, eugenol, and vanillin.

In the literature, a work by Yang et al. (2019) reported a significant increase on vanillin and *p*-hydroxybenzaldehyde after treatment of *kraft* and organosolv lignins with a thermoalkaliphilic laccase from *Caldalkalibacillus thermarum*; whereas Stevens et al. (2020), investigating interactions between three ionic liquids (including [$C_2$mim][OAc]) and a laccase from *Thermus Thermophilus* for biocatalytic lignin conversion to aromatic monomers, verified that the major products obtained from alkaline lignin were vanillin, acetosyringone, syringaldehyde, and acetovanillone. By comparison with the results in Table 4.10, the relevance of the specific laccase in the type of low molecular weight phenolic compounds most significantly produced in the enzyme-based depolymerisation processes is evidenced.

**Table 4.10.** Concentration of phenolic compounds (expressed in mg/L) identified in the aqueous phase of the different treatments.

| Phenolic compound | Indulin AT washing water | Treatment | | | | | | | | | |
|---|---|---|---|---|---|---|---|---|---|---|---|
| | | Ctrl | 1 | 1O | 2 | 2O | Ctrl-IL | 1-IL | 1O-IL | 2-IL | 2O-IL |
| Caffeic acid (G) | 0 | 19 | 19 | 18 | 22 | 21 | 40 | 40 | 39 | 40 | 40 |
| Carvacrol (G) | 166 | 293 | 295 | 284 | 322 | 290 | 340 | 334 | 341 | 324 | 356 |
| Chlorogenic acid (G) | 0 | 0 | 0 | 0 | 0 | 31 | 18 | 18 | 18 | 18 | 31 |
| *p*-Coumaric acid (H) | 16 | 46 | 48 | 44 | 52 | 58 | 135 | 141 | 136 | 142 | 141 |
| *p*-Cymene (H) | 0 | 27 | 26 | 23 | 28 | 24 | 23 | 22 | 22 | 16 | 16 |
| Ellagic acid (G) | 17 | 116 | 106 | 94 | 71 | 130 | 195 | 190 | 169 | 427 | 406 |
| Eugenol (G) | 12 | 15 | 16 | 19 | 12 | 13 | 173 | 172 | 129 | 268 | 188 |
| Ferulic acid (G) | 12 | 12 | 10 | 10 | 11 | 14 | 29 | 28 | 26 | 314 | 313 |
| Guaiacol (G) | 0 | 505 | 756 | 434 | 644 | 615 | 253 | 255 | 73 | 5925 | 5449 |
| Homovanillic acid (G) | 11 | 25 | 29 | 25 | 27 | 31 | 114 | 109 | 101 | 110 | 108 |
| 3-Hydroxytyrosol (G) | 0 | 0 | 0 | 0 | 0 | 0 | 0 | 0 | 0 | 0 | 12 |
| Methyl syringate (S) | 16 | 13 | 19 | 10 | 14 | 23 | 40 | 48 | 40 | 61 | 59 |
| Naringenin (H) | 28 | 42 | 45 | 33 | 56 | 59 | 142 | 138 | 85 | 101 | 108 |
| Oleuropein (G) | 0 | 161 | 0 | 0 | 8234 | 6560 | 301 | 286 | 208 | 282 | 191 |
| Rosmarinus acid (G) | 0 | 74 | 0 | 0 | 4214 | 4698 | 188 | 182 | 148 | 149 | 148 |
| Syringaldehyde (S) | 39 | 542 | 618 | 375 | 331 | 571 | 965 | 913 | 861 | 4531 | 3813 |
| Syringic acid (S) | 1 | 21 | 21 | 21 | 20 | 22 | 40 | 39 | 37 | 37 | 39 |
| Taxifolin (G) | 24 | 39 | 42 | 30 | 52 | 61 | 141 | 137 | 83 | 298 | 106 |
| Thymol (G) | 144 | 198 | 199 | 195 | 209 | 202 | 218 | 214 | 209 | 209 | 219 |
| Tyrosol (H) | 0 | 45 | 28 | 27 | 37 | 35 | 23 | 24 | 24 | 24 | 24 |
| Vanillin (G) | 4 | 48 | 52 | 39 | 49 | 70 | 130 | 130 | 130 | 185 | 175 |
| Others | 17 | 125 | 113 | 99 | 121 | 156 | 246 | 191 | 236 | 253 | 221 |

*[a] Letters in parentheses after the names of the compounds refer to the unit from which they originate: H for p-hydroxyphenyl units, G for guaiacyl units, and S for syringyl units.*

# 5. CONCLUSIONS

# CONCLUSIONS

In view of the scientific fundamentals developed in this doctoral thesis, strategies based on the combination of molecular solvents and ionic liquids are promising as the basis of new technologies for the valorisation of the two major constituents of lignocellulosic biomass (cellulose and lignin) in a more sustainable framework.

Specific conclusions drawn from the original results reported and discussed in this work are presented below, grouped according to the distribution of the contents in Chapters 3 and 4.

***Pretreatment of cellulose for its improved reactivity***

The ionic liquid [$P_{4444}$][OAc] is capable of reducing the crystallinity of cellulose (MCC or Avicel PH-101 were particularly tested) by means of a non-dissolving pretreatment under mild conditions (atmospheric pressure, 343 K, and pretreatment times as short as 2 h), with easy recovery of the pretreated cellulose and of the pretreatment liquid by filtration. This crystallinity reduction leads to an improvement of the reactivity, illustrated through the analysis of the rate of enzymatic hydrolysis of the pretreated samples.

The combination of [$P_{4444}$][OAc] with the polar aprotic solvent DMSO ($x_{DMSO}$ = 0.20 or 0.40) for its utilisation as a pretreatment liquid, while preserving the non-dissolving character and its associated advantages, results in a significantly larger reduction of the crystallinity of cellulose and also in a faster rate of enzymatic hydrolysis. Moreover, due to its eutectic behaviour, the system [$P_{4444}$][OAc] + DMSO can be used as pretreatment liquid at lower temperatures than the pure [$P_{4444}$][OAc] (which has a melting temperature of 331 K), for example at 323 K.

Mixtures of [$P_{4444}$][OAc] with polar protic solvents such as water and ethanol can be also used in analogous pretreatments for the reduction of the crystallinity of cellulose. This reduction, however, is more modest than the one achieved with the [$P_{4444}$][OAc] + DMSO system, and even equivalent to the one obtained with pure [$P_{4444}$][OAc]. The rate of enzymatic hydrolysis of the cellulose samples pretreated with [$P_{4444}$][OAc] + water or [$P_{4444}$][OAc] + ethanol is, accordingly, slower than the one obtained for the samples pretreated with [$P_{4444}$][OAc] + DMSO.

The binary systems of [$P_{4444}$][OAc] with its homologous halides [$P_{4444}$]Cl and [$P_{4444}$]Br present a eutectic behaviour, with eutectic temperatures of 297 K and 305 K, respectively; notably below the melting temperature of pure [$P_{4444}$][OAc]. Nevertheless, the use of the eutectic mixtures as pretreatment liquids in the approach proposed herein lead to ineffective reduction of the crystallinity index of cellulose, and only to a minor improvement over untreated cellulose in terms of rate of enzymatic hydrolysis.

None of the pretreatments with any of the fluids mentioned above affects relevantly the thermal stability or the degree of polymerisation of cellulose, an aspect of interest in the industry of cellulose-derived polymeric products.

In line with the latter, and in the context of a practical application, the improved reactivity of cellulose (Avicel) pretreated with [$P_{4444}$][OAc] and with a mixture of [$P_{4444}$][OAc] and DMSO has been evidenced through its carboxymethylation. Thanks to the proposed pretreatments, carboxymethylcellulose with degrees of substitution in the commercial range can be obtained under notably simpler and milder conditions than the benchmark process for industrial production of carboxymethylcellulose.

In future work, the pretreatment of lignocellulosic biomass with the proposed liquid systems is envisioned for improved accessibility and subsequent facilitated reactivity (e.g., toward enzymatic hydrolysis) of its cellulosic fraction directly within the lignocellulosic matrix.

To sum up, the work reported herein constitutes a basis of great potential for the future development of affordable non-dissolving pretreatment processes to assist in the production of cellulose-derived chemicals and materials.

***Valorisation of technical lignin***

The treatment of a representative water-insoluble technical lignin (Indulin AT) with a 70 % aqueous solution of the ionic liquid [$C_2$mim][OAc], at ambient temperature and pressure, leads to measurable yields of a variety of value-added phenolic compounds resulting from the lignin depolymerisation. In particular, yields of ca. 3 g of vanillin and ca. 1 g of guaiacol per kilogram of lignin treated can be highlighted. The solid residue left after the treatment has a lower proportion of guaicyl units (G-units) with respect to the original lignin, in agreement with the fact that the phenolic compounds more largely produced derive from G-units.

The assistance of the above treatment with UV irradiation for the photoreaction of lignin depolymerisation catalysed by $TiO_2$ or AgCl nanoparticles does not provide any significant improvement. The supplementation with $H_2O_2$ in this photoreaction-assisted mode does even show a counterproductive effect.

In the direct treatment with a 10 % solution of [$C_2$mim][OAc], the yields obtained are notably lower, possibly due to limited solubility of lignin. However, the ionic liquid in this concentration can be used as adjuvant to tune the performance of the treatment of lignin (at 298 K) with a recombinant laccase from *Myceliophthora thermophila*, or with a laccase-mediator system composed by such laccase and the mediator ABTS, in a mildly acid medium. The higher yields of phenolic compounds in the laccase-mediator treatments with presence of ionic liquid correspond to guaiacol and syringaldehyde, whereas in its absence they correspond to oleuropein and rosmarinic acid. After any of the treatments, nevertheless, a number of other phenolic compounds resulting from the depolymerisation of lignin are also produced in detectable yields.

The solids recovered from the biological treatments showed a lower proportion of G-units with respect to raw Indulin AT, especially when a pre-saturation of the treatment media with $O_2$ was carried out. Interestingly, the solids recovered after the laccase-mediator treatments with a pre-saturation with $O_2$ exhibit enhanced antimicrobial activity against *Staphylococcus aureus*, in comparison to raw Indulin AT.

Overall, the ionic liquid [$C_2$mim][OAc] shows potential for its participation, either as concentrated solute in aqueous solution or as adjuvant of laccase-mediator systems, in schemes of valorisation of lignin via its (partial) depolymerisation. Future work on the development of the approaches proposed herein should focus in strategies oriented to boost the (so far limited) level of depolymerisation.

# List of symbols

# List of symbols

| | |
|---|---|
| $a$ | fit parameter |
| $A$ | pre-exponential factor in the Arrhenius-type equation |
| $A$ | fit parameter in the VFT equation for viscosity |
| $b$ | fit parameter |
| $c$ | fit parameter |
| $C$ | molar concentration |
| $d_1$ | time of recycle delay |
| $E$ | extinction of light |
| $E_a$ | activation energy in the Arrhenius-type equation |
| $H_m$ | molar enthalpy of fusion |
| $^1J_{CH}$ | one-bond proton-carbon coupling constant |
| $k$ | fit parameter in the VFT equation for viscosity |
| $K$ | constant of the capillary viscometer |
| $l$ | layer thickness |
| $MW$ | molecular weight |
| $m$ | mass |
| $n$ | number of moles |
| $R$ | universal constant of gases |
| $R_{CM}$ | FTIR absorbance ratio between the signals for the asymmetric carboxylic stretching and the methylenic/methinic stretching |
| $t$ | time |
| $T$ | temperature |
| $T_d$ | decomposition temperature |
| $T_{exc}$ | melting temperature of the excess compound |
| $T_{eut}$ | melting temperature of the eutectic composition |
| $T_g$ | glass transition temperature |
| $T_m$ | melting temperature |
| $T_{max}$ | temperature of maximum of rate of decomposition |
| $T_0$ | fit parameter in the VFT equation for viscosity |
| $T_1$ | spin-lattice relaxation time |

| | |
|---|---|
| $V$ | volume |
| v/v | volume-to-volume ratio |
| w/v | mass-to-volume ratio |
| w/w | mass-to-mass ratio |
| $x$ | mole fraction in liquid phase |

***Greek letters***

| | |
|---|---|
| $\alpha$ | molar proportion of compound decomposed |
| $\varepsilon$ | molar absorption coefficient |
| $\Delta$ | variation of property |
| $\eta$ | dynamic viscosity |
| $[\eta]_c$ | intrinsic viscosity |
| $\lambda$ | wavelength in the absorption spectrum |
| $\nu$ | kinematic viscosity |
| $\rho$ | density |

# List of abbreviations and acronyms

# List of abbreviations and acronyms

| | |
|---|---|
| ABTS | 2,2′-azino-bis(3-ethylbenzothiazoline-6-sulfonic acid) diammonium salt |
| ATR-FTIR | attenuated total reflectance Fourier-transform infrared |
| BHT | butylated hydroxytoluene |
| CFU | colony-forming unit |
| CMC | carboxymethylcellulose |
| *CI* | crystallinity index |
| *Ctrl* | control |
| DMSO | dimethylsulfoxide |
| *DP* | degree of polymerisation |
| DPPH | 2,2-diphenyl-1-picrylhydrazyl |
| *DS* | degree of substitution |
| DSC | differential scanning calorimetry |
| FID | free induction decay |
| FTIR | Fourier-transform infrared |
| H-CMC | acid-form carboxymethylcellulose |
| HPLC | high-pressure liquid chromatography |
| HSQC NMR | heteronuclear single quantum coherence nuclear magnetic resonance |
| $IC_{50}$ | concentration necessary to achieve 50 % inhibition of radical species |
| INEPT | intensive nuclei enhanced by polarisation transfer |
| IL | ionic liquid |
| MCC | microcrystalline cellulose powder |
| MIC | minimal inhibitory concentration |
| NA | nutrient agar |
| Na-CMC | sodium carboxymethylcellulose |
| NB | nutrient broth |
| NMR | nuclear magnetic resonance |
| PXRD | powder X-ray diffractometry |
| RSA | radical scavenging activity |
| UHPLC | ultra-high-pressure liquid chromatography |

| | |
|---|---|
| UV | ultraviolet |
| UV-vis | ultraviolet-visible |
| TEM | transmission electron microscopy |
| TGA | thermogravimetric analysis |
| XRD | X-ray diffraction |
| 2D | two-dimensional |
| 3D | three-dimensional |
| *%LOD* | percentage of weight loss |
| [$C_2$mim][OAc] | 1-ethyl-3-methylimidazolium acetate |
| [$P_{4444}$]Br | tetrabutylphosphonium bromide |
| [$P_{4444}$]Cl | tetrabutylphosphonium chloride |
| [$P_{4444}$][OAc] | tetrabutylphosphonium acetate |

# References

# References

## A

Abe, M.; Kuroda, K.; Ohno H. (2015). "Maintenance-Free Cellulose Solvents Based on Onium Hydroxides", *ACS Sustainable Chemistry and Engineering*, 3, 1771-1776. https:/7doi.org/10.1021/acssuschemeng.5b00303

Adamová, G.; Gardas, R. L.; Nieuwenhuyzen, M.; Puga, A. V.; Rebelo, L. P. N.; Robertson, A. J.; Seddon, K. R. (2012). "Alkyltributylphosphonium chloride ionic liquids: synthesis, physicochemical properties and crystal structure", *Dalton Transactions*, 41, 8316-8332. https://doi.org/10.1039/c1dt10466g

Ahvenianen, P.; Kontro, I.; Svedström, K. (2016). "Comparison of sample crystallinity determination methods by X-ray diffraction for challenging cellulose I materials", *Cellulose*, 23, 1073-1086. https://doi.org/10.1007/s10570-016-0881-6

Alder, C. M.; Hayler, J. D.; Henderson, R. K.; Redman, A. M.; Shukla, L.; Shuster, L. E.; Sneddon, H. F. (2016). "Updating and further expanding GSK's solvent sustainability guide". *Green Chemistry*, 18, 3879-3890. https://doi.org/10.1039/C6GC00611F

Asaadi, S.; Hummel, M.; Ahvenainen, P.; Gubitosi, M.; Olsson, U.; Sixta, H. (2018). "Structural analysis of Ioncell-F fibres from birch wood", *Carbohydrate Polymers*, 181, 893-901. https://doi.org/10.1016/j.carbpol.2017.11.062

## B

Bozell, J. J.; Holladay, J. E.; Johnson, D.; White, J. F. (2007). *Top Value-Added Chemicals from Biomass. Volume II—Results of Screening for Potential Candidates from Biorefinery Lignin*, Pacific Northwest National Laboratory, report prepared for the US Department of Energy under contract DE-AC05-76RL01830.

Bradaric, C. J.; Downard, A.; Kennedy, C.; Robertson, A. J.; Zhou, Y. (2003). "Industrial preparation of phosphonium ionic liquids", *Green Chemistry*, 5, 143-152. https://doi.org/10.1039/B209734F

Brandt, A.; Gräsvik, J.; Hallett, J. P.; Welton, T. (2013). "Deconstruction of lignocellulosic biomass with ionic liquids", *Green Chemistry,* 15, 550-583. https://doi.org/10.1039/C2GC36364J

Buswell, J. A.; Cai, Y.; Chang, S.-T. (1995). "Effect of nutrient nitrogen and manganese on manganese peroxidase and laccase production by *Lentinula (Lentinus) edodes*", *FEMS Microbiology Letters*, 128, 81-87. https://doi.org/10.1111/j.1574-6968.1995.tb07504.x

## C

Casas, A.; Oliet, M.; Alonso, M. V.; Rodríguez, F. (2012). "Dissolution of *Pinus radiata* and *Eucalyptus globulus* woods in ionic liquids under microwave radiation: Lignin regeneration and characterization", *Separation and Purification Technology,* 97, 115-122. https://doi.org/10.1016/j.seppur.2011.12.032

Casimiro, F. M.; Costa, C. A. E.; Vega-Aguilar, C.; Rodrigues, A. E. (2022). "Hardwood and softwood lignins from sulfite liquors: Structural characterization and valorization through depolymerization", *International Journal of Biological Macromolecules*, 215, 272-279. https://doi.org/10.1016/j.ijbiomac.2022.06.067

Castro, M. C.; Rodríguez, H.; Arce, A.; Soto, A. (2014). "Mixtures of Ethanol and the Ionic Liquid 1-Ethyl-3-methylimidazolium Acetate for the Fractionated Solubility of Biopolymers of Lignocellulosic Biomass", *Industrial and Engineering Chemistry Research,* 53, 11850-11861. https://doi.org/10.1021/ie501956x

Chang, K.-L.; Wang, X.-Q.; Han, Y.-J.; Deng, H.; Liu, J.-Y.; Lin, Y.-C. (2018). "Enhanced Enzymatic Hydrolysis of Rice Straw Pretreated by Oxidants Assisted with Photocatalysis Technology", *Materials*, 11, article no. 802. https://doi.org/10.3390/ma11050802

Chatel, G.; Rogers, R. D. (2014). "Review: Oxidation of Lignin Using Ionic Liquids – An Innovative Strategy To Produce Renewable Chemicals", *ACS Sustainable Chemistry and Engineering,* 2, 322-339. https://doi.org/10.1021/sc4004086

Cheng, G.; Kent, M. S.; He, L.; Varanasi, P.; Dibble, D.; Arora, R.; Deng, K.; Hong, K.; Melnichenko, Y. B.; Simmons, B. A.; Singh, S. (2012). "Effect of Ionic Liquid Treatment on the Structures of Lignins in Solutions: Molecular Subunits Released from Lignin", *Langmuir*, 28, 11850-11857. https://doi.org/10.1021/la300938b

Cherubini, F.; Jungmeier, G.; Wellisch, M.; Willke, T.; Skiadas, I.; Ree, R. V.; Jong, E. (2009). "Toward a common classification approach for biorefinery systems", *Biofuels, Bioproducts and Biorefining,* 3, 534-546. https://doi.org/10.1002/bbb.172

Clough, M. T.; Geyer, K.; Hunt, P. A.; Mertes, J.; Welton, T. (2013). "Thermal decomposition of carboxylate ionic liquids: trends and mechanism". *Physical Chemistry Chemical Physics,* 15, 20480-20495. https://doi.org/10.1039/C3CP53648C

CLSI—Clinical and Laboratory Standards Institute (2009). *Methods for Dilution Antimicrobial Susceptibility Tests for Bacteria that Grow Aerobically*, 17th ed., Approved Standard, Document M07-A8, CLSI, Wayne, PA, USA.

Cohen, M. H.; Turnbull, D. (1959). "Molecular Transport in Liquids and Glasses", *Journal of Chemical Physics*, 31, 1164-1169. https://doi.org/10.1063/1.1730566

Colmenares, J. C.; Varma, R. S.; Nair, V. (2017). "Selective photocatalysis of lignin-inspired chemicals by integrating hybrid nanocatalysis in microfluidic reactors", *Chemical Society Reviews,* 46, 6675-6686. https://doi.org/10.1039/c7cs00257b

Cortesão, A. M.; Henriques, J. G.; Castro, R. A. E.; Maria, T. M. R.; Canotilho, J.; Eusébio, M. E. S. (2017). "Binary phase diagrams of pyridiniecarboxamide isomers", *Journal of Thermal Analysis and Calorimetry*, 130, 1727-1733. https://doi.org/10.1007/s10973-017-6474-2

## D

Dai, J.; Patti, A. F.; Saito, K. (2016). "Recent developments in chemical degradation of lignin: catalytic oxidation and ionic liquids", *Tetrahedron Letters,* 57, 4945-4951. https://doi.org/10.1016/j.tetlet.2016.09.084

Dai, J.; Styles, G. N.; Patti, A. F.; Saito, K. (2018). "$CuSO_4/H_2O_2$-Catalyzed Lignin Depolymerization under the Irradiation of Microwaves", *ACS Omega*, 3, 10433-10441. https://doi.org/10.1021/acsomega.8b01978

del Río, J. C.; Rencoret, J.; Prinsen, P.; Martínez, A. T.; Ralph, J.; Gutiérrez, A. (2012). "Structural Characterization of Wheat Straw Lignin as Revealed by Analytical Pyrolysis, 2D-NMR, and Reductive Cleavage Methods", *Journal of Agricultural and Food Chemistry*, 60, 5922-5935. https://doi.org/10.1021/jf301002n

Devore, J. L. (2004). *Probability and Statistics for Engineering and the Sciences*, 6th ed., Brooks/Cole, Belmont, CA, USA. ISBN: 978-0006210177

Dibble, D. C.; Li, C.; Sun, L.; George, A.; Cheng, A.; Çetinkol, Ö. P.; Benke, P.; Holmes, B. M.; Singh, S.; Simmons, B. A. (2011). "A facile method for the recovery of ionic liquid and lignin from biomass pretreatment", *Green Chemistry*, 13, 3255-3264. https://doi.org/10.1039/C1GC15111H

Domínguez, A.; Rodríguez, O.; Tavares, A. P. M.; Macedo, E. A.; Longo, M. A.; Sanromán, M. A. (2011). "Studies of laccase from *Trametes versicolor* in aqueous solutions of several methylimidazolium ionic liquids", *Bioresource Technology*, 102, 7494–7499. https://doi.org/10.1016/j.biortech.2011.05.063

Duchemin, B. J. C. (2015). "Mercerisation of cellulose in aqueous NaOH at low concentrations", *Green Chemistry*, 17, 3941-3947. https://doi.org/10.1039/C5GC00563A

Dutta, T.; Isern, N. G.; Sun, J.; Wang, E.; Hull, S.; Cort, J. R.; Simmons, B. A.; Singh, S. (2017). "Survey of Lignin-Structure Changes and Depolymerization during Ionic Liquid Pretreatment", *ACS Sustainable Chemistry and Engineering,* 5, 10116-10127. https://doi.org/10.1021/acssuschemeng.7b02123

## E

El-Hosainy, H.; Mine, S.; Toyao, T.; Shimizu, K.; Tsunoji, N.; Esmat, M.; Doustkhah, E.; El-Kemary, M.; Ide, Y. (2022). "Layered silicate stabilises diiron to mimic UV-shielding $TiO_2$ nanoparticle", *Materials Today Nano,* 19, article no. 100227. https://doi.org/10.1016/j.mtnano.2022.100227

El Seoud, O. A.; Fidale, L. C.; Ruiz, N.; D'Almeida, M. L.; Frollini, E. (2008). "Cellulose swelling by protic solvents: which properties of the biopolymer and the solvent matter?", *Cellulose*, 15, 371–392. https://doi.org/10.1007/s10570-007-9189-x

Eyler, R. W.; Klug, E. D.; Diephuis, F. (1947). "Determination of Degree of Substitution of Sodium Carboxymethylcellulose", *Analytical Chemistry*, 19, 24-27. https://doi.org/10.1021/ac60001a007

## F

Fache, M.; Boutevin, B.; Caillol, S. (2016). "Vanillin Production from Lignin and Its Use as a Renewable Chemical", *ACS Sustainable Chemistry and Engineering*, 4, 35-46. https://doi.org/10.1021/acssuschemeng.5b01344

Faix, O.; Jakab, E.; Till, F.; Székely, T. (1988). "Study on low mass thermal degradation products of milled wood lignins by thermogravimetry-mass-spectrometry", *Wood Science and Technology*, 22, 323-334. https://doi.org/10.1007/BF00353322

Fedyaeva, O. N.; Vostrikov, A. A.; Artamonov, D. O.; Shishkin, A. V.; Sokol, M. Y. (2020). "Combustion of Sludge-Lignin in Water-Oxygen Mixture", *Journal of Engineering Thermophysics*, 29, 26-41. https://doi.org/10.1134/S1810232820010038

Feng, N.; Guo, L.; Ren, H.; Xie, Y.; Jiang, Z.; Ek, M.; Zhai, H. (2019). "Changes in chemical structures of wheat straw auto-hydrolysis lignin by 3-hydroxyanthranilic acid as a laccase mediator", *International Journal of Biological Macromolecules*, 122, 210-215. https://doi.org/10.1016/j.ijbiomac.2018.10.153

Ferguson, J. L.; Holbrey, J. D.; Ng, S.; Plechkova, N. V.; Seddon, K. R., Tomaszowska, A. A.; Wassell, D. F. (2012). "A greener, halide-free approach to ionic liquid synthesis", *Pure and Applied Chemistry*, 84, 723-744. https://doi.org/10.1351/PAC-CON-11-07-21

Ferro, M.; Mannu, A.; Panzeri, W.; Theeuwen, C. H. J.; Mele, A. (2020). "An Integrated Approach to Optimizing Cellulose Mercerization", *Polymers*, 12, article no. 1559. https://doi.org/10.3390/polym12071559

FitzPatrick, M.; Champagne, P.; Cunningham, M. F.; Whitney, R. A. (2010). "A biorefinery processing perspective: Treatment of lignocellulosic materials for the production of value-added products", *Bioresource Technology,* 101, 8915-8922. https://doi.org/10.1016/j.biortech.2010.06.125

Freemantle, M. (2010). *An Introduction to Ionic Liquids*, The Royal Society of Chemistry. Cambridge, UK. ISBN: 978-1-84755-161-0

Freire, M. G.; Teles, A. R. R.; Rocha, M. A. A.; Schröder, B.; Neves, C. M. S. S.; Carvalho, P. J.; Evtuguin, D. V.; Santos, L. M. N. B. F.; Coutinho, J. A. P. (2011). "Thermophysical Characterization of Ionic Liquids Able To Dissolve Biomass", *Journal of Chemical and Engineering Data*, 56, 4813-4822. https://doi.org/10.1021/je200790q

## G

Geniselli da Silva, V. (2021). "Laccases and ionic liquids as an alternative method for lignin depolymerization: A review", *Bioresource Technology Reports*, 16, article no. 100824. https://doi.org/10.1016/j.biteb.2021.100824

George, A.; Tran, K.; Morgan, T. J.; Benke, P. I.; Berrueco, C.; Lorente, E.; Wu, B. C.; Keasling, J. D.; Simmons, B. A.; Holmes, B. M. (2011). "The effect of ionic liquid cation and anion combinations on the macromolecular structure of lignins", *Green Chemistry*, 13, 3375-3385. https://doi.org/10.1039/C1GC15543A

Glasser, W. G.; Jain, R. K. (1993). "Lignin Derivatives. I. Alkanoates", *Holzforschung*, 47, 225-233. https://doi.org/10.1515/hfsg.1993.47.3.225

## H

Hall, M.; Bansal, P.; Lee, J. H.; Realff, M. J.; Bommarius, A. S. (2010). "Cellulose crystallinity – a key predictor of the enzymatic hydrolysis rate", *FEBS Journal*, 277, 1571-1582. https://doi.org/10.1111/j.1742-4658.2010.07585.x

Harwardt, N.; Stripling, N.; Roth, S.; Liu, H.; Schwaneberg, U.; Spiess, A. C. (2014). "Effects of ionic liquids on the reaction kinetics of a laccase–mediator system", *RSC Advances*, 4, 17097-17104. https://doi.org/10.1039/C4RA00733F

He, M.-K.; He, Y.-L.; Li, Z.-Q.; Zhao, L.-N.; Zhang, S.-Q.; Liu, H.-M.; Qin, Z. (2022). "Structural characterization of lignin and lignin-carbohydrate complex (LCC) of sesame hull", *International Journal of Biological Macromolecules*, 209, 258-267, https://doi.org/10.1016/j.ijbiomac.2022.04.009

Hernández-Beltrán, J. U.; Hernández-De Lira, I. O.; Cruz-Santos, M. M.; Saucedo-Luevanos, A.; Hernández-Terán, F.; Balagurusamy, N. (2019). "Insight into Pretreatment Methods of Lignocellulosic Biomass to Increase Biogas Yield: Current State, Challenges, and Opportunities", *Applied Sciences*, 9, article no. 3721. https://doi.org/10.3390/app9183721

Holding, A. J.; Heikkilä, M.; Kilpeläinen, I.; King, A. W. T. (2014). "Amphiphilic and Phase-Separable Ionic Liquids for Biomass Processing", *ChemSusChem*, 7, 1422-1434. https://doi.org/10.1002/cssc.201301261

Holding, A. J.; Parviainen, A.; Kilpeläinen, I.; Soto, A.; King, A. W. T.; Rodríguez, H. (2017). "Efficiency of hydrophobic phosphonium ionic liquids and DMSO as recyclable

cellulose dissolution and regeneration media", *RSC Advances*, 7, 17451-17461. https://doi.org/10.1039/C7RA01662J

Hu, J.; Zhang, Q.; Lee, D.-J. (2018). "Kraft lignin biorefinery: A perspective", *Bioresource Technology*, 247, 1181-1183. https://doi.org/10.1016/j.biortech.2017.08.169

Huang, Y.; Liu, H.; Yuan, H.; Zhuang, X.; Yuan, S.; Yin, X.; Wu, C. (2018). "Association of chemical structure and thermal degradation of lignins from crop straw and softwood", *Journal of Analytical and Applied Pyrolysis*, 134, 25-34. https://doi.org/10.1016/j.jaap.2018.04.008

Huang, Y.-B.; Xin, P.-P.; Li, J.-X.; Shao, Y.-Y.; Huang, C.-B.; Pan, H. (2016). "Room-Temperature Dissolution and Mechanistic Investigation of Cellulose in a Tetra-butylammonium Acetate/Dimethyl Sulfoxide System", *ACS Sustainable Chemistry and Engineering*, 4, 2286-2294. https://doi.org/10.1021/acssuschemeng.5b01749

Huber, G. W.; Iborra, S.; Corma, A. (2006). "Synthesis of transportation fuels from biomass: Chemistry, catalysts, and engineering", *Chemical Reviews,* 106, 4044-4098. https://doi.org/10.1021/cr068360d

## I

Itoh, T.; Takagi, Y. (2021) "Laccase-Catalyzed Reactions in Ionic Liquids for Green Sustainable Chemistry", *ACS Sustainable Chemistry and Engineering*, 9, 1443-1458. https://doi.org/10.1021/acssuschemeng.0c07097

Isikgor, F. H.; Becer, C. R. (2015). "Lignocellulosic biomass: a sustainable platform for the production of bio-based chemicals and polymers", *Polymer Chemistry*, 6, 4497-4559. https://doi.org/10.1039/C5PY00263J

## K

Kamwilaisak, K.; Wright, P. C. (2012). "Investigating Laccase and Titanium Dioxide for Lignin Degradation", *Energy and Fuels*, 26, 2400-2406. https://doi.org/10.1021/ef3000533

Kärkäs, M. D.; Bosque, I.; Matsuura, B. S.; Stephenson C. R. J. (2016). "Photocatalytic Oxidation of Lignin Model Systems by Merging Visible-Light Photoredox and Palladium Catalysis", *Organic Letters,* 18, 5166-5169. https://doi.org/10.1021/acs.orglett.6b02651

Kim, H.; Ralph, J. (2010). "Solution-state 2D NMR of ball-milled plant cell wall gels in DMSO-d6/pyridine-d5", *Organic and Biomolecular Chemistry*, 8, 576-591. https://doi.org/10.1039/b916070a

Klemm, D.; Heublein, B.; Fink, H. P.; Bohn, A. (2005). "Cellulose: Fascinating Biopolymer and Sustainable Raw Material", *Angewandte Chemie International Edition*, 44, 3358-3393. https://doi.org/10.1002/anie.200460587

Klemm, D.; Philipp, B.; Heinze, T.; Heinze, U.; Wagenknecht, W. (1998). *Comprehensive Cellulose Chemistry*, Wiley-VCH, Weinheim, Germany. ISBN: 9783527601929

Klug, E. D.; Tinsley, J. S. (1950). "Carboxyalkyl ethers of cellulose", US Patent 2,517,577.

Kono, H.; Oshima, K.; Hashimoto, H.; Shimizu, Y.; Tajima, K. (2016). "NMR characterization of sodium carboxymethyl cellulose: Substituent distribution and mole fraction of monomers in the polymer chains", *Carbohydrate Polymers*, 146, 1-9. https://doi.org/10.1016/j.carbpol.2016.03.021

Krässig, H.; Schurz, J.; Steadman, R. G.; Schliefer, K.; Albrecht, W.; Mohring, M.; Schlosser, H. (2012). "Cellulose", in: *Ullmann's Encyclopedia of Industrial Chemistry*, Wiley-VCH Verlag, Weinheim, Germany. https://doi.org/10.1002/14356007.a05_375.pub2

Kuga, S.; Takagi, S.; Brown, R. M. (1993). "Native folded-chain cellulose II", *Polymer*, 34, 3293-3297. https://doi.org/10.1016/0032-3861(93)90404-X

## L

Langan, P.; Nishiyama, Y.; Chanzy, H. (2001). "X-ray Structure of Mercerized Cellulose II at 1 Å Resolution", *Biomacromolecules*, 2, 410-416. https://doi.org/10.1021/bm005612q

Leitch, A. C.; Abdelghany, T. M.; Probert, P. M.; Dunn, M. P.; Meyer, S. K.; Palmer, J. M.; Cooke, M. P.; Blake, L. I.; Morse, K.; Rosenmai, A. K.; Oskarsson, A.; Bates, L.; Figueiredo, R. S.; Ibrahim, I.; Wilson, C.; Abdelkader, N. F.; Jones, D. E.; Blain, P. G.; Wright, M. C. (2020). "The toxicity of the methylimidazolium ionic liquids, with a focus on M8OI and hepatic effects", *Food and Chemical Toxicology,* 136, article no. 111069. https://doi.org/10.1016/j.fct.2019.111069

Li, C.; Zhao, X.; Wang, A.; Huber, G. W.; Zhang, T. (2015). "Catalytic Transformation of Lignin for the Production of Chemicals and Fuels", *Chemical Reviews*, 115, 11559-11624. https://doi.org/10.1021/acs.chemrev.5b00155

Li, H.; McDonald, A. G. (2014). "Fractionation and characterization of industrial lignins", *Industrial Crops and Products*, 62, 67-76. https://doi.org/10.1016/j.indcrop.2014.08.013

Li, L.; Zhou, W.; Wu, H.; Yu, Y.; Liu, F.; Zhu, D. (2014). "Relationship between crystallinity index and enzymatic hydrolysis performance of celluloses separated from aquatic and terrestrial plants materials", *BioResources*, 9, 3993-4005.

Li, W.; Wang, Y.; Li, D.; Jiang, J.; Li, K.; Zhang, K.; An, Q.; Zhai, S.; Wei, L. (2021). "1-Ethyl-3-methylimidazolium acetate ionic liquid as simple and efficient catalytic system for the oxidative depolymerization of alkali lignin", *International Journal of Biological Macromolecules*, 183, 285-294. https://doi.org/10.1016/j.ijbiomac.2021.04.118

Liebert, T. (2010). "Cellulose Solvents – Remarkable History, Bright Future", in: *Cellulose Solvents: For Analysis, Shaping and Chemical Modification* (Eds: Liebert, T. F.; Heinze, T. J.; Edgar, K. J.), ACS Symposium Series, vol. 1033, American Chemical Society, Washington, DC, USA. https://doi.org/10.1021/bk-2010-1033.ch001

Liu, G.; Bao, J. (2019). "Maximizing phosphorous and potassium recycling by supplementation of lignin combustion ash from dry biorefining of lignocellulose", *Biochemical Engineering Journal*, 144, 104-109. https://doi.org/10.1016/j.bej.2019.01.011

Liu, Y.; Wang, Z.; Wang, J.; Yang, G.; Huang, F.; Lucia, L. (2012). "Evaluation of the structural and molecular weight changes of lignin during the treatment of hardwood alkaline peroxide mechanical pulp with laccase and a laccase-mediator-system", *Bioresources*, 7, 4284-4293.

Liu, Z.-H.; Le, R. K.; Kosa, M.; Yang, B.; Yuan, J.; Ragauskas, A. J. (2019). "Identifying and creating pathways to improve biological lignin valorization", *Renewable and Sustainable Energy Reviews,* 105, 349-362. https://doi.org/10.1016/j.rser.2019.02.009

Longe, L. F.; Couvreur, J.; Grandchamp, M. L.; Garnier, G.; Allais, F.; Saito, K. (2018). "Importance of Mediators for Lignin Degradation by Fungal Laccase", *ACS Sustainable Chemistry and Engineering*, 6, 10097-10107. https://doi.org/10.1021/acssuschemeng.8b01426

## M

Majewicz, T. G.; Podlas, T. J. (2000). "Cellulose Ethers", in: *Kirk-Othmer Encyclopedia of Chemical Technology*, John Wiley & Sons, New York, NY, USA. https://doi.org/10.1002/0471238961.0305121213011005.a01

Makhotkina, O. A.; Preis, S. V.; Parkhomchuk, E. V. (2008). "Water delignification by advances oxidation processes: Homogeneous and heterogeneous Fenton and $H_2O_2$ photo-assisted reactions", *Applied Catalysis B: Environmental*, 84, 821-826. https://doi.org/10.1016/j.apcatb.2008.06.015

Makkar, H. P. S.; Singh, B.; Vats, S. K.; Sood, R. P. (1993). "Total phenols, tannins and condensed tannins in different parts of *Rumex hastatus*", *Bioresource Technology*, 45, 69-71. https://doi.org/10.1016/0960-8524(93)90147-4

Manna, B.; Datta, S.; Ghosh, A. (2021). "Understanding the dissolution of softwood lignin in ionic liquid and water mixed solvents", *International Journal of Biological Macromolecules,* 182, 402-412. https://doi.org/10.1016/j.ijbiomac.2021.04.006

Martins, M. A. R.; Pinho, S. P.; Coutinho, J. A. P. (2019). "Insights into the Nature of Eutectic and Deep Eutectic Mixtures", *Journal of Solution Chemistry*, 48, 962-982. https://doi.org/10.1007/s10953-018-0793-1

Michelin, M.; Liebentritt, S.; Vicente, A. A.; Teixeira, J. A. (2018). "Lignin from an integrated process consisting of liquid hot water and ethanol organosolv: Physicochemical and antioxidant properties", *International Journal of Biological Macromolecules,* 120, 159-169. https://doi.org/10.1016/j.ijbiomac.2018.08.046

Mikkola, S.-K.; Robciuc, A.; Lokajová, J.; Holding, A. J.; Lämmerhofer, M.; Kilpeläinen, I.; Holopainen, J. M.; King, A. W. T.; Wiedmer, S. K. (2015). "Impact of Amphiphilic Biomass-Dissolving Ionic Liquids on Biological Cells and Liposomes", *Environmental Science and Technology*, 49, 1870-1878. https://doi.org/10.1021/es505725g

Munk, L.; Andersen, M. L.; Meyer, A. S. (2018). "Influence of mediators on laccase catalyzed radical formation in lignin", *Enzyme and Microbial Technology*, 116, 48-56. https://doi.org/10.1016/j.enzmictec.2018.05.009

Munk, L.; Sitarz, A. K.; Kalyani, D. C.; Mikkelsen, J. D.; Meyer, A. S. (2015). "Can laccases catalyze bond cleavage in lignin?", *Biotechnology Advances*, 33, 13-24. https://doi.org/10.1016/j.biotechadv.2014.12.008

## N

Nagarajan, S.; Skillen, N. C.; Irvine, J. T. S.; Lawton, L. A.; Robertson, P. K. J. (2017). "Cellulose II as bioethanol feedstock and its advantages over native cellulose", *Renewable and Sustainable Energy Reviews*, 77, 182-192. https://doi.org/10.1016/j.rser.2017.03.118

Nanayakkara, S.; Patti, A. F.; Saito, K. (2014). "Chemical depolymerization of lignin involving the redistribution mechanism with phenols and repolymerization of depolymerized products", *Green Chemistry*, 16, 1897-1903. https://doi.org/10.1039/C3GC41708E

Ninomiya, K.; Ochiai, K.; Eguchi, M.; Kuroda, K.; Tsuge, Y.; Ogino, C.; Taima, T.; Takahashi, K. (2018). "Oxidative depolymerization potential of biorefinery lignin obtained by ionic liquid pretreatment and subsequent enzymatic saccharification of eucalyptus", *Industrial Crops and Products*, 111, 457-461. https://doi.org/10.1016/j.indcrop.2017.10.056

## O

O'Sullivan, A. C. (1997). "Cellulose: the structure slowly unravels", *Cellulose*, 4, 173-207. https://doi.org/10.1023/A:1018431705579

## P

Park, S.; Baker, J. O.; Himmel, M. E.; Parilla, P. A.; Johnson, D. K. (2010). "Cellulose crystallinity index: measurement techniques and their impact on interpreting cellulase performance", *Biotechnology for Biofuels*, 3, article no. 10. https://doi.org/10.1186/1754-6834-3-10

Prado, R.; Erdocia, X.; De Gregorio, G. F.; Labidi, J.; Welton, T. (2016). "Willow Lignin Oxidation and Depolymerization under Low Cost Ionic Liquid", *ACS Sustainable Chemistry and Engineering*, 4, 5277-5288. https://doi.org/10.1021/acssuschemeng.6b00642

Pushpamalar, V.; Langford, S. J.; Ahmad, M.; Lim, Y. Y. (2006). "Optimization of reaction conditions for preparing carboxymethyl cellulose from sago waste", *Carbohydrate Polymers*, 64, 312-318. https://doi.org/10.1016/j.carbpol.2005.12.003

## Q

Queirós, C. S. G. P.; Paredes, X.; Avelino, T. F. S.; Bastos, D. E. N.; Ferreira, M.; Santos, F. J. V.; Santos, A. F.; Lopes, M. L. M.; Lourenço, M. J. V.; Pereira, H.; Nieto de Castro, C. A. (2020). "The influence of water on the thermophysical properties of 1-ethyl-3-methylimidazolium acetate", *Journal of Molecular Liquids,* 297, article no. 111925. https://doi.org/10.1016/j.molliq.2019.111925

## R

Radhakrishnan, R.; Patra, P.; Das, M.; Ghosh, A. (2021). "Recent advancements in the ionic liquid mediated lignin valorization for the production of renewable materials and value-added chemicals", *Renewable and Sustainable Energy Reviews*, 149, article no. 111368. https://doi.org/10.1016/j.rser.2021.111368

Ragauskas, A. J.; Beckham, G. T.; Biddy, M. J.; Chandra, R.; Chen, F.; Davis, M. F.; Davison, B. H.; Dixon, R. A.; Gilna, P.; Keller, M.; Langan, P.; Naskar, A. K.; Saddler, J. N.; Tschaplinski, T. J.; Tuskan, G. A.; Wyman, C. E. (2014). "Lignin Valorization: Improving Lignin Processing in the Biorefinery", *Science*, 344, article no. 1246843. https://doi.org/10.1126/science.1246843

Ralph, J.; Lapierre, C.; Boerjan, W. (2019). "Lignin structure and its engineering", *Current Opinion in Biotechnology*, 56, 240-249. https://doi.org/10.1016/j.copbio.2019.02.019

Ramezani, N.; Sain, M. (2018). "Thermal and Physiochemical Characterization of Lignin Extracted from Wheat Straw by Organosolv Process", *Journal of Polymers and the Environment*, 26, 3109-3116. http://dx.doi.org/10.1007/s10924-018-1199-2

Rico, A.; Rencoret, J.; del Río, J. C.; Martínez, A. T.; Gutiérrez, A. (2014). "Pretreatment with laccase and a phenolic mediator degrades lignin and enhances saccharification of *Eucalyptus* feedstock", *Biotechnology for Biofuels,* 7, article no. 6. https://doi.org/10.1186/1754-6834-7-6

Rico del Cerro, D.; Koso, T. V.; Kakko, T.; King, A. W. T.; Kilpeläinen, I. (2020). "Crystallinity reduction and enhancement in the chemical reactivity of cellulose by non-dissolving pre-treatment with tetrabutylphosphonium acetate", *Cellulose*, 27, 5545-5562. https://doi.org/10.1007/s10570-020-03044-6

Rodríguez, H. (2021). "Ionic liquids in the pretreatment of lignocellulosic biomass", *Acta Innovations*, 38, 22-35. https://doi.org/10.32933/ActaInnovations.38.3

Rodríguez-Cabo, B.; Rodríguez-Palmeiro, I.; Rodil, R.; Rodil, E.; Arce A.; Soto A. (2015). "Synthesis of AgCl nanoparticles in ionic liquid and their application in photodegradation of Orange II", *Journal of Materials Science*, 50, 3576-3585. https://doi.org/10.1007/s10853-015-8917-0

Ruokonen, S.-K.; Sanwald, C.; Sundvik, M.; Polnick, S.; Vyavaharkar, K.; Duša, F.; Holding, A. J.; King, A. W. T.; Kilpeläinen, I.; Lämmerhofer, M.; Panula, P.; Wiedmer, S. K. (2016). "Effect of Ionic Liquids on Zebrafish (*Danio rerio*) Viability, Behavior, and Histology; Correlation between Toxicity and Ionic Liquid Aggregation", *Environmental Science and Technology*, 50, 7116-7125. https://doi.org/10.1021/acs.est.5b06107

## S

Saake, B.; Lehnen, R. (2012). "Lignin", in: *Ullmann's Encyclopedia of Industrial Chemistry*, Wiley-VCH Verlag, Weinheim, Germany. https://doi.org/10.1002/14356007.a15_305.pub3

Schmidt, U.; Koch, G.; Lehnen, R. (2013). "Wood", in: *Ullmann's Encyclopedia of Industrial Chemistry*, Wiley-VCH Verlag, Weinheim, Germany. https://doi.org/10.1002/14356007.a28_305

Shibazaki, H.; Saito, M.; Kuga, S.; Okano, T. (1998). "Native cellulose II production by acetobacter xylinum under physical constraints", *Cellulose*, 5, 165-173. https://doi.org/10.1023/A:1009277122329

Shin, S. K.; Ko, Y. J.; Hyeon, J. E.; Han, S. O. (2019). "Studies of advanced lignin valorization based on various types of lignolytic enzymes and microbes", *Bioresource Technology*, 289, article no. 121728. https://doi.org/10.1016/j.biortech.2019.121728

Singer, S. W.; Reddy, A. P.; Gladden, J. M.; Guo, H.; Hazen, T. C.; Simmons, B. A.; VanderGheynst, J. S. (2011). "Enrichment, isolation and characterization of fungi tolerant to 1-ethyl-3-methylimidazolium acetate", *Journal of Applied Microbiology*, 110, 1023-1031. https://doi.org/10.1111/j.1365-2672.2011.04959.x

Singh, S.; Varanasi, P.; Simmons B. (2019). "Renewable aromatics from lignocellulosic lignin", US Patent 10,233,292 B2, 2019.

Singhvi, M.; Kim, B. S. (2021). "Lignin valorization using biological approach", *Biotechnology and Applied Biochemistry*, 68, 459-468. https://doi.org/10.1002/bab.1995

Singhvi, M. S.; Gokhale, D. V. (2019). "Lignocellulosic biomass: Hurdles and challenges in its valorization", *Applied Microbiology and Biotechnology*, 103, 9305-9320. https://doi.org/10.1007/s00253-019-10212-7

Sixta, H.; Michud, A.; Hauru, L.; Asaadi, S.; Ma, Y.; King, A. W. T.; Kilpeläinen, I.; Hummel, M. (2015). "Ioncell-F: A High-strength regenerated cellulose fibre", *Nordic Pulp and Paper Research Journal*, 30, 43-57. https://doi.org/10.3183/npprj-2015-30-01-p043-057

Sjöström, E. (1993). *Wood chemistry, Fundamentals and Applications*, 2nd ed., Academic Press, San Diego, CA, USA.

Smiglak, M.; Bridges, N. J.; Dilip, M.; Rogers, R. D. (2008). "Direct, Atom Efficient, and Halide-Free Syntheses of Azolium Azolate Energetic Ionic Liquids and Their Eutectic Mixtures, and Method for Determining Eutectic Composition", *Chemistry – A European Journal*, 14, 11314–11319. https://doi.org/10.1002/chem.200801811

Song, Y.; Chen, W.; Niu, X.; Fang, G.; Min, H.; Pan, H. (2018). "An Energy-Efficient One-Pot Swelling/Esterification Method to Prepare Cellulose Nanofibers with Uniform Diameter", *ChemSusChem*, 11, 3714–3718. https://doi.org/10.1002/cssc.201801794

Spinreact (2016). *Quantitative determination of glucose*. Available at: spinreact.com/files/Inserts/Bioquimica/BSIS17_GLU_TR_02_2016.pdf (last accessed: July 2022).

Stevens, J. C.; Das, L.; Mobley, J. K.; Asare, S. O.; Lynn, B. C.; Rodgers, D. W.; Shi, J. (2019). "Understanding Laccase-Ionic Liquid Interactions toward Biocatalytic Lignin Conversion in Aqueous Ionic Liquids", *ACS Sustainable Chemistry and Engineering*, 7, 15928-15938. https://doi.org/10.1021/acssuschemeng.9b02151

Stevens, J. C.; Rodgers, D. W.; Dumon, C.; Shi, J. (2020). "Characterization and Enzyme Engineering of a Hyperthermophilic Laccase Toward Improving Its Activity in Ionic Liquid", *Frontiers in Energy Research*, 8, article no. 158. https://doi.org/10.3389/fenrg.2020.00158

Strassberger, Z.; Prinsen, P.; van der Klis, F.; van Es, D. S.; Tanase, S.; Rothenberg, G. (2015). "Lignin solubilisation and gentle fractionation in liquid ammonia", *Green Chemistry*, 17, 325-334. https://doi.org/10-1039/c4gc01143k

Sun, N.; Parthasarathi, R.; Socha, A. M.; Shi, J.; Zhang, S.; Stavila, V.; Sale, K. L.; Simmons, B. A.; Singh, S. (2014). "Understanding pretreatment efficacy of four cholinium and imidazolium ionic liquids by chemistry and computation", *Green Chemistry*, 16, 2546-2557. https://doi.org/10.1039/C3GC42401D

Sun, Z.; Fridrich, B.; de Santi, A.; Elangovan, S.; Barta, K. (2018). "Bright Side of Lignin Depolymerization: Toward New Platform Chemicals", *Chemical Reviews,* 118, 614-678. https://doi.org/10.1021/acs.chemrev.7b00588

Swatloski, R. P.; Spear, S. K.; Holbrey, J. D.; Rogers, R. D. (2002). "Dissolution of Cellulose with Ionic Liquids", *Journal of the American Chemical Society*, 124, 4974-4975. https://doi.org/10.1021/ja025790m

## T

Tejado, A.; Peña, C.; Labidi, J.; Echeverria, J. M.; Mondragon, I. (2007). "Physico-chemical characterization of lignins from different sources for use in phenol-formaldehyde resin synthesis", *Bioresource Technology*, 98, 1655-1663. https://doi.org/10.1016/j.biortech.2006.05.042

The United States Pharmacopeia (2017). *The United States 883 Pharmacopeia USP 41 and The National Formulary NF 36*, The United States Pharmacopeial Convention: Rockville, MD, USA.

Thielking, H.; Schmidt, M. (2006). "Cellulose Ethers", in: *Ullmann's Encyclopedia of Industrial Chemistry*, Wiley-VCH Verlag, Weinheim, Germany. https://doi.org/10.1002/14356007.a05_461.pub2

Trinder, P. (1969). "Determination of Glucose in Blood using Glucose Oxidase with an alternative oxygen acceptor", *Annals of Clinical Biochemistry*, 6, 24-27. https://doi.org/10.1177/000456326900600108

## U

Usmani, Z.; Sharma, M.; Gupta, P.; Karpichev, Y.; Gathergood, N.; Bhat, R.; Gupta, V.K. (2020). "Ionic liquid based pretreatment of lignocellulosic biomass for enhanced

bioconversion", *Bioresource Technology*, 304, article no. 123003. https://doi.org/10.1016/j.biortech.2020.123003

## V

Verma, S.; Kuila, A. (2020). "Principles of Sustainable Biorefinery", in: *Biorefinery Production Technologies for Chemicals and Energy*, Scrivener Publishing, Beverly, MA, USA. ISBN: 978-1-119-59142-9

## W

Wang, H.; Gurau, G.; Rogers, R. D. (2012). "Ionic liquid processing of cellulose", *Chemical Society Reviews*, 41, 1519-1537. https://doi.org/10.1039/C2CS15311D

Wang, Y.; Sun, S.; Li, F.; Cao, X.; Sun, R. (2018). "Production of vanillin from lignin: The relationship between β-*O*-4 linkages and vanillin yield", *Industrial Crops and Products*, 116, 116-121. https://doi.org/10.1016/j.indcrop.2018.02.043

Wu, Z.; Xu, J.; Gong, J.; Li, J.; Mo, L. (2018). "Preparation, characterization and acetylation of cellulose nanocrystal allomorphs", *Cellulose*, 25, 4905–4918. https://doi.org/10.1007/s10570-018-1937-6

Wyman, C. E.; Decker, S. R.; Himmel, M. E.; Brady, J. W.; Skopec, C. E.; Viikari, L. (2005). "Hydrolysis of Cellulose and Hemicellulose", in: *Polysaccharides: Structural Diversity and Functional Versatility* (Ed.: Dumitriu, S.), 2nd ed., Marcel Dekker, New York, NY, USA.

## Y

Yamaguchi, A.; Mimura, N.; Segawa, A.; Mazaki, H.; Sato, O. (2020). "Lignin Depolymerization into Aromatic Monomers Using Supported Metal Catalysts in Supercritical Water", *Journal of the Japan Petroleum Institute*, 63, 221-227. https://doi.org/10.1627/jpi.63.221

Yang, Y.; Song, W.-Y.; Hur, H.-G.; Kim, T.-Y.; Ghatge, S. (2019). "Thermoalkaliphilic laccase treatment for enhanced production of high-value benzaldehyde chemicals from lignin", *International Journal of Biological Macromolecules*, 124, 200-208. https://doi.org/10.1016/j.ijbiomac.2018.11.144

Yang, Y.-T.; Qin, M.-K.; Sun, Q.; Gao, Y.-F.; Ma, C.-Y.; Wen, J.-L. (2022). "Structural elucidation and targeted valorization of poplar lignin from the synergistic hydrothermal-deep eutectic solvent pretreatment", *International Journal of Biological Macromolecules*, 209, 1882-1892. https://doi.org/10.1016/j.ijbiomac.2022.04.162

Yoo, C. G.; Meng, X.; Pu, Y.; Ragauskas, A. J. (2020). "The critical role of lignin in lignocellulosic biomass conversion and recent pretreatment strategies: A comprehensive review", *Bioresource Technology*, 301, article no. 122784. https://doi.org/10.1016/j.biortech.2020.122784

Yun, J.; Wei, L.; Li, W.; Gong, D.; Qin, H.; Feng, X.; Li, G.; Ling, Z.; Wang, P.; Yin, B. (2021). "Isolating High Antimicrobial Ability Lignin From Bamboo Kraft Lignin by Organosolv Fractionation", *Frontiers in Bioengineering and Biotechnology*, 9, article no. 363. https://doi.org/10.3389/fbioe.2021.683796

## Z

Zakzeski, J.; Bruijnincx, P. C.; Jongerius, A. L.; Weckhuysen, B. M. (2010). "The Catalytic Valorization of Lignin for the Production of Renewable Chemicals", *Chemical Reviews*, 110, 3552-3599. https://doi.org/10.1021/cr900354u

Zakrzewska, M. E.; Bogel-Łukasik, E.; Bogel-Łukasik, R. (2010). "Solubility of Carbohydrates in Ionic Liquids", *Energy and Fuels*, 24, 737-745. https://doi.org/10.1021/ef901215m

Zhang, L.; Huang, C.; Zhang, C.; Pan, H. (2021). "Swelling and dissolution of cellulose in binary systems of three ionic liquids and three co-solvents", *Cellulose*, 28, 4643–4653. https://doi.org/10.1007/s10570-021-03844-4

Zhang, Q.; Benoit, M.; De Oliveira Vigier, K.; Barrault, J.; Jérôme, F. (2012). "Green and Inexpensive Choline-Derived Solvents for Cellulose Decrystallization". *Chemistry – A European Journal*, 18, 1043–1046. https://doi.org/10.1002/chem.201103271

Zhang, X.; Qu, T.; Mosier, N. S.; Han, L.; Xiao, W. (2018). "Cellulose modification by recyclable swelling solvents", *Biotechnology for Biofuels,* 11, article no. 191. https://doi.org/10.1186/s13068-018-1191-z

# Appendix A:
# $^{1}H$ and $^{13}C$ NMR spectra of ionic liquids

# Appendix A:

# $^{1}H$ and $^{13}C$ NMR spectra of ionic liquids

In this Appendix, the $^{1}H$ and $^{13}C$ NMR spectra of the purified ionic liquids used in this Thesis are presented. Please refer to Chapters 3 and 4 for further details (supplier/synthesis, purification, NMR spectrometer and recording of the spectra, etc.).

Table A.1 presents a list of the ionic liquids, including full names, CAS numbers, and the corresponding abbreviations. In Figures A.1 to A.8 in the following pages, for each of them the $^{1}H$ NMR spectrum is presented first and then the $^{13}C$ NMR spectrum.

**Table A.1.** Full names, CAS numbers, and abbreviations of the ionic liquids involved in the experimental work of this Thesis, and for which the $^{1}H$ and $^{13}C$ NMR spectra are collected in this Appendix.

| Name | CAS number | Abbreviation |
|---|---|---|
| Tetrabutylphosphonium chloride | 2304-30-5 | $[P_{4444}]Cl$ |
| Tetrabutylphosphonium bromide | 3115-68-2 | $[P_{4444}]Br$ |
| Tetrabutylphosphonium acetate | 30345-49-4 | $[P_{4444}][OAc]$ |
| 1-Ethyl-3-methylimidazolium acetate | 143314-17-4 | $[C_2mim][OAc]$ |

## Tetrabutylphosphonium chloride ([P4 4 4 4]Cl)

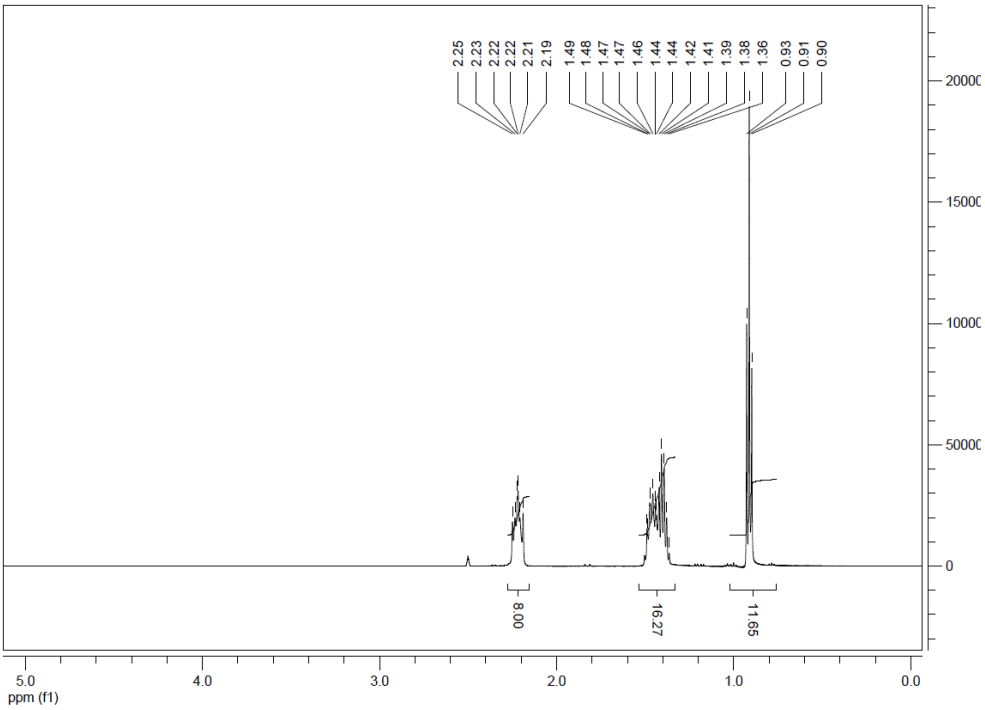


Figure A.1. $^1$H NMR spectrum of [P4 4 4 4]Cl, $\delta_H$ (DMSO-$d_6$, 300 MHz): 0.91 (t, $J$ = 7.1 Hz, 12H, 4 × P(CH2)3C$\underline{H}$3), 1.34-1.51 (unresolved, 16H, 4 × PCH2(C$\underline{H}$2)2), 2.18-2.26 (unresolved, 8H, 4 × PCH2). The peak at 2.5 ppm corresponds to the residual proton signal of the deuterated solvent.

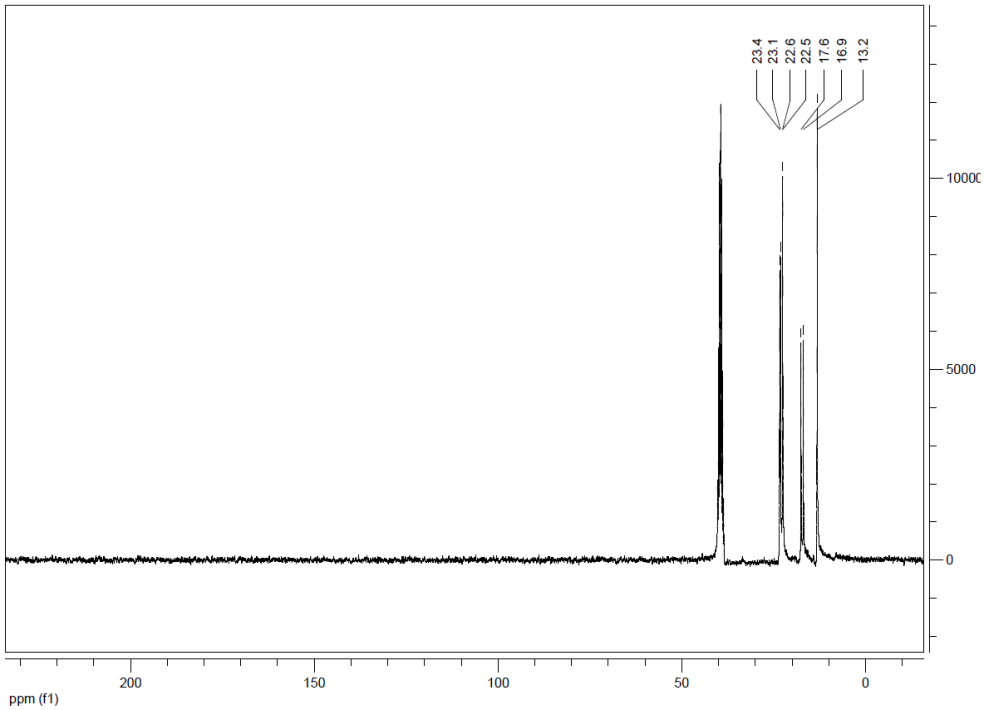


Figure A.2. $^{13}C$ NMR spectrum of $[P_{4\,4\,4\,4}]Cl$, $\delta_C$ (DMSO-$d_6$, 75.4 MHz): 13.2 (s, 4 × $P(CH_2)_3\underline{C}H_3$), 17.3 (d, $J_{C\text{-}P}$ = 48 Hz, 4 × $PCH_2$), 22.6 (d, $J$ = 4 Hz, 4 × $P(CH_2)_2\underline{C}H_2$), 23.2 (d, $J$ = 16 Hz, 4 × $PCH_2\underline{C}H_2$). The peak at 39.4 ppm corresponds to the deuterated solvent.

## Tetrabutylphosphonium bromide ([$P_{4\,4\,4\,4}$]Br)

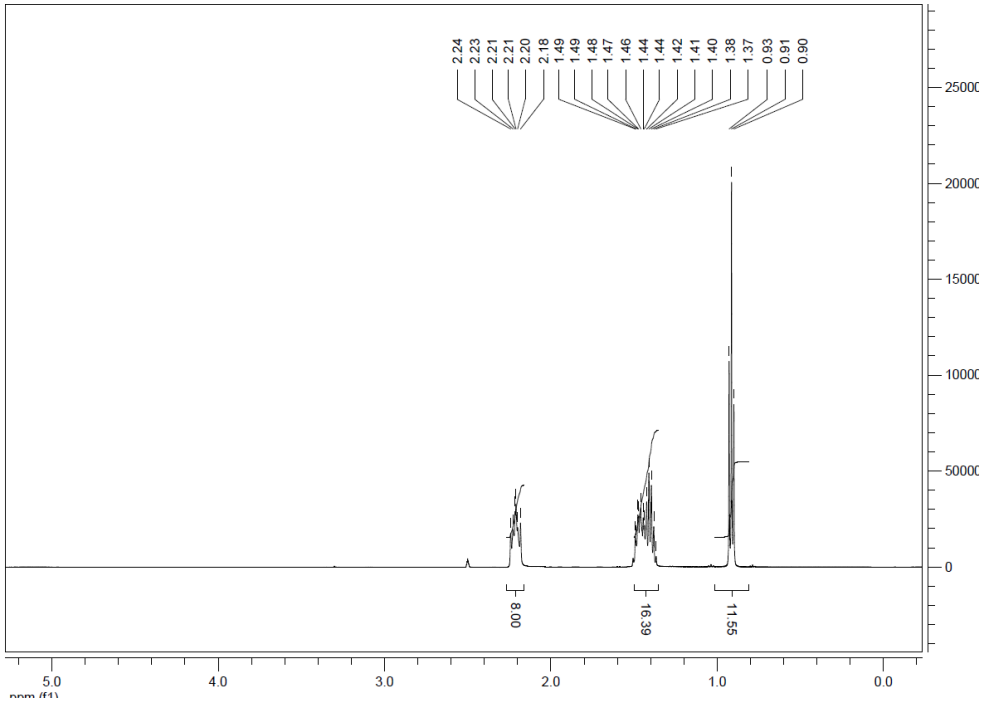


Figure A.3. $^1$H NMR spectrum of [$P_{4\,4\,4\,4}$]Br, $\delta_H$ (DMSO-$d_6$, 300 MHz): 0.91 (t, $J$ = 7.1 Hz, 12H, 4 × $P(CH_2)_3C\underline{H}_3$), 1.31-1.55 (unresolved, 16H, 4 × $PCH_2(C\underline{H}_2)_2$), 2.09-2.28 (unresolved, 8H, 4 × $PCH_2$). The peak at 2.5 ppm corresponds to the residual proton signal of the deuterated solvent.

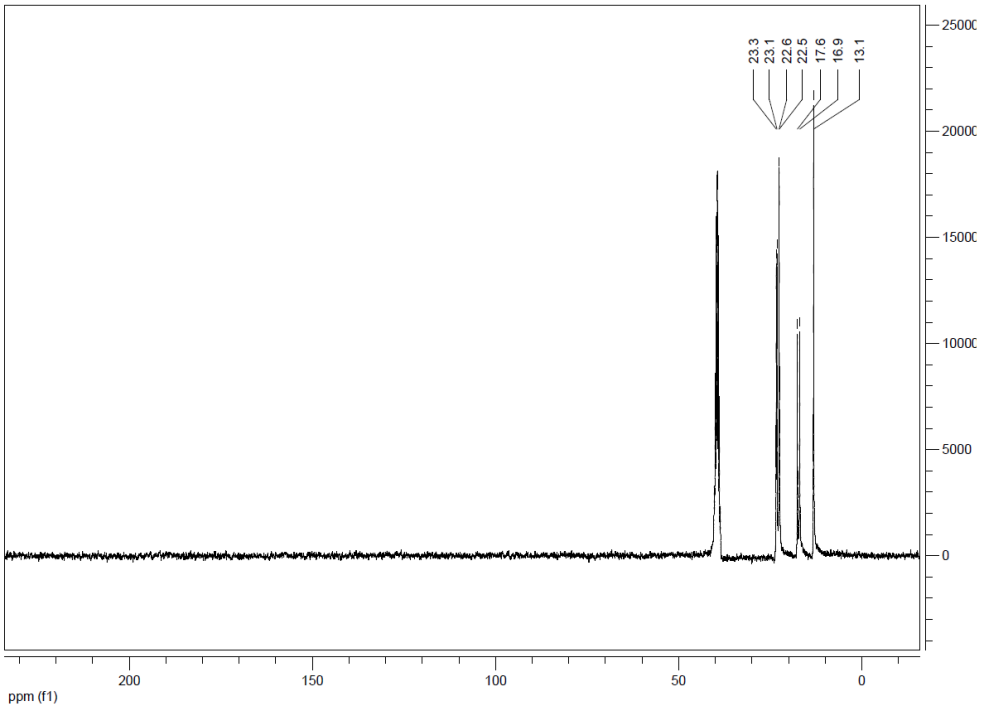


**Figure A.4.** $^{13}C$ NMR spectrum of $[P_{4\,4\,4\,4}]Br$, $\delta_C$ (DMSO-$d_6$, 75.4 MHz): 13.1 (s, 4 × $P(CH_2)_3\underline{C}H_3$), 17.3 (d, $J_{C\text{-}P}$ = 48 Hz, 4 × $PCH_2$), 22.6 (d, $J$ = 4 Hz, 4 × $P(CH_2)_2\underline{C}H_2$), 23.2 (d, $J$ = 16 Hz, 4 × $PCH_2\underline{C}H_2$). The peak at 39.4 ppm corresponds to the deuterated solvent.

## Tetrabutylphosphonium acetate ([P4 4 4 4][OAc])

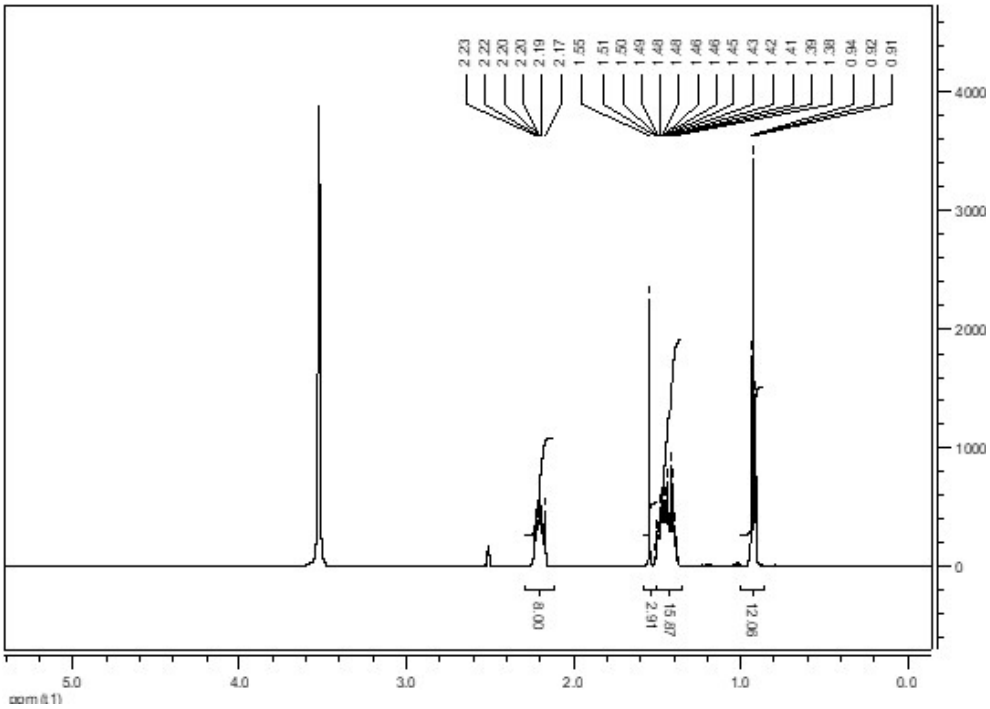


Figure A.5. $^1$H NMR spectrum of [P4 4 4 4][OAc], $\delta_H$ (DMSO-$d_6$, 300 MHz): 0.92 (t, $J$ = 7.1 Hz, 12H, 4 × P(CH$_2$)$_3$C$\underline{H}_3$), 1.34-1.52 (unresolved, 16H, 4 × PCH$_2$(C$\underline{H}_2$)$_2$), 1.55 (s, 3H, CH$_3$COO), 2.12-2.25 (unresolved, 8H, 4 × PCH$_2$). The peaks at 2.5 ppm and 3.6 ppm correspond, respectively, to the residual proton signal of the deuterated solvent and to traces of water present in the mixture (solvent + sample).

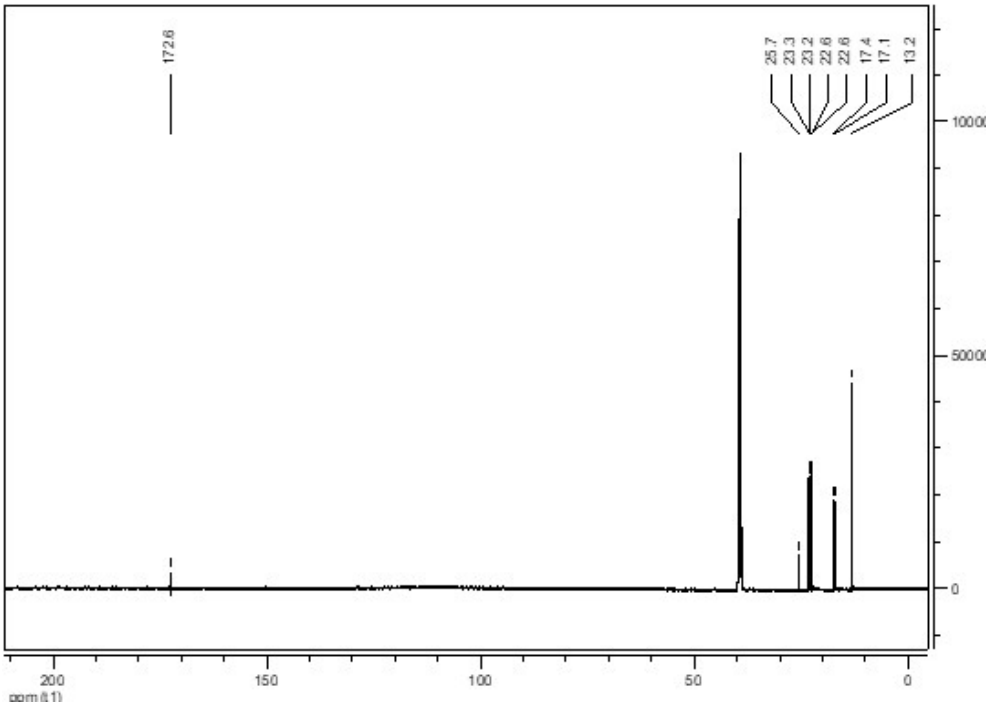


Figure A.6. $^{13}C$ NMR spectrum of $[P_{4\,4\,4\,4}][OAc]$, $\delta_C$ (DMSO-$d_6$, 75.4 MHz): 13.2 (s, 4 × $P(CH_2)_3\underline{C}H_3$), 17.3 (d, $J_{C\text{-}P}$ = 48 Hz, 4 × $PCH_2$), 22.6 (d, $J$ = 4 Hz, 4 × $P(CH_2)_2\underline{C}H_2$), 23.3 (d, $J$ = 16 Hz, 4 × $PCH_2\underline{C}H_2$), 25.7 (s, $\underline{C}H_3COO$), 172.6 (s, $CH_3\underline{C}OO$). The peak at 39.4 ppm corresponds to the deuterated solvent.

## 1-Ethyl-3-methylimidazolium acetate ([C2mim][OAc])

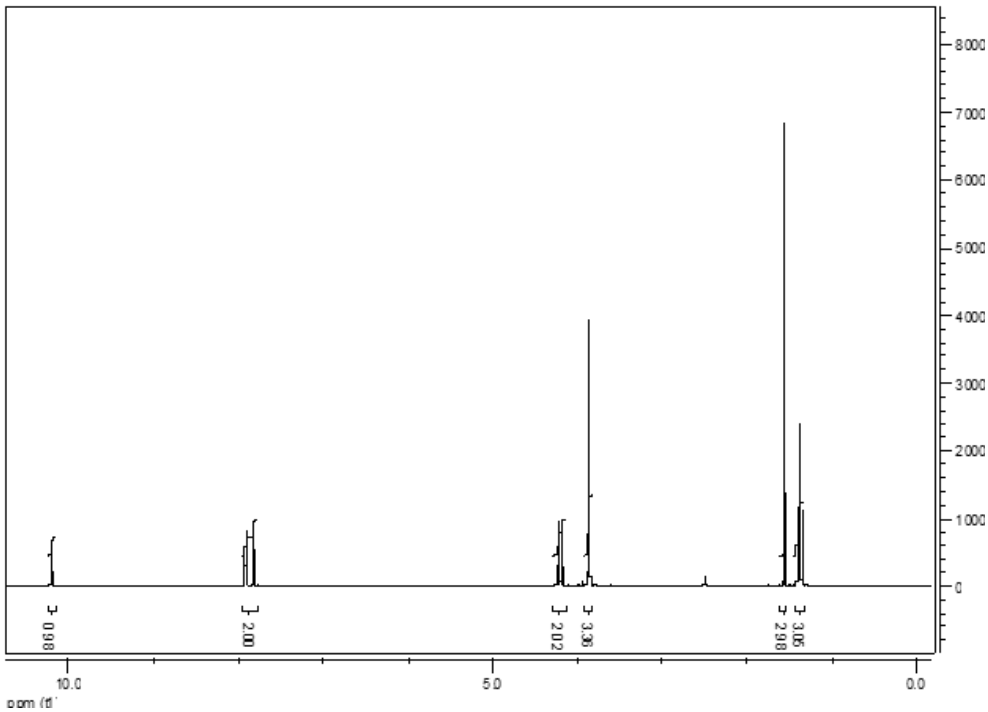


Figure A.7. $^{1}$H NMR spectrum of [C2mim][OAc], $\delta_H$(DMSO-$d_6$, 300 MHz): 1.39 (t, $J$= 7.3 Hz, 3H, $NCH_2C\underline{H}_3$), 1.56 (s, 3H, $CH_3COO$), 3.87 (s, 3H, $NCH_3$), 4.22 (q, $J$= 7.3 Hz, 2H, $NCH_2$), 7.78-7.96 (unresolved, 2H, C(5)H and C(4)H), 10.20 (s, 1H, C(2)H). The peak at 2.50 ppm corresponds to the residual proton signal of the deuterated solvent.

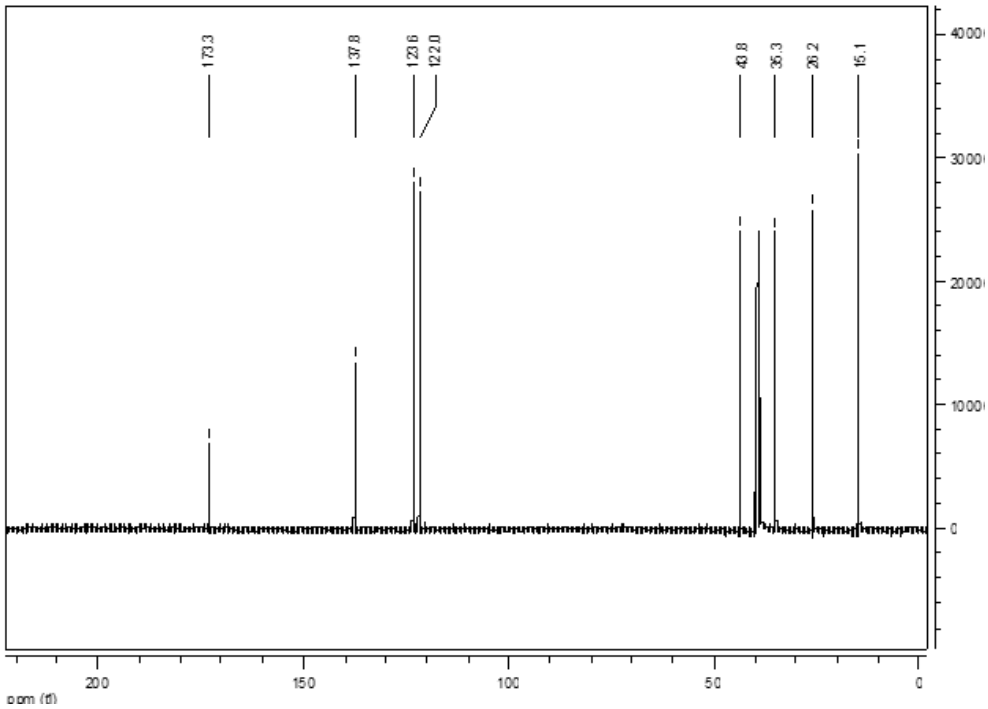


Figure A.8. $^{13}C$ NMR spectrum of $[C_2mim][OAc]$, $\delta_C$ (DMSO-$d_6$, 75.4 MHz): 15.1 ($NCH_2\underline{C}H_3$), 26.2 ($\underline{C}H_3COO$), 35.3 ($NCH_3$), 43.8 ($NCH_2$), 122.0 (C(4)H), 123.6 (C(5)H), 137.8 (C(2)H), 173.3 ($CH_3\underline{C}OO$). The multiplet at 40 ppm corresponds to the deuterated solvent.

# Appendix B:
# Solid-liquid equilibrium data

# Appendix B:

# Solid-liquid equilibrium data

**Table B.1.** Experimentally determined thermal events ($T_{exc}$: melting temperatures of the excess compounds; $T_{eut}$: melting temperatures of the eutectic composition) of mixtures of [P4 4 4 4][OAc] and [P4 4 4 4]Cl of different compositions (expressed as mole fractions of [P4 4 4 4][OAc], $x_{[P4444][OAc]}$), covering the entire compositional range of the binary system.

| $x_{[P4444][OAc]}$ | $T_{exc}$ (K) | $T_{eut}$ (K) |
|---|---|---|
| 0.000 | 357 | — |
| 0.090 | 345 | — |
| 0.200 | 335 | — |
| 0.299 | 316 | 294 |
| 0.410 | 310 | 296 |
| 0.503 | 297 | — |
| 0.614 | 300 | 292 |
| 0.702 | 305 | 288 |
| 0.805 | 313 | — |
| 0.901 | 319 | — |
| 0.998 | 328 | — |

**Table B.2.** Experimentally determined thermal events ($T_{exc}$: melting temperatures of the excess compounds; $T_{eut}$: melting temperatures of the eutectic composition) of mixtures of [P4 4 4 4][OAc] and [P4 4 4 4]Br of different compositions (expressed as mole fractions of [P4 4 4 4][OAc], $x_{[P4444][OAc]}$), covering the entire compositional range of the binary system.

| $x_{[P4444][OAc]}$ | $T_{exc}$ (K) | $T_{eut}$ (K) |
|---|---|---|
| 0.000 | 374 | — |
| 0.110 | 362 | — |
| 0.206 | 353 | — |
| 0.312 | 340 | 305 |
| 0.420 | 329 | 306 |
| 0.500 | 327 | 305 |
| 0.600 | 310 | 305 |
| 0.686 | 306 | — |
| 0.806 | 315 | 305 |
| 0.902 | 320 | — |
| 0.998 | 332 | — |

**Table B.3.** Experimentally determined melting temperatures ($T_m$) of mixtures of [$P_{4\,4\,4\,4}$][OAc] and ethanol of different compositions (expressed as mole fractions of ethanol, $x_{ethanol}$), covering the compositional range of the binary system from $x_{ethanol}$ = 0 to $x_{ethanol}$ = 0.70.

| $x_{ethanol}$ | $T_m$ (K) |
|---|---|
| 0.000 | 331 |
| 0.104 | 313 |
| 0.200 | 304 |
| 0.296 | 295 |
| 0.395 | 288 |
| 0.497 | 280 |
| 0.600 | 269 |
| 0.659 | 247 |
| 0.700 | 229 |

**Table B.4** Experimentally determined thermal events ($T_{exc}$: melting temperatures of the excess compounds; $T_{eut}$: melting temperatures of the eutectic composition) of mixtures of [$P_{4\,4\,4\,4}$][OAc] and DMSO of different compositions (expressed as mole fractions of DMSO, $x_{DMSO}$), covering the entire compositional range of the binary system.

| $x_{DMSO}$ | $T_{exc}$ (K) | $T_{eut}$ (K) |
|---|---|---|
| 0.000 | 331 | — |
| 0.109 | 314 | 264 |
| 0.220 | 302 | 260 |
| 0.296 | 294 | 267 |
| 0.399 | 288 | 267 |
| 0.505 | 276 | 268 |
| 0.601 | 273 | 264 |
| 0.699 | — | 261 |
| 0.800 | 271 | 267 |
| 0.900 | 279 | 267 |
| 1.000 | 290 | — |

# Appendix C:
# TGA thermograms of Avicel samples

# Appendix C:

# TGA thermograms of Avicel samples

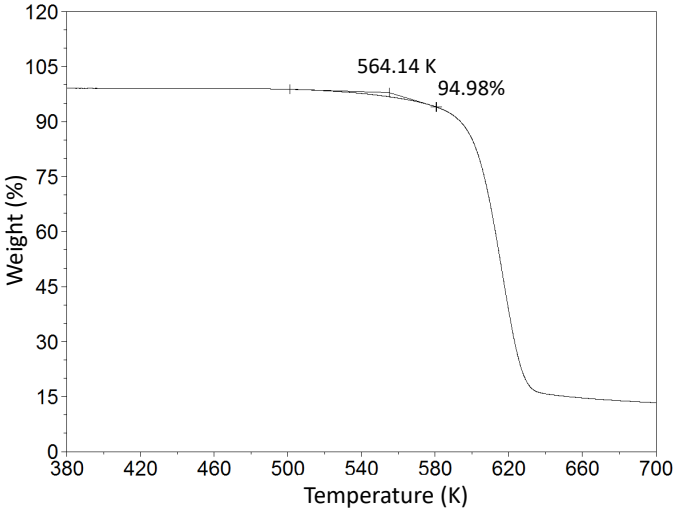


Figure C.1. Dynamic TGA thermogram of untreated Avicel cellulose showing the determination of the 5 % onset decomposition temperature.

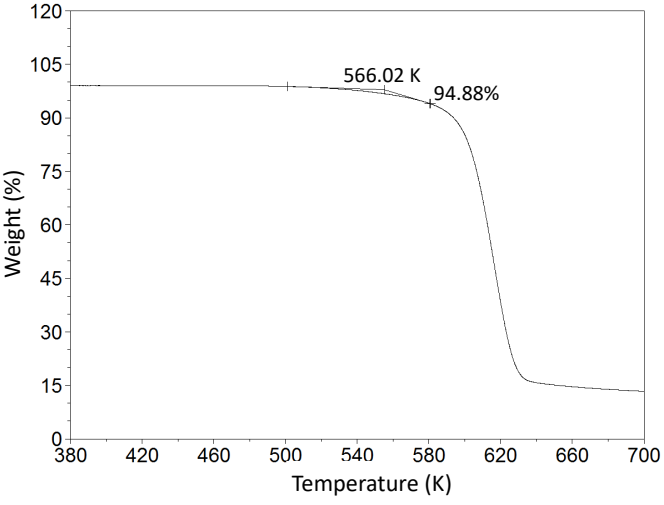


Figure C.2. Dynamic TGA thermogram of Avicel cellulose pretreated at 343.2 K with neat [$P_{4444}$][OAc], showing the determination of the 5 % onset decomposition temperature.

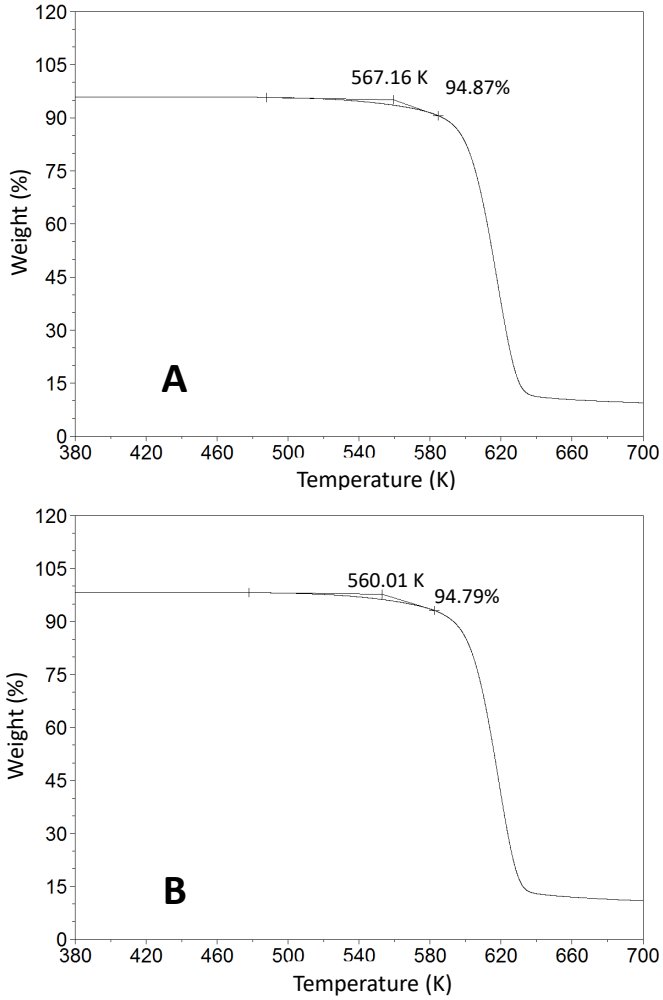


**Figure C.3. Dynamic TGA thermogram of Avicel cellulose pretreated with the eutectic mixture of [$P_{4444}$][OAc] + [$P_{4444}$]Cl at 313.2 K (A) and 343.2 K (B), showing the determination of the 5 % onset decomposition temperature.**

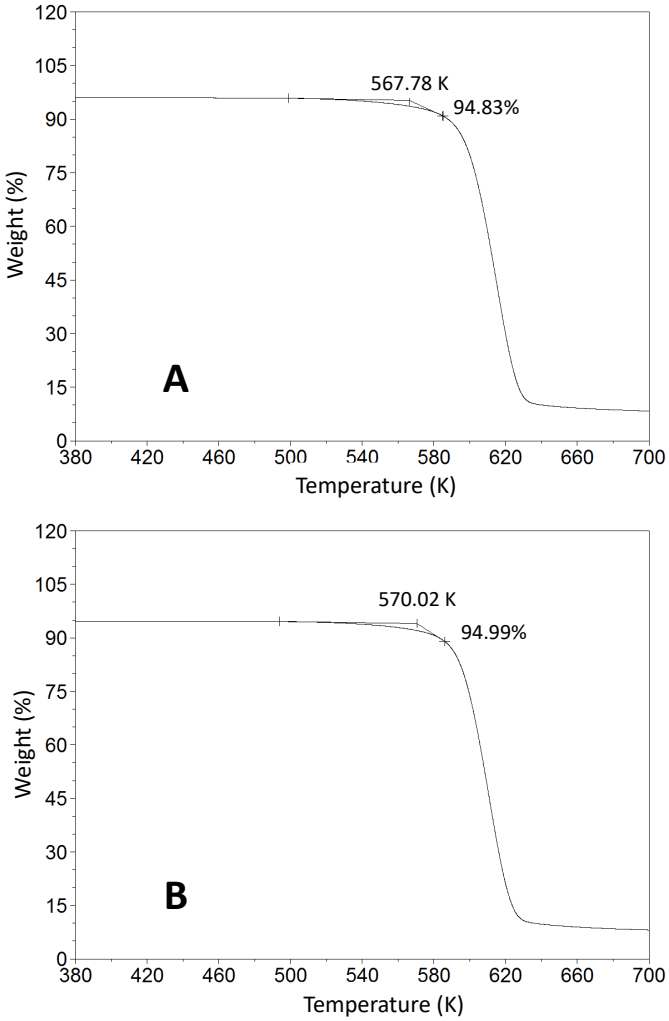


**Figure C.4. Dynamic TGA thermogram of Avicel cellulose pretreated with the eutectic mixture of [P4444][OAc] + [P4444]Br at 313.2 K (A) and 343.2 K (B), showing the determination of the 5 % onset decomposition temperature.**

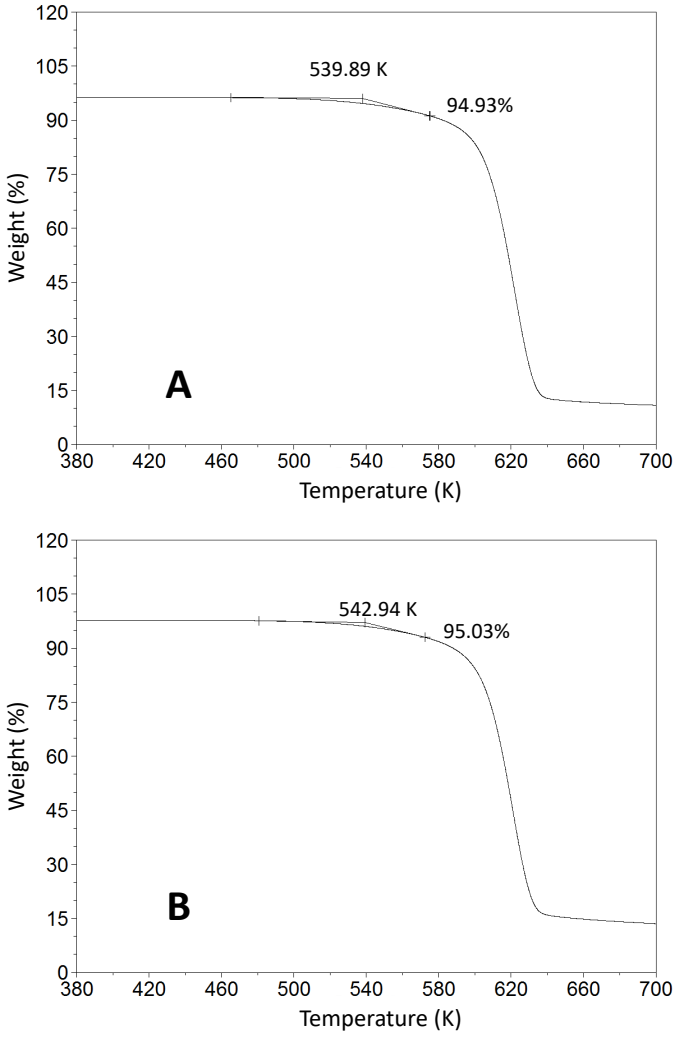


**Figure C.5. Dynamic TGA thermogram of Avicel cellulose pretreated with the mixture of [$P_{4\,4\,4\,4}$][OAc] + ethanol ($x_{ethanol}$ = 0.20) at 323.2 K (A) and 343.2 K (B), showing the determination of the 5 % onset decomposition temperature.**

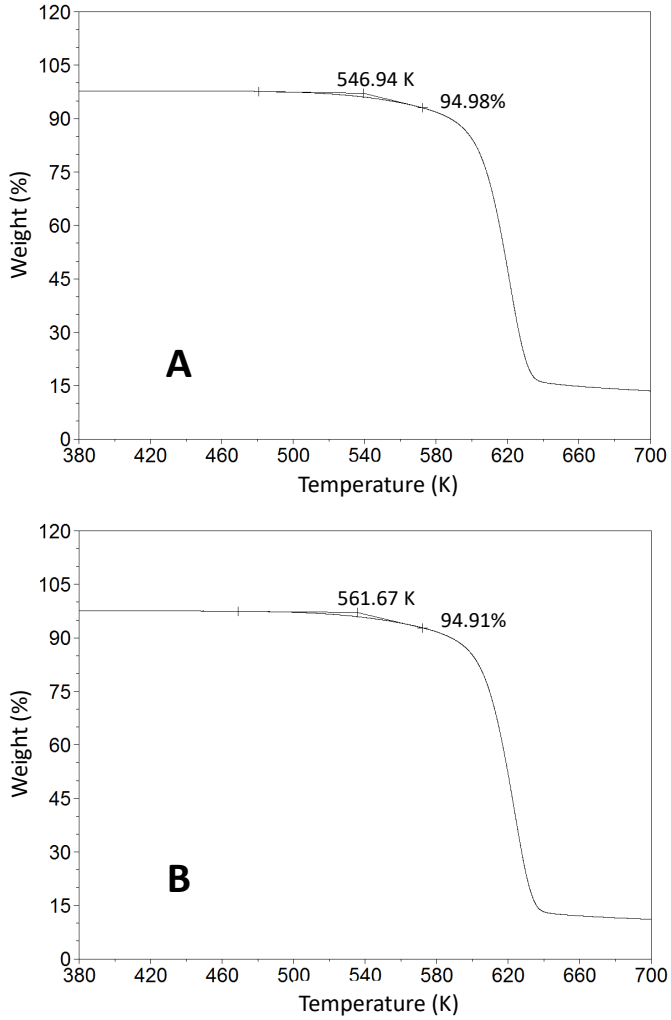


**Figure C.6. Dynamic TGA thermogram of Avicel cellulose pretreated with the mixture of [$P_{4\,4\,4\,4}$][OAc] + ethanol ($x_{ethanol}$ = 0.40) at 323.2 K (A) and 343.2 K (B), showing the determination of the 5 % onset decomposition temperature.**

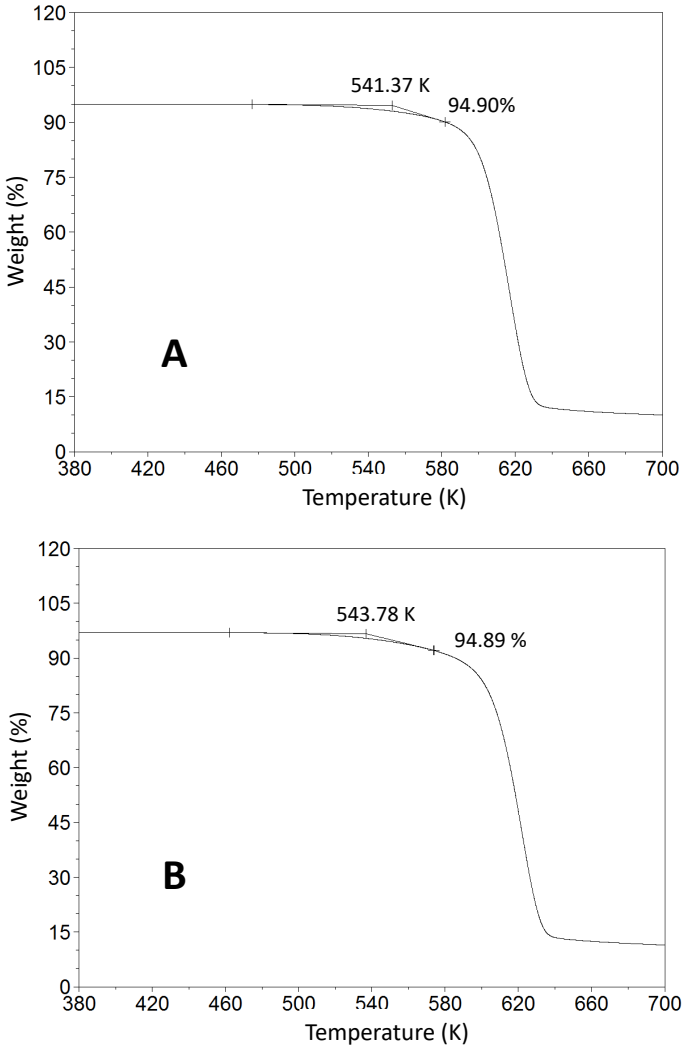


**Figure C.7. Dynamic TGA thermogram of Avicel cellulose pretreated with the mixture of $[P_{4\,4\,4}][OAc]$ + DMSO ($x_{DMSO}$ = 0.20) at 323.2 K (A) and 343.2 K (B), showing the determination of the 5 % onset decomposition temperature.**

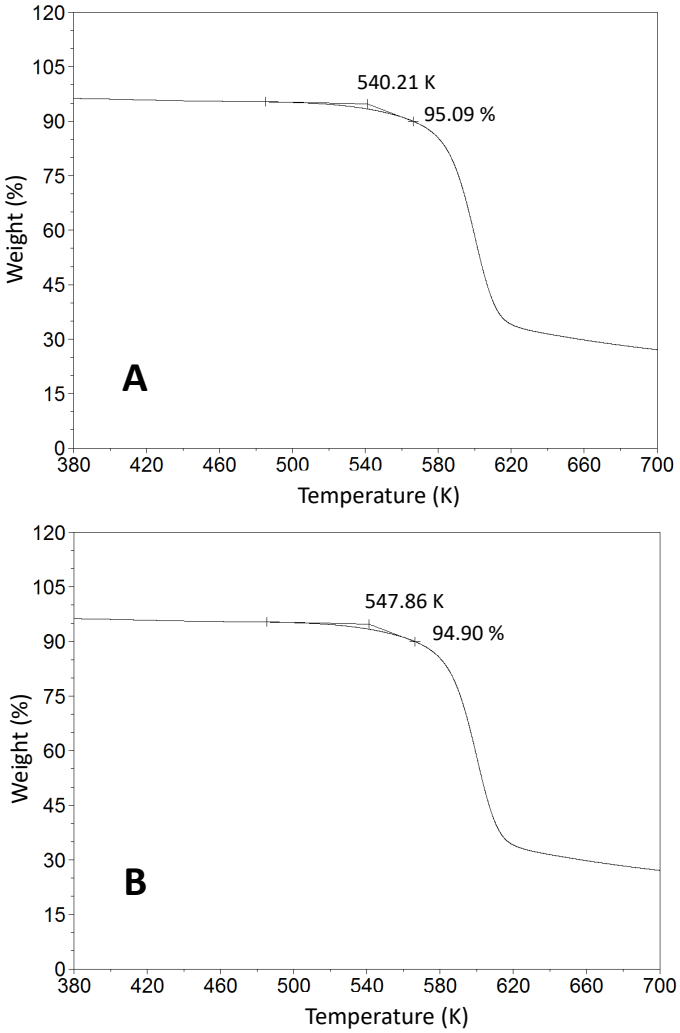


**Figure C.8. Dynamic TGA thermogram of Avicel cellulose pretreated with the mixture of [$P_{4\,4\,4\,4}$][OAc] + DMSO ($x_{DMSO}$ = 0.40) at 323.2 K (A) and 343.2 K (B), showing the determination of the 5 % onset decomposition temperature.**

# Appendix D:
# Additional TGA and DSC thermograms of lignin samples treated with laccase-based systems

# Appendix D:

# Additional TGA and DSC thermograms of lignin samples treated with laccase-based systems

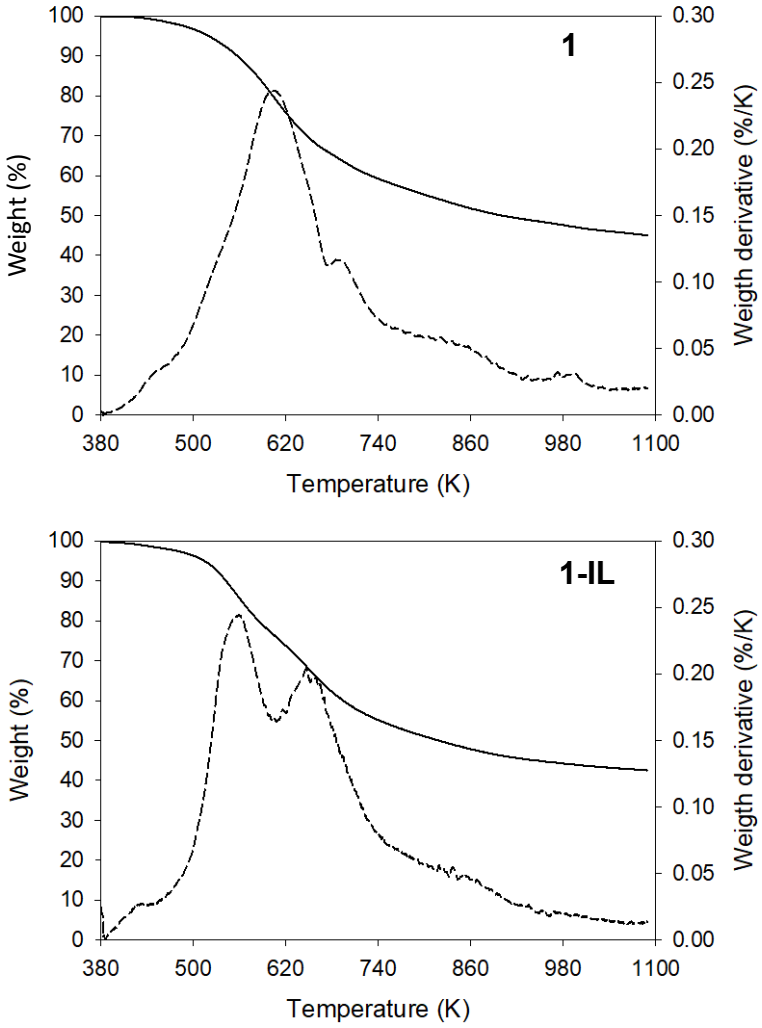


Figure D.1. Dynamic TGA thermograms (solid lines), and their derivative curves (dashed lines), for the solids recovered after the treatments 1 and 1-IL.

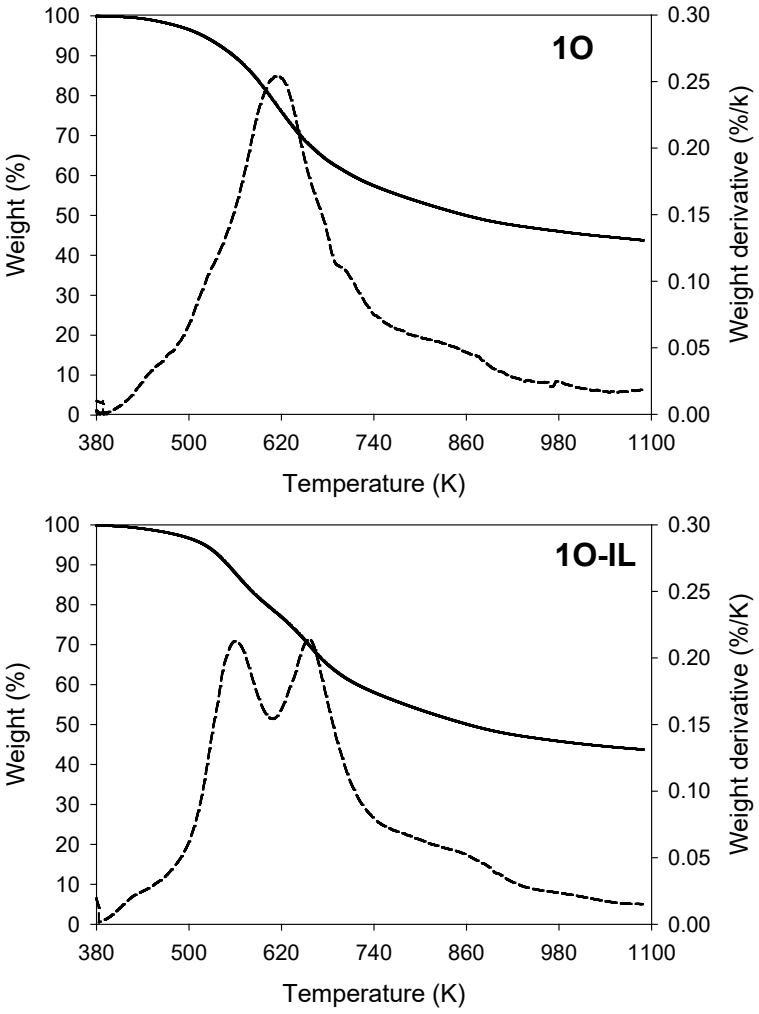


**Figure D.2. Dynamic TGA thermograms (solid lines), and their derivative curves (dashed lines), for the solids recovered after the treatments 10 and 10-IL.**

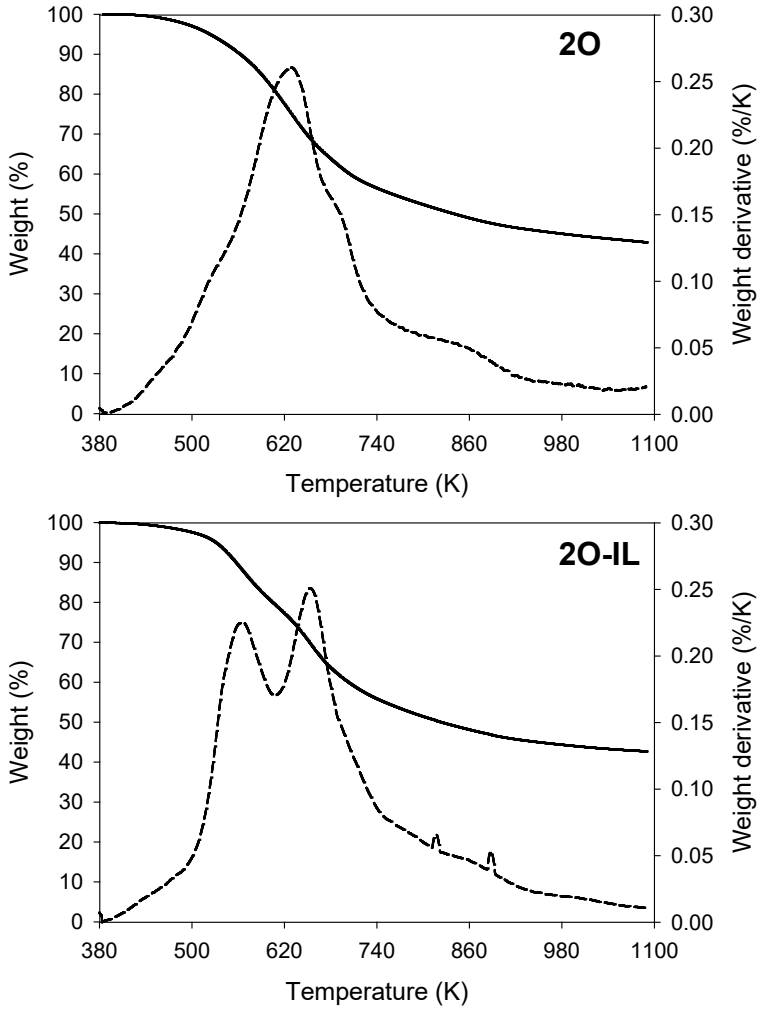


Figure D.3. Dynamic TGA thermograms (solid lines), and their derivative curves (dashed lines), for the solids recovered after the treatments 2O and 2O-IL.

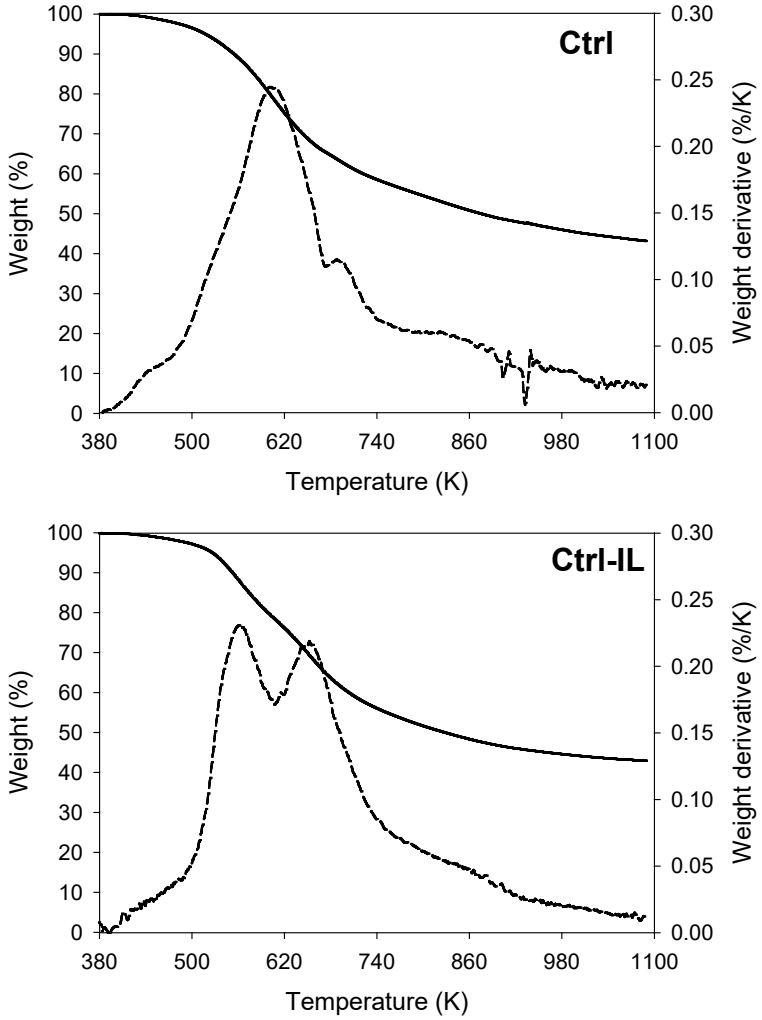


**Figure D.4. Dynamic TGA thermograms (solid lines), and their derivative curves (dashed lines), for the solids recovered from the control runs (Ctrl and Ctrl-IL).**

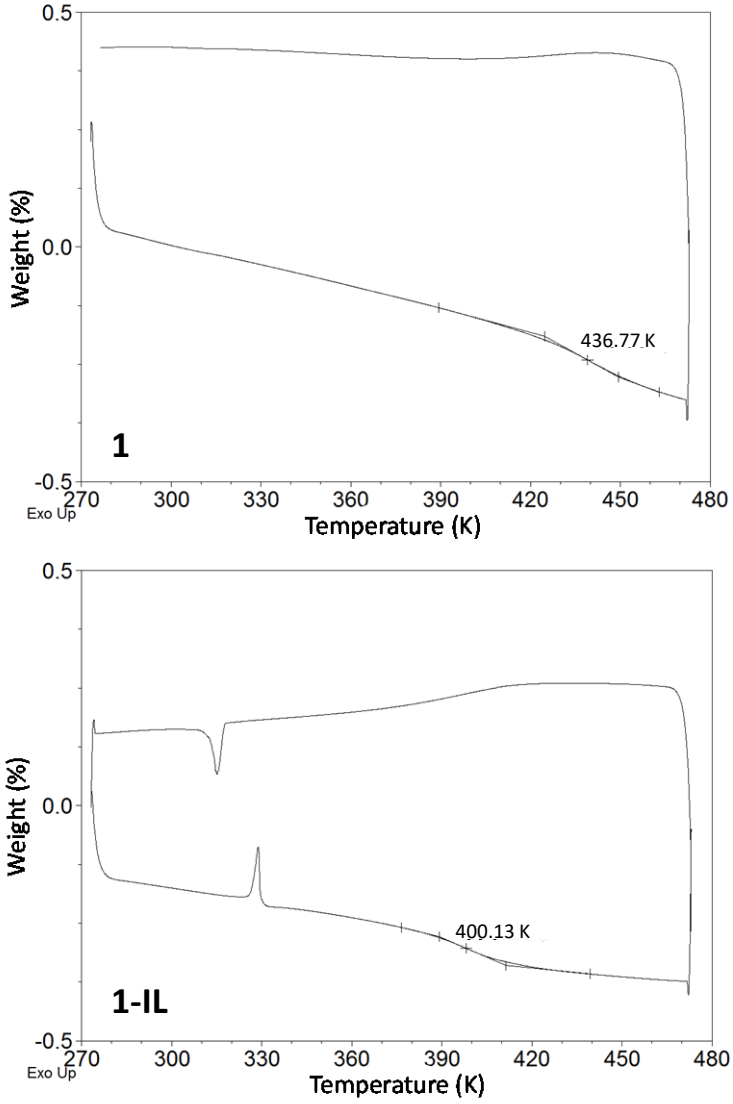


Figure D.5. DSC thermograms (exo up) for the solids recovered after the treatments 1 and 1-IL.

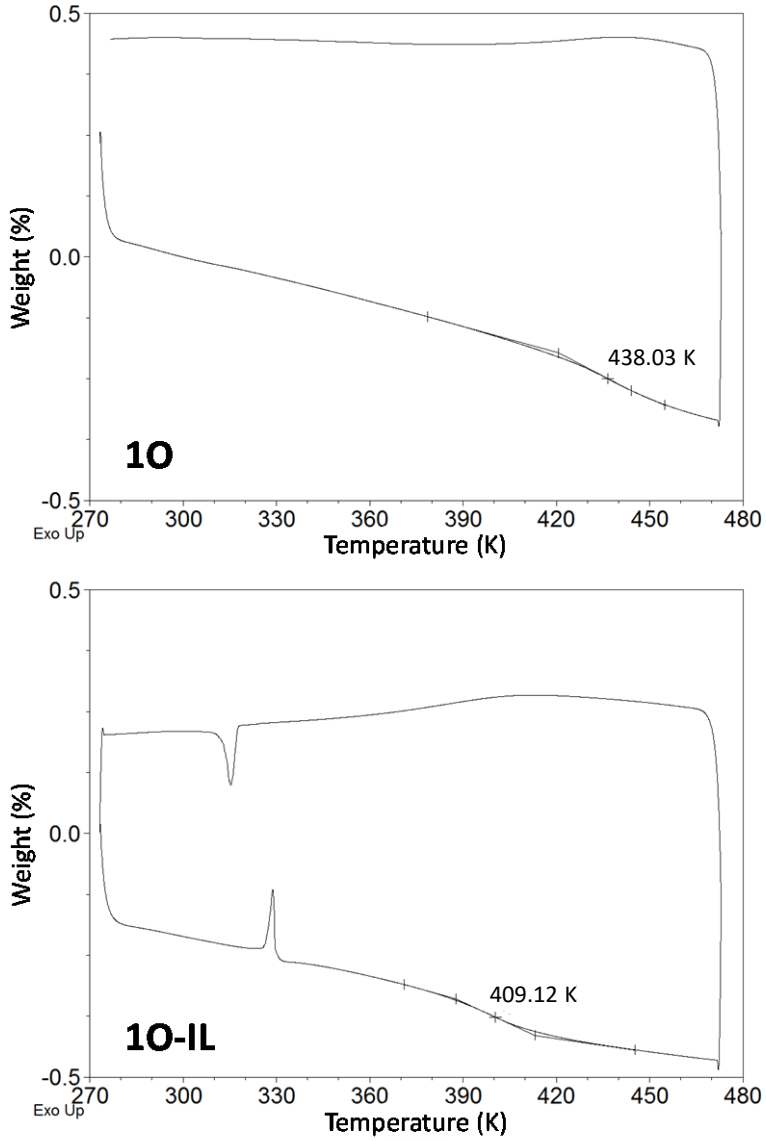


Figure D.6. DSC thermograms (exo up) for the solids recovered after the treatments 10 and 10-IL.

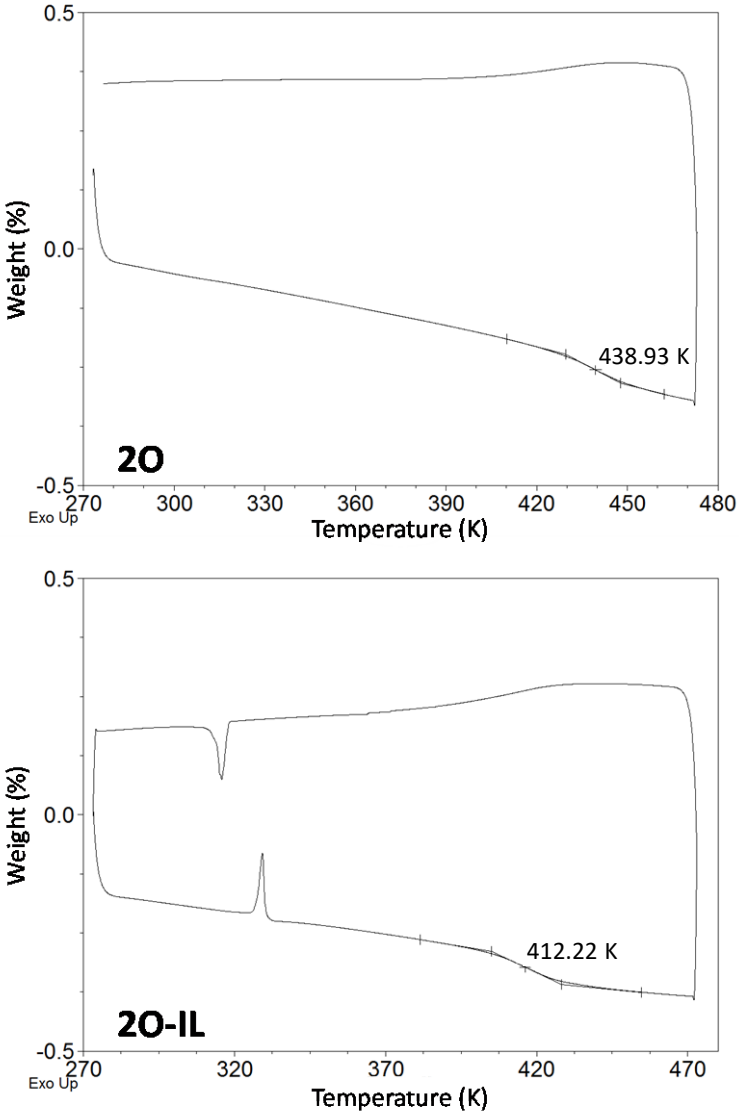


Figure D.7. DSC thermograms (exo up) for the solids recovered after the treatments 20 and 20-IL.

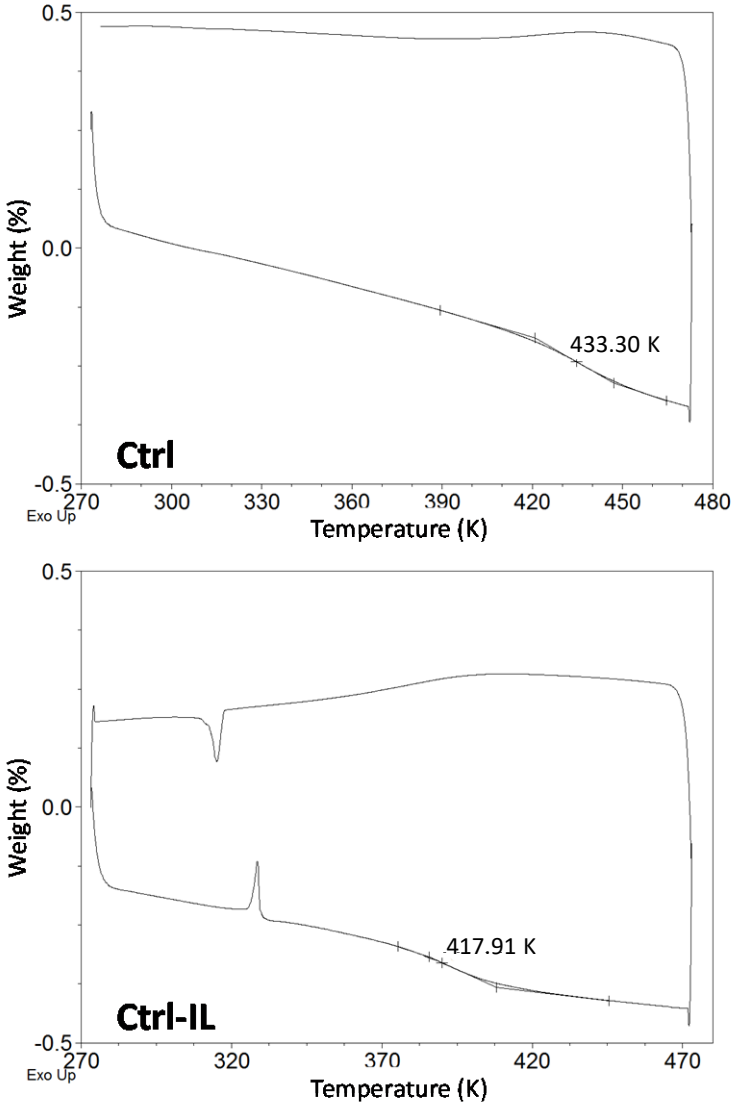


Figure D.8. DSC thermograms (exo up) for the solids recovered from the control runs (Ctrl and Ctrl-IL).

# Appendix E:
# Journal articles on which this thesis is based

# Appendix E:

# Journal articles on which this thesis is based

## Improved Reactivity of Cellulose via its Crystallinity Reduction by Non-Dissolving Pretreatment with an Ionic Liquid

Carlos A. Pena[a], Ana Soto[a], Alistair W. T. King[b], Héctor Rodríguez[a]

[a] Department of Chemical Engineering, Universidade de Santiago de Compostela, E-15782 Santiago de Compostela, Spain.
[b] Department of Chemistry, University of Helsinki, A. I. Virtasen Aukio 1, 00014 Helsinki, Finland

**Journal:** ACS Sustainable Chemistry & Engineering (2019), ed. American Chemical Society (ISSN: 2168-0485), volume 7, pages 9164-9171. DOI: https://doi.org/10.1021/acssuschemeng.8b06357. Impact factor = 7.632 (year 2019), ranking it 8/143 in the JCR category Chemical Engineering (Q1). The journal allows the use of this full article in the present thesis, both in print and electronic format, without requesting further permissions, provided that it is not published commercially and that it is properly referenced:

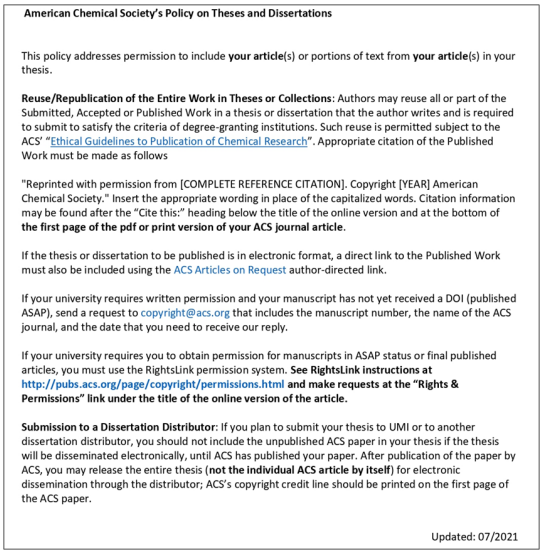

**American Chemical Society's Policy on Theses and Dissertations**

This policy addresses permission to include **your article**(s) or portions of text from **your article**(s) in your thesis.

**Reuse/Republication of the Entire Work in Theses or Collections**: Authors may reuse all or part of the Submitted, Accepted or Published Work in a thesis or dissertation that the author writes and is required to submit to satisfy the criteria of degree-granting institutions. Such reuse is permitted subject to the ACS' "Ethical Guidelines to Publication of Chemical Research". Appropriate citation of the Published Work must be made as follows

"Reprinted with permission from [COMPLETE REFERENCE CITATION]. Copyright [YEAR] American Chemical Society." Insert the appropriate wording in place of the capitalized words. Citation information may be found after the "Cite this:" heading below the title of the online version and at the bottom of **the first page of the pdf or print version of your ACS journal article**.

If the thesis or dissertation to be published is in electronic format, a direct link to the Published Work must also be included using the ACS Articles on Request author-directed link.

If your university requires written permission and your manuscript has not yet received a DOI (published ASAP), send a request to copyright@acs.org that includes the manuscript number, the name of the ACS journal, and the date that you need to receive our reply.

If your university requires you to obtain permission for manuscripts in ASAP status or final published articles, you must use the RightsLink permission system. **See RightsLink instructions at http://pubs.acs.org/page/copyright/permissions.html and make requests at the "Rights & Permissions" link under the title of the online version of the article.**

**Submission to a Dissertation Distributor**: If you plan to submit your thesis to UMI or to another dissertation distributor, you should not include the unpublished ACS paper in your thesis if the thesis will be disseminated electronically, until ACS has published your paper. After publication of the paper by ACS, you may release the entire thesis (**not the individual ACS article by itself**) for electronic dissemination through the distributor; ACS's copyright credit line should be printed on the first page of the ACS paper.

Updated: 07/2021

**Author contribution (CRediT taxonomy):** Methodology, Formal analysis, Investigation, Writing – Original draft, Visualisation.

**Chapters reproducing the article content:** Chapter 3 is based on this publication.

## Tetrabutylphosphonium acetate and its eutectic mixtures with common-cation halides as solvents for carbon dioxide capture

Carlos A. Pena[a], Ana Soto[a], Héctor Rodríguez[a]

[a] CRETUS Institute, Department of Chemical Engineering, Universidade de Santiago de Compostela, E–15782 Santiago de Compostela, Spain

**Journal:** Chemical Engineering Journal (2021), ed. Elsevier Science (ISSN: 1385-8947), volume 409, article no. 128191. DOI: https://doi.org/10.1016/j.cej.2020.128191. Impact factor = 16.744 (2021), ranking it 4/142 in the JCR category Chemical Engineering (Q1). This journal allows the use of this full article in the present thesis, both in print and electronic format, without requesting further permissions, provided that it is not published commercially and that it is properly referenced.

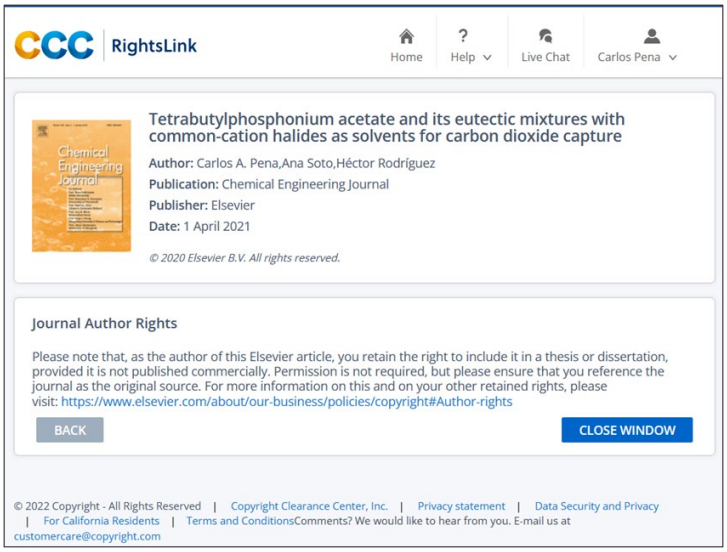


**Author contribution (CRediT taxonomy):** Formal analysis, Investigation, Writing – original draft, Conceptualization.

**Chapters reproducing the article content:** Chapter 3 is based on this publication.

## Liquid Systems Based on Tetra(*n*-butyl)phosphonium Acetate for the Non-dissolving Pretreatment of a Microcrystalline Cellulose (Avicel PH-101)

Carlos A. Pena[a], Alberto V. Puga[b], Andreas Metlen[c], Ana Soto[a], Héctor Rodríguez[a]

[a] CRETUS, Department of Chemical Engineering, Universidade de Santiago de Compostela, E15782 Santiago de Compostela, Spain.
[b] Departament d'Enginyeria Química, Universitat Rovira i Virgili, 43007 Tarragona, Spain.
[c] AMT1-Translations & Chemistry, 2910 Essen Antwerp, Belgium

**Journal:** Biomacromolecules (2022), ed. American Chemical Society (ISSN: 1525-7797), volume 23, pages 1970-1980. DOI: https://doi.org/10.1021/acs.biomac.1c01683. Impact factor = 6.978 (2021), ranking it 8/90 in the JCR category Polymer Science (Q1). This journal allows the use of this full article in the present thesis, both in print and electronic format, without requesting further permissions, provided that it is not published commercially and that it is properly referenced.

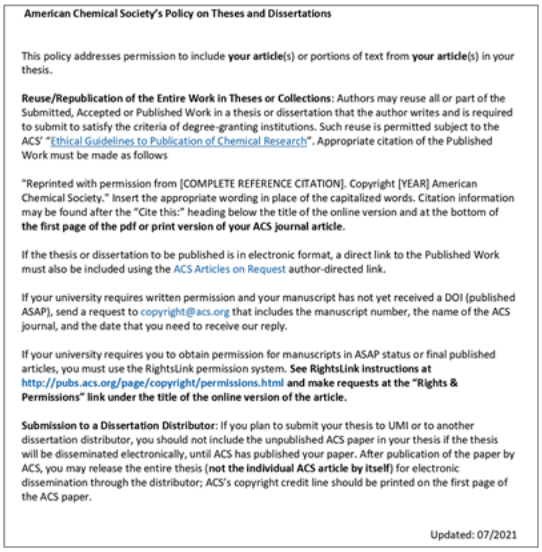

**American Chemical Society's Policy on Theses and Dissertations**

This policy addresses permission to include **your article**(s) or portions of text from **your article**(s) in your thesis.

**Reuse/Republication of the Entire Work in Theses or Collections**: Authors may reuse all or part of the Submitted, Accepted or Published Work in a thesis or dissertation that the author writes and is required to submit to satisfy the criteria of degree-granting institutions. Such reuse is permitted subject to the ACS' "Ethical Guidelines to Publication of Chemical Research". Appropriate citation of the Published Work must be made as follows

"Reprinted with permission from [COMPLETE REFERENCE CITATION]. Copyright [YEAR] American Chemical Society." Insert the appropriate wording in place of the capitalized words. Citation information may be found after the "Cite this:" heading below the title of the online version and at the bottom of **the first page of the pdf or print version of your ACS journal article.**

If the thesis or dissertation to be published is in electronic format, a direct link to the Published Work must also be included using the ACS Articles on Request author-directed link.

If your university requires written permission and your manuscript has not yet received a DOI (published ASAP), send a request to copyright@acs.org that includes the manuscript number, the name of the ACS journal, and the date that you need to receive our reply.

If your university requires you to obtain permission for manuscripts in ASAP status or final published articles, you must use the RightsLink permission system. **See RightsLink instructions at http://pubs.acs.org/page/copyright/permissions.html and make requests at the "Rights & Permissions" link under the title of the online version of the article.**

**Submission to a Dissertation Distributor**: If you plan to submit your thesis to UMI or to another dissertation distributor, you should not include the unpublished ACS paper in your thesis if the thesis will be disseminated electronically, until ACS has published your paper. After publication of the paper by ACS, you may release the entire thesis (**not the individual ACS article by itself**) for electronic dissemination through the distributor; ACS's copyright credit line should be printed on the first page of the ACS paper.

Updated: 07/2021

**Author contribution (CRediT taxonomy):** Methodology, Formal analysis, Investigation, Writing – Original draft, Visualisation.

**Chapters reproducing the article content:** Chapter 3 is based on this publication.

- At the time of presenting this thesis, two manuscripts have been submitted for publication, corresponding to the work presented in Chapter 4:

**Laccase-mediator system for the ionic liquid-assisted treatment of a technical lignin with partial dissolution**

Carlos A. Pena[a,b], Lina F. Ballesteros[b], Héctor Rodríguez[a], Eva Rodil[a], José A. Teixeira[a], Michele Michelin[a]

[a] Centre of Biological Engineering, University of Minho, Campus de Gualtar, 4710-057 Braga, Portugal
[b] CRETUS, Department of Chemical Engineering, Universidade de Santiago de Compostela, E–15782 Santiago de Compostela, Spain

**Journal:** submitted for publication to a journal edited by Elsevier Science, ranked Q1 according to the JCR 2021 impact factors.

**Author contribution (CRediT taxonomy):** Methodology, Formal analysis, Investigation, Writing – Original draft, Visualisation.

**Chapters reproducing the article content:** Chapter 4 is based on this publication.

**Lignin depolymerisation with aqueous solutions of the ionic liquid 1 ethyl-3-methylimidazolium acetate**

Carlos A. Pena[a], Eva Rodil[a], Héctor Rodríguez[a]

[a] CRETUS, Department of Chemical Engineering, Universidade de Santiago de Compostela, E–15782 Santiago de Compostela, Spain

**Journal:** submitted for publication to a journal edited by Elsevier Science, ranked Q1 according to the JCR 2021 impact factors.

**Author contribution (CRediT taxonomy):** Investigation, Methodology, Data curation, Visualisation, Writing – original draft.

**Chapters reproducing the article content:** Chapter 4 is based on this publication.

# Appendix F:

# “Resumo” (Summary, in Galician)

# Appendix F:

# "Resumo" (Summary, in Galician)

No actual contexto socioeconómico existe unha incuestionable dependencia dos recursos non renovables e combustibles fósiles, implicando inevitablemente unha degradación do medio ambiente. A tendencia actual do sector industrial é a procura de procesos máis sostibles e con menor impacto ambiental. Non obstante, na industria química, as substancias de orixe non renovable aínda teñen unha presencia elevada na maioría de procesos. A biomasa lignocelulósica é un recurso renovable que ofrece o potencial para satisfacer unha gran parte desta demanda. Este biorrecurso presenta unha distribución xeográfica máis uniforme que as materias primas de orixe fósil, facilitando a súa accesibilidade e diminuíndo as necesidades de transporte. A variabilidade que presenta, tanto desde unha perspectiva xeográfica como de especie vexetal -entre outros factores-, afecta de xeito importante a súa composición, pero en xeral está formada por tres compoñentes maioritarios: celulosa, hemicelulosa e lignina, que poden constituír ata un 95 % do seu peso seco. Co obxectivo de lograr un óptimo aproveitamento deste recurso, xorde o concepto de biorrefinería, definido como unha planta industrial onde os biorrecursos son aproveitados de forma integral co fin de obter produtos, enerxía e combustibles por medio de procesos que minimizan o impacto ambiental e a xeración de residuos. Para lograr a óptima implantación da biorrefinería desenvolvéronse procesos destinados a maximizar o aproveitamento da biomasa, porén, os procesos estandarizados para a valorización de lignina e celulosa están baseados en disolventes problemáticos ou altas temperaturas e presións, supoñendo unha forte limitación no beneficio ambiental do aproveitamento do referido recurso biorrenovable. Polo tanto, para alcanzar o obxectivo de lograr unha industria química sostible no marco do paradigma de biorrefinería, é imprescindible desenvolver novos procesos cunhas credenciais máis sostibles.

A **celulosa** é o biopolímero máis abundante na Terra. É o compoñente maioritario da biomasa lignocelulósica, cunha función estrutural nos vexetais. Este recurso, non tóxico, é producido de forma natural a unha taxa suficiente para satisfacer as necesidades da industria química global. Así, a súa óptima explotación é chave nun

contexto de biorrefinería, onde ten un alto valor na industria de polímeros e biocombustibles. Estruturalmente, a celulosa é un carbohidrato formado por monómeros de D-glucopiranosa unidos por enlaces β-1,4-O-glucosídicos, formando longas cadeas ligadas entre si por enlaces de hidróxeno. Estes enlaces de hidróxeno repítense de forma periódica conferíndolle unha estrutura cristalina. Das catro principais estruturas cristalinas coñecidas (á parte de outros subtipos), a máis abundante na Natureza é a tipo I. A celulosa tipo II habitualmente é obtida por solubilización da celulosa tipo I e posterior rexeneración, mentres que os outros tipos son considerados de menor importancia xa que son obtidos a partir destes dous, presentando unha menor estabilidade. A estrutura da celulosa tipo I, a pesar de ser menos estable termodinámicamente que a celulosa tipo II, é menos reactiva ó presentar unha disposición espacial moi compacta, conferíndolle un carácter recalcitrante. Esta baixa reactividade orixina que, para o aproveitamento deste recurso, sexan necesarios tratamentos que transforman a celulosa tipo I en celulosa tipo II ou, idealmente, en celulosa amorfa. As actuais metodoloxías baséanse en dúas técnicas: a disolución de celulosa seguida dunha rápida rexeneración por precipitación e a mercerización. Esta última metodoloxía, a pesar de superar o problema da rexeneración da celulosa, emprega disolucións corrosivas baseadas en NaOH. En ambos casos é necesario o emprego de disolventes problemáticos e un elevado aporte enerxético, limitando a súa compatibilidade ambiental. Así, é evidente a necesidade de desenvolver mellores procesos de pretratamento de celulosa.

Neste contexto, existen antecedentes de disolución de celulosa en condicións suaves co emprego de líquidos iónicos. Os líquidos iónicos son sales cunha baixa temperatura de fusión ou de transición vítrea (arbitrariamente considérase o límite de 100 °C). As propiedades destas substancias varían considerablemente segundo a súa natureza pero, de forma xeral, pódese considerar que presentan varias características que lles confiren mellores propiedades que os disolventes tradicionais ós que poden substituír: presión de vapor depreciable, evitando a contribución á polución ambiental e á creación de atmosferas inflamables; xeralmente boa estabilidade térmica; gran capacidade de solvantación; etc. Estes disolventes abriron as portas de novas tecnoloxías para os pretratamentos de celulosa baseados na súa disolución e posterior rexeneración como celulosa de tipo II. Porén, os procesos baseados na disolución de celulosa requiren grandes cantidades de antidisolvente para a rexeneración da celulosa,

o que supón un elevado gasto enerxético na recuperación do líquido iónico, xeralmente por destilación. A alternativa investigada nesta tese é un proceso equivalente á mercerización, na que o líquido iónico altera a estrutura cristalina da celulosa sen disolvela, por contacto directo heteroxéneo, permitindo recuperar a celulosa pretratada simplemente mediante filtración.

Por outra banda, na biomasa lignocelulósica a **lignina** pode constituír ata un 40 % do seu peso seco (dependendo da orixe da biomasa). Este biopolímero presenta unha estrutura tridimensional constituída maioritariamente pola repetición de tres unidades: *p*-hidroxifenil (unidades H), guaiacil (unidades G) e sirinxil (unidades S), as cales constitúen unha abundante materia prima para múltiples produtos de alto valor engadido como bioplásticos, resinas, lubricantes ou aeroxeles. Non obstante, este potencial está fortemente limitado polo carácter recalcitrante da súa estrutura, limitando a viabilidade do seu aproveitamento a nivel industrial. Por este motivo, tradicionalmente veu sendo considerado como un produto secundario de baixo valor ou incluso como un residuo, empregándose na meirande parte como mero combustible nas propias plantas nas que se produce. Recentemente deseñáronse novos procedementos para, mediante a súa despolimerización, obter produtos de alto valor engadido. Aínda así, estas técnicas adoitan basearse en tratamentos a altas presións e temperaturas superiores a 100 °C, habitualmente coa asistencia de osíxeno e/ou catalizadores metálicos ou ácidos. Na procura de novas tecnoloxías para a despolimerización de lignina en procesos ambientalmente máis compatibles, existen antecedentes empregando o máis popular líquido iónico para o tratamento de biomasa: o acetato de 1-etil-3-metilimidazolio ([$C_2$mim][OAc]). Agora ben, presentan igualmente o inconveniente do emprego de alta temperatura e alta presión de osíxeno molecular para acadar unha despolimerización parcial da lignina. Neste contexto, acentúase a necesidade de desenvolver métodos alternativos de despolimerización da lignina, que non precisen condicións de operación de tanta dureza.

**Obxectivos**

O obxectivo xeral desta tese é o avance no coñecemento científico sobre o potencial uso de sistemas líquidos baseados en líquidos iónicos e/ou disolventes moleculares en novas tecnoloxías máis sostibles e cun baixo impacto ambiental para a valorización de celulosa e lignina, compoñentes poliméricos maioritarios da biomasa lignocelulósica.

Este obxectivo xeral inclúe obxectivos específicos referentes a cada un destes biopolímeros. Así, un primeiro obxectivo baséase na procura dun pretratamento heteroxéneo (sen disolución) mediante sistemas baseados no líquido iónico acetato de tetrabutilfosfonio ([$P_{4444}$][OAc]) para mellorar a reactividade da celulosa empregando condicións suaves (temperatura moderada e presión atmosférica). Os estudos preliminares realízanse con celulosa microcristalina (MCC) para continuar cunha investigación máis definida usando a popular celulosa comercial Avicel PH-101. A maiores do líquido iónico puro, estúdanse combinacións deste con disolventes moleculares convencionais de baixo impacto ambiental e baixa toxicidade. Empréganse unha representación de disolventes próticos e apróticos para avaliar esta característica na eficacia do pretratamento. Ademais, coa finalidade de poder executar os pretratamentos a temperatura inferior á do punto de fusión deste líquido iónico, efectúase a determinación dos equilibrios sólido-líquido das mesturas do líquido iónico cos co-disolventes seleccionados. Do mesmo xeito investigarase o potencial comportamento eutéctico do [$P_{4444}$][OAc] cos seus haluros homólogos, con cloruro e bromuro como anións, para, deste xeito, manter a natureza completamente iónico do fluído de pretratamento tamén nos pretratamentos a menor temperatura. O efecto do pretratamento analízase na celulosa pretratada mediante determinación do índice de cristalinidade e do grado de polimerización, así como do estudo da estabilidade térmica. A mellora na reactividade valórase mediante a cinética dunha hidrólise enzimática e, no caso da celulosa Avicel PH-101, tamén coa produción de carboximetilcelulosa (CMC) en condicións de reacción máis suaves que os procesos actuais de referencia.

O segundo obxectivo céntrase na mellora dos procesos de valorización de lignina.v En primeiro lugar, investígase como axente despolimerizador dunha lignina de calidade técnica, Indulin AT, o líquido iónico [$C_2$mim][OAc] en disolución acuosa, a temperatura e presión ambientais. Ademais, complétase o estudo co efecto de nanopartículas metálicas coa asistencia de radiación ultravioleta como axente catalizador desta despolimerización. Nunha liña similar, estúdase o efecto conxunto deste líquido iónico coas enzimas de referencia neste campo: as lacasas. Empregarase unha lacasa recombinante comercial ben de maneira illada ou en sistemas lacasa-mediador, actuando como mediador o 2,2'-azino-bis(ácido 3-etilbenzotiazolina-6-sulfónico), comunmente coñecido como ABTS, sempre en condicións ambientais. En ámbolos casos búscase a identificación de compostos fenólicos de alto valor engadido,

obtidos a partir da despolimerización de lignina, así como a caracterización estrutural do residuo sólido, que será comparado coa Indulin AT orixinal.

**Líquidos baseados en acetato de tetrabutilfosfonio para o pretratamento sen disolución de celulosa**

A alternativa investigada nesta tese para o pretratamento da celulosa, co obxectivo da transformación da celulosa I a celulosa II ou preferiblemente a celulosa amorfa, é un proceso equivalente á mercerización, no que a substancia empregada é un líquido que altera a estrutura cristalina da celulosa nun contacto heteroxéneo sen disolución, permitindo recuperar a celulosa doadamente mediante filtración. Os pretratamentos de celulosa realízanse en dúas fases: estudos preliminares sobre celulosa microcristalina en pó MCC e estudos avanzados empregando celulosa Avicel. En calquera dos casos, as mostras orixinais de celulosa foron secadas a 383 K para axustar o seu contido en auga a aproximadamente 1.5 %. O líquido base seleccionado para o estudo foi o líquido iónico $[P_{4444}][OAc]$, ampliándose ó uso combinado deste líquido iónico con disolventes moleculares, co fin de intentar reducir a temperatura de fusión e viscosidade dos fluídos de pretratamento e así facilitar o seu uso a nivel industrial. Con este obxectivo investíganse dous disolventes próticos (auga e etanol) e un aprótico (dimetilsulfóxido, normalmente denominado DMSO).

En primeiro lugar determináronse os rangos de temperatura como líquido estable do $[P_{4444}][OAc]$, entre a súa temperatura de fusión (ou de transición vítrea) e a súa temperatura de descomposición. As temperaturas de fusión determínanse mediante calorimetría diferencial de barrido (DSC) e a estabilidade térmica por análise termogravimética (TGA). Obtivéronse unha temperatura de fusión de 331 K e unha temperatura de descomposición de 590 K polo método de TGA dinámico, se ben experimentos de medio-longo prazo con TGA isotermo indicaron que a taxa de descomposición é insignificante a unha temperatura máis reducida: 403 K. Estableceuse, como valor de equilibrio, 343.2 K como temperatura de pretratamento da celulosa que garante unha viscosidade suficientemente baixa e un líquido estable.

Os pretratamentos de celulosa realízanse en celdas de vidro termostatizadas, cun 10 % (w/w) de celulosa respecto ó fluído de pretratamento. Ó rematar o pretratamento, as mostras de celulosa recupéranse empregando filtros sintéticos axudándose de baleiro suave. A celulosa lávase con auga sobre o mesmo filtro ata que

a auga de lavado contén menos de 50 ppm do fluído de pretratamento. A celulosa pretratada caracterízase por: análise termogravimétrica (TGA) dinámica para estudar a estabilidade térmica, índice de cristalinidade por difractometría de raios X, empregando a estratexia de subtracción do contido amorfo (celulosa amorfizada nun muíño de bolas), e grao de polimerización por medio do procedemento baseado na viscosidade intrínseca, seguindo o procedemento descrito pola *United States Pharmacopeia*. Os primeiros pretratamentos da MCC co [$P_{4444}$][OAc] a 343.2 K centráronse na análise do efecto do tempo mediante a determinación do índice de cristalinidade. Obsérvase unha redución de cristalinidade na MCC, pasando de 48 % para a celulosa sen tratar, a un 38 % a celulosa tratada durante 2 h, 30 % para a celulosa tratada durante 4 h e 24 % para o tratamento de 8 h. Nos pretratamentos con co-disolventes en 2 h, coa mestura deste líquido iónico con $x_{DMSO}$ = 0.20 a cristalinidade reduciuse ata o 12 %, mentres que no tratamento con $x_{DMSO}$ = 0.40 tivo lugar un considerable efecto de xelación, producindo agregados moi compactos e de elevada dureza, pouco interesantes para o propósito desta tese, sendo así descartado ese fluído de pretratamento. No caso da auga, a cristalinidade situouse en 31 % e 34 % para fracción molares de auga de 0.20 e 0.40 respectivamente. No referente ó grao de polimerización, non se atoparon variación significativas, manténdose en todos os casos entre 219 e 228.

Unha das desvantaxes deste líquido iónico é a súa relativa alta temperatura de fusión. Por ese motivo, na segunda fase, nos estudos avanzados con celulosa Avicel, investigouse a posible formación de sistemas eutécticos (a través de estudos de equilibrio sólido-líquido), co mesmo líquido iónico e co mesmo co-disolvente polar aprótico (o DMSO) mentres que a auga como co-disolvente prótico substituíuse por etanol na procura dunha eficacia máis pronunciada. Só se evidenciou comportamento eutéctico para o DMSO, pero aínda así observouse unha baixada na temperatura de fusión para as mesturas do [$P_{4444}$][OAc] cos dous disolventes moleculares investigados en fraccións molares de co-disolvente de 0.20 e 0.40, o que permitiu a realización dos pretratamentos a 323.2 K. A cristalinidade da celulosa Avicel viuse reducida de 51 % a 46 % con 2 h de pretratamento con [$P_{4444}$][OAc] puro. Nos pretratamentos que empregan etanol como codisolvente conseguiuse unha redución de cristalinidade similar á do líquido iónico puro, proporcionando índices de cristalinidade entre o 44 % e o 48 % para todos os casos que involucraron este co-disolvente. No caso do DMSO, a

redución de cristalinidade foi notable, especialmente salientable no pretratamento cunha fracción molar de 0.20 de DMSO a 343.2 K, reducindo a cristalinidade da celulosa ata o 20 %. Este mesmo tratamento a 323.2 K logra a redución de cristalinidade ata o 29 %, mentres que empregando $x_{DMSO}$ = 0.40 a cristalinidade da celulosa situouse no 23 % e no 28 % para os tratamentos a 323.2 K e 343.2 K respectivamente. Os difractogramas das mostras de celulosa cos pretratamentos que involucran o DMSO non só evidencian unha redución de cristalinidade, senón tamén unha transformación da estrutura cristalina, pasando de celulosa I á máis reactiva estructura celulosa II.

Tendo en conta os resultados obtidos decidiuse probar como fluído de pretratamento a combinación do [$P_{4444}$][OAc] cos seus haluros homólogos [$P_{4444}$]Cl e [$P_{4444}$]Br, que mantería íntegras as vantaxes do carácter iónico do disolvente. Co desenvolvemento do diagrama de fases sólido-líquido das correspondentes mesturas observáronse comportamentos eutécticos, cunha composición eutéctica de $x_{[P4444][OAc]}$ de 0.50 e 0.70 respectivamente, e temperaturas eutécticas suficientemente baixas como para permitir realizar os pretratamentos con estas mesturas a 313.2 K. O comportamento eutéctico destes sistemas é ben descrito polo modelo de Schröder-van Laar. Estas mesturas eutécticas non evidenciaron ningunha redución de cristalinidade nas dúas temperaturas estudiadas. Estes fluídos de pretratamento caracterizáronse mediante a densidade e viscosidade, e cos datos experimentais, modeláronse estas dúas magnitudes con, respectivamente, ecuacións polinómicas e a versión da ecuación de Vogel-Fulcher-Tammann modificada por Cohen e Turnbull. En todos os tratamentos sobre cellulosa Avicel prodúcese unha lixeira redución no grao de polimerización, entre o 5 % e o 10 %. A estabilidade térmica da celulosa pretratada con líquidos integramente iónicos mantívose invariable, mentres que empregando co-disolventes moleculares observouse unha lixeira redución, sempre inferior ó 8 %.

Por último, a verificación empírica da mellora da reactividade realizouse mediante hidrólises enzimáticas, tanto para MCC como para Avicel, nas que o seguimento da súa cinética se realizou a través da monitorización da concentración de glucosa no medio. As curvas cinéticas obtidas amosan unha aceptable relación aproximadamente lineal entre a cristalinidade e a velocidade de reacción. Non obstante, deben existir outros factores non estudiados nesta tese que tamén xogan un papel importante máis alá do índice de cristalinidade. Nos estudos avanzados sobre Avicel tamén se efectuou unha carboximentilación en condición máis suaves que as

estandarizadas para esta reacción. A celulosa pretratada con [$P_{4444}$][OAc] e DMSO ($x_{DMSO}$ = 0.20) a 343.2 K obtivo unha clara mellora do 47 % con respecto á celulosa non tratada.

En todos os casos verificouse o carácter non disolvente dos fluídos de pretratamento, mantendo en axitación 0.01 g de celulosa durante 24 h nunha celda termostatizada con 2 g de fluído para, posteriormente mediante microscopía, observar a non disolución das partículas.

**Valorización dunha lignina técnica en medios acuosos con acetato de 1-etil-3-metilimidazolio**

Nos primeiros estudos de despolimerización de lignina explórase a posibilidade de empregar o líquido iónico [$C_2$mim][OAc] en disolución acuosa en condicións suaves de operación. A combinación deste líquido iónico con auga permite modular a súa capacidade de solvatación ó tempo que mitiga o problema da súa viscosidade relativamente elevada. Como modelo de lignina emprégase a Indulin AT, unha lignina tipo *kraft* cun baixo contido de xofre (2.12 %), o cal lle proporciona un carácter insoluble en auga, ó igual que a lignina natural e a diferenza doutras moitas ligninas empregadas profusamente na bibliografía científica. En todos os experimentos empréganse 5 g de Indulin AT por cada 100 g de medio de reacción a temperatura ambiente e con axitación suficiente para asegurar unha boa homoxeneización.

Os tratamentos iniciais de Indulin AT realizáronse con disolucións acuosas de [$C_2$mim][OAc] para dúas concentracións de líquido iónico diferentes (10 % e 70 %) e para diferentes tempos de tratamento (ata 6 h). As mostras acuosas obtidas tras os tratamentos de lignina coas disolucións acuosas de [$C_2$mim][OAc] analizáronse mediante cromatografía líquida de alta resolución (HPLC). Os compostos obtidos cun maior rendemento son a vainillina e o guaiacol. Estas substancias son probablemente producidas pola ruptura de enlaces β-O-4 na estrutura polimérica da lignina pola acción do líquido iónico. En canto ás fases sólidas recuperadas despois do tratamento (que normalmente representan o 80-90 % da lignina inicial antes do tratamento), caracterízanse estruturalmente por resonancia magnética nuclear de coherencia cuántica simple heteronuclear $^{1}$H-$^{13}$C (2D $^{1}$H-$^{13}$C HSQC NMR), así como mediante análise termogravimétrica (TGA) e calorimetría diferencial de barrido (DSC) para a caracterización térmica. Os resultados destes experimentos indican un claro aumento

na concentración de vainillina e guaiacol, na fase acuosa, a medida que a concentración de líquido iónico aumenta. Isto coincide coa observación no sólido dunha menor proporción de unidades G, que son aquelas das que derivan a vainillina e o guaiacol. Respecto da caracterización térmica dos sólidos por DSC e TGA, pódese dicir que os tratamentos coas disolucións acuosas de [$C_2$mim][OAc] non implican unha modificación relevante do comportamento de transición vítrea do material de lignina e que o comportamento térmico dos sólidos recuperados é bastante semellante ó da Indulin AT crúa.

Co propósito de mellorar o rendemento do tratamento con disolución acuosa de [$C_2$mim][OAc] investígase a despolimerización da lignina mediante a fotorreacción inducida pola irradiación de luz ultravioleta con nanopartículas de $TiO_2$ ou AgCl como catalizadores. Tamén se investiga o efecto dun axente oxidante ($H_2O_2$) como aditivo na acción das nanopartículas. Usando a disolución ó 70 % de [$C_2$mim][OAc] como fluído de tratamento de referencia, probáronse varias concentracións de nanopartículas en tratamentos rápidos de 45 min baixo irradiación UV. Centrándose no rendemento dos dous principais compostos fenólicos identificados nas fases acuosas posteriores ó tratamento (vainillina e guaiacol), obsérvase que a concentración do 0,05 % de nanopartículas de $TiO_2$ conduce a unha mellora simultánea dos rendementos de ambos fenois con respecto ó caso de utilizar a irradiación ultravioleta sen nanopartículas (que, á súa vez, proporciona resultados equivalentes ó tratamento análogo sen irradiación). Os tratamentos coas outras concentracións de nanopartículas de $TiO_2$ probadas non conducen a unha mellora simultánea de ambos rendementos. Respecto das nanopartículas de AgCl, non se detectou ningunha mellora significativa dos rendementos de fenois en ningunha concentración; e mesmo se observa unha clara diminución do rendemento de vainillina para as concentracións máis altas (≥0,25 %). Polo tanto, descártanse as nanopartículas de AgCl e selecciónase unha concentración do 0,05 % de nanopartículas de $TiO_2$ para posteriores experimentos. Estúdase o efecto do aumento do tempo de irradiación de 45 min a 6 h pero non se observa ningunha variación significativa nos rendementos de vainillina ou guaiacol. A continuación, tentando mellorar a actividade catalítica das nanopartículas de $TiO_2$, investígase como aditivo o peróxido de hidróxeno (a unha concentración de 5 mM). Non obstante, estes experimentos con $H_2O_2$ levaron realmente a uns rendementos máis baixos dos compostos fenólicos, especialmente no caso da vainillina. En canto ós resultados

obtidos da análise das fases sólidas recuperadas despois dos tratamentos, obsérvase que, na maioría dos casos, a diminución relativa de unidades G garda correspondencia cun maior rendemento de vainillina e guaiacol, que son compostos fenólicos derivados das unidades G de lignina. A excepción vén marcada polos tratamentos que involucran $H_2O_2$, probablemente por causa de que, a partir de moitas unidades G que desaparecen do sólido, se produzan compostos totalmente oxidados de baixo peso molecular, como o $CO_2$, que abandonan o sistema.

Por último, como alternativa ós catalizadores metálicos, estúdanse diferentes tratamentos baseados nunha lacasa recombinante. A actividade das lacasas habitualmente diminúe en concentracións altas de sal, polo que a presencia do líquido iónico no medio de reacción pode ser prexudicial para a súa capacidade despolimerizadora. Porén, a súa presenza, coa capacidade exhibida de acción sobre a lignina, pode compensar a diminución de actividade das lacasas e ser interesante o seu emprego como aditivo tamén nesta estratexia enzimática de despolimerización. Nestes tratamentos emprégase unha lacasa recombinante de *Myceliophthora thermophila*. A súa actividade e estabilidade determínase con distintas concentracións de [$C_2$mim][OAc] en tampón acetato 0,1 M e pH 5,0, concluíndo que mantén unha actividade aceptable ata o 10 % (w/w) de [$C_2$mim][OAc]. Como mediador actúa o ABTS nunha concentración de 25 mM e tamén se investiga o efecto dunha presaturación con osíxeno molecular mediante un burbulleo de 30 minutos de forma previa ó inicio dos experimentos. Para finalizar os tratamentos, os recipientes de reacción introdúcense en auga fervendo, para desta forma desnaturalizar as enzimas. Os controis, a pesar de non conter lacasas, sométense a esta fase para que o efecto da temperatura non interfira nos resultados. En todos os tratamentos se obtivo unha fase sólida e outra acuosa. A fase sólida lávase con auga para asegurar a eliminación de restos de líquido iónico ou de líquido iónico e lacasas. A identificación de compostos fenólicos nas fases acuosas lévase a cabo por cromatografía UHPLC e, ademais, nos tratamentos deseñados para estudar o sistema lacasa-mediador, determínase o contido total de compostos fenólicos empregando o reactivo de Folin Ciocâlteu, obtendo o resultado como equivalentes de ácido gálico. A maiores, o sólido procedente dos tratamentos destinados a estudar o efecto do sistema lacasa-mediador someteuse a espectroscopía ATR-FTIR, a determinación da actividade antioxidante mediante un método baseado na redución do 2,2-difenil-1-picrilhidracil (DPPH) e a determinación da capacidade de inhibición do

crecemento de dúas bacterias: *S. aureus* e *E. coli*. Nos resultados obtidos obsérvanse considerables variación nos produtos fenólicos obtidos na fase acuosa, en función dos elementos involucrados no tratamento. Isto permite modular a despolimerización cara ós produtos desexados. No contido total de fenólicos, os tratamentos involucrando lacasas e ABTS amosan un claro incremento. No referente ás fases sólidas, obsérvase unha diminución relativa de unidades G cando está involucrado o líquido iónico, potenciado pola pre-osixenación. Os sólidos recuperados dos tratamentos involucrando lacasas e osixenación (con e sen líquido iónico) amosaron unha elevada capacidade antimicrobiana fronte a *S. aureus.* Tanto as análises térmicos como o ATR-TIR confirmaron os datos estruturais proporcionados pola espectrometría de RMN.

**Conclusións**

Á vista dos resultados obtidos nesta teses, as estratexias baseadas na combinación de disolventes moleculares e líquidos iónicos son prometedoras como base das novas tecnoloxías para a valorización dos dous principais constituíntes da biomasa lignocelulósica (celulosa e lignina) a través dunha perspectiva máis sostible. A continuación enuméranse unha serie de conclusións específicas extraídas dos resultados:

- ***Pretratamento da celulosa para a mellora da súa reactividade:***

- O líquido iónico $[P_{4444}][OAc]$ é capaz de reducir a cristalinidade da celulosa (en particular, MCC ou Avicel PH 101) mediante un pretratamento sen disolución en condicións suaves (presión atmosférica, 343 K) con fácil recuperación da celulosa pretratada e do líquido de pretratamento, por filtración. Esta redución da cristalinidade leva a unha mellora da reactividade, comprobada a través da análise da cinética de hidrólise enzimática das mostras pretratadas.
- Os sistemas binarios de $[P_{4444}][OAc]$ cos seus haluros homólogos $[P_{4444}]Cl$ e $[P_{4444}]Br$ presentan un comportamento eutéctico, con temperaturas eutécticas de 297 K e 305 K, respectivamente; marcadamente por debaixo da temperatura de fusión do $[P_{4444}][OAc]$ puro. Non obstante, o uso de mesturas eutécticas como líquidos de pretratamento da celulosa leva a unha redución cativa do índice de cristalinidade da celulosa e só se observa unha pequena

mellora con respecto a celulosa non tratada en termos de cinética de hidrólise enzimática.

- Ningún dos pretratamentos feitos á celulosa con calquera dos fluídos mencionados afecta significativamente á estabilidade térmica nin ó grao de polimerización da celulosa, aspecto de interese na industria de produtos poliméricos derivados da celulosa. En liña con isto, e no contexto dunha aplicación práctica, a mellora da reactividade da celulosa (Avicel) pretratada con $[P_{4444}][OAc]$ e cunha mestura de $[P_{4444}][OAc$ ] e DMSO demostrouse a través da súa carboximetilación. Grazas ós pretratamentos propostos, é posible obter carboximetilcelulosa con graos de substitución no rango comercial en condicións considerablemente máis suaves que o proceso de referencia para a produción industrial de carboximetilcelulosa.
- Os traballos futuros contemplan o pretratamento da biomasa lignocelulósica cos sistemas líquidos propostos para mellorar a accesibilidade e facilitar a reactividade posterior (por exemplo, cara á hidrólise enzimática) da súa fracción celulósica directamente dentro da matriz lignocelulósica. En resumo, o traballo presentado constitúe unha base de gran potencial para o desenvolvemento futuro de procesos de pretratamento de baixo custo e sen disolventes para axudar na produción de produtos químicos e materiais derivados da celulosa.

➢ ***Valorización da lignina técnica:***

- O tratamento dunha lignina técnica insoluble en auga (Indulin AT) cunha disolución acuosa ó 70 % do líquido iónico $[C_2mim][OAc]$, a temperatura e presión ambientais, conduce a rendementos medibles de diversos compostos fenólicos de valor engadido resultantes da despolimerización da lignina. En particular, pódense destacar os rendementos de aproximadamente 3 g de vainillina e 1 g de guaiacol por quilo de lignina tratada. O residuo sólido que queda despois do tratamento presenta unha menor proporción de unidades guaicil (unidades G) con respecto á lignina orixinal, de acordo co feito de que os compostos fenólicos producidos en maior medida derivan de unidades G. A asistencia do tratamento anterior con irradiación ultravioleta e nanopartículas de $TiO_2$ ou AgCl non proporciona ningunha mellora significativa. Ademais, a suplementación con $H_2O_2$ incluso amosa un efecto contraproducente.

- Os rendementos obtidos son notablemente máis baixos no caso de tratamento directo da lignina cunha disolución acuosa ó 10 % de [$C_2$mim][OAc], posiblemente debido á limitada solubilidade da lignina. Non obstante, o líquido iónico nesta concentración pódese utilizar como axudante para axustar o rendemento do tratamento da lignina a temperatura ambiente cunha lacasa recombinante de *Myceliophthora thermophila*, ou cun sistema lacasa-mediador composto por lacasa e o mediador ABTS, nun medio lixeiramente ácido. Os maiores rendementos de compostos fenólicos nos tratamentos con mediadores de lacasa con presenza de líquido iónico corresponden a guaiacol e siringaldehído, mentres que na súa ausencia corresponden a oleuropeína e ácido rosmarínico. Despois dalgún dos tratamentos, con todo, tamén se producen outros compostos fenólicos resultantes da despolimerización da lignina con rendementos detectables.
- Os sólidos recuperados dos tratamentos biolóxicos da lignina amosaron unha menor proporción de unidades G con respecto á Indulin AT sen tratar, especialmente cando se realizou unha pre-saturación dos medios de tratamento con $O_2$. Curiosamente, os sólidos recuperados despois dos tratamentos con mediadores de lacasa cunha presaturación con $O_2$ presentan unha actividade antimicrobiana mellorada contra *Staphylococcus aureus*, en comparación coa Indulin AT non tratada.
- En xeral, o líquido iónico [$C_2$mim][OAc] amosa potencial para a súa participación, ben como soluto concentrado en solución acuosa ou como aditivo de sistemas mediadores de lacasa, en esquemas de valorización da lignina mediante a súa despolimerización (parcial). Os traballos futuros sobre o desenvolvemento dos enfoques aquí propostos deberían centrarse en estratexias orientadas a aumentar o (ata o de agora discreto) nivel de despolimerización.



Lignocellulosic biomass is a key biorenewable source of the current industrial platform for the production of chemicals and materials to a more sustainable scheme. It is presently accepted that the viable exploitation of this type of biomass should include an integral valorisation of its major constituent biopolymers. The work of this thesis focuses on the two main ones: cellulose and lignin. In a rst part, the pretreatment of cellulose with liquid formulations based on ionic liquids was studied, with the purpose of improving its reactivity. Better reaction rates were observed both in the enzyme hydrolysis and in the carboxymethylation of the pretreated samples. In a second part, the depolymerisation of lignin via aqueous solutions of an ionic liquid or alternative aqueous systems was explored. Although in limited yields, a number of value-added phenolic compounds were identified after the treatments.